Phenomenology of the Higgs sectors of the $\mu\nu$SSM and the N2HDM

Memoria de Tesis Doctoral realizada por
Thomas Biekötter
presentada ante el Departamento de Física Teórica
de la Universidad Autónoma de Madrid
para optar el título de Doctor en Física Teórica

Tesis dirigida por el **Prof. Sven Heinemeyer**
y el **Prof. Carlos Muñoz López**

Instituto de Física Teórica UAM-CSIC

Departamento de Física Teórica
Universidad Autónoma de Madrid

Instituto de Física Teórica UAM-CSIC

June 18, 2019

If you've learnt something,
then the day's not been waisted.

Karl Pilkington

This thesis is based on the following scientific articles:

T. Biekötter, S. Heinemeyer, and C. Muñoz, "Precise prediction for the Higgs-boson masses in the $\mu\nu$SSM", *Eur. Phys. J.* **C78** (2018), no. 6, 504, arXiv:1712.07475

T. Biekötter, M. Chakraborti, and S. Heinemeyer, "A 96 GeV Higgs Boson in the N2HDM", *submitted to Eur. Phys. J.* **C**, 2019 arXiv:1903.11661

T. Biekötter, M. Chakraborti, and S. Heinemeyer, "An N2HDM Solution for the possible 96 GeV Excess", *18th Hellenic School and Workshops on Elementary Particle Physics and Gravity (CORFU2018) Corfu, Greece, August 31-September 28, 2018*, 2019 arXiv:1905.03280

T. Biekötter, S. Heinemeyer, and C. Muñoz, "Precise prediction for the Higgs-Boson Masses in the $\mu\nu$SSM with three right-handed neutrino superfields", arXiv:1906.06173

Acknowledgments

First of all, I want to express my gratitude to my supervisors Prof. Sven Heinemeyer y Prof. Carlos Muñoz López. You gave me the opportunity to work on an extremely interesting topic. I am also deeply grateful for your guidance during the four years of my Ph.D.

My sincere thanks also go to the other members of the $\mu\nu$SSM group in Madrid: Iñaki Lara Pérez and Donald Kpatcha. During our discussions I learnt a lot on the academic, but also on the personal level.

I also would like to thank my office mate Jorge Fernández Pendás who accompanied my journey from the very first to the very last day. I especially thank you for the enlightening discussions and for sorting out the subjuntivo in the chapters of this thesis written in Spanish.

Apart from that, I would like to thank the people with whom I collaborated or worked with during my Ph.D.: Florian Domingo, Manimala Chakraborti and Daniel E. López Fogliani. I am thankful for the organizers of the KUTS workshops during which my learning curve received large threshold corrections.

I thank all the members of the IFT and the Department of Theoretical Physics for creating such a pleasant working atmosphere.

I gratefully acknowledge the financial support of the Fundación La Caixa under the 'La Caixa-Severo Ochoa' international predoctoral grant.

Finally, I thank my parents Dorothea and Bernd for supporting me throughout my life in general.

Resumen

Con el descubrimiento del bosón de Higgs la última, y posiblemente más importante, pieza del modelo estándar (SM) puede haber sido encontrada. La existencia del bosón de Higgs es un requisito esencial del mecanismo de Brout-Englert-Higgs. Sin este mecanismo el SM no puede explicar el origen de las masas de todas las partículas fundamentales, de forma que los átomos no podrían formarse y la materia ordinaria no existiría. El SM predice con exactitud casi todos los fenómenos observados en experimentos a escalas de energía muy distintas y con una precisión destacable.

Sin embargo, el SM no predice todas las observaciones experimentales. El SM no explica la asimetría bariónica del universo. En el SM los neutrinos no tienen masa por construcción, así que no hay un mecanismo que dé lugar a las pequeñas masas de los neutrinos. El SM no contiene un candidato que pudiese contribuir a la abundancia de materia oscura fría. Además, existe el llamado problema de la jerarquía, que consiste en que la masa del bosón de Higgs parece estar ajustada muy finamente, si no hay un mecanismo que la proteja contra las correcciones cuánticas. Todos los problemas mencionados llevan a la conclusión de que el SM está incompleto y tiene que ser extendido para incorporar nueva física más allá del SM (BSM). Los modelos propuestos para llevar a cabo esa tarea se centran en determinados fenómenos BSM.

Durante la elaboración de esta tesis hemos investigado la fenomenología de dos teorías BSM distintas. Las dos tienen en común que cuentan con un sector de Higgs extendido respecto al del SM. La primera parte de la tesis trata sobre una extensión supersimétrica del SM, llamada en inglés μ-from-ν Supersymmetric Standard Model ($\mu\nu$SSM). Por medio de supersimetría, se resuelve el problema de la jerarquía y la unificación de los acoplamientos gauge se logra a una escala de alta energía. Además, en este modelo se añaden neutrinos *right-handed* al contenido de partículas del SM, de tal forma que las masas pequeñas de los neutrinos se originan a traves de un mecanismo de *seesaw* a la escala electrodébil. El gravitino, que tiene una vida media más grande que la edad del universo, representa un candidato para matería oscura. En el $\mu\nu$SSM tanto la escala de ruptura de supersimetría como la escala del mecanismo de seesaw están relacionadas con la escala electrodébil. Por eso, el espacio de parametros del $\mu\nu$SSM podría ser explorado con el Gran Colisionador de Hadrones (LHC) o con otros futuros colisionadores.

En extensiones supersimétricas del SM hay compañeros supersimétricos escalares para los fermiones del SM. Por lo tanto, en el $\mu\nu$SSM también los neutrinos right-handed tienen como compañeros sus escalares correspondientes. En el caso de una generación, es decir el $\mu\nu$SSM con un neutrino right-handed, el sector escalar neutro consiste en un número total de seis campos complejos, que son los dos campos dobletes de Higgs, los tres campos de neutrinos escalares left-handed, y el campo de neutrino escalar right-handed. En el caso de tres generaciones están presentes tres neutrinos right-handed. Los campos escalares correspondientes dan lugar a una extensión del sector escalar con un total de ocho campos complejos. Durante la ruptura de la simetría electrodébil todos

estos campos obtienen un valor esperado en el vacío. Asumiendo la conservación de $\mathcal{CP}$, las componentes reales e imaginarias producen un total de 6(8) partículas escalares pares bajo $\mathcal{CP}$ y 5(7) impares bajo $\mathcal{CP}$ en el caso de una(tres) generación(es).

Las masas de los escalares neutros de los modelos supersimétricos se pueden obtener a partir de los parámetros del modelo investigado. Sin embargo, las relaciones entre los parámetros y las masas físicas de los escalares dependen fuertemente de las correcciones cuánticas, que hay que considerar mediante el cálculo de correcciones de órdenes superiores en la teoría de perturbaciones. Todos los cálculos que incorporan órdenes superiores en teorías de campos cuánticos sufren la aparición de divergencias. Las divergencias tienen que ser eliminadas consistentemente por un procedimiento llamado renormalización. Durante el desarrollo de la tesis establecimos una prescripción de renormalización para el potencial escalar neutro del $\mu\nu$SSM que, a diferencia de cálculos automatizados, se aprovecha de unas condiciones de renormalización denominadas *on-shell*. De este modo, las relaciones entre ciertos parámetros y los observables físicos apropiados se mantienen al mismo orden de la teoría de perturbaciones estudiado.

Nuestro trabajo en el $\mu\nu$SSM se centró en predecir con precisión las masas de los escalares neutros a partir de las contribuciones renormalizadas a órdenes superiores. Utilizamos diagramas de Feynman, de forma que a orden n en teoría de perturbaciones se consideran los diagramas con n loops. Evaluamos las correcciones a un loop incluyendo el conjunto entero de parámetros del modelo, pero para una predicción con exactitud de la masa del bosón de Higgs del SM el resultado de un loop no es suficiente. Por ello, también consideramos correcciones parciales de ordenes superiores que están disponibles en la literatura. En nuestro análisis numérico obtuvimos una masa del bosón de Higgs del SM consistente con el valor experimental. Ilustramos lo especial que es la fenomenología del sector escalar del $\mu\nu$SSM estudiando escenarios representativos en los que aparecen otros escalares ligeros. Para el caso de tres generaciones pudimos presentar escenarios de referencia que concuerdan con las propiedades del bosón de Higgs del SM medido por el LHC, mientras reprodujimos al mismo tiempo los valores experimentales de las diferencias de masa de los neutrinos y los ángulos de mezcla.

En la segunda fase de la tesis investigamos una extensión no-supersimetrica del SM llamada en inglés Next-to 2 Higgs Doublet Model (N2HDM). El N2HDM extiende el sector de Higgs del SM con otro campo de Higgs doblete y un campo escalar real sin ninguna carga. Tales adiciones al sector de Higgs mínimo del SM son comunes en una gran cantidad de teorías BSM. Investigar la fenomenología del N2HDM cubre ampliamente la fenomenología de esas teorías relacionadas con el sector de Higgs. El sector de Higgs del N2HDM consiste de un total de cuatro bosones de Higgs neutros y dos cargados. Las predicciones teóricas del N2HDM se diferencian de las del SM por la presencia de los bosones de Higgs adicionales. Los resultados experimentales de las búsquedas en colisionadores, de la física de sabores o de los observables electrodébiles imponen límites sobre las posibles configuraciones de parámetros del N2HDM.

Nuestro análisis numérico del N2HDM buscaba explicar dos excesos experimentales, medidos con el Large Electron-Positron collider (LEP) y el Large Hadron Collider (LHC), que apuntan a la existencia de un segundo bosón de Higgs con una masa de ~ 96 GeV. Investigando el $\mu\nu$SSM descubrimos que los excesos pueden ser explicados con una fiabilidad de $\sim 1\sigma$, identificando así el posible bośon de Higgs nuevo como un sneutrino right-handed. Sin embargo, ciertas relaciones supersimétricas que deben ser cumplidas por el potencial escalar restringen esta explicación. Mediante un escaneo exhaustivo demostramos que los excesos pueden ser reproducidos en ciertos tipos de N2HDM, en

perfecta concordancia con los valores medidos experimentalmente. En el N2HDM un bosón de Higgs con una componente singlete dominante puede jugar el papel de la presunta partícula con masa igual a ~ 96 GeV. Verificamos que nuestra solución respeta todas las restricciones teóricas y experimentales. Por último, demostramos que nuestra solución puede ser comprobada con los colisionadores actuales o con los que se construirán en el futuro.

Summary

With the discovery of the Higgs boson the last missing, and arguably most important, piece of the Standard Model (SM) may have been found. The existence of the Higgs boson is an essential requirement of the Brout-Englert-Higgs mechanism. Without this mechanism the SM cannot account for the masses of all fundamental particles, such that no atoms would form and ordinary matter could not exist. The SM accurately predicts most of the phenomena observed at experiments at vastly different energy scales and at remarkable precision.

However, the SM is not able to predict all experimental observations. The baryon asymmetry of the universe is not explained. In the SM neutrinos are massless by construction, so that the origin of tiny neutrino masses is not accounted for. The SM contains no particle that contributes to the relic abundance of cold dark matter. The so-called hierarchy problem states that the Higgs-boson mass appears to be extremely fine-tuned without any mechanism protecting it from quantum corrections. All the aforementioned flaws lead to the conclusion that the SM is incomplete. It has to be extended to incorporate new physics, referred to as physics beyond the SM (BSM). Each BSM theory addresses a different set of BSM phenomena.

In this thesis the phenomenology of two BSM theories was investigated. Both models have in common that they feature an extended Higgs sector compared to the SM. The first part of the thesis deals with a supersymmetric extension of the SM, called μ-from-ν Supersymmetric SM ($\mu\nu$SSM). By means of supersymmetry, the hierarchy problem is not present and gauge coupling unification at very high energies is possible. Furthermore, in this model right-handed neutrinos are added to the SM particle content in order to explain the origin of neutrino masses, via a seesaw mechanism at the electroweak scale. A dark matter candidate is present with a gravitino having a lifetime longer than the age of the universe. In the $\mu\nu$SSM both the supersymmetry-breaking scale and the scale of the seesaw mechanism are related to the electroweak symmetry-breaking scale. Thus, the parameter space of the $\mu\nu$SSM is testable at the Large Hadron Collider (LHC) or future collider experiments.

In supersymmetric extensions of the SM there are scalar supersymmetry partners present for each SM fermion. Consequently, in the $\mu\nu$SSM also the right-handed neutrinos are accompanied by corresponding scalar particles. In the one-generation case, i.e., the $\mu\nu$SSM with one right-handed neutrino, the neutral scalar sector consists of a total of six complex fields, which are two Higgs-doublet fields, three left-handed scalar neutrinos fields, and one right-handed scalar neutrino field. In the three generation case, three right-handed neutrinos are present. The corresponding scalar supersymmetry partners yield a further extension of the scalar sector to a total of eight complex scalar fields. During electroweak symmetry breaking, all these fields acquire a vacuum expectation value. Assuming $\mathcal{CP}$-conservation, the real and imaginary components lead to a total of 6(8) $\mathcal{CP}$-even and 5(7) $\mathcal{CP}$-odd neutral scalar particles in the one(three)-generation case.

The physical masses of the scalars present in a supersymmetric model can be derived from the model parameters. However, the relations between the parameters and the masses strongly depend on quantum corrections which have to be incorporated by taking into account higher-order corrections in perturbation theory. Higher-order calculations in quantum field theories are plagued by the appearance of divergences. The divergences have to be consistently removed by a procedure called renormalization. In this work, we established a renormalization prescription for the neutral scalar sector of the $\mu\nu$SSM which, in contrast to automated calculations, makes use of so-called on-shell renormalization condition. In this way, the relations between certain parameters and appropriate physical observables are maintained at the order of perturbation theory explored.

Our work in the $\mu\nu$SSM was aimed to precisely predict the masses of the neutral scalars including the renormalized higher-order contributions. We employ the Feynman-diagrammatic approach in which at n^{th} order in perturbation theory diagrams containing n closed loops have to be considered. We evaluated the corrections at the one-loop level, including the full set of model parameters. For an accurate prediction of the SM-like Higgs-boson mass, the one-loop result is not sufficient. Therefore, we supplemented the one-loop corrections by partial higher-order contributions available in the literature. In our numerical analysis, we obtained a SM-like Higgs-boson mass consistent with the experimental value. We illustrated the unique phenomenlogy of the scalar sector of the $\mu\nu$SSM in representative scenarios that incorporate additional light scalars. In the three-generation case, we were able to present benchmark scenarios that are in agreement with the measurements of the properties of the SM-like Higgs boson and of the neutrino mass differences and mixing angles.

In the second part of the thesis, a non-supersymmetric extension of the SM called Next-to 2 Higgs Doublet Model (N2HDM) was studied. In the N2HDM the Higgs sector of the SM is enhanced by a second Higgs doublet field and a real scalar singlet field. Such additions to the minimal Higgs sector of the SM are common in a vast amount of BSM theories. To a large extend, the phenomenology related to the Higgs sector of these theories can be covered by investigating the phenomenology of the N2HDM. The Higgs sector of the N2HDM consists of a total of four neutral and two charged Higgs bosons. Theory predictions of the N2HDM are modified compared to the SM, because of the presence of the additional Higgs bosons. Combining experimental constraints from different areas, such as collider searches, flavor physics or electroweak precision observables, yields limitations on the possible parameter configurations of the N2HDM.

Our numerical analysis in the N2HDM was aimed to explain simultaneously two experimental excesses measured at the Large Electron-Positron collider (LEP) and the LHC that hint to the existence of a second Higgs boson with a mass of ~ 96 GeV. Investigating the $\mu\nu$SSM, we discovered that the excesses can be explained at the level of $\sim 1\sigma$ by identifying the potentially new Higgs boson with a right-handed sneutrino. The explanation was limited due to supersymmetric relations the scalar potential of the $\mu\nu$SSM has to obey. With an extensive analysis we showed that the excesses can be reproduced in certain types of the N2HDM in perfect agreement with the experimentally measured signal strengths. Here, a dominantly singlet-like Higgs boson acts as the potential ~ 96 GeV particle state. We verified that our solution respects all relevant theoretical and experimental constraints. We finally showed that our solution in the N2HDM is testable at current and future collider experiments.

Contents

Chapter 1

Introduction

Modern high-energy particle physics finds itself in a peculiar situation. The Standard Model (SM) of particle physics, established in the 70$^{\text{th}}$ of the past century [1–4], accurately predicts most of the phenomena measured at experiments over a vast range of energy scales. The SM is a renormalizable and anomaly-free gauge theory. It describes the most fundamental particles we know of and how they interact. The last missing piece of the SM, the Higgs boson predicted by the Brout-Englert-Higgs mechanism [5, 6], was finally detected at the Large Hadron Collider (LHC) [7, 8]. The measurements of the Higgs-boson mass already reached an astonishingly precise value of [9–12],

$$m_{h^{\text{SM}}} = 125.09 \pm 0.24 \text{ GeV} . \tag{1.1}$$

So far, all measurements of the Higgs-boson properties are in perfect agreement with the SM predictions [13–15], having in mind the theoretical and experimental uncertainties. This should not surprise too much, as the SM established itself via a lengthy historical curriculum of successful particle predictions.

In 1970 the Glashow–Iliopoulos–Maiani mechanism [16] demanded the existence of a fourth quark, referred to as charme quark, which was found just four years later at the Stanford Linear Accelerator Laboratory [17] and the Brookhaven National Laboratory [18]. The measurement of $\mathcal{CP}$-violation [19] and the detection of a third generation lepton [20] motivated the existence of a third generation of quarks [21]. The bottom quark was discovered soon after at Fermilab [22], while it took over 20 years and the Tevatron collider to find the top quark [23, 24]. The W and the Z boson, the gauge bosons theorized to be the mediators of the electroweak interaction, were detected at CERN with the help of the Super Proton Synchrotron in 1983 [25–27]. The ratio of their masses was in remarkable agreement with the theoretical predictions. And of course the particularly important discovery of the Higgs boson. Without the Higgs field all fundamental particles of the SM would be massless.

Nevertheless, there is absolute certainty that the SM is not a complete theory describing all aspects of nature. The SM does not contain gravity at all. Until today, it is unclear how to combine the general theory of relativity [28], a theory formulated without quantum effects, with the SM being a quantum field theory. Related to this is the origin of dark energy. In principle, the effects attributed to the existence of dark energy can be accommodated by a finite cosmological constant [29]. The SM expectation for this constant, however, disagrees with the experimental value by more than 100 orders of magnitude [30]. The light Higgs-boson mass demands an enormous amount of fine-tuning. The Higgs potential of the SM seems to be independent of any physics at larger

energy scales, even though a large sensitivity should be present (see also Sect. 2.1.2). The Higgs boson is the only fundamental scalar of the SM, while there are three different copies of the fermionic matter fields. The appearance of different copies of fermions lead to a certain arbitrariness in the Yukawa sector of the SM. In particular, there is no mechanism present in the SM to explain the large hierarchy between the fermion masses. This problem became even more severe after the detection of tiny neutrino masses [31] which in the SM are strictly massless. The SM cannot naturally account for an inflationary epoch of the universe to explain the observed homogeneity and isotropy of the universe [32]. Based on purely theoretical reasons, the SM will become inconsistent at the energy scale of the Landau pole of the hypercharge gauge group. Admittedly, the Landau pole lies far beyond the Planck scale. One of the most concrete evidences for new physics is the relic abundance of cold dark matter [33, 34] for which the SM does not provide an elementary candidate whatsoever.

Considering all these experimental and theoretical problems of the SM, there is a desperate need for theories beyond the Standard Model (BSM) that provide solutions to the above mentioned flaws by incorporating new physics. This thesis contains phenomenological investigations of two such models; the μ-from-ν Supersymmetric Standard Model ($\mu\nu$SSM) and the Next-to 2 Higgs Doublet Model (N2HDM). The $\mu\nu$SSM solves several issues of the SM by means of Supersymmetry (Susy). Among other things, Susy solves the so-called hierarchy problem related to the fine-tuning in the SM Higgs sector. In addition, the $\mu\nu$SSM addresses the origin of neutrino masses. The main motivations for Susy in general and for the $\mu\nu$SSM in particular will be discussed in Ch. 2 and Ch. 3, respectively. The N2HDM is a non-superysymmetric extension of the SM featuring a second Higgs doublet field and a real scalar singlet field. Motivations for considering models with more than one Higgs doublets will be given in Ch. 7. One of them, also in relation to the presence of a singlet scalar, can be attributed to Susy. Several Susy models contain such particles. In the limit of large Susy-breaking scales, they can be mapped onto models like the N2HDM at energies far below the breaking scale. In any case, there is no reason to believe that there is only one fundamental scalar in nature. The mere discovery of the SM Higgs boson encourages to investigate models with additional scalars.

One exceptional reason to investigate the N2HDM in the scope of this thesis was the occurrence of two experimental excesses. Considering the experimental uncertainties, the excesses appear at an identical mass of ~ 96 GeV. As we will see, they hint to the presence of an additional Higgs boson with this mass. We were able to accommodate these excesses in the $\mu\nu$SSM with a particle called the right-handed sneutrino, the scalar partner of a right-handed neutrino. However, the potential signals could only be reproduced at the 1σ level, because of tight constraints on the form of the scalar potential that has to obey Susy relations. Thus, the interest arose to investigate to what extent the explanation of the excesses improves in non-Susy models containing similar Higgs sectors. We demonstrated that perfect agreement with the experimental data can be reached in the N2HDM [35, 36].

In our work in the $\mu\nu$SSM we elaborated a renormalization prescription for the neutral scalar potential of the $\mu\nu$SSMwhich is a prerequisite to calculate quantum corrections. This rather technical task will be explained in Chs. 5 and 6 for the $\mu\nu$SSM with one and three right-handed neutrino superfields, respectively. Therein, we give details about the precise definition of the renormalization scheme and the resulting radiative corrections to the physical scalar mass eigenstates. The renormalization was preformed by making use of the Feynman-diagrammatic approach at the one-loop level. We took into account

the full set of free parameters in a mixed on-shell/$\overline{\text{DR}}$ scheme. Thus, our calculation goes beyond already existing calculations of radiative corrections in the $\mu\nu$SSM [37]. At first, we considered the simpler version of the $\mu\nu$SSM with just one family of right-handed neutrinos [38]. Afterwards, we completed our aspirations by considering the full $\mu\nu$SSM with three families of right-handed neutrinos [39]. The latter three-generation case permitted a deeper understanding of the relations of fermionic and scalar sector, because neutrino masses can be incorporated accurately already at tree level. We propose representative benchmark scenarios which, in addition to accommodate a SM-like Higgs boson and neutrino states in agreement with experimental constraints, feature further light Higgs bosons.

The thesis is organized as follows. In Ch. 2 we introduce Susy. We give reasons why Susy-extensions of the SM are well motivated, and we explain the construction of supersymmetric Lagrangians. Exact Susy predicts new particles with masses equal to the ones of their SM partners. Thus, Susy cannot be an exact symmetry of nature, but has to be spontaneously broken at some scale. The phenomenological footprints of Susy breaking will be clarified. The final section introduces the minimal version of a supersymmetric SM, as well as general remarks about further extensions. A comprehensive study of the $\mu\nu$SSM can be found in Ch. 3. There we introduce the superpotential and the corresponding soft Lagrangian of the model. We point out the importance of the exact and spontaneously broken symmetries. This is followed by a summary of the particle spectrum. Also details about the electroweak seesaw mechanism from which the tiny neutrino masses originate will be given. In Ch. 4 we briefly describe the relevant ingredients required for the renormalization of general gauge theories. They are applied to the scalar potential of the $\mu\nu$SSM with one and three right-handed neutrinos in Ch. 5 and Ch. 6, respectively. Afterwards, we present a summary of the N2HDM in Ch. 7. The numerical analysis in the N2HDM which is dedicated to the explanation of experimental excesses is reported in Ch. 8, There we also reveal our earlier attempts in the $\mu\nu$SSM. We conclude in Ch. 9.

Bibliography

[1] S. L. Glashow, "Partial Symmetries of Weak Interactions", *Nucl. Phys.* **22** (1961) 579–588.

[2] S. Weinberg, "A Model of Leptons", *Phys. Rev. Lett.* **19** (1967) 1264–1266.

[3] A. Salam, "Weak and Electromagnetic Interactions", *Conf. Proc.* **C680519** (1968) 367–377.

[4] G. 't Hooft and M. J. G. Veltman, "Regularization and Renormalization of Gauge Fields", *Nucl. Phys.* **B44** (1972) 189–213.

[5] F. Englert and R. Brout, "Broken Symmetry and the Mass of Gauge Vector Mesons", *Phys. Rev. Lett.* **13** (1964) 321–323, [,157(1964)].

[6] P. W. Higgs, "Broken Symmetries and the Masses of Gauge Bosons", *Phys. Rev. Lett.* **13** (1964) 508–509, [,160(1964)].

[7] **ATLAS** Collaboration, G. Aad *et al.*, "Observation of a new particle in the search for the Standard Model Higgs boson with the ATLAS detector at the LHC", *Phys. Lett.* **B716** (2012) 1–29, arXiv:1207.7214.

[8] **CMS** Collaboration, S. Chatrchyan *et al.*, "Observation of a new boson at a mass of 125 GeV with the CMS experiment at the LHC", *Phys. Lett.* **B716** (2012) 30–61, arXiv:1207.7235.

[9] **Particle Data Group** Collaboration, M. Tanabashi *et al.*, "Review of Particle Physics", *Phys. Rev.* **D98** (2018), no. 3, 030001.

[10] **CMS** Collaboration, A. M. Sirunyan *et al.*, "Measurements of properties of the Higgs boson decaying into the four-lepton final state in pp collisions at $\sqrt{s} = 13$ TeV", *JHEP* **11** (2017) 047, arXiv:1706.09936.

[11] **ATLAS, CMS** Collaboration, G. Aad *et al.*, "Combined Measurement of the Higgs Boson Mass in *pp* Collisions at $\sqrt{s} = 7$ and 8 TeV with the ATLAS and CMS Experiments", *Phys. Rev. Lett.* **114** (2015) 191803, arXiv:1503.07589.

[12] **ATLAS** Collaboration, M. Aaboud *et al.*, "Measurement of the Higgs boson mass in the $H \to ZZ^* \to 4\ell$ and $H \to \gamma\gamma$ channels with $\sqrt{s} = 13$ TeV *pp* collisions using the ATLAS detector", *Phys. Lett.* **B784** (2018) 345–366, arXiv:1806.00242.

[13] **ATLAS, CMS** Collaboration, G. Aad *et al.*, "Measurements of the Higgs boson production and decay rates and constraints on its couplings from a combined ATLAS and CMS analysis of the LHC pp collision data at $\sqrt{s} = 7$ and 8 TeV", *JHEP* **08** (2016) 045, arXiv:1606.02266.

[14] **ATLAS Collaboration** Collaboration, "Combined measurements of Higgs boson production and decay using up to 80 fb^{-1} of proton–proton collision data at $\sqrt{s} =$ 13 TeV collected with the ATLAS experiment", ATLAS-CONF-2018-031, CERN, Geneva, Jul 2018

[15] **CMS** Collaboration, A. M. Sirunyan *et al.*, "Combined measurements of Higgs boson couplings in proton-proton collisions at $\sqrt{s} = 13$ TeV", *Submitted to: Eur. Phys. J.*, 2018 arXiv:1809.10733.

[16] S. L. Glashow, J. Iliopoulos, and L. Maiani, "Weak Interactions with Lepton-Hadron Symmetry", *Phys. Rev.* **D2** (1970) 1285–1292.

[17] **SLAC-SP-017** Collaboration, J. E. Augustin *et al.*, "Discovery of a Narrow Resonance in e^+e^- Annihilation", *Phys. Rev. Lett.* **33** (1974) 1406–1408, [Adv. Exp. Phys.5,141(1976)].

[18] **E598** Collaboration, J. J. Aubert *et al.*, "Experimental Observation of a Heavy Particle *J*", *Phys. Rev. Lett.* **33** (1974) 1404–1406.

[19] J. H. Christenson, J. W. Cronin, V. L. Fitch, and R. Turlay, "Evidence for the 2π Decay of the K_2^0 Meson", *Phys. Rev. Lett.* **13** (1964) 138–140.

[20] M. L. Perl *et al.*, "Evidence for Anomalous Lepton Production in e+ - e- Annihilation", *Phys. Rev. Lett.* **35** (1975) 1489–1492, [,193(1975)].

[21] M. Kobayashi and T. Maskawa, "CP Violation in the Renormalizable Theory of Weak Interaction", *Prog. Theor. Phys.* **49** (1973) 652–657.

[22] S. W. Herb *et al.*, "Observation of a Dimuon Resonance at 9.5-GeV in 400-GeV Proton-Nucleus Collisions", *Phys. Rev. Lett.* **39** (1977) 252–255.

[23] **CDF** Collaboration, F. Abe *et al.*, "Observation of top quark production in $\bar{p}p$ collisions", *Phys. Rev. Lett.* **74** (1995) 2626–2631, arXiv:hep-ex/9503002.

[24] **D0** Collaboration, S. Abachi *et al.*, "Search for high mass top quark production in $p\bar{p}$ collisions at $\sqrt{s} = 1.8$ TeV", *Phys. Rev. Lett.* **74** (1995) 2422–2426, arXiv:hep-ex/9411001.

[25] **UA2** Collaboration, M. Banner *et al.*, "Observation of Single Isolated Electrons of High Transverse Momentum in Events with Missing Transverse Energy at the CERN anti-p p Collider", *Phys. Lett.* **B122** (1983) 476–485, [,7.45(1983)].

[26] **UA2** Collaboration, P. Bagnaia *et al.*, "Evidence for Z0 —> e+ e- at the CERN anti-p p Collider", *Phys. Lett.* **B129** (1983) 130–140, [,7.69(1983)].

[27] **UA1** Collaboration, G. Arnison *et al.*, "Experimental Observation of Lepton Pairs of Invariant Mass Around 95-GeV/c**2 at the CERN SPS Collider", *Phys. Lett.* **B126** (1983) 398–410, [,7.55(1983)].

[28] A. Einstein, "The Foundation of the General Theory of Relativity", *Annalen Phys.* **49** (1916), no. 7, 769–822, [Annalen Phys.354,no.7,769(1916)].

[29] Y. B. Zeldovich, "Cosmological Constant and Elementary Particles", *JETP Lett.* **6** (1967) 316, [Pisma Zh. Eksp. Teor. Fiz.6,883(1967)].

[30] S. Weinberg, "The Cosmological Constant Problem", *Rev. Mod. Phys.* **61** (1989) 1–23, [,569(1988)].

[31] **Super-Kamiokande** Collaboration, Y. Fukuda *et al.*, "Evidence for oscillation of atmospheric neutrinos", *Phys. Rev. Lett.* **81** (1998) 1562–1567, arXiv:hep-ex/9807003.

[32] J. L. F. Barbon and J. R. Espinosa, "On the Naturalness of Higgs Inflation", *Phys. Rev.* **D79** (2009) 081302, arXiv:0903.0355.

[33] F. Zwicky, "Die Rotverschiebung von extragalaktischen Nebeln", *Helv. Phys. Acta* **6** (1933) 110–127, [Gen. Rel. Grav.41,207(2009)].

[34] V. C. Rubin, N. Thonnard, and W. K. Ford, Jr., "Rotational properties of 21 SC galaxies with a large range of luminosities and radii, from NGC 4605 /R = 4kpc/ to UGC 2885 /R = 122 kpc/", *Astrophys. J.* **238** (1980) 471.

[35] T. Biekötter, M. Chakraborti, and S. Heinemeyer, "A 96 GeV Higgs Boson in the N2HDM", *submitted to Eur. Phys. J.* **C**, 2019 arXiv:1903.11661.

[36] T. Biekötter, M. Chakraborti, and S. Heinemeyer, "An N2HDM Solution for the possible 96 GeV Excess", *18th Hellenic School and Workshops on Elementary Particle Physics and Gravity (CORFU2018) Corfu, Greece, August 31-September 28, 2018*, 2019 arXiv:1905.03280.

[37] H.-B. Zhang, T.-F. Feng, X.-Y. Yang, S.-M. Zhao, and G.-Z. Ning, "Higgs boson mass corrections in the $\mu\nu$SSM with effective potential methods", *Phys. Rev.* **D95** (2017), no. 7, 075013, arXiv:1704.03388.

[38] T. Biekötter, S. Heinemeyer, and C. Muñoz, "Precise prediction for the Higgs-boson masses in the $\mu\nu$SSM", *Eur. Phys. J.* **C78** (2018), no. 6, 504, arXiv:1712.07475.

[39] T. Biekötter, S. Heinemeyer, and C. Muñoz, "Precise prediction for the Higgs-Boson Masses in the $\mu\nu$SSM with three right-handed neutrino superfields", arXiv:1906.06173.

Chapter 2

Supersymmetry

Supersymmetry (Susy) [1–3] is one of the most attractive frameworks for BSM theories. It combines fermionic and bosonic degrees of freedom in a unified superspace formalism. Unification has proven to be a good guiding principle in the past. The unification of electromagnetism led to the discovery of Maxwell's equations. Later on, the electroweak theory unified electromagnetism and the weak interaction. Special relativity treats space and time as a unified object. There are good reasons to believe that a future Grand Unified Theory (GUT) in some way or the other relies on Susy. In particular, first attempts to unify the SM gauge forces into a single gauge group predicted the weak mixing angle and the proton lifetimes in agreement with experimental data only when Susy is incorporated [4, 5]. The only ways in which a unified framework for the SM gauge interactions and gravity was achieved were based on Supergravity (Sugra), where gravity automatically emerges from local Susy transformations (see Sect. 2.1.4).

An extensive literature can be found introducing the topic of Susy (see Refs. [6–9] for reviews). We briefly summarize only the most important general aspects of Susy, focusing on phenomenological implications of models with spontaneously broken Susy. One of these implications is the presence of Susy partners for the SM particles. For each SM fermion there are two corresponding scalars (called sfermions) in the particle spectrum. For each SM gauge boson there is an additional fermion (called gaugino) present. Also the bosonic degrees of freedom in the Higgs sector are mirrored into fermionic degrees of freedom. However, due to other reasons the resulting spectrum is more complicated and will be discussed later (see Sect. 2.5). If Susy would be an exact symmetry, the Susy partners would have exactly the same mass as their SM ally. This is obviously not the case in nature. Thus, Susy must be spontaneously broken. The mechanism behind the Susy breaking is unclear, but relevant Susy-breaking operators present at energy scales below the Susy-breaking scale can be parametrized by adding a so-called soft Lagrangian to the Susy-conserving piece. The form of these additional operators will be specified in Sect. 2.4.

The outline of this chapter is as follows. Firstly, we illustrate in Sect. 2.1 four of the main motivations to consider Susy models. Of particular importance is the hierarchy problem formulated in Sect. 2.1.2. It provides a compelling argument that the relevant scales of Susy breaking are in the vicinity of the electroweak symmetry breaking (EWSB) scale. Therefore, signals at colliders and other experiments are expected. Afterwards, we introduce in Sect. 2.2 the Susy algebra and the two fundamental building blocks of the superpotential, i.e., the chiral and the vector superfield. Based on this formalism, we explain the construction of Susy Lagrangians and the Susy-breaking part in Sect. 2.3

and Sect. 2.4, respectively. The final section is dedicated to the simplest SUSY extensions of the SM. Their open problems motivate to go beyond the simplest models, as was done in the scope of this thesis by considering the $\mu\nu$SSM.

2.1 Motivations for Supersymmetry

There are several reasons to incorporate SUSY in BSM theories. We point out four of them which are valid for all SUSY models, and so do not rely on further model-specific assumptions.

2.1.1 The Coleman-Mandula theorem

We already argued that symmetries have shown to be a good guiding principle in the pursuit for new physics. However, the SM symmetry cannot be extended arbitrarily. In fact, the Coleman-Mandula theorem states that combining the internal symmetry groups and the spacetime symmetry group of the SM can only be done in a trivial way, i.e., by Lorentz scalars [10]. The spacetime symmetry of the SM is the Poincaré group [11], which consists of the generator of translations P_μ, and the antisymmetric tensor $M_{\mu\nu}$ generating Lorentz transformations. Adding additional charges transforming non-trivially under the Poincaré group, in other words, carrying a Lorentz index, would overconstrain possible interactions. For example, assuming a further conserved symmetric tensorial charge $Q_{\mu\nu}$ would lead to the unreasonable conclusion that two particles could only scatter in forward or backward direction [8, 12].

It turns that a certain kind of symmetry can circumvent the no-go theorem of Coleman-Mandula, namely SUSY. As already mentioned, SUSY relates bosonic and fermionic degrees of freedom. Thus, it is natural to assume that the generators of SUSY will carry a spinor index. Therefore, they cannot transform trivially under the Lorentz symmetry, and should be in contradiction with the Coleman-Mandula therom. However, the theorem only considers bosonic spacetime charges. Spinor charges fulfill anti-commutation relations, instead of commutation relations like the familiar generators of internal gauge groups and Poincaré spacetime symmetry of the SM. The Haag-Lopuszanki-Sohnius theorem states that an extension of the spacetime symmetry of an interactive quantum field theory is possible as long as the additional generators anti-commute with each other [13], forming a so-called graded Lie algebra or superalgebra. Assuming Q_a to be the generators of such transformations, with a being a spinor index, and letting this act on a state with spin J, the resulting state will have a different spin, so that [8]

$$Q_a \left|J\right\rangle = \left|J'\right\rangle \quad \text{with} \quad J \neq J' \,. \tag{2.1}$$

The action of Q_a on the S-matrix of the underlying quantum field theory does not overconstrain scattering processes and the Coleman-Mandula does not apply. In the following discussion, we will deal with two-component Weyl spinor charges Q_a, so that the spins of particles states will transform by half a unit, i.e., $J' = J \pm 1/2$. A symmetry having such generators leads to $N = 1$ supersymmetry. It is precisely the one relevant for SUSY extensions of the SM. The exact definition of the algebra will be given in Sect. 2.2.

At this point, the relevant message is that SUSY is the only possible way to extend the spacetime symmetry of the SM. Thus, SUSY is well motivated based purely on theoretical arguments. Unfortunately, one cannot deduce the energy scales at which the phenomenological impact of SUSY become important from the arguments presented here. In the

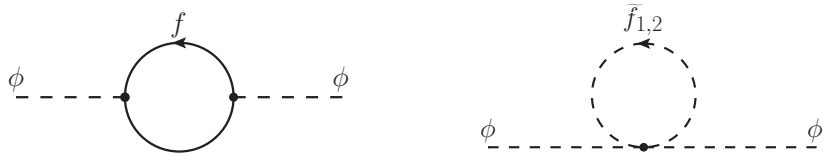

Figure 2.1: One-loop diagrams contributing to the radiative corrections to the mass of the scalar ϕ in the presence of a Dirac fermion f (*left*) and a sfermion $\widetilde{f}$ (*right*).

following section, we give a compelling argument why low-scale Susy, not too far from the EWSB scale, might be realized in nature.

2.1.2 Hierarchy problem

Following the discussion in Ch. 1, where we emphasized the necessity of BSM theories accommodating new physics, we have to assume that the SM is an effective field theory valid at the electroweak scale and below. However, the form of the complete high-energy theory in the ultraviolet (UV) from which the SM should be deducible is unknown. The Higgs-boson mass is regarded as a fundamental scalar in the SM. It is naively expected to be extremely sensitive to any large energy scale that might be present in the UV theory. See, for instance, the Feynman diagram on the left-hand side of Fig. 2.1. The diagram contributes to the radiative corrections to the mass m_ϕ of fundamental complex scalar ϕ coupled to a Dirac fermion f, via a Yukawa coupling of the form $-Y^f \phi \bar{\psi}_f \psi_f$ [7].[1] This diagram introduces a quadratic dependence

$$\Delta m_\phi^2 \propto -\frac{|Y^f|^2}{8\pi^2}\Lambda_{\mathrm{UV}}^2 \,, \tag{2.2}$$

of the loop-corrected scalar mass on the UV cutoff Λ_{UV}. The SM is renormalizable. The limit $\Lambda_{\mathrm{UV}} \to \infty$ can be taken, and the appearing UV divergences can be consistently canceled by introducing counterdivergences in the bare parameters of the Lagrangian, like in this case the bare mass parameter m_ϕ. However, a big problem arises as soon as new physics enters the theory. The scale of this new physics Λ_{NP} will be the momentum cutoff from where the SM is not anymore valid without taking into account new physics effects. The Higgs-boson mass would depend quadratically on this cutoff. Imagine, for instance, a mechanism that incorporates a quantized gravitational interaction. The scale at which this will be necessary is expected to be of the order of the Planck mass

$$\Lambda_{\mathrm{NP}} \sim M_P \sim 10^{19}\ \mathrm{GeV} \,, \tag{2.3}$$

yielding exorbitant radiative corrections to the scalar mass, tenth of orders of magnitudes larger than its actual value

$$\mathcal{O}\big((10^{19}\ \mathrm{GeV})^2\big) \gg \mathcal{O}\big((10^{2}\ \mathrm{GeV})^2\big) \,. \tag{2.4}$$

The question is then why in the SM the Higgs-boson mass is so small, if there is such a large sensitivity to the UV physics. Somehow, a cancellation of the UV dependence must be present. Another way of stating this circumstance is to ask why gravity is so weak. The natural value for the SM Higgs-boson mass is of the order of the Planck mass. The vacuum expectation value (vev) of the Higgs boson is also most naturally of the same order. It enters linearly in the masses of all SM particles. Hence, the SM particles are

[1] All Feynman diagram shown in this thesis were produced with `JaxoDraw` [14].

naively expected to have masses of the order of the Planck scale, so that gravity should be many times stronger compared to the other forces.

Most probably, there will be new physics already at lower scales than the Planck mass. Even then the quadratic dependency induces a problematic sensitivity to the scale of new physics. Consider, a heavy neutral Dirac fermion with a mass M_f of several TeV which could be a dark matter candidate, for instance. Integrating out the new Dirac fermion and matching the theory to the SM at lower energy introduces a dependence of the bilinear term in the Higgs sector on M_f^2. Thus, the scalar potential would receive corrections many orders of magnitude larger then the desired values of the parameters. The SM Higgs-boson mass would be much below its natural scale. If we imagine that there is new physics in the UV at several different scales, these would all leave footprints like the one stated above. This makes a low value of the SM Higgs-boson mass, as we observe it, highly fine-tuned and unnatural. It is important to note that the new physics does not even have to be coupled directly to the Higgs boson [7]. When higher-orders beyond the one-loop level are considered, large corrections can be induced via mediators that couple both to the scalar and the new fields. The graviton, for instance, couples to energy. As soon as gravity is considered, a mediator field between the new physics and the Higgs boson is automatically present.

The issues explained above are referred to as the hierarchy problem. It deals with the question why the SM works so astonishingly well as an effective theory without the need to know anything about the UV completion. The physics in the UV does not leave a trace in the Higgs sector, even though it naturally should, and the SM Higgs-boson mass somehow remains light.

What could be the mechanism behind this cancellation? One way to answer this question is by understanding why there is no hierarchy problem in the other sectors of the SM. This will emphasize the importance of symmetries. The SM is a chiral theory. Left-handed and right-handed fermions are differently charged under the SU(2) gauge group. Writing down explicit Dirac mass terms for the leptons and quarks is forbidden, because such terms mix both left- and right-handed fields. Consequently, a chiral symmetry is present. The chiral symmetry is broken during the electroweak phase transition, when effective Dirac masses for the fermions are generated via the Brout-Englert-Higgs mechanism. Quantum corrections to the masses of the SM fermions m_f exist. However, they are proportional to the fermion masses themselves [8],

$$\delta m_f \propto m_f \log \frac{\Lambda_{\mathrm{UV}}}{m_f} \,, \tag{2.5}$$

since their own Dirac mass terms are the ones breaking the chiral symmetry in the first place. The logarithmic dependence on Λ_{UV} is harmless. Consequently, the fermion masses in the SM are natural, because they are protected by a symmetry. Similarly, the massive SM gauge bosons obtain their masses dynamically after EWSB, when the Goldstone bosons of the broken SU(2)×U(1) gauge symmetry are gauged away into the longitudinal degrees of freedoms of the $W^{\pm}$ and the Z bosons. Hence, their masses are naturally of the order of the EWSB scale, protected by the SM gauge symmetry.

Can there be a symmetry protecting the Higgs-boson mass against large radiative corrections? The answer is yes, and the most elegant solution is Susy. Consider the diagram on the right-hand side of Fig. 2.1, depicting the one-loop contribution stemming from two complex scalar fields $\varphi_{1,2}^{\widetilde{f}}$, coupled to the scalar ϕ with a quartic coupling of

the form $-\lambda^{\widetilde{f}}|\phi|^2|\varphi^{\widetilde{f}}_{1,2}|^2$ [7]. The diagram yields contributions given by

$$\Delta m_\phi^2 \propto \frac{\lambda^{\widetilde{f}}}{16\pi^2}\left(2\Lambda_{\mathrm{UV}}^2 - m_{\widetilde{f}_1}^2 \log\frac{\Lambda_{\mathrm{UV}}}{m_{\widetilde{f}_1}} - m_{\widetilde{f}_2}^2 \log\frac{\Lambda_{\mathrm{UV}}}{m_{\widetilde{f}_2}}\right) . \tag{2.6}$$

In Susy bosonic and fermionic degrees of freedom are related to each other. A SM Dirac fermion f will have two complex scalar superpartners, one for the left- and one for the right-handed component, respectively. Assuming that $\widetilde{f}_1$ and $\widetilde{f}_2$ are these superpartners of f, then (as we will see below) the quartic couplings of the sfermions will be related to the Yukawa coupling of the corresponding fermions, such that

$$\lambda^{\widetilde{f}} = |Y^f|^2 . \tag{2.7}$$

The minus sign in Eq. (2.2) stems from the Dirac statistic for fermions. The quadratic cutoff dependence from the fermion loop will cancel against the term from the scalar loop diagrams proportional to Λ_{UV}^2. In addition, when Susy is an exact symmetry, one finds

$$m_f = m_{\widetilde{f}_1} = m_{\widetilde{f}_2} , \tag{2.8}$$

so that the terms logarithmically dependent on the cutoff are comparable in size to the Higgs-boson mass. Then the hierarchy problem is solved.

However, we know that the Susy partners of the SM particles must be heavier than the SM particles. Susy must be spontaneously broken. The breaking leads to mass difference between SM particles and their Susy partners which will be of the order of the Susy-breaking scale Λ_{Susy}. If this scale is very large, the sfermion masses are very large, and the hierarchy problem is reintroduced through the logarithmic terms in Eq. (2.6). Thus, for Susy to solve the hierarchy problem, one has to demand

$$\Lambda_{\mathrm{Susy}} \gtrsim \Lambda_{\mathrm{EWSB}} . \tag{2.9}$$

This is a crucial point, because low-scale Susy then also allows for several other issues of the SM to be solved simultaneously. Furthermore, it means that the Susy partners can be in reach of collider experiments like the Large Hadron Colliders (LHC). It is therefore a testable theory. Possible particle discoveries can provide information on the type of Susy model realized in nature.

2.1.3 Gauge coupling unification

The parameters of a quantum field theory depend on the energy scale Q at which a certain observable is calculated. The running can be computed in perturbation theory. It is formulated in terms of differential equations called Running Group Equations (RGEs). The RGEs depend on the particles that contribute to the higher-order vertex corrections. In the SM, the coupling g_1 of the abelian hypercharge U(1) gauge interaction grows with the energy scale, while the couplings g_2 and g_3 of the non-abelian SU(2) and SU(3) gauge groups become smaller when Q increases. The three values come closest to each other at roughly $Q \sim 10^{15}$ GeV. However, they do not intersect in a single point. This is a problem, because the notion of Grand Unified Theories (GUT), i.e., a unification of all forces of nature, predict a point in which the SM gauge couplings have equal values [15].

In Susy the additional particles start contributing to the running beyond the Susy-breaking scale. This modifies the energy dependence of the gauge couplings. Almost

miraculously, one finds that in the minimal SUSY extension of the SM (see Sect. 2.5) all three gauge couplings do intersect in a single point [15–18]. The necessary conditions for this to happen are that the SUSY-breaking scale is not too far beyond the TeV scale and that the normalization of g_1 is adequate to allow for a unification of the SM gauge groups into SU(5) or SO(10). We consider this as a strong motivation for SUSY, even though it could be just an unfortunate coincidence.

2.1.4 Supergravity

Another motivation for SUSY arises from the apparent segregation of gravity from the electroweak and the strong interaction [19]. The SM is a quantum field theory. The electroweak and the strong forces arise from gauge symmetries, defined by the groups $\mathrm{SU}(3)\times\mathrm{SU}(2)\times\mathrm{U}(1)$. On the other hand, the gravitational force is described by general relativity which is a classical theory. A naive attempt to formulate a quantum theory of gravity, treating the metric as a dynamical field, and in which gravitational interactions arise from gauging global spacetime transformations, leads to the appearance of an infinite number of UV divergences. The resulting quantum field theory is not renormalizable, because the gravitational coupling constant has negative mass dimensions. In Sect. 2.1.2 we already saw that SUSY can help in this regard. In particular, the presence of a fermionic superpartner of the graviton, called gravitino, yields a partial cancellation of the UV divergences.

Apart from that, there is a connection between SUSY and gravity stemming from the SUSY algebra. Just by matching degrees of freedom, one can derive that the form of the anti-commutation relation of two spinor charges Q_a must be [8]

$$\{Q_a, Q_b\} = A^{\mu}_{ab} P_{\mu} \,, \tag{2.10}$$

where P_μ is the spacetime translation operator, and A for now some unknown object (we give the precise form of the SUSY algebra in Sect. 2.2). The localized version of this anti-commutation relation automatically implies gravity which, as stated before, arises as gauge interaction from local spacetime transformations $P_\mu(x)$. This is why the local version of SUSY is called Supergravity (SUGRA). The distinct frameworks of general relativity and the SM can be linked by SUSY.

However, even a quantum field theory incorporating SUGRA cannot be renormalized. The only known way to obtain a renormalizable SUGRA theory is to consider fundamental particles as higher-dimensional extended objects. These so-called strings live in a higher-dimensional spacetime and only appear to be point-like at energies below a certain scale [19]. SUGRA in four-dimensional spacetime can then be realized as a low-energy effective theory from so-called superstring theories. The important point though is that even in such superstring theories SUSY is mandatory, because the presence of both fermions and bosons, as in the SM, requires SUSY [20]. In conclusion, SUSY might be the crucial ingredient to combine the SM and general relativity. Only this circumstance on its own is an outstanding motivation to study possible realizations of SUSY.

2.2 Supersymmetry algebra

In this section we will give the precise formulation of a SUSY field theory. We closely follow the introduction of Ref. [7]. We focus on the details with phenomenological implications. In SUSY the fundamental pieces of the theory are superfields $S(x, \theta, \theta^\dagger)$ which

are functions of the superspace coordinates

$$x^\mu \ , \quad \theta^\alpha \ , \quad \theta^\dagger_{\dot\alpha} \ , \tag{2.11}$$

where x^μ is the usual four-component spacetime coordinate. θ^α and $\theta^\dagger_{\dot\alpha}$ are Grassman variables, i.e., anti-commuting complex two-component spinors with negative mass dimension of $1/2$. α and $\dot\alpha$ are the undotted and dotted indices from the Van der Waerden notation [21]. The most general form of a superfield is

$$\begin{aligned} S(x,\theta,\theta^\dagger) = a(x) + \theta\ \xi(x) + \theta^\dagger\ \chi^\dagger(x) + \theta\theta\ b(x) + \theta^\dagger\theta^\dagger\ c(x) + \theta^\dagger\bar\sigma^\mu\theta\ v_\mu(x) \\ + \theta^\dagger\theta^\dagger\theta\ \eta(x) + \theta\theta\theta^\dagger\ \zeta(x) + \theta\theta\theta^\dagger\theta^\dagger\ d(x) \ , \end{aligned} \tag{2.12}$$

where we assume that S is commuting and does not have spinor or Lorentz indices. The SUSY transformations given by the anti-commuting spinor charges Q and $Q^\dagger$ act on a superfield.[2] The SUSY algebra is given by

$$\{Q_\alpha, Q^\dagger_{\dot\beta}\} = -2\sigma^\mu_{\alpha\dot\beta} P_\mu \ , \tag{2.13}$$

$$\{Q_\alpha, Q_{\dot\beta}\} = 0 \ , \tag{2.14}$$

$$\{Q^\dagger_\alpha, Q^\dagger_{\dot\beta}\} = 0 \ , \tag{2.15}$$

$$[P_\mu, Q_\alpha] = 0 \ , \tag{2.16}$$

$$[P_\mu, P_\nu] = 0 \ , \tag{2.17}$$

where $\sigma^{1,2,3}$ are the Pauli matrices and σ^0 is the identity matrix. A supermultiplet is a vector transforming in the irreducible representation of the SUSY algebra. A supermultiplet combines the bosonic and fermionic superpartners into a single object. The operator $-P^2$ commutes with Q and $Q^\dagger$, so that particles within a supermultiplet must have the same mass. Q and $Q^\dagger$ commute with the generators of gauge transformations, so that particles within a supermultiplet also carry the same gauge charges. Each supermultiplet contains the same number of bosonic and fermionic degrees of freedom. Relevant for the studies in this thesis are the three simplest representation of a supermultiplet. The SM fermions and their superpartners are arranged into chiral supermultiplets containing a Weyl fermion and a complex scalar. The SM gauge bosons and their superpartners constitute a vector supermultiplet consisting of a vector boson and a Weyl fermion. Finally, for gravity, the spin-2 graviton can form a supermultiplet with the help of a spin-$3/2$ gravitino fermion field.

The SUSY generators can be expressed as differential operators in superspace (denoted by a hat),

$$\hat Q_\alpha = \mathrm{i}\frac{\partial}{\partial\theta^\alpha} - (\sigma^\mu\theta^\dagger)_\alpha\partial_\mu \ , \quad \hat Q^\alpha = -\mathrm{i}\frac{\partial}{\partial\theta_\alpha} + (\theta^\dagger\bar\sigma^\mu)^\alpha\partial_\mu \ , \tag{2.18}$$

$$\hat Q^{\dagger\dot\alpha} = \mathrm{i}\frac{\partial}{\partial\theta^\dagger_{\dot\alpha}} - (\bar\sigma^\mu\theta)^{\dot\alpha}\partial_\mu \ , \quad \hat Q^\dagger_{\dot\alpha} = -\mathrm{i}\frac{\partial}{\partial\theta^{\dagger\dot\alpha}} + (\theta\sigma^\mu)_{\dot\alpha}\partial_\mu \ , \tag{2.19}$$

such that $\hat P_\mu = -\mathrm{i}\partial_\mu$ is identified with the usual spacetime translation operator. These operators define a translation in superspace. They are linear operators, so that a linear combination of superfields is a superfield transforming in the same way.

[2] We only consider $N = 1$ SUSY with a single generator Q_α. It is the one with phenomenological relevance given the chiral structure of the SM [8].

It is obvious from Eq. (2.12) that the general form of a superfield has too many degrees of freedom to represent a chiral or vector supermultiplet. Therefore, one defines the chiral covariant derivatives

$$D_\alpha = \frac{\partial}{\partial\theta^\alpha} - 2\mathrm{i}(\sigma^\mu\theta^\dagger)_\alpha\frac{\partial}{\partial y^\mu}\ , \quad D^\alpha = -\frac{\partial}{\partial\theta_\alpha} + 2\mathrm{i}(\theta^\dagger\bar\sigma^\mu)^\alpha\frac{\partial}{\partial y^\mu}\ , \tag{2.20}$$

and accordingly the anti-chiral covariant derivatives

$$\bar D^{\dot\alpha} = \frac{\partial}{\partial\theta^\dagger_{\dot\alpha}}\ , \quad \bar D_{\dot\alpha} = -\frac{\partial}{\partial\theta^{\dagger\dot\alpha}}\ , \tag{2.21}$$

where it is made use of the coordinates

$$y^\mu = x^\mu + \mathrm{i}\theta^\dagger\bar\sigma^\mu\theta\ , \quad \theta^\alpha\ , \quad \theta^\dagger_{\dot\alpha}\ . \tag{2.22}$$

The covariant derivatives anti-commute with the differential SUSY operators, such that $D_\alpha S$ and $\bar D_{\dot\alpha}S$ are superfields when S is a superfield. With the help of the covariant derivatives one defines the left-chiral superfield Φ by imposing

$$\bar D_{\dot\alpha}\Phi = 0\ , \tag{2.23}$$

and the right-chiral superfield Φ^* by imposing

$$D_\alpha\Phi^* = 0\ . \tag{2.24}$$

Chiral fields can be constructed from a general superfield by applying

$$\Phi = \bar D_{\dot\alpha}\bar D^{\dot\alpha}S\ , \quad \Phi^* = D^\alpha D_\alpha S^*\ . \tag{2.25}$$

Expressed by the component fields they read

$$\begin{aligned}\Phi =&\phi(y) + \sqrt{2}\theta\psi(y) + \theta\theta F(y)\ ,\\ \Phi^* =&\phi^*(y^*) + \sqrt{2}\theta^\dagger\psi^\dagger(y) + \theta^\dagger\theta^\dagger F^*(y^*)\ ,\end{aligned} \tag{2.26}$$

where ϕ is the scalar and ψ the fermionic component of the chiral superfield. F is an auxiliary function. A product or linear combination of chiral fields gives a chiral field. Hence, holomorphic functions $W(\Phi_i)$ or $W(\Phi_i^*)$ will themselves be left-chiral or right-chiral, respectively.

A vector superfield V is defined by imposing

$$V = V^*\ . \tag{2.27}$$

It can be constructed out of chiral and anti-chiral superfields by combinations like

$$\Phi + \Phi^*\ , \quad \mathrm{i}(\Phi - \Phi^*)\ , \quad \Phi\Phi^*\ . \tag{2.28}$$

After gauging away some auxiliary components by a supergauge transformation

$$V \to V + \mathrm{i}(\Omega^* - \Omega)\ , \tag{2.29}$$

with Ω being a chiral superfield, the vector superfield is given in the Wess-Zumino gauge by

$$V_{\mathrm{WZ}} = \theta^\dagger\bar\sigma^\mu\theta A_\mu(x) + \theta^\dagger\theta^\dagger\theta\lambda(x) + \theta\theta\theta^\dagger\lambda^\dagger(x) + \theta\theta\theta^\dagger\theta^\dagger D(x)\ . \tag{2.30}$$

Here, A_μ is the vector field component and λ the corresponding Weyl fermion, while D is an auxiliary field. The field strength is given by

$$\mathcal{W}_\alpha = -\frac{1}{4}\bar{D}_{\dot{\alpha}}\bar{D}^{\dot{\alpha}}\left(\mathrm{e}^{-V}D_\alpha \mathrm{e}^{V}\right) \ . \tag{2.31}$$

It is a chiral superfield and transforms under the supergauge transformation shown in Eq. (2.28) as

$$\mathcal{W}_\alpha \to \mathrm{e}^{\mathrm{i}\Omega}\mathcal{W}_\alpha \mathrm{e}^{-\mathrm{i}\Omega} \ . \tag{2.32}$$

We now have defined all the ingredients to write down an action which is invariant under global Susy and supergauge transformations.

2.3 Supersymmetric Lagrangians

In usual quantum field theories the action is defined as the spacetime integral over the Lagrangian density. If the integration is extended to superspace, an action A invariant under global Susy transformation can be constructed by integrating over a general superfield S, such that

$$A = \int d^4x \int d^2\theta d^2\theta^\dagger \ S(x,\theta,\theta^\dagger) \ . \tag{2.33}$$

The transformations defined in Eqs. (2.18) and (2.19) acting on a superfield S generate a translation in superspace. Therefore, the spacetime integral A is invariant under such transformations. The superfield Lagrangian S must be a real superfield to ensure that the action A is real. S is constructed out of chiral and vector superfields Φ and V, respectively. The change of the F-term component of a chiral superfield and the D-term component of a vector superfield under Susy transformation is a total derivative. These components can be projected out via an integration over the fermionic coordinates,

$$[\Phi]_F = \int d^2\theta d^2\theta^\dagger \ \delta^{(2)}(\theta^\dagger)\Phi \ , \tag{2.34}$$

$$[V]_D = \int d^2\theta d^2\theta^\dagger \ V \ , \tag{2.35}$$

where $\delta^{(2)}$ is the anti-commuting Dirac delta function

$$\delta^{(2)}(\theta-\theta') = \left(\theta-\theta'\right)\left(\theta-\theta'\right) \ . \tag{2.36}$$

Hence, a Lagrangian $\mathcal{L}$ invariant under Susy transformations should have the form

$$\mathcal{L}(x) = \int d^2\theta d^2\theta^\dagger \left\{ \ [\text{vector superfield}]_D + \left(\delta^{(2)}(\theta^\dagger)[\text{chiral superfield}]_F + \text{c.c.}\right)\right\} \ , \tag{2.37}$$

where the complex conjugate term of the chiral component ensures that the action is real. For general gauge theories the action is demanded to be invariant under supergauge transformations under which chiral and vector superfields transform as

$$\Phi_i \to \left(\mathrm{e}^{2\mathrm{i}g_a\Omega^a T^a}\right)_i^{\ j}\Phi_j \ , \quad \Phi^{*i} \to \Phi^{*j}\left(\mathrm{e}^{-2\mathrm{i}g_a\Omega^a T^a}\right)_j^{\ i} \ , \tag{2.38}$$

$$\mathrm{e}^{2g_a(T^a)_i^{\ j}V^a} \to \mathrm{e}^{\mathrm{i}(2g_a(T^a)_i^{\ j}\Omega^a)^\dagger}\mathrm{e}^{2g_a(T^a)_i^{\ j}V^a}\mathrm{e}^{-\mathrm{i}(2g_a(T^a)_i^{\ j}\Omega^a)} \ . \tag{2.39}$$

Here, g_a are the gauge couplings, T^a are the generators of the Lie algebra, and Ω^a are the gauge parameter superfields. The renormalizable Lagrangian invariant under these transformations can be written as

$$\mathcal{L}(x) = \frac{1}{4}\left(\left[\mathcal{W}^{a\alpha}\mathcal{W}^a_\alpha\right]_F + \text{c.c}\right) + \left[\Phi^{*i}\left(\mathrm{e}^{2g_a T^a V^a}\right)_i^{\ j}\Phi_j\right]_D + \left(\left[W(\Phi_i)\right]_F + \text{c.c.}\right) \ , \quad (2.40)$$

where we neglected possible $\mathcal{CP}$-violating Θ_a-parameters, because they are not relevant in the scope of this thesis. W is a holomorphic function of chiral superfields called superpotential. It contains possible interactions of the chiral superfields allowed by the gauge symmetries. The most general form of W in renormalizable theories is

$$W = L^i\Phi_i + \frac{1}{2}M^{ij}\Phi_i\Phi_j + \frac{1}{6}y^{ijk}\Phi_i\Phi_j\Phi_k \ . \quad (2.41)$$

The terms stemming from the superpotential are given in scalar and fermionic components of the chiral superfields by

$$\left[W(\Phi_i) + \text{c.c}\right]_F = W^i F_i + W^*_i F^{*i} - \frac{1}{2}\left(W^{ij}\psi_i\psi_j + W^*_{ij}\psi^{\dagger i}\psi^{\dagger j}\right) \ , \quad (2.42)$$

where

$$W^i = \left.\frac{\delta W}{\delta\Phi_i}\right|_{\Phi_i\to\phi_i} \ , \quad \text{and} \quad W^{ij} = \left.\frac{\delta^2 W}{\delta\Phi_i\Phi_j}\right|_{\Phi_i\to\phi_i} \ , \quad (2.43)$$

with ϕ_i and ψ_i being the scalar and fermionic component of the chiral superfields, respectively (see Eq. (2.26)). The second term on the right-hand side of Eq. (2.40) provides the terms

$$\begin{aligned}\left[\Phi^{*i}\left(\mathrm{e}^{2g_a T^a V^a}\right)_i^{\ j}\Phi_j\right]_D = {} & F^{*i}F_i - \Delta_\mu\phi^{*i}\Delta^\mu\phi_i + \mathrm{i}\psi^{\dagger i}\bar\sigma^\mu\Delta_\mu\psi_i - \sqrt{2}g_a\left(\phi^* T^a\psi\right)\lambda^a \\ & - \sqrt{2}g_a\lambda^\dagger\left(\psi^\dagger T^a\phi\right) + g_a\left(\phi^* T^a\phi\right)D^a \ . \end{aligned} \quad (2.44)$$

with the gauge-covariant derivatives

$$\Delta_\mu\phi_i = \partial\phi_i - \mathrm{i}gA^a_\mu\left(T^a\phi\right)_i \ , \quad (2.45)$$

$$\Delta_\mu\phi^{*i} = \partial\phi^{*i} + \mathrm{i}gA^a_\mu\left(\phi^* T^a\right)^i \ , \quad (2.46)$$

$$\Delta_\mu\psi_i = \partial_\mu\psi_i - \mathrm{i}gA^a_\mu\left(T^a\psi\right)_i \ . \quad (2.47)$$

The first term on the right-hand side of Eq. (2.40) reads in component form

$$\left[\mathcal{W}^{a\alpha}\mathcal{W}^a_\alpha\right]_F = D^a D^a + 2\mathrm{i}\lambda^a\sigma^\mu\Delta_m u\lambda^{\dagger a} - \frac{1}{2}F^{a\,\mu\nu}F^a_{\mu\nu} + \frac{\mathrm{i}}{4}\epsilon^{\mu\nu\rho\sigma}F^a_{\mu\nu}F^a_{\rho\sigma} \ . \quad (2.48)$$

The terms containing the auxiliary fields F_i and D_a in Eqs. (2.43), (2.44) and (2.48) contribute to the scalar potential. By making use of the equations of motions

$$F_i = -W^*_i \quad \text{and} \quad D_a = g_a\left(\phi^* T^a\phi\right) \ , \quad (2.49)$$

they form the F-terms and D-terms of the scalar potential

$$V(\phi_i,\phi^*_i) = F^{*i}F_i + \frac{1}{2}\sum_a D^a D^a = W^*_i W^i + \frac{1}{2}\sum_a g_a^2\left(\phi^* T^a\phi\right)^2 \ . \quad (2.50)$$

This relation illustrates two important features of scalar potentials in SUSY models. Firstly, the scalar potential is a sum of squares, so it is non-negative. Secondly, the quartic couplings are determined by the gauge couplings and the superpotential couplings. This is the reason why it is possible to predict the SM-like Higgs-boson mass in SUSY models, while in the SM the quartic coupling of the Higgs boson, and consequently its mass, are free parameters.

2.4 Supersymmetry breaking

The Lagrangian derived in the previous section (see Eq. (2.40)) is invariant under global supergauge transformation. We argued that particles within the same supermultiplet have the same mass and the same quantum numbers. Since this is not observed in nature, the global SUSY has to be broken to obtain a phenomenologically viable theory. The precise mechanism for this breaking is unknown. Nevertheless, the low-energy operators, effectively generated through the SUSY breaking, can be parametrized and added to the Susy-conserving Lagrangian. An important constraint for these additional operators is that they do not reintroduce quadratic divergences, thus spoiling the solution of the hierarchy problem. This implies that their coefficients have positive mass dimension. Such operators are called soft. The most general form of a soft Lagrangian that can arise from spontaneous SUSY breaking is given by [7, 22]

$$\begin{aligned}\mathcal{L}_{\text{soft}} = &-\left(\frac{1}{2}M_a\lambda^a\lambda^a + \frac{1}{6}T^{ijk}\phi_i\phi_j\phi_k + \frac{1}{2}b^{ij}\phi_i\phi_j + t^i\phi_i - M^a_{\text{Dirac}}\lambda^a\psi_a + \text{c.c.}\right)\\ &- \left(m^2\right)^i_j\,\phi^{*j}\phi_i\ .\end{aligned} \tag{2.51}$$

Each term explicitly breaks SUSY. The first term provides Majorana masses M_a for the gauginos λ^a, the superpartners of the gauge bosons. The third and the last term provide additional mass parameters b^{ij} and $(m^2)^i_j$ for the scalar components ϕ_i of the chiral superfields. The Dirac mass terms proportional to M^a_{Dirac} can only be present when there is a chiral supermultiplet transforming in the adjoint representation of the corresponding gauge group. In SUSY-extensions of the SM that is usually (and in particular in the models treated here) not the case. The soft tadpole terms proportional to t^i can only be present if there is chiral superfield not charged under the gauge groups. Mass terms for the fermionic components of chiral fields ψ_i are redundant, because they can be eliminated by a redefinition of superpotential terms.

As already mentioned, the parameters within $\mathcal{L}_{\text{soft}}$ parametrize our ignorance about the precise mechanism behind SUSY breaking. However, some general aspects can be derived from the form of the potential in SUSY theories [9]. From the anti-commutation relation of the generators of Q and $Q^\dagger$ (see Eq. (2.13)) one can show that a SUSY-conserving vacuum has zero energy. As was explained in the previous discussion, the SUSY potential cannot be negative. Thus, for SUSY to be spontaneously broken, the SUSY-conserving states must have positive non-zero energies, so that a deeper SUSY-breaking vacuum can exist. Apart from that, SUSY-breaking vacua have non-zero positive energy, since the generators do not annihilate such vacuum states. From Eq. (2.50) we see that there are only two possibilities for this to happen. Either terms terms in a chiral supermultiplet break SUSY, leading to so-called F-type SUSY breaking, so that

$$\langle 0|\, F_i\, |0\rangle > 0\ , \tag{2.52}$$

where $|0\rangle$ is the vacuum state, or terms in a vector multiplet break SUSY, yielding D-type SUSY breaking, so that

$$\langle 0|\, D^a\, |0\rangle > 0\ . \tag{2.53}$$

The latter type of SUSY breaking usually implies unacceptable breaking of the gauge symmetries in SUSY extensions of the SM. Consequently, F-type SUSY breaking is favored [8].

In any case, purely spontaneous SUSY breaking evokes certain sum rules for the component fields of chiral supermultiplets [23] which are incompatible with observations,

Superfield	scalar comp.	fermionic comp.	$SU(3)_c$	$SU(2)_L$	$U(1)_y$
$\hat{Q}_i = (\hat{Q}_{iu}, \hat{Q}_{id})$	$(\widetilde{u}_{iL}, \widetilde{d}_{iL})$	(u_{iL}, d_{iL})	3	2	1/3
$\hat{u}_i^c$	$\widetilde{u}_{iR}^c$	u_{iR}^c	$\bar{3}$	1	-4/3
$\hat{d}_i^c$	$\widetilde{d}_{iR}^c$	d_{iR}^c	$\bar{3}$	1	2/3
$\hat{L}_i = (\hat{L}_{i\nu}, \hat{L}_{ie})$	$(\widetilde{\nu}_{iL}, \widetilde{e}_{iL})$	(ν_{iL}, e_{iL})	1	2	-1
$\hat{e}_i^c$	$\widetilde{e}_{iR}^c$	e_{iR}^c	1	1	2
$\hat{H}_u = (\hat{H}_u^+, \hat{H}_u^0)$	(H_u^+, H_u^0)	$(\widetilde{H}_u^+, \widetilde{H}_u^0)$	1	2	1
$\hat{H}_d = (\hat{H}_d^0, \hat{H}_d^-)$	(H_d^0, H_d^-)	$(\widetilde{H}_d^0, \widetilde{H}_d^-)$	1	2	-1

Table 2.1: Chiral superfields of the MSSM and how they transform under the SM gauge groups. $i = 1, 2, 3$ is the family index.

when only SM gauge interactions are considered. To avoid these constraints, one has to assume additional explicit Susy breaking that originates from spontaneous Susy breaking in a so-called hidden sector at much higher energies. The hidden sector must be decoupled from SM interactions. The breaking in the SM sector arises through mediators interacting in the hidden sector and the SM. Several possibilities for this were considered in the the past, such as gravity-mediated or gauge-mediated Susy breaking, which yield different conditions on the parameters in the soft Lagrangian (see Ref. [24] for a review). In the scope of this thesis no particular Susy-breaking mechanism will be assumed, so that we will not go into further details here.

Finally, we remark that the spontaneous breaking of Susy in the context of Sugra is related to the appearance of a massless field. The Susy generators are fermionic. Consequently, in contrast to Goldstone bosons present in broken gauge theories, the massless field will be a fermion called goldstino [25]. In the SM, the goldstone bosons are gauged away into the vector bosons of the broken SU(2), which then acquire masses. The goldstino can be gauged away into the longitudinal degrees of freedom of the gravitino which then becomes massive. This is called the Super-Higgs mechanism [26–29].

2.5 The MSSM and simple extenstions

In this section we will introduce the Minimal Supersymmetric Standard Model (MSSM) [30, 31]. It is minimal in the sense that it incorporates the most minimal particle content necessary to obtain a Susy version of the SM. The MSSM has several shortcomings so that popular extensions of the MSSM exist. One of these non-minimal models is the $\mu\nu$SSM which is the one studied in this thesis (see Ch. 3). Nevertheless, since various different comparisons between the MSSM and the $\mu\nu$SSM will be drawn, it is worthwhile to introduce the MSSM. Afterwards, we use it as a starting point for more realistic models.

In analogy to the SM, the MSSM is constructed demanding invariance under the gauge groups $SU(3)_c \times SU(2)_L \times U(1)_y$. The MSSM matter fields are the chiral superfields summarized in Tab. 2.1. The chiral superfields are denoted with a hat. The superfields in the first five rows represent the left- and right-handed SM quarks and leptons. The scalar components of these superfields are denoted with a tilde. The charges of the

Superfield	vector comp.	fermionic comp.	$\mathrm{SU}(3)_c$	$\mathrm{SU}(2)_L$	$\mathrm{U}(1)_y$
$\hat{g}$	g	$\widetilde{g}$	8	1	0
$\hat{W}$	$W^\pm, W^0$	$\widetilde{W}^\pm, \widetilde{W}^0$	1	3	0
$\hat{B}$	B	$\widetilde{B}$	1	1	0

Table 2.2: Vector superfields of the MSSM and how they transform under the SM gauge groups.

chiral fields are chosen to coincide with the charges of the SM fermions. The right-handed fermions have to be put into left-chiral superfields to be able to construct a holomorphic superpotential (see Sect. 2.2). Thus, they are given as charge-conjugate left-chiral antiparticle superfields. For the same reason, there have to be two Higgs-doublet superfields present. During EWSB up-type fermions will acquire masses via couplins to $\hat{H}_u$ and down-type fermions via the coupling to $\hat{H}_d$, shown in the last two rows of Tab. 2.1. One Higgs-doublet field, as in the SM, is not sufficient. A field and its charge conjugate cannot be used simultaneously in the superpotential.[3] Consequently, in the $\mathcal{CP}$-conserving case the Higgs sector of the MSSM consists of two $\mathcal{CP}$-even Higgs bosons h and H, one $\mathcal{CP}$-odd Higgs boson A, and two charged Higgs bosons $H^\pm$. The SM gauge bosons are included as the bosonic part of vector superfields, which are depicted in Tab. 2.2. After EWSB the vector components B and W^0 will mix into the Z boson and the photon, in total analogy to the SM. However, in the MSSM also the fermionic components of the vector superfields will mix to give rise to the so-called zino and photino.

The superpotenital of the MSSM is chosen to be renormalizable, invariant under the SM gauge groups, and conserving a discrete symmetry called R-parity, yielding

$$W^{\mathrm{MSSM}} = \epsilon_{ab} \left(Y^e_{ij}\, \hat{H}^a_d\, \hat{L}^b_i\, \hat{e}^c_j + Y^d_{ij}\, \hat{H}^a_d\, \hat{Q}^b_i\, \hat{d}^c_j + Y^u_{ij}\, \hat{H}^b_u\, \hat{Q}^a_i\, \hat{u}^c_j + \mu\, \hat{H}^a_d\, \hat{H}^b_u \right) , \tag{2.54}$$

where ϵ_{ab} is the fully antisymmetric tensor with $\epsilon_{12} = 1$. Color indices are undisplayed. Under R-parity the components of the supermultiplets transform as

$$R = (-1)^{3B+L+2s} , \tag{2.55}$$

where B is the baryon number, L the lepton number, and s the spin. For SM fields one finds $R = 1$ and for their Susy partners $R = -1$. Enforcing this symmetry has the purpose of forbidding dangerous tree-level operators enabling fast proton decay. Additionally, the lightest supersymmetric particle (LSP) will be stable, such that it can be a dark matter candidate. According to Eq. (2.51), the general form of the Susy-breaking Lagrangian is given by

$$\begin{aligned} -\mathcal{L}^{\mathrm{MSSM}}_{\mathrm{soft}} = {} & \epsilon_{ab} \left(T^e_{ij}\, H^a_d\, \widetilde{L}^b_{iL}\, \widetilde{e}^*_{jR} + T^d_{ij}\, H^a_d\, \widetilde{Q}^b_{iL}\, \widetilde{d}^*_{jR} + T^u_{ij}\, H^b_u \widetilde{Q}^a_{iL} \widetilde{u}^*_{jR} + b_\mu H^a_d H^b_u + \mathrm{h.c.} \right) \\ & + \left(m^2_{\widetilde{Q}} \right)_{ij} \widetilde{Q}^{a*}_{iL} \widetilde{Q}^a_{jL} + \left(m^2_{\widetilde{u}} \right)_{ij} \widetilde{u}^*_{iR} \widetilde{u}_{jR} + \left(m^2_{\widetilde{d}} \right)_{ij} \widetilde{d}^*_{iR} \widetilde{d}_{jR} + \left(m^2_{\widetilde{L}} \right)_{ij} \widetilde{L}^{a*}_{iL} \widetilde{L}^a_{jL} \\ & + \left(m^2_{\widetilde{e}} \right)_{ij} \widetilde{e}^*_{iR} \widetilde{e}_{jR} + m^2_{H_d} H^{a*}_d H^a_d + m^2_{H_u} H^{a*}_u H^a_u \\ & + \frac{1}{2} \left(M_3\, \widetilde{g}\, \widetilde{g} + M_2\, \widetilde{W}\, \widetilde{W} + M_1\, \widetilde{B}^0\, \widetilde{B}^0 + \mathrm{h.c.} \right) . \end{aligned} \tag{2.56}$$

[3] Another reason is that two Higgs doublet fields ensure anomaly cancellation regarding the gauge groups.

In the first row we find the scalar operator corresponding to the superpotential couplings. In the second and the third row we find soft scalar masses for the scalar components of the chiral superfields. In the last row the fermionic parts of the vector fields, transforming in the adjoint representation of the gauge groups, receive soft masses. The scale of the SUSY breaking defines the mass scale of the SUSY partners of the SM particles.

The MSSM has been the most popular SUSY extension of the SM in the past. If the SUSY-breaking scale is not far above the TeV scale, the hierarchy problem is solved and the SM gauge couplings unification can be achieved. The neutralino LSP, a stable weakly interacting massive particle (WIMP), can naturally serve as a dark matter candidate [32, 33]. Because of the conservation of R-parity, any SUSY particle possibly produced at colliders would decay into final states containing the stable LSP escaping the detector. Thus, the particle spectrum of the MSSM was expected to be measurable at the LHC making use of signals with missing energy or monojets. The predictions for the top quark mass assuming unification of the SM forces into SU(5) or SO(10) were in remarkable agreement with the measured value soon after [34, 35]. The measured SM-like Higgs-boson mass is not above the mass range that can be accommodated [36, 37]. Furthermore, the EWSB arises naturally, because the relevant scalar soft mass parameter becomes negative while running from the GUT scale to the electroweak scale [38, 39].

However, recent observation (or the lack of them) tightly constrain the parameter space of the MSSM for SUSY scales providing a solution to the hierarchy problem, or are in complete disagreement with the MSSM prediction. Firstly, direct searches for SUSY particles at the LHC found no evidence whatsoever of the presence of a particle spectrum predicted by the MSSM. In particular the scalar SUSY partner of the quarks were expected to be produced at the LHC, since they are charged under the $\mathrm{SU}(3)_c$. The WIMP dark matter explanation via a neutralino LSP is challenged by the absence of signals in direct detection experiments and LHC searches [40, 41]. Most importantly, neutrino-oscillation data demand the presence of (at least two) finite neutrino masses [42, 43]. The MSSM does not address the origin of neutrino masses and mixings at all.

There are also theoretical problems related to the form of the MSSM superpotential shown in Eq. (2.54). It contains a parameter μ with mass dimension two. The term is part of the SUSY-preserving sector, such that it should be of the order of the UV scale (for instance the Planck mass) where the operator is generated. For phenomenological reasons, however, it must be of the order of the electroweak scale. This is called the μ-problem [44] (see Ref. [45] for a recent review). Another theoretical problem in the MSSM is that the tree-level mass of the lightest Higgs boson is bounded from above by the Z-boson mass [36, 46, 47]. Even though a particle taking the role of the SM-like Higgs boson can be accommodated, large quantum corrections to its mass are required to obtain a value of ~ 125 GeV (see Ref. [48] for a recent review). The largest radiative corrections arise from the interaction with the scalar top quark partners (stops). Hence, the Higgs sector and the stop sector of the MSSM are tightly linked. The non-observation of stops at the LHC leads to constraints in both sectors.

Both the experimental and theoretical problems motivate SUSY extensions of the SM beyond the MSSM. We mention extensions addressing either the μ-problem or the origin of neutrino masses here, because they are the ones relevant in the scope of this thesis. Solutions to the μ-problem usually consist of forbidding the term in the superpotential, for instance by a symmetry, and then generating it effectively at the electroweak scale. In the Next-to MSSM (NMSSM) a gauge-singlet chiral superfield $\hat{s}$ is added to the particle content [49–51] (see Refs. [52, 53] for reviews). Forbidding the explicit μ-term by a Z_3

symmetry under which the Higgs doublet fields are charged, and introducing the term

$$W^{\mathrm{NMSSM}} \sim -\epsilon_{ab}\,\lambda\,\hat{s}\,\hat{H}_u^b\hat{H}_d^a\ , \tag{2.57}$$

an effective μ-term is generated when the scalar component $\widetilde{s}$ acquires a vev. A simliar solution is found in the nearly-MSSM in which also a gauge-singlet chiral superfield is added. There, the explicit μ-term is forbidden by demanding a discrete R-symmetry [54, 55]. R-symmetries do not commute with the SUSY generators, so that they act non-trivially on the bosonic and fermionic components of superfields. Several other models consider an additional chiral superfield exclusively charged under an extra $\mathrm{U}(1)'$ gauge group that forbids certain terms with mass dimensions in the superpotential (see Ref. [44] for an overview).

To explain the origin of neutrino masses there are two generic possibilities. Several SUSY models feature at least one of them [56]. First of all, right-handed chiral superfields can be added to the particle spectrum of the MSSM. These are gauge singlets. Thus, anomaly cancellation stays intact. Then, a seesaw mechanism with large Majorana masses for the right-handed neutrinos can be implemented. Such a solution works just as well in the SM [57] so that this mechanism is not necessarily related to SUSY. Other solution to generate neutrino masses more related to SUSY depend on the introduction of lepton-number violating operators. In the MSSM these are forbidden due to the conservation of R-parity. This condition can be relaxed to only assume conservation of baryon number, since it is enough to prevent fast proton decay. Then the MSSM superpotential can be expanded to contain lepton-number violating operators. Neutrino masses are produced radiatively without the need to extend the particle content of the MSSM.

This thesis deals with a SUSY model capable of solving both the μ-problem and the generation of neutrino masses simultaneously by relating both issues to the EWSB scale. This is done by interpreting the gauge-singlet chiral superfield $\hat{s}$ used to solve the μ-problem in models like the NMSSM as right-handed neutrino superfields;

$$\hat{s} \leftrightarrow \hat{\nu}_R\ . \tag{2.58}$$

The precise mechanism behind this will be explained in the following chapter in which we give a brief summary of this model.

Bibliography

[1] V. I. Ogievetsky and L. Mezincescu, "Symmetries Between Bosons and Fermions and Superfields", *Sov. Phys. Usp.* **18** (1975) 960–982, [Usp. Fiz. Nauk117,637(1975)].

[2] A. Salam and J. A. Strathdee, "Supersymmetry and Nonabelian Gauges", *Phys. Lett.* **51B** (1974) 353–355.

[3] S. Ferrara and B. Zumino, "Supergauge Invariant Yang-Mills Theories", *Nucl. Phys.* **B79** (1974) 413.

[4] S. Dimopoulos and H. Georgi, "Softly Broken Supersymmetry and SU(5)", *Nucl. Phys.* **B193** (1981) 150–162.

[5] N. Sakai, "Naturalness in Supersymmetric Guts", *Z. Phys.* **C11** (1981) 153.

[6] H. Kalka and G. Soff, "Supersymmetry. (In German)", *Teubner*, 1997.

[7] S. P. Martin, "A Supersymmetry primer", arXiv:hep-ph/9709356, [Adv. Ser. Direct. High Energy Phys.18,1(1998)].

[8] I. J. R. Aitchison, "Supersymmetry and the MSSM: An Elementary introduction", arXiv:hep-ph/0505105.

[9] M. Drees, R. Godbole, and P. Roy, "Theory and phenomenology of sparticles: An account of four-dimensional N=1 supersymmetry in high energy physics", 2004.

[10] S. R. Coleman and J. Mandula, "All Possible Symmetries of the S Matrix", *Phys. Rev.* **159** (1967) 1251–1256.

[11] M. H. Poincaré, "Sur la dynamique de l'électron", *Rendiconti del Circolo Matematico di Palermo (1884-1940)* **21** Dec (1906) 129–175.

[12] N. Ellis and J. March-Russell, "2001 European school of high-energy physics, Beatenberg, Switzerland, 26 Aug-8 Sep 2001: Proceedings", CERN-2002-002, Geneva, Switzerland: CERN (2002) 401 p, 2002

[13] R. Haag, J. T. Lopuszanski, and M. Sohnius, "All Possible Generators of Supersymmetries of the s Matrix", *Nucl. Phys.* **B88** (1975) 257, [,257(1974)].

[14] D. Binosi, J. Collins, C. Kaufhold, and L. Theussl, "JaxoDraw: A Graphical user interface for drawing Feynman diagrams. Version 2.0 release notes", *Comput. Phys. Commun.* **180** (2009) 1709–1715, arXiv:0811.4113.

[15] U. Amaldi, W. de Boer, and H. Furstenau, "Comparison of grand unified theories with electroweak and strong coupling constants measured at LEP", *Phys. Lett.* **B260** (1991) 447–455.

[16] J. R. Ellis, S. Kelley, and D. V. Nanopoulos, "Probing the desert using gauge coupling unification", *Phys. Lett.* **B260** (1991) 131–137.

[17] P. Langacker and M.-x. Luo, "Implications of precision electroweak experiments for M_t, ρ_0, $\sin^2\theta_W$ and grand unification", *Phys. Rev.* **D44** (1991) 817–822.

[18] C. Giunti, C. W. Kim, and U. W. Lee, "Running coupling constants and grand unification models", *Mod. Phys. Lett.* **A6** (1991) 1745–1755.

[19] D. G. Cerdeno and C. Munoz, "An introduction to supergravity", 1998, [PoScorfu98,011(1998)].

[20] K. Becker, M. Becker, and J. H. Schwarz, "String theory and M-theory: A modern introduction", Cambridge University Press, 2006.

[21] B. L. van der Waerden, "Spinornalyse", *Nachrichten von der Gesellschaft der Wissenschaftern zu Göttingen, Mathematisch-Physikalische Klasse*, (1929) 100–109.

[22] L. Girardello and M. T. Grisaru, "Soft Breaking of Supersymmetry", *Nucl. Phys.* **B194** (1982) 65.

[23] S. Ferrara, L. Girardello, and F. Palumbo, "A General Mass Formula in Broken Supersymmetry", *Phys. Rev.* **D20** (1979) 403.

[24] S. S. AbdusSalam *et al.*, "Benchmark Models, Planes, Lines and Points for Future SUSY Searches at the LHC", *Eur. Phys. J.* **C71** (2011) 1835, arXiv:1109.3859.

[25] P. Fayet and J. Iliopoulos, "Spontaneously Broken Supergauge Symmetries and Goldstone Spinors", *Phys. Lett.* **51B** (1974) 461–464.

[26] D. V. Volkov and V. A. Soroka, "Higgs Effect for Goldstone Particles with Spin 1/2", *JETP Lett.* **18** (1973) 312–314, [Pisma Zh. Eksp. Teor. Fiz.18,529(1973)].

[27] S. Deser and B. Zumino, "Broken Supersymmetry and Supergravity", *Phys. Rev. Lett.* **38** (1977) 1433–1436.

[28] E. Cremmer, B. Julia, J. Scherk, P. van Nieuwenhuizen, S. Ferrara, and L. Girardello, "Super-higgs effect in supergravity with general scalar interactions", *Phys. Lett.* **79B** (1978) 231–234.

[29] P. Fayet, "Mixing Between Gravitational and Weak Interactions Through the Massive Gravitino", *Phys. Lett.* **70B** (1977) 461.

[30] P. Fayet, "Supersymmetry and Weak, Electromagnetic and Strong Interactions", *Phys. Lett.* **64B** (1976) 159.

[31] P. Fayet, "Spontaneously Broken Supersymmetric Theories of Weak, Electromagnetic and Strong Interactions", *Phys. Lett.* **69B** (1977) 489.

[32] H. Goldberg, "Constraint on the Photino Mass from Cosmology", *Phys. Rev. Lett.* **50** (1983) 1419, [,219(1983)].

[33] J. R. Ellis, J. S. Hagelin, D. V. Nanopoulos, K. A. Olive, and M. Srednicki, "Supersymmetric Relics from the Big Bang", *Nucl. Phys.* **B238** (1984) 453–476, [,223(1983)].

[34] L. J. Hall, R. Rattazzi, and U. Sarid, "The Top quark mass in supersymmetric SO(10) unification", *Phys. Rev.* **D50** (1994) 7048–7065, arXiv:hep-ph/9306309.

[35] J. Kubo, M. Mondragon, and G. Zoupanos, "Reduction of couplings and heavy top quark in the minimal SUSY GUT", *Nucl. Phys.* **B424** (1994) 291–307.

[36] Y. Okada, M. Yamaguchi, and T. Yanagida, "Upper bound of the lightest Higgs boson mass in the minimal supersymmetric standard model", *Prog. Theor. Phys.* **85** (1991) 1–6.

[37] G. Degrassi, S. Heinemeyer, W. Hollik, P. Slavich, and G. Weiglein, "Towards high precision predictions for the MSSM Higgs sector", *Eur. Phys. J.* **C28** (2003) 133–143, arXiv:hep-ph/0212020.

[38] J. R. Ellis, D. V. Nanopoulos, and K. Tamvakis, "Grand Unification in Simple Supergravity", *Phys. Lett.* **121B** (1983) 123–129.

[39] L. Alvarez-Gaume, J. Polchinski, and M. B. Wise, "Minimal Low-Energy Supergravity", *Nucl. Phys.* **B221** (1983) 495.

[40] F. Mahmoudi, A. Arbey, and M. Battaglia, "Light neutralino dark matter in MSSM", *PoS* **ICHEP2012** (2013) 447, arXiv:1211.2795.

[41] A. Arbey, M. Boudaud, F. Mahmoudi, and G. Robbins, "Robustness of dark matter constraints and interplay with collider searches for New Physics", *JHEP* **11** (2017) 132, arXiv:1707.00426.

[42] **Super-Kamiokande** Collaboration, Y. Fukuda *et al.*, "Evidence for oscillation of atmospheric neutrinos", *Phys. Rev. Lett.* **81** (1998) 1562–1567, arXiv:hep-ex/9807003.

[43] **KamLAND** Collaboration, S. Abe *et al.*, "Precision Measurement of Neutrino Oscillation Parameters with KamLAND", *Phys. Rev. Lett.* **100** (2008) 221803, arXiv:0801.4589.

[44] J. E. Kim and H. P. Nilles, "The mu Problem and the Strong CP Problem", *Phys. Lett.* **138B** (1984) 150–154.

[45] K. J. Bae, H. Baer, V. Barger, and D. Sengupta, "Revisiting the SUSY mu problem and its solutions in the LHC era", arXiv:1902.10748.

[46] H. E. Haber and R. Hempfling, "Can the mass of the lightest Higgs boson of the minimal supersymmetric model be larger than m(Z)?", *Phys. Rev. Lett.* **66** (1991) 1815–1818.

[47] J. R. Ellis, G. Ridolfi, and F. Zwirner, "Radiative corrections to the masses of supersymmetric Higgs bosons", *Phys. Lett.* **B257** (1991) 83–91.

[48] P. Draper and H. Rzehak, "A Review of Higgs Mass Calculations in Supersymmetric Models", *Phys. Rept.* **619** (2016) 1–24, arXiv:1601.01890.

[49] H. P. Nilles, M. Srednicki, and D. Wyler, "Weak Interaction Breakdown Induced by Supergravity", *Phys. Lett.* **120B** (1983) 346.

[50] J. M. Frere, D. R. T. Jones, and S. Raby, "Fermion Masses and Induction of the Weak Scale by Supergravity", *Nucl. Phys.* **B222** (1983) 11–19.

[51] J. P. Derendinger and C. A. Savoy, "Quantum Effects and SU(2) x U(1) Breaking in Supergravity Gauge Theories", *Nucl. Phys.* **B237** (1984) 307–328.

[52] U. Ellwanger, C. Hugonie, and A. M. Teixeira, "The Next-to-Minimal Supersymmetric Standard Model", *Phys. Rept.* **496** (2010) 1–77, arXiv:0910.1785.

[53] M. Maniatis, "The Next-to-Minimal Supersymmetric extension of the Standard Model reviewed", *Int. J. Mod. Phys.* **A25** (2010) 3505–3602, arXiv:0906.0777.

[54] C. Panagiotakopoulos and K. Tamvakis, "New minimal extension of MSSM", *Phys. Lett.* **B469** (1999) 145–148, arXiv:hep-ph/9908351.

[55] C. Panagiotakopoulos and A. Pilaftsis, "Higgs scalars in the minimal nonminimal supersymmetric standard model", *Phys. Rev.* **D63** (2001) 055003, arXiv:hep-ph/0008268.

[56] E. Ma, "Supersymmetry and neutrino masses", arXiv:hep-ph/9902450, [PoScorfu98,047(1998)].

[57] P. Minkowski, "$\mu \to e\gamma$ at a Rate of One Out of 10^9 Muon Decays?", *Phys. Lett.* **67B** (1977) 421–428.

Chapter 3

The μ-from-ν Supersymmetric Standard Model

The μ-from-ν Supersymmetric Standard Model ($\mu\nu$SSM) [1, 2] is a SUSY extension of the SM that can accommodate neutrino masses and mixings in agreement with experimental data by augmenting the particle content with right-handed neutrino superfields. The astonishing property of the $\mu\nu$SSM is that this is set to happen via a seesaw mechanism at the electroweak scale. Therefore, no new energy scale has to be introduced. In fact, the superpotential of the $\mu\nu$SSM does not contain dimensionful parameters at all. The only BSM energy scale is the SUSY-breaking scale. The importance of this cannot be overestimated, since a priori one might think that, due to the tiny neutrino masses, their origin is related to physics either at very low or very high energy scales, far from the electroweak scale.

Consider the ratio of the electron mass, the lightest massive fermion in the SM spectrum, and the neutrino masses. The precise values of the neutrino masses are unknown, but an upper value to the sum of neutrino masses can be obtained from cosmology [3] or the tail of the electron spectrum in β-decay experiments [4, 5];

$$\frac{m_e}{m_\nu} \lesssim 10^6 \, . \tag{3.1}$$

In the SM, fermion masses are generated via an effective Dirac mass term which is proportional to the Higgs-boson vev. In principle, the same can be applied to neutrinos, when the presence of right-handed neutrinos is assumed. However, the smallness of the neutrino masses would yield a tiny Yukawa coupling of the order of

$$Y^\nu \sim 10^{-13} \, . \tag{3.2}$$

The usual hierarchy in the fermionic mass spectrum of the SM can already be considered unnatural, as one sees a span of six orders of magnitude in the sizes of the different Yukawa couplings. Surely, considering that small neutrino Yukawa couplings is an extremely unsatisfactory proposal at least. Apart from that, it is not even possible to realize that small Yukawa couplings in certain string constructions in which the Yukawa couplings arise geometrically and can be calculated [6]. Thus, it is tempting to consider a BSM mechanism that can explain the origin of the tiny neutrino masses. If new physics coupled to neutrinos is assumed to be present in a UV completion of the SM, it could manifest itself at lower energies in the form of effective operators. Considering the SM particle content and gauge symmetries, the only allowed five-dimensional operator (not counting

flavor indices) is the Weinberg operator [7]

$$\frac{(Y^\nu_{ij})^2}{\Lambda_\nu}\left(\bar{L}_i\widetilde{\phi}^*\right)\left(\widetilde{\phi}^\dagger L_j\right) + \text{h.c.}\,. \tag{3.3}$$

Here, $L_i = (\nu_i, l_i)$ are the left-handed lepton doublets, $\phi = (\phi^+, \phi^0)$ is the SM Higgs doublet, and $\widetilde{\phi} = \mathrm{i}\sigma H^*$. Λ_ν is the energy scale of new physics at which this operator is generated. It can arise when an SU(2)-singlet or -triplet fermion or an SU(2)-singlet fermion mediator is heavy and can be integrated out. In the $\mu\nu$SSM the mediator particles are, for instance, the right-handed neutrinos. After EWSB this term would lead to Majorana masses for the neutrinos of the form

$$\sim \frac{(Y^\nu_{ij})^2 v^2}{\Lambda_\nu}\,, \tag{3.4}$$

where $v \sim 246$ GeV is the SM vev. In these kind of scenario, the smallness of the neutrino masses is induced by the size of the energy scale Λ_ν. It is inversely proportional to the effectively generated neutrino masses. If we assume Yukawa couplings of order one, the new energy scale will be

$$\Lambda_\nu \gtrsim 10^{13}\ \text{GeV}\,. \tag{3.5}$$

Nothing really can be said against this option theoretically, and nature might very well have chosen this possibility. Considering the current and future reach of particle colliders, this is however the most unfortunate one. Also, since the hierarchy problem demands new physics at much lower scales, it is certainly more exciting to explore ways to obtain massive neutrinos at the electroweak scale.

In the $\mu\nu$SSM this is made possible by compromising. If the new physics responsible for the neutrino masses is related to EWSB and SUSY breaking,

$$\mathcal{O}(\Lambda_\nu) \sim \mathcal{O}(\Lambda_{\text{SUSY}}) \gtrsim \mathcal{O}(\Lambda_{\text{EWSB}}) \sim \mathcal{O}(100\ \text{GeV})\,, \tag{3.6}$$

one can get away with values for the neutrino Yukawa couplings close to the value of the electron Yukawa coupling,

$$Y^\nu \lesssim Y^e \sim 10^{-6}\,. \tag{3.7}$$

Obviously, this is still a small value, but it is not orders of magnitudes smaller than the ones we are familiar with from the SM. Thus, no harm is done in terms of naturalness. In fact, it is rather surprising that, assuming the energy scale Λ_ν to be of the order of the SUSY-breaking scale Λ_{SUSY}, yields the approximate relation in Eq. (3.7).

Besides solving the ν-problem, i.e., the appearance of neutrino masses, there is a second task assigned to the right-handed superfields in the $\mu\nu$SSM. Since they are gauge-singlets, the μ-problem (see Sect. 2.5) can be solved in total analogy to the NMSSM (see Eq. (2.57)). An effective μ-term is automatically present at the correct scale, when the scalar components of the right-handed neutrino superfields obtain a vev. Hence, the μ-problem is solved simultaneously with the ν-problem. This feature also explains the name of the model. The Z_3 symmetry is theoretically justified in the context of string theory, in which in the low energy limit only trilinear terms arise in the superpotential, while parameters with energy dimensions are suppressed [1].

We will describe the details of the $\mu\nu$SSM in the following subsections, including the concrete realization of the electroweak seesaw mechanism. The most important ingredient for the construction of the superpotential, introduced in Sect. 3.1, are the symmetries

applied, to which we dedicate Sect. 3.2. A side effect of associating the scale Λ_ν with the dynamics of SUSY is that the lepton-number violation, naturally present in seesaw scenarios, also induces the breaking of R-parity. We discuss the consequences of R-parity breaking regarding the spectrum of the model, in particular the more complicated particle mixings and other phenomenological issues in Sect. 3.3. Finally, we give a brief overview of the work that has already been done in the context of the $\mu\nu$SSM, and summarize a few further extensions that can be applied to the $\mu\nu$SSM in Sect. 3.4.

3.1 Superpotential and soft terms

Based on the flavor structure of the SM, the most natural assumptions is to add three families of right-handed neutrino superfields to the particle content. The superpotential and the corresponding soft SUSY-breaking Lagrangian of this *full* $\mu\nu$SSM will be introduced in this section. A simpler version of the $\mu\nu$SSM only considers one family of right-handed neutrinos. This is still enough to accommodate neutrino masses, but only one neutrino mass is present at tree-level, while the remaining masses have to arise from radiative corrections. Both versions of the $\mu\nu$SSM were studied in the literature (see Sect. 3.4). Accordingly, during the work of this thesis, both the one-generation [8] and the three-generation case [9] were considered. We present here the full model from which the one-generation case is simply obtained by removing the generation index of the right-handed neutrino superfields.

The superpotential of the $\mu\nu$SSM with three generations of right-handed neutrinos is written as [1, 9]

$$\begin{aligned} W = {} & \epsilon_{ab}\left(Y^e_{ij}\,\hat{H}^a_d\,\hat{L}^b_i\,\hat{e}^c_j + Y^d_{ij}\,\hat{H}^a_d\,\hat{Q}^b_i\,\hat{d}^c_j + Y^u_{ij}\,\hat{H}^b_u\,\hat{Q}^a_i\,\hat{u}^c_j\right) \\ & + \epsilon_{ab}\left(Y^\nu_{ij}\,\hat{H}^b_u\,\hat{L}^a_i\,\hat{\nu}^c_j - \lambda_i\,\hat{\nu}^c_i\,\hat{H}^b_u\hat{H}^a_d\right) + \frac{1}{3}\kappa_{ijk}\hat{\nu}^c_i\hat{\nu}^c_j\hat{\nu}^c_k\ , \end{aligned} \tag{3.8}$$

where $\hat{H}^T_d = (\hat{H}^0_d, \hat{H}^-_d)$ and $\hat{H}^T_u = (\hat{H}^+_u, \hat{H}^0_u)$ are the MSSM-like doublet Higgs superfields, $\hat{Q}^T_i = (\hat{u}_i, \hat{d}_i)$ and $\hat{L}^T_i = (\hat{\nu}_i, \hat{e}_i)$ are the left-chiral quark and lepton superfield doublets, and $\hat{u}^c_j$, $\hat{d}^c_j$, $\hat{e}^c_j$ and $\hat{\nu}^c$ are the right-chiral quark and lepton superfields. i and j are family indices running from one to three, and $a, b = 1, 2$ are indices of the fundamental representation of SU(2) with ϵ_{ab} the totally antisymmetric tensor and $\varepsilon_{12} = 1$. The color indices are not written out. The first row in Eq. (3.8) is nothing else than the familiar superpotential of the MSSM, except that the bilinear μ-term is dropped. In the second row one sees the additional terms genuine to the $\mu\nu$SSM that can be constructed in the presence of the fields $\hat{\nu}^c$. Therein, the second and the third term are analogues to the couplings of the singlet of the Z_3-symmetric NMSSM, besides that in the $\mu\nu$SSM several gauge-singlet fields are present. The λ_i parameter carries one and the κ_{ijk} parameter carries three indices, with κ_{ijk} being symmetric under permutation of the indices. The remarkable difference to the NMSSM is the additional Yukawa coupling Y^ν_{ij} which induces explicit breaking of lepton-number conservation and R-parity through the λ_i- and κ_{ijk}-terms. The presence of the Y^ν_{ij}-terms justifies the interpretation of the singlet superfields as right-handed neutrino superfields. We will discuss in detail the preserved and broken symmetries of the superpotential in Sect. 3.2. There, we also give reasons for not considering further terms in the superpotential thar are in principle allowed once R-parity is broken.

For now we will go on with establishing the form of the broken sector. Working in the framework of low-energy SUSY the corresponding soft SUSY-breaking Lagrangian is

given by [10]

$$
\begin{aligned}
-\mathcal{L}_{\text{soft}} = \; & \epsilon_{ab}\left(T^e_{ij}\, H^a_d\, \widetilde{L}^b_{iL}\, \widetilde{e}^*_{jR} + T^d_{ij}\, H^a_d\, \widetilde{Q}^b_{iL}\, \widetilde{d}^*_{jR} + T^u_{ij}\, H^b_u \widetilde{Q}^a_{iL} \widetilde{u}^*_{jR} + \text{h.c.}\right) \\
& + \epsilon_{ab}\left(T^\nu_{ij}\, H^b_u\, \widetilde{L}^a_{iL} \widetilde{\nu}^*_{jR} - T^\lambda_i\, \widetilde{\nu}^*_{iR}\, H^a_d H^b_u + \frac{1}{3} T^\kappa_{ijk}\, \widetilde{\nu}^*_{iR} \widetilde{\nu}^*_{jR} \widetilde{\nu}^*_{kR} \; + \text{h.c.}\right) \\
& + \left(m^2_{\widetilde{Q}}\right)_{ij} \widetilde{Q}^{a*}_{iL} \widetilde{Q}^a_{jL} + \left(m^2_{\widetilde{u}}\right)_{ij} \widetilde{u}^*_{iR} \widetilde{u}_{jR} + \left(m^2_{\widetilde{d}}\right)_{ij} \widetilde{d}^*_{iR} \widetilde{d}_{jR} + \left(m^2_{\widetilde{L}}\right)_{ij} \widetilde{L}^{a*}_{iL} \widetilde{L}^a_{jL} \\
& + \left(m^2_{\widetilde{\nu}}\right)_{ij} \widetilde{\nu}^*_{iR} \widetilde{\nu}_{jR} + \left(m^2_{\widetilde{e}}\right)_{ij} \widetilde{e}^*_{iR} \widetilde{e}_{jR} + m^2_{H_d} H^{a*}_d H^a_d + m^2_{H_u} H^{a*}_u H^a_u + \left(m^2_{H_d \widetilde{L}}\right)_i H^{a*}_d \widetilde{L}^a_{iL} \\
& + \frac{1}{2}\left(M_3\, \widetilde{g}\, \widetilde{g} + M_2\, \widetilde{W}\, \widetilde{W} + M_1\, \widetilde{B}^0\, \widetilde{B}^0 + \text{h.c.}\right) . \qquad (3.9)
\end{aligned}
$$

In the first four lines the fields denote the scalar component of the corresponding superfields. In the last line the fields denote the fermionic superpartners of the gauge bosons, with $M_{1,2,3}$ being the gaugino masses for the corresponding gauge group. The scalar trilinear parameters $T^{e,\nu,d,u,\lambda,\kappa}$ correspond to the trilinear couplings in the superpotential. The soft mass parameters $m^2_{\widetilde{Q},\widetilde{u},\widetilde{d},\widetilde{L},\widetilde{\nu},\widetilde{e}}$ are hermitian 3×3 matrices in family space. $m^2_{H_d,H_u}$ are the soft masses of the doublet Higgs fields. $m^2_{H_d\widetilde{L}}$ is a 3-dimensional vector in family space, which is always regarded to be absent in the tree-level Lagrangian of the $\mu\nu$SSM, because it spoils the electroweak seesaw mechanism (see Sect. 3.3.1). We include it here, because the operator is allowed by gauge symmetries since $\hat{H}_d$ and $\hat{L}_i$ share exactly the same quantum numbers. Tiny contributions to $m^2_{H_d\widetilde{L}}$ are generated via quantum corrections. Consequently, the parameters $m^2_{H_d\widetilde{L}}$ are required to renormalize the scalar potential, and we include them here. Theoretically, the absence of soft mass parameters mixing different fields at tree level, $(m^2_{H_d\widetilde{L}})_i$, $(m^2_{\widetilde{L}})_{i\neq j}$, $(m^2_{\widetilde{Q}})_{i\neq j}$, etc., can be justified by the diagonal structure of the Kähler metric in certain supergravity models, or when the dilaton field is the source of SUSY breaking in string constructions [11]. Notice also that when the down-type Higgs doublet superfield is interpreted as a fourth family of leptons, the parameters $m^2_{H_d\widetilde{L}}$ can be seen as non-diagonal elements of $m^2_{\widetilde{L}}$ [12].

Throughout this thesis, we will make use of these assumptions. We will neglect flavor mixing at tree-level in the squark and the quark sector, so that the soft masses are diagonal. We write $m^2_{\widetilde{Q}_i}$, $m^2_{\widetilde{u}_i}$ and $m^2_{\widetilde{d}_i}$, as well as for the soft trilinears $T^u_i = A^u_i Y^u_i$, $T^d_i = A^d_i Y^d_i$, where the summation convention on repeated indices is not implied. The quark Yukawas $Y^u_{ii} = Y^u_i$ and $Y^d_{ii} = Y^d_i$ are assumed to be diagonal as well. For the sleptons we define $T^e_{ij} = A^e_{ij} Y^e_{ij}$ and $T^\nu_{ij} = A^\nu_{ij} Y^\nu_{ij}$, again without summation over repeated indices. The latter condition is vital for the electroweak seesaw mechanism, as will be shown in Sect. 3.3.1. Without the proportionality

$$T^\nu_{ij} \propto Y^\nu_{ij} \qquad (3.10)$$

the correct hierarchy between vevs of the scalar fields is not guaranteed (see Sect. 3.3.1).

3.2 Symmetries

The construction of the Lagrangian of the $\mu\nu$SSM, like in any other SUSY model, is based on symmetries and how they are broken. Firstly, there is SUSY itself, whose breaking is parametrized by the soft terms in Eq. (3.9). Besides assumptions on the flavor structure of the soft terms, we do not make explicit assumptions on the mechanism of SUSY-breaking.

The soft terms rather reflect a parametrization of our inability to capture the underlying mechanism. Therefore, all soft coefficients are free parameters. The important point to note is that no quadratic divergences arise at any order in perturbation theory from the terms in Eq. (3.9), even though the terms break SUSY [13]. Due to the gaugino mass terms no continuous R-symmetry can be present [14].

During EWSB, when the real scalar components will acquire a vev (see below), not only the local gauge group $\mathrm{U}(1)_Y \times \mathrm{SU}(2)_L$ will be broken, but also the global Z_3 symmetry, under which any chiral superfields transform as

$$\Phi \to e^{\frac{2\pi \mathrm{i}}{3}} \Phi \,, \tag{3.11}$$

and vector superfields are invariant. This symmetry makes the superpotential scale invariant. In particular, as explained in the introduction, it enables a solution to the μ-problem. Furthermore, it forbids dangerous bilinear terms

$$W \sim \epsilon_{ab} \left(\mu_{iL} \hat{H}_u^b \hat{L}_i^a \right) \,, \tag{3.12}$$

that would introduce arbitrary large sources of lepton-number violation. Also, since the right-handed neutrinos are gauge-singlets, linear *tadpole* terms and explicit bilinear Majorana mass terms of the form

$$W \sim L_i \hat{\nu}_i^c + M_{ij}^M \hat{\nu}_i^c \hat{\nu}_j^c \,, \tag{3.13}$$

would be allowed without the Z_3 symmetry. The latter Majorana mass terms are unwanted, because they should arise dynamically during EWSB via the κ_{ijk}-terms, such that no additional scale has to be put into the model by hand for the electroweak seesaw mechanism to be successful. The former tadpole term is better avoided, because it can reintroduce quadratic divergences in the framework of supergravity [15].

For cosmological reasons global symmetries are problematic due to the appearance of degenerate vacua. They are associated with the so-called domain wall problem [16]; topological defects during the electroweak phase transition in which the Z_3 symmetry is broken spontaneously. Their energy can grow very large, so that they would contribute unacceptably to the cosmological evolution of the universe. The usual solution to this problem can be applied, as in the trilinear NMSSM, also to the $\mu\nu$SSM [1]. Non-renormalizable operators, small enough to not be important for the low-energy phenomenology, and which do not reintroduce the hierarchy problem, break the global symmetry, such that the degeneracy of the vacuum is broken [17, 18].

By writing down the term proportional to the neutrino Yukawa couplings Y_{ij}^ν, the singlet fields are identified as lepton fields. Lepton-number conservation is then is explicitly broken by the λ_i- and κ_{ijk}-terms. Thus, even though lepton-number violating Majorana mass terms are spontaneously generated during EWSB, no massless Goldstone boson called *Majoron* appears, because lepton-number conservation is not a good symmetry of the superpotential anyway [1]. On top of that, the κ_{ijk}-terms are essential to break a global U(1) symmetry, under which the singlet and doublet fields transform as [19]

$$\hat{\nu}_i \to e^{2\mathrm{i}\Theta} \,, \quad \hat{H}_d \to e^{-\mathrm{i}\Theta} \,, \quad \hat{H}_u \to e^{-\mathrm{i}\Theta} \,, \tag{3.14}$$

leaving the λ_i-terms invariant. This symmetry can trivially be extended to the Yukawa terms of the superpotential by assigning the proper charges to the lepton and quark fields. In the absence of the κ_{ijk}-terms, it would be broken only spontaneously during EWSB, leading to the presence of an unwanted Peccei-Quinn axion [1].

We complete this section by discussing the non-existence of R-parity, in contrast to models like the (N)MSSM. Similar to lepton-number conservation, R-parity cannot be conserved once the neutrino Yukawa terms and either the λ_i-terms or the κ_{ijk}-terms are present. Only in the limit

$$Y^\nu_{ij} \to 0 \quad \text{or} \quad (\lambda_i \to 0\,, \kappa_{ijk} \to 0)\ , \tag{3.15}$$

R-parity is restored. Following the reasoning above, both limits are phenomenologically uninteresting. However, we argued in the introduction that the values of Y^ν_{ij} have to be small (see Eq. (3.7)). Therefore, dangerous R-parity breaking phenomena are always suppressed, i.e., they are relevant when they do not have to compete against R-parity conserving processes. The only exceptions arise from the right-handed (s)neutrinos, whose couplings to the doublet-like Higgs bosons and their Susy partners are not suppressed by Y^ν_{ij}.

Despite the suppression caused by the smallness of Y^ν_{ij}, the phenomenology of the $\mu\nu$SSM is conceptually changed compared to R-parity conserving models. Firstly, there are several additional terms that could in principle be included to the superpotential, as soon as R-parity is broken [11]. Notice that the left-handed lepton superfields $\hat{L}_i$ and the down-type Higgs superfield $\hat{H}_d$ share the same quantum numbers, since also lepton-number is not conserved anymore. Hence, each term in the superpotential containing $\hat{L}_i$ can also be written down with the field $\hat{H}_d$ instead, and vice versa. For instance, from the terms proportional to Y^e_{ij} and Y^d_{ij} one can deduce the terms

$$\epsilon_{ab}\left(\lambda_{ijk}\hat{L}^a_i\hat{L}^b_j\hat{e}^c_k + \lambda'_{ijk}\hat{L}^a_i\hat{Q}^b_j\hat{d}^c_k\right)\ , \tag{3.16}$$

which are lepton-number violating. The second term can lead to fast proton decay, if it appears together with the baryon-number violating term

$$\epsilon^{\alpha\beta\gamma}\left(\lambda''_{ijk}\hat{d}^c_{i\alpha}\hat{d}^c_{j\beta}\hat{u}^c_{k\gamma}\right)\ , \tag{3.17}$$

where $\epsilon^{\alpha\beta\gamma}$ is totally antisymmetric and $\epsilon^{123} = 1$. To save the proton, one forbids the term in Eq. (3.17), for instance, by demanding conservation of baryon triality, such that operators inducing proton decay of dimension five or lower are forbidden. The two terms in Eq. (3.16), however, cannot be forbidden by symmetries. Still, there are two reasons to not consider them. Firstly, while the terms included in the superpotential genuine to the $\mu\nu$SSM (see second row in Eq. (3.8)) solve certain phenomenological or theoretical problems, the terms shown in Eq. (3.16) are not particularly motivated by new physics, nor do they play a role in the origin of EWSB. Secondly, there are very strong constraints on the products $\lambda_{ijk}\lambda_{lmn}$, $\lambda_{ijk}\lambda'_{lmn}$ and $\lambda'_{ijk}\lambda'_{lmn}$ [20, 21], for instance, from μ-e conversion experiments [22, 23], and searches for lepton-flavor violating decays [24, 25]. Consequently, the terms written in Eq. (3.16) are considered to be negligible in what follows.

Since any Susy particle is allowed to decay to SM particles, there is no stable lightest supersymmetric particle (LSP). Nevertheless, the $\mu\nu$SSM can still offer a dark matter candidate. A gravitino LSP, whose decay is suppressed by the inverse of the Planck mass squared and the smallness of Y^ν_{ij} can have a lifetime longer than the age of the universe, thus contributing to the relic abundance of dark matter [26, 27]. Apart from that, the LSP of the $\mu\nu$SSM can carry electric or color charge, because it is not stable.

3.3 The spectrum and phenomenology

The breaking of R-parity also has a profound impact on the spectrum of the $\mu\nu$SSM. All SM particles, except the quarks and squarks which are protected by baryon triality, mix with the SUSY particles with equal quantum numbers. Due to the smallness of the parameters Y^{ν}_{ij}, the mixing of the SM fermions with SUSY particles is always suppressed, so that the SM is recovered as the low-energy effective field theory. In the following sections we will give details about the particle mixings in each sector of the $\mu\nu$SSM separately. Again, we give the relevant expressions for the more general case of the $\mu\nu$SSM with three families of right-handed neutrino superfields here [9]. The corresponding expressions for the one-generation case can be found in Ref. [8].

3.3.1 Neutral scalar potential

The neutral scalar potential of the $\mu\nu$SSM is given at tree-level and assuming $\mathcal{CP}$-conservation, as we will do throughout this thesis, by the soft terms and the F- and D-term contributions of the superpotential. One finds

$$V^{(0)} = V_{\rm soft} + V_F + V_D \ , \tag{3.18}$$

with

$$\begin{aligned} V_{\rm soft} = & \left(T^{\nu}_{ij}\, H^0_u\, \widetilde{\nu}_{iL}\, \widetilde{\nu}^*_{jR} - T^{\lambda}_i\, \widetilde{\nu}^*_{iR}\, H^0_d H^0_u + \frac{1}{3} T^{\kappa}_{ijk}\, \widetilde{\nu}^*_{iR} \widetilde{\nu}^*_{jR} \widetilde{\nu}^*_{kR} \ + \text{h.c.} \right) \\ & + \left(m^2_{\widetilde{L}} \right)_{ij} \widetilde{\nu}^*_{iL} \widetilde{\nu}_{jL} + \left(m^2_{\widetilde{\nu}} \right)_{ij} \widetilde{\nu}^*_{iR} \widetilde{\nu}_{jR} + m^2_{H_d} H^{0*}_d H^0_d + m^2_{H_u} H^{0*}_u H^0_u \ , \end{aligned} \tag{3.19}$$

$$\begin{aligned} V_F = & \lambda_j \lambda_j H^0_d H^{0^*}_d H^0_u H^{0^*}_u + \lambda_i \lambda_j \tilde{\nu}^*_{iR} \tilde{\nu}_{jR} H^0_d H^{0*}_d + \lambda_i \lambda_j \tilde{\nu}^*_{iR} \tilde{\nu}_{jR} H^0_u H^{0*}_u \\ & + \kappa_{ijk} \kappa_{ljm} \tilde{\nu}^*_{iR} \tilde{\nu}_{lR} \tilde{\nu}^*_{kR} \tilde{\nu}_{mR} - \big(\kappa_{ijk} \lambda_j \tilde{\nu}^*_{iR} \tilde{\nu}^*_{kR} H^{0*}_d H^{0*}_u - Y^{\nu}_{ij} \kappa_{ljk} \tilde{\nu}_{iL} \tilde{\nu}_{lR} \tilde{\nu}_{kR} H^0_u \\ & + \ Y^{\nu}_{ij} \lambda_j \tilde{\nu}_{iL} H^{0*}_d H^{0*}_u H^0_u + Y^{\nu}_{ij} \lambda_k \tilde{\nu}^*_{iL} \tilde{\nu}_{jR} \tilde{\nu}^*_{kR} H^0_d + \text{h.c.} \big) \\ & + Y^{\nu}_{ij} Y^{\nu}_{ik} \tilde{\nu}^*_{jR} \tilde{\nu}_{kR} H^0_u H^{0*}_u + Y^{\nu}_{ij} Y^{\nu}_{lk} \tilde{\nu}_{iL} \tilde{\nu}^*_{lL} \tilde{\nu}^*_{jR} \tilde{\nu}_{kR} + Y^{\nu}_{ji} Y^{\nu}_{ki} \tilde{\nu}_{jL} \tilde{\nu}^*_{kL} H^0_u H^{0*}_u \ , \end{aligned} \tag{3.20}$$

$$V_D = \frac{1}{8} \left(g_1^2 + g_2^2 \right) \left(\widetilde{\nu}_{iL} \widetilde{\nu}^*_{iL} + H^0_d H^{0*}_d - H^0_u H^{0*}_u \right)^2 \ . \tag{3.21}$$

After the EWSB the neutral scalar fields will acquire a vev. This includes the left- and right-handed sneutrino fields, because they are not protected by lepton-number conservation, as is the case in the MSSM and the NMSSM. We define the decomposition

$$H^0_d = \frac{1}{\sqrt{2}} \left(H^{\mathcal{R}}_d + v_d + \mathrm{i}\, H^{\mathcal{I}}_d \right) \ , \tag{3.22}$$

$$H^0_u = \frac{1}{\sqrt{2}} \left(H^{\mathcal{R}}_u + v_u + \mathrm{i}\, H^{\mathcal{I}}_u \right) \ , \tag{3.23}$$

$$\widetilde{\nu}_{iR} = \frac{1}{\sqrt{2}} \left(\widetilde{\nu}^{\mathcal{R}}_{iR} + v_{iR} + \mathrm{i}\, \widetilde{\nu}^{\mathcal{I}}_{iR} \right) , \tag{3.24}$$

$$\widetilde{\nu}_{iL} = \frac{1}{\sqrt{2}} \left(\widetilde{\nu}^{\mathcal{R}}_{iL} + v_{iL} + \mathrm{i}\, \widetilde{\nu}^{\mathcal{I}}_{iL} \right) \ , \tag{3.25}$$

in such a way that after the EWSB they develop the real vevs

$$\langle H_d^0 \rangle = \frac{v_d}{\sqrt{2}} \,, \quad \langle H_u^0 \rangle = \frac{v_u}{\sqrt{2}} \,, \quad \langle \widetilde{\nu}_{iR} \rangle = \frac{v_{iR}}{\sqrt{2}} \,, \quad \langle \widetilde{\nu}_{iL} \rangle = \frac{v_{iL}}{\sqrt{2}} \,. \tag{3.26}$$

The subscripts $^{\mathcal{R}}$ and $^{\mathcal{I}}$ denote $\mathcal{CP}$-even and -odd components of each scalar field, respectively.[1]

Using the decomposition from Eqs. (3.23) - (3.25), the linear and bilinear terms in the fields define the tadpoles T_φ and the scalar $\mathcal{CP}$-even and $\mathcal{CP}$-odd neutral mass matrices m_φ^2 and m_σ^2,

$$V_H = \cdots - T_{\varphi_i} \varphi_i + \frac{1}{2} \varphi_i^T \left(m_\varphi^2 \right)_{ij} \varphi_j + \frac{1}{2} \sigma_i^T \left(m_\sigma^2 \right)_{ij} \sigma_j + \cdots \,. \tag{3.27}$$

where we collectively denote with $\varphi^T = (H_d^{\mathcal{R}}, H_u^{\mathcal{R}}, \widetilde{\nu}_{1R}^{\mathcal{R}}, \widetilde{\nu}_{2R}^{\mathcal{R}}, \widetilde{\nu}_{3R}^{\mathcal{R}}, \widetilde{\nu}_{1L}^{\mathcal{R}}, \widetilde{\nu}_{2L}^{\mathcal{R}}, \widetilde{\nu}_{3L}^{\mathcal{R}})$ and $\sigma^T = (H_d^{\mathcal{I}}, H_u^{\mathcal{I}}, \widetilde{\nu}_{1R}^{\mathcal{I}}, \widetilde{\nu}_{2R}^{\mathcal{I}}, \widetilde{\nu}_{3R}^{\mathcal{I}}, \widetilde{\nu}_{1L}^{\mathcal{I}}, \widetilde{\nu}_{2L}^{\mathcal{I}}, \widetilde{\nu}_{3L}^{\mathcal{I}})$ the $\mathcal{CP}$-even and $\mathcal{CP}$-odd scalar fields, respectively. The linear terms are only allowed for $\mathcal{CP}$-even fields and given by

$$\begin{aligned}
T_{H_d^{\mathcal{R}}} =& - m_{H_d}^2 v_d - \left(m_{H_d \widetilde{L}}^2 \right)_i v_{iL} - \frac{1}{8} \left(g_1^2 + g_2^2 \right) v_d \left(v_d^2 + v_{iL} v_{iL} - v_u^2 \right) \\
& - \frac{1}{2} v_d v_u^2 \lambda_i \lambda_i + \frac{1}{\sqrt{2}} v_u v_{iR} T_i^\lambda + \frac{1}{2} v_u^2 Y_{ji}^\nu \lambda_i v_{jL} - \frac{1}{2} v_d v_{iR} \lambda_i v_{jR} \lambda_j \\
& + \frac{1}{2} v_u \kappa_{ikj} \lambda_i v_{jR} v_{kR} + \frac{1}{2} v_{iR} \lambda_i v_{jL} Y_{jk}^\nu v_{kR} \,,
\end{aligned} \tag{3.28}$$

$$\begin{aligned}
T_{H_u^{\mathcal{R}}} =& - m_{H_u}^2 v_u + \frac{1}{8} \left(g_1^2 + g_2^2 \right) v_u \left(v_d^2 + v_{iL} v_{iL} - v_u^2 \right) \\
& - \frac{1}{2} v_d^2 v_u \lambda_i \lambda_i + \frac{1}{\sqrt{2}} v_d v_{iR} T_i^\lambda + v_d v_u Y_{ji}^\nu \lambda_i v_{jL} - \frac{1}{\sqrt{2}} v_{iL} T_{ij}^\nu v_{jR} - \frac{1}{2} v_u v_{iR} \lambda_i v_{jR} \lambda_j \\
& - \frac{1}{2} v_u Y_{ji}^\nu Y_{ki}^\nu v_{jL} v_{kL} - \frac{1}{2} v_u Y_{ij}^\nu Y_{ik}^\nu v_{jR} v_{kR} + \frac{1}{2} v_d \kappa_{ijk} \lambda_i v_{jR} v_{kR} - \frac{1}{2} Y_{li}^\nu \kappa_{ikj} v_{jR} v_{kR} v_{lL} \,,
\end{aligned} \tag{3.29}$$

$$\begin{aligned}
T_{\widetilde{\nu}_{iR}^{\mathcal{R}}} =& - \left(m_{\widetilde{\nu}}^2 \right)_{ij} v_{jR} - \frac{1}{\sqrt{2}} v_u v_{jL} T_{ji}^\nu - \frac{1}{2} v_u^2 Y_{ji}^\nu Y_{jk}^\nu v_{kR} + v_d v_u \kappa_{ijk} \lambda_j v_{kR} - \frac{1}{\sqrt{2}} T_{ijk}^\kappa v_{jR} v_{kR} \\
& + \frac{1}{2} v_d v_{jL} Y_{ji}^\nu v_{kR} \lambda_k - v_u Y_{lj}^\nu \kappa_{ijk} v_{kR} v_{lL} - \frac{1}{2} v_{jL} Y_{ji}^\nu v_{kL} Y_{kl}^\nu v_{lR} - \kappa_{ijm} \kappa_{jlk} v_{kR} v_{lR} v_{mR} \\
& - \frac{1}{2} \left(v_d^2 + v_u^2 \right) \lambda_i \lambda_j v_{jR} + \frac{1}{2} v_d v_{jL} Y_{jk}^\nu v_{kR} \lambda_i + \frac{1}{\sqrt{2}} v_d v_u T_i^\lambda \,,
\end{aligned} \tag{3.30}$$

$$\begin{aligned}
T_{\widetilde{\nu}_{iL}^{\mathcal{R}}} =& - \left(m_{\widetilde{L}}^2 \right)_{ij} v_{jL} - \left(m_{H_d \widetilde{L}}^2 \right)_i v_d - \frac{1}{8} \left(g_1^2 + g_2^2 \right) v_{iL} \left(v_d^2 + v_{jL} v_{jL} - v_u^2 \right) \\
& + \frac{1}{2} v_d v_u^2 Y_{ij}^\nu \lambda_j - \frac{1}{\sqrt{2}} v_u v_{jR} T_{ij}^\nu - \frac{1}{2} v_u^2 Y_{ij}^\nu Y_{kj}^\nu v_{kL} + \frac{1}{2} v_d v_{jR} Y_{ij}^\nu v_{kR} \lambda_k \\
& - \frac{1}{2} v_u Y_{ij}^\nu \kappa_{jkl} v_{kR} v_{lR} - \frac{1}{2} v_{jR} Y_{ij}^\nu v_{kL} Y_{kl}^\nu v_{lR} \,.
\end{aligned} \tag{3.31}$$

The tadpoles are the first derivative of the scalar potential, meaning that in the true vacuum of the model they have to vanish. A crucial property of the $\mu\nu$SSM is that this implies a hierarchy between the vevs of the left-handed sneutrinos v_{iL} and the vevs of the right-handed sneutrinos v_{iR} and the doublet Higgses v_d and v_u. To see this we recall that the neutrino Yukawa couplings must have small values of the order of the

[1] Spontaneous $\mathcal{CP}$-violation is possible in the $\mu\nu$SSM [28], but not considered during this thesis.

electron Yukawa coupling. In very good approximation we can take the limit $Y^\nu_{ij} \to 0$ in Eq. (3.31),

$$T_{\widetilde{\nu}^{\mathcal{R}}_{iL}} \sim -\left(m^2_{\widetilde{L}}\right)_{ij} v_{jL} - \left(m^2_{H_d\widetilde{L}}\right)_i v_d - \frac{1}{8}\left(g_1^2+g_2^2\right) v_{iL}\left(v_d^2 + v_{jL}v_{jL} - v_u^2\right) \ , \tag{3.32}$$

making use of the fact that the soft parameter T^ν_{ij} are taken to be proportional to Y^ν_{ij}. As was explained in Sect. 3.1, the tree-level values of the parameters $m^2_{H_d\widetilde{L}_i}$ are taken to be zero, i.e., they are absent at tree level.[2] The remaining terms in Eq. (3.32) are proportional to v_{iL}. For the tadpole coefficient $T_{\widetilde{\nu}^{\mathcal{R}}_{iL}}$ to vanish, v_{iL} has to go to zero as well. This correlation is broken by the small terms containing Y^ν_{ij} that we neglected. Hence, the vevs v_{iL} will acquire a finite value which is, however, orders of magnitude smaller than the values of the other vevs [29],

$$v_{iL} \sim 10^{-4}\ \text{GeV} \ll v_d, v_u, v_{iR} \sim 10^2\text{–}10^3\ \text{GeV} \ . \tag{3.33}$$

This hierarchy is reflecting the fact that all lepton-number violating phenomena related to SM fermions are suppressed by the smallness of Y^ν_{ij}. It not only guarantees the viability of the model in terms of constraints regarding lepton-number violating observables, but is also crucial for the electroweak seesaw mechanism to work out, as will be shown in detail in Sect. 3.3.3.

The bilinear terms of the scalar potential in Eq. (3.27) define the mass matrices in the interaction basis for the $\mathcal{CP}$-even scalar φ_i,

$$m^2_\varphi = \begin{pmatrix} m^2_{H_d^{\mathcal{R}}H_d^{\mathcal{R}}} & m^2_{H_d^{\mathcal{R}}H_u^{\mathcal{R}}} & m^2_{H_d^{\mathcal{R}}\widetilde{\nu}^{\mathcal{R}}_{jR}} & m^2_{H_d^{\mathcal{R}}\widetilde{\nu}^{\mathcal{R}}_{jL}} \\ m^2_{H_u^{\mathcal{R}}H_d^{\mathcal{R}}} & m^2_{H_u^{\mathcal{R}}H_u^{\mathcal{R}}} & m^2_{H_u^{\mathcal{R}}\widetilde{\nu}^{\mathcal{R}}_{jR}} & m^2_{H_u^{\mathcal{R}}\widetilde{\nu}^{\mathcal{R}}_{jL}} \\ m_{\widetilde{\nu}^{\mathcal{R}}_{iR}H_d^{\mathcal{R}}} & m_{\widetilde{\nu}^{\mathcal{R}}_{iR}H_u^{\mathcal{R}}} & m^2_{\widetilde{\nu}^{\mathcal{R}}_{iR}\widetilde{\nu}^{\mathcal{R}}_{jR}} & m^2_{\widetilde{\nu}^{\mathcal{R}}_{iR}\widetilde{\nu}^{\mathcal{R}}_{jL}} \\ m^2_{\widetilde{\nu}^{\mathcal{R}}_{iL}H_d^{\mathcal{R}}} & m^2_{\widetilde{\nu}^{\mathcal{R}}_{iL}H_u^{\mathcal{R}}} & m^2_{\widetilde{\nu}^{\mathcal{R}}_{iL}\widetilde{\nu}^{\mathcal{R}}_{jR}} & m^2_{\widetilde{\nu}^{\mathcal{R}}_{iL}\widetilde{\nu}^{\mathcal{R}}_{jL}} \end{pmatrix} \ , \tag{3.34}$$

and the $\mathcal{CP}$-odd scalars σ_i,

$$m^2_\sigma = \begin{pmatrix} m^2_{H_d^{\mathcal{I}}H_d^{\mathcal{I}}} & m^2_{H_d^{\mathcal{I}}H_u^{\mathcal{I}}} & m^2_{H_d^{\mathcal{I}}\widetilde{\nu}^{\mathcal{I}}_{jR}} & m^2_{H_d^{\mathcal{I}}\widetilde{\nu}^{\mathcal{I}}_{jL}} \\ m^2_{H_u^{\mathcal{I}}H_d^{\mathcal{I}}} & m^2_{H_u^{\mathcal{I}}H_u^{\mathcal{I}}} & m^2_{H_u^{\mathcal{I}}\widetilde{\nu}^{\mathcal{I}}_{jR}} & m^2_{H_u^{\mathcal{I}}\widetilde{\nu}^{\mathcal{I}}_{jL}} \\ m^2_{\widetilde{\nu}^{\mathcal{I}}_{iR}H_d^{\mathcal{I}}} & m^2_{\widetilde{\nu}^{\mathcal{I}}_{iR}H_u^{\mathcal{I}}} & m^2_{\widetilde{\nu}^{\mathcal{I}}_{iR}\widetilde{\nu}^{\mathcal{I}}_{jR}} & m^2_{\widetilde{\nu}^{\mathcal{I}}_{iR}\widetilde{\nu}^{\mathcal{I}}_{jL}} \\ m^2_{\widetilde{\nu}^{\mathcal{I}}_{iL}H_d^{\mathcal{I}}} & m^2_{\widetilde{\nu}^{\mathcal{I}}_{iL}H_u^{\mathcal{I}}} & m^2_{\widetilde{\nu}^{\mathcal{I}}_{iL}\widetilde{\nu}^{\mathcal{I}}_{jR}} & m^2_{\widetilde{\nu}^{\mathcal{I}}_{iL}\widetilde{\nu}^{\mathcal{I}}_{jL}} \end{pmatrix} \ . \tag{3.35}$$

These are 8×8-dimensional matrices in family space. A genuine feature of the $\mu\nu$SSM, in contrast to more familiar models like the MSSM and the NMSSM, becomes visible. Since R-parity and lepton-number conservation are broken, the mixing between particles is much more complicated. In this case, the $\mathcal{CP}$-even and -odd sneutrinos will mix with the doublet Higgs bosons and the pseudoscalar. The $\mathcal{CP}$-even scalar mass matrix elements are given by

$$m^2_{H_d^{\mathcal{R}}H_d^{\mathcal{R}}} = m^2_{H_d} + \frac{1}{8}\left(g_1^2+g_2^2\right)\left(3v_d^2 + v_{iL}v_{iL} - v_u^2\right) + \frac{1}{2}\left(v_u^2\lambda_i\lambda_i + (v_{iR}\lambda_i)^2\right) \ , \tag{3.36}$$

$$m^2_{H_u^{\mathcal{R}}H_u^{\mathcal{R}}} = m^2_{H_u} + \frac{1}{8}\left(g_1^2+g_2^2\right)\left(3v_u^2 - v_d^2 - v_{iL}v_{iL}\right) + \frac{1}{2}\lambda_i\lambda_i v_d^2 - v_d Y^\nu_{ji}\lambda_i v_{jL}$$

[2] We will argue in Ch. 5 that radiative corrections will only induce negligible contributions to this operator, so that the absence of $m^2_{H_d\widetilde{L}_i}$ is stable and practically scale-invariant.

$$+\frac{1}{2}\left(v_{iR}\lambda_i\right)^2+\frac{1}{2}Y^{\nu}_{ji}Y^{\nu}_{ki}v_{jL}v_{kL}+\frac{1}{2}Y^{\nu}_{ij}Y^{\nu}_{ik}v_{jR}v_{kR}\,, \tag{3.37}$$

$$m^2_{H^{\mathcal{R}}_u H^{\mathcal{R}}_d}=-\frac{1}{4}\left(g_1^2+g_2^2\right)v_d v_u+v_d v_u\lambda_i\lambda_i-\frac{1}{\sqrt{2}}T^{\lambda}_i v_{iR}-v_u Y^{\nu}_{ji}\lambda_i v_{jL}-\frac{1}{2}\kappa_{ijk}\lambda_i v_{jR}v_{kR}\,, \tag{3.38}$$

$$m^2_{\widetilde{\nu}^{\mathcal{R}}_{iR}H^{\mathcal{R}}_d}=-v_u\kappa_{ijk}\lambda_j v_{kR}-\frac{1}{2}v_{jR}\lambda_j v_{kL}Y^{\nu}_{ki}+v_d v_{jR}\lambda_j\lambda_i-\frac{1}{2}v_{jL}Y^{\nu}_{jk}v_{kR}\lambda_i-\frac{1}{\sqrt{2}}v_u T^{\lambda}_i\,, \tag{3.39}$$

$$\begin{aligned}m^2_{\widetilde{\nu}^{\mathcal{R}}_{iR}H^{\mathcal{R}}_u}=&\frac{1}{\sqrt{2}}v_{jL}T^{\nu}_{ji}+v_u Y^{\nu}_{ji}Y^{\nu}_{jk}v_{kR}-v_d\kappa_{ijk}\lambda_j v_{kR}+Y^{\nu}_{lj}\kappa_{ijk}v_{kR}v_{lL}+v_u v_{jR}\lambda_j\lambda_i\\&-\frac{1}{\sqrt{2}}v_d T^{\lambda}_i\,,\end{aligned} \tag{3.40}$$

$$\begin{aligned}m^2_{\widetilde{\nu}^{\mathcal{R}}_{iR}\widetilde{\nu}^{\mathcal{R}}_{jR}}=&\left(m^2_{\widetilde{\nu}_R}\right)_{ij}+\frac{1}{2}v_u^2Y^{\nu}_{ki}Y^{\nu}_{kj}-v_d v_u\kappa_{ijk}\lambda_k+\sqrt{2}v_{kR}T^{\kappa}_{ijk}+v_u Y^{\nu}_{lk}\kappa_{ijk}v_{lL}\\&+\frac{1}{2}v_{kL}Y^{\nu}_{ki}v_{lL}Y^{\nu}_{lj}+2\kappa_{ikl}\kappa_{jkm}v_{lR}v_{mR}+\kappa_{ijk}\kappa_{klm}v_{lR}v_{mR}-\frac{1}{2}v_d v_{kL}Y^{\nu}_{kj}\lambda_i\\&-\frac{1}{2}v_d v_{kL}Y^{\nu}_{ki}\lambda_j+\frac{1}{2}\left(v_d^2+v_u^2\right)\lambda_i\lambda_j\,,\end{aligned} \tag{3.41}$$

$$m^2_{\widetilde{\nu}^{\mathcal{R}}_{iL}H^{\mathcal{R}}_d}=\left(m^2_{H_d\widetilde{L}}\right)_i+\frac{1}{4}\left(g_1^2+g_2^2\right)v_d v_{iL}-\frac{1}{2}v_u^2Y^{\nu}_{ij}\lambda_j-\frac{1}{2}v_{jR}\lambda_j v_{kR}Y^{\nu}_{ik}\,, \tag{3.42}$$

$$\begin{aligned}m^2_{\widetilde{\nu}^{\mathcal{R}}_{iL}H^{\mathcal{R}}_u}=&-\frac{1}{4}\left(g_1^2+g_2^2\right)v_u v_{iL}-v_d v_u Y^{\nu}_{ij}\lambda_j+\frac{1}{\sqrt{2}}v_{jR}T^{\nu}_{ij}+v_u Y^{\nu}_{ij}Y^{\nu}_{kj}v_{kL}\\&+\frac{1}{2}Y^{\nu}_{ij}\kappa_{jkl}v_{kR}v_{lR}\,,\end{aligned} \tag{3.43}$$

$$\begin{aligned}m^2_{\widetilde{\nu}^{\mathcal{R}}_{iR}\widetilde{\nu}^{\mathcal{R}}_{jL}}=&v_u Y^{\nu}_{jk}\kappa_{ikl}v_{lR}+\frac{1}{2}v_{kL}Y^{\nu}_{ki}v_{lR}Y^{\nu}_{jl}-\frac{1}{2}v_d v_{kR}\lambda_k Y^{\nu}_{ji}+\frac{1}{2}v_{kL}Y^{\nu}_{kl}v_{lR}Y^{\nu}_{ji}\,,\\&-\frac{1}{2}v_d v_{kR}Y^{\nu}_{jk}\lambda_i+\frac{1}{\sqrt{2}}v_u T^{\nu}_{ji}\,,\end{aligned} \tag{3.44}$$

$$\begin{aligned}m^2_{\widetilde{\nu}^{\mathcal{R}}_{iL}\widetilde{\nu}^{\mathcal{R}}_{jL}}=&\left(m^2_{\widetilde{L}}\right)_{ij}+\frac{1}{8}\delta_{ij}\left(g_1^2+g_2^2\right)\left(v_d^2-v_u^2+v_{kL}v_{kL}\right)+\frac{1}{4}\left(g_1^2+g_2^2\right)v_{iL}v_{jL}\\&+\frac{1}{2}v_u^2Y^{\nu}_{ik}Y^{\nu}_{jk}+\frac{1}{2}v_{kR}Y^{\nu}_{jk}v_{lR}Y^{\nu}_{il}\,.\end{aligned} \tag{3.45}$$

The transformation to the mass eigenstate basis of the $\mathcal{CP}$-even scalars is given by a unitary transformation defined by the matrix U^H_{ij} that diagonalizes the mass matrix $(m^2_{\varphi})_{ij}$,

$$U^H_{ik}(m^2_{\varphi})_{kl}\;U^H_{jl}=(m^2_h)_{ij}\,, \tag{3.46}$$

with

$$\varphi_i=U^H_{ji}h_j\,, \tag{3.47}$$

where the h_i are the $\mathcal{CP}$-even scalar fields in the mass eigenstate basis. Without $\mathcal{CP}$-violation in the scalar sector the matrix U^H is real. The lengthy expression for the mass matrix elements are not very intuitive. However, one can easily verify that the mixing between left-handed sneutrinos and the doublet fields and the right-handed sneutrinos is suppressed by the smallness of v_{iL} and Y^{ν}_{ij} (see Eqs. (3.42)-(3.44)). Therefore, it is possible to find approximate formulas for the masses of the three left-handed sneutrinos

$\widetilde{\nu}_{iL}^{\mathcal{R}}$. The dominant terms of the submatrix $m^2_{\widetilde{\nu}_{iL}^{\mathcal{R}}\widetilde{\nu}_{jL}^{\mathcal{R}}}$ are proportional to the inverse of the vevs v_{iL}. One finds for the diagonal entries after replacing the soft mass parameters $(m^2_{\widetilde{L}})_{ii}$ via the tadpole Eqs. (3.31)

$$m^2_{\widetilde{\nu}_{iL}^{\mathcal{R}}\widetilde{\nu}_{iL}^{\mathcal{R}}} \sim \frac{Y^{\nu}_{ii}}{2v_{iL}}\left(v_d v_u^2 \lambda_i + \sqrt{2} v_d v_{iR}\mu - v_u v_{iR}\left(\sqrt{2}A^{\nu}_{ii} + \kappa_{iii} v_{iR}\right)\right) \,, \tag{3.48}$$

where we defined the effective μ-term as

$$\mu = \frac{1}{\sqrt{2}}\left(v_{1R}\lambda_1 + v_{2R}\lambda_2 + v_{3R}\lambda_3\right) \,. \tag{3.49}$$

This is the obvious generalization of the effective μ-term of the NMSSM when three instead of one gauge-singlet are present. For the right-handed sneutrinos $\widetilde{\nu}_{iR}$ approximate tree-level formulas for their masses can be obtained under the assumption that there is no substantial missing with the doublet Higgs fields H_d and H_u. We find for the submatrix $m^2_{\widetilde{\nu}_{iR}^{\mathcal{R}}\widetilde{\nu}_{jR}^{\mathcal{R}}}$, under the assumptions that non-diagonal elements of κ_{ijk} and $(m^2_{\widetilde{\nu}})_{ij}$ vanish, and after eliminating the diagonal elements $(m^2_{\widetilde{\nu}})_{ii}$ via the tadpole Eqs. (3.30),

$$m^2_{\widetilde{\nu}_{iR}^{\mathcal{R}}\widetilde{\nu}_{jR}^{\mathcal{R}}} \sim \frac{1}{2}v^2\lambda_i\lambda_j + \delta_{ij}\left[\frac{1}{\sqrt{2}}v_{iR}\kappa_{iii}A^{\kappa}_{iii} + 2\kappa^2_{iii}v^2_{iR} - \frac{\lambda_i}{\sqrt{2}v_{iR}}\left(\mu v^2 - v_d v_u A^{\lambda}_i\right)\right] \,. \tag{3.50}$$

In this approximation the submatrix has the form

$$m^2_{\widetilde{\nu}_{iR}^{\mathcal{R}}\widetilde{\nu}_{jR}^{\mathcal{R}}} = \begin{pmatrix} a & b & b \\ b & a & b \\ b & b & a \end{pmatrix} \,. \tag{3.51}$$

The eigenvalues of this matrix are $a-b$, $a-b$ and $a+2b$. In this limit only the mass eigenstate corresponding to the latter eigenvalue potentially mixes with the SM-like Higgs boson [30]. If it does, the corresponding tree-level mass squared will be substantially different from the eigenvalue obtained under the approximation used here. Since the other two mass eigenstates do not mix with the doublet Higgs fields, they will be decoupled from the remaining scalars. Being gauge-singlets, they interact very weakly with SM particles. In extensions of the NMSSM with several gauge singlets, this decoupling can lead to stable particles. In the $\mu\nu$SSM this is not possible, because the decoupling cannot be exact, even when κ_{ijk} and $(m^2_{\widetilde{\nu}})_{ij}$ are diagonal. Terms suppressed by factors of Y^{ν}_{ij} and v_{iL} will always induce a remnant coupling to the SM particle spectrum. Usually the right-handed vevs v_{iR} are somewhat larger than the doublet vevs v_d and v_u, whose scale is fixed by the SM vev

$$v^2 = v_u^2 + v_d^2 + v_{1L}^2 + v_{2L}^2 + v_{3L}^2 \sim v_u^2 + v_d^2 \,. \tag{3.52}$$

Hence, Eq. (3.50) further simplifies to

$$m^2_{\widetilde{\nu}_{iR}^{\mathcal{R}}\widetilde{\nu}_{iR}^{\mathcal{R}}} \sim \frac{1}{\sqrt{2}}v_{iR}\kappa_{iii}A^{\kappa}_{iii} + 2\kappa^2_{iii}v^2_{iR} \,, \tag{3.53}$$

As in the NMSSM [31], the upper bound on the lowest Higgs mass squared at tree-level $m^{(0)}_{h_1}$ is relaxed through additional contributions from the right-handed sneutrinos [29];

$$\left(m^{(0)}_{h_1}\right)^2 \leq M_Z^2\left(\cos^2 2\beta + \frac{2\boldsymbol{\lambda}^2}{g_1^2+g_2^2}\sin^2 2\beta\right) \,, \quad \text{with} \quad \boldsymbol{\lambda}^2 := \lambda_1^2+\lambda_2^2+\lambda_3^2 \,, \tag{3.54}$$

where β is defined in accordance to the definition in the MSSM by the ratio of doublet vevs, such that

$$\tan\beta = \frac{v_u}{v_d} \ . \tag{3.55}$$

This means that, depending on the value of the λ_i, it is easier to obtain a SM-like Higgs boson mass compared to the MSSM, because less quantum corrections are required.

For the $\mathcal{CP}$-odd scalar sector, the mass matrix elements are given by

$$m^2_{H_d^{\mathcal{I}} H_d^{\mathcal{I}}} = m^2_{H_d} + \frac{1}{8}\left(g_1^2+g_2^2\right)\left(v_d^2 + v_{iL}v_{iL} - v_u^2\right) + \frac{1}{2}\left(v_u^2\lambda_i\lambda_i + (v_{iR}\lambda_i)^2\right) \ , \tag{3.56}$$

$$\begin{aligned} m^2_{H_u^{\mathcal{I}} H_u^{\mathcal{I}}} = {} & m^2_{H_u} + \frac{1}{8}\left(g_1^2+g_2^2\right)\left(v_u^2 - v_d^2 - v_{iL}v_{iL}\right) + \frac{1}{2}v_d^2\lambda_i\lambda_i - v_d Y^\nu_{ji}\lambda_i v_{jL} \\ & + \frac{1}{2}\left(v_{iR}\lambda_i\right)^2 + \frac{1}{2}Y^\nu_{ji}Y^\nu_{ki}v_{jL}v_{kL} + \frac{1}{2}Y^\nu_{ij}Y^\nu_{ik}v_{jR}v_{kR} \ , \end{aligned} \tag{3.57}$$

$$m^2_{H_u^{\mathcal{I}} H_d^{\mathcal{I}}} = \frac{1}{2}\kappa_{ijk}\lambda_i v_{jR}v_{kR} + \frac{1}{\sqrt{2}}v_{iR}T^\lambda_i \ , \tag{3.58}$$

$$m^2_{\widetilde{\nu}_{iR}^{\mathcal{I}} H_d^{\mathcal{I}}} = v_u\kappa_{ijk}\lambda_j v_{kR} + \frac{1}{2}v_{jR}\lambda_j v_{kL}Y^\nu_{ki} - \frac{1}{2}v_{jL}Y^\nu_{jk}v_{kR}\lambda_i - \frac{1}{\sqrt{2}}v_u T^\lambda_i \ , \tag{3.59}$$

$$m^2_{\widetilde{\nu}_{iR}^{\mathcal{I}} H_u^{\mathcal{I}}} = \frac{1}{\sqrt{2}}v_{jL}T^\nu_{ji} + v_d\kappa_{ijk}\lambda_j v_{kR} - Y^\nu_{lj}\kappa_{ijk}v_{kR}v_{lL} - \frac{1}{\sqrt{2}}v_d T^\lambda_i \ , \tag{3.60}$$

$$\begin{aligned} m^2_{\widetilde{\nu}_{iR}^{\mathcal{I}}\widetilde{\nu}_{jR}^{\mathcal{I}}} = {} & \left(m^2_{\widetilde{\nu}}\right)_{ij} + \frac{1}{2}v_u^2 Y^\nu_{ki}Y^\nu_{kj} + v_d v_u\kappa_{ijk}\lambda_k - \sqrt{2}v_{kR}T^\kappa_{ijk} - v_u Y^\nu_{lk}\kappa_{ijk}v_{lL} \\ & + \frac{1}{2}v_{kL}Y^\nu_{ki}v_{lL}Y^\nu_{lj} + \kappa_{ikm}\kappa_{jkl}v_{lR}v_{mR} - \kappa_{ijk}\kappa_{klm}v_{lR}v_{mR} - \frac{1}{2}v_d v_{kL}Y^\nu_{kj}\lambda_i \\ & - \frac{1}{2}v_d v_{kL}Y^\nu_{ki}\lambda_j + \frac{1}{2}\left(v_d^2+v_u^2\right)\lambda_i\lambda_j \ , \end{aligned} \tag{3.61}$$

$$m^2_{\widetilde{\nu}_{iL}^{\mathcal{I}} H_d^{\mathcal{I}}} = \left(m^2_{H_d\widetilde{L}}\right)_i - \frac{1}{2}v_u^2 Y^\nu_{ij}\lambda_j - \frac{1}{2}v_{jR}\lambda_j v_{kR}Y^\nu_{ik} \ , \tag{3.62}$$

$$m^2_{\widetilde{\nu}_{iL}^{\mathcal{I}} H_u^{\mathcal{I}}} = -\frac{1}{\sqrt{2}}v_{jR}T^\nu_{ij} - \frac{1}{2}Y^\nu_{ij}\kappa_{jkl}v_{kR}v_{lR} \ , \tag{3.63}$$

$$\begin{aligned} m^2_{\widetilde{\nu}_{iR}^{\mathcal{I}}\widetilde{\nu}_{jL}^{\mathcal{I}}} = {} & -v_u Y^\nu_{jk}\kappa_{ikl}v_{lR} - \frac{1}{2}v_{kL}Y^\nu_{ki}v_{lR}Y^\nu_{jl} - \frac{1}{2}v_d v_{kR}\lambda_k Y^\nu_{ji} + \frac{1}{2}v_{kL}Y^\nu_{kl}v_{lR}Y^\nu_{ji} \\ & + \frac{1}{2}v_d v_{kR}Y^\nu_{jk}\lambda_i + \frac{1}{\sqrt{2}}v_u T^\nu_{ji} \ , \end{aligned} \tag{3.64}$$

$$m^2_{\widetilde{\nu}_{iL}^{\mathcal{I}}\widetilde{\nu}_{jL}^{\mathcal{I}}} = \left(m^2_{\widetilde{L}}\right)_{ij} + \frac{1}{8}\delta_{ij}\left(g_1^2+g_2^2\right)\left(v_d^2 + v_{kL}v_{kL} - v_u^2\right) + \frac{1}{2}v_u^2 Y^\nu_{ik}Y^\nu_{jk} + \frac{1}{2}v_{kR}Y^\nu_{ik}v_{lR}Y^\nu_{jl} \ . \tag{3.65}$$

We define the rotation matrix U^A_{ij}, that diagonalizes the mass matrix $(m^2_\sigma)_{ij}$,

$$U^A_{ik}(m^2_\sigma)_{kl}U^A_{jl} = (m^2_A)_{ij} \ , \qquad \text{with } \sigma_i = U^A_{ji}A_j \ . \tag{3.66}$$

One of the mass eigenstates constitutes the unphyiscal neutral Goldstone boson $A_1 = G^0$. Under the same approximations as for the $\mathcal{CP}$-even scalars, we can find approximate analytical results for the pseudoscalar mass spectrum. Each $\mathcal{CP}$-odd left-handed sneutrino is nearly degenerate with the corresponding $\mathcal{CP}$-even one, though they are slightly lighter due to different D-term contributions proportional to the gauge couplings,

$$m^2_{\widetilde{\nu}_{iL}^{\mathcal{I}}\widetilde{\nu}_{iL}^{\mathcal{I}}} - m^2_{\widetilde{\nu}_{iL}^{\mathcal{R}}\widetilde{\nu}_{iL}^{\mathcal{R}}} = -\frac{1}{4}\left(g_1^2+g_2^2\right)v_{iL}^2 \ . \tag{3.67}$$

For the right-handed $\mathcal{CP}$-odd sneutrinos we find

$$m^2_{\widetilde{\nu}^{\mathcal{R}}_{iR}\widetilde{\nu}^{\mathcal{R}}_{iR}} \sim -\frac{3}{\sqrt{2}} A^{\kappa}_{iii}\kappa_{iii}v_{iR}\,. \tag{3.68}$$

Thus, to avoid tachyons in the $\mathcal{CP}$-odd scalar spectrum, we adopt the sign convention

$$A^{\kappa}_{iii} < 0\,. \tag{3.69}$$

Consequently, comparing to Eq. (3.53), one has to chose

$$\kappa_{iii} > 0 \quad \text{and} \quad v_{iR} > 0\,, \tag{3.70}$$

to prevent tachyons in the $\mathcal{CP}$-even scalar spectrum. For both the scalar and pseudoscalar left-handed sneutrinos, as can be seen from Eqs. (3.48) and (3.67), the parameters A^{ν}_{ii} enter with a minus sign, so that under the sign convention above it is appropriate to chose

$$A^{\nu}_{ii} < 0\,. \tag{3.71}$$

We conclude the discussion of the neutral scalar potential at tree level by emphasizing that the analytical expressions stated above will, in many cases, not be accurate enough. The scalar spectrum is strongly dependent on quantum corrections. In Ch. 5 and Ch. 6 we demonstrate this fact in scenarios in which these corrections can be of the same order or even larger than the tree-level masses. Surely, for the SM like Higgs-boson mass this is a well known fact from studying the Higgs sector of the MSSM, see e.g. Refs. [32–34] for reviews. However, during the work of this thesis we showed that in the framework of the $\mu\nu$SSM also the higher-order contributions to the mass eigenstates corresponding to the sneutrinos can be of the same order as the tree-level masses [8, 9]. Still, the approximate formulas are a useful tool to get an idea of the rough structure of the scalar masses.

3.3.2 Charged scalars

Since R-parity and lepton-number are not conserved, the six charged left- and right-handed sleptons $\widetilde{e}_{iL}$ and $\widetilde{e}_{jR}$ mix with the two charged scalars H_d^- and H_u^+ from the Higgs doublets fields. Also, lepton-flavor universality is necessarily broken once the left-handed sneutrinos obtain a vev. Thus, the sleptons of different flavor have a non-zero admixture with each other. In the basis $C^T = (H_d^{-*}, H_u^+, \widetilde{e}^*_{iL}, \widetilde{e}^*_{jR})$ we can express the mass terms in the Lagrangian as

$$\mathcal{L}_C \;=\; -C^{*T} m^2_{C^+}\, C\,, \tag{3.72}$$

where, assuming $\mathcal{CP}$-conservation, $m^2_{C^+}$ is a symmetric matrix of dimension 8,

$$m^2_{C^+} = \begin{pmatrix} m^2_{H_d^- H_d^{-*}} & m^2_{H_d^- H_u^+} & m^2_{H_d^- \widetilde{e}^*_{jL}} & m^2_{H_d^- \widetilde{e}^*_{jR}} \\ m^2_{H_u^{+*} H_d^{-*}} & m^2_{H_u^{+*} H_u^+} & m^2_{H_u^{+*} \widetilde{e}^*_{jL}} & m^2_{H_u^{+*} \widetilde{e}^*_{jR}} \\ m^2_{\widetilde{e}_{iL} H_d^{-*}} & m^2_{\widetilde{e}_{iL} H_u^+} & m^2_{\widetilde{e}_{iL} \widetilde{e}^*_{jL}} & m^2_{\widetilde{e}_{iL} \widetilde{e}^*_{jR}} \\ m^2_{\widetilde{e}_{iR} H_d^{-*}} & m^2_{\widetilde{e}_{iR} H_u^+} & m^2_{\widetilde{e}_{iR} \widetilde{e}^*_{jL}} & m^2_{\widetilde{e}_{iR} \widetilde{e}^*_{jR}} \end{pmatrix}\,. \tag{3.73}$$

The entries are given by

$$m^2_{H_d^- H_d^{-*}} = m^2_{H_d} + \frac{1}{8}g_1^2\left(v_d^2 + v_{iL}v_{iL} - v_u^2\right) + \frac{1}{8}g_2^2\left(v_d^2 - v_{iL}v_{iL} + v_u^2\right) + \frac{1}{2}\left(v_{iR}\lambda_i\right)^2$$

$$+\frac{1}{2}Y^e_{ij}Y^e_{ik}v_{jL}v_{kL}\ , \tag{3.74}$$

$$m^2_{H_u^{+*}H_u^+} = m^2_{H_u}+\frac{1}{8}g_1^2\left(v_u^2-v_d^2-v_{iL}v_{iL}\right)+\frac{1}{8}g_2^2\left(v_u^2+v_d^2+v_{iL}v_{iL}\right)+\frac{1}{2}\left(v_{iR}\lambda_i\right)^2$$
$$+\frac{1}{2}Y^\nu_{ij}Y^\nu_{ik}v_{jR}v_{kL}\ , \tag{3.75}$$

$$m^2_{H_d^-H_u^+} = \frac{1}{4}g_2^2v_dv_u-\frac{1}{2}v_dv_u\lambda_i\lambda_i+\frac{1}{\sqrt{2}}v_{iR}T^\lambda_i+\frac{1}{2}v_uY^\nu_{ji}\lambda_iv_{jL}+\frac{1}{2}\kappa_{ijk}\lambda_iv_{jR}v_{kR}\ , \tag{3.76}$$

$$m^2_{H_d^-\widetilde{e}^*_{iL}} = \left(m^2_{H_d\widetilde{L}}\right)_i+\frac{1}{4}g_2^2v_dv_{iL}-\frac{1}{2}v_dY^e_{ji}Y^e_{jk}v_{kL}-\frac{1}{2}v_{jR}Y^\nu_{ij}v_{kR}\lambda_k\ , \tag{3.77}$$

$$m^2_{H_u^{+*}\widetilde{e}^*_{iL}} = \frac{1}{4}g_2^2v_uv_{iL}+\frac{1}{2}v_dv_uY^\nu_{ij}\lambda_j-\frac{1}{\sqrt{2}}v_{jR}T^\nu_{ij}-\frac{1}{2}v_uY^\nu_{ij}Y^\nu_{kj}v_{kL}-\frac{1}{2}Y^\nu_{ij}\kappa_{jkl}v_{kR}v_{lR}\ , \tag{3.78}$$

$$m^2_{H_d^-\widetilde{e}^*_{iR}} = -\frac{1}{\sqrt{2}}v_{jL}T^e_{ij}-\frac{1}{2}v_uY^e_{ij}Y^\nu_{jk}v_{jR}\ , \tag{3.79}$$

$$m^2_{H_u^{+*}\widetilde{e}^*_{iR}} = -\frac{1}{2}v_dY^e_{ij}Y^\nu_{jk}v_{kR}-\frac{1}{2}v_{jR}\lambda_jv_{kL}Y^e_{ik}\ , \tag{3.80}$$

$$m^2_{\widetilde{e}_{iL}\widetilde{e}^*_{jL}} = \left(m^2_{\widetilde{L}}\right)_{ij}+\frac{1}{8}\delta_{ij}\left(g_1^2-g_2^2\right)\left(v_d^2-v_u^2+v_{kL}v_{kL}\right)+\frac{1}{4}g_2^2v_{iL}v_{jL}+\frac{1}{2}v_d^2Y^e_{ki}Y^e_{kj}$$
$$+\frac{1}{2}v_{kR}Y^\nu_{jk}v_{lR}Y^\nu_{il}\ , \tag{3.81}$$

$$m^2_{\widetilde{e}_{iR}\widetilde{e}^*_{jR}} = \left(m^2_{\widetilde{e}}\right)_{ij}+\frac{1}{4}\delta_{ij}g_1^2\left(v_u^2-v_d^2-v_{kL}v_{kL}\right)+\frac{1}{2}v_d^2Y^e_{ik}Y^e_{jk}+\frac{1}{2}v_{kL}Y^e_{ik}v_{lL}Y^e_{jl}\ , \tag{3.82}$$

$$m^2_{\widetilde{e}_{iL}\widetilde{e}^*_{jR}} = \frac{1}{\sqrt{2}}v_dT^e_{ij}-\frac{1}{2}v_uv_{kR}\lambda_kY^e_{ij}\ . \tag{3.83}$$

As can be seen in Eqs. (3.77) - (3.80), elements mixing the scalar SUSY partners of the SM fermions and the Higgs-doublet fields are suppressed by factors of Y^ν_{ij} and v_{iL}. The mass matrix is diagonalized by an orthogonal matrix U^+_{ij}:

$$U^+_{ik}(m^2_{C^+})_{kl}U^+_{jl} = (m^2_{H^+})_{ij}\ , \tag{3.84}$$

where the elements of the diagonal matrix $(m^2_{H^+})_{ij}$ are the squared masses of the mass eigenstates

$$H^+_i = U^+_{ij}C_j\ , \tag{3.85}$$

which include the unphysical charged Goldstone boson $H^+_1 = G^\pm$. For the left-handed sleptons, the mass differences to the corresponding sneutrinos is approximately given by

$$m^2_{\widetilde{e}_{iL}\widetilde{e}^*_{iL}}-m^2_{\widetilde{\nu}^{\mathcal{R}}_{iL}\widetilde{\nu}^{\mathcal{R}}_{iL}} \sim -M_W^2\cos 2\beta+m_l^2\ , \tag{3.86}$$

where m_l is the lepton mass of the same family. Hence, the left-handed slepton mass will always be slightly larger than the left-handed sneutrino masses of that family at tree level. This circumstance is especially important in scenarios in which a left-handed sneutrino is the LSP. Usually, then the next-to LSP is the corresponding slepton which decays to the LSP, because decays directly to SM particles are suppressed by factors of Y^ν_{ij}. Then the slepton decay is an important production channel of the sneutrino LSPs at colliders [11].

3.3.3 Neutral fermions

The neutral fermion sector consists of a total of 10 massive Majorana fermions. The three left-handed neutrinos and the right-handed neutrinos mix with the neutral Higgsinos and gauginos. Following Ref. [11] we write the relevant part of the Lagrangian in terms of two-component spinors $(\chi^0)^T = \left((\nu_{iL})^{c^*}, \widetilde{B}^0, \widetilde{W}^0, \widetilde{H}_d^0, \widetilde{H}_u^0, \nu_{jR}^*\right)$ as

$$\mathcal{L}_{\chi^0} \;=\; -\frac{1}{2}(\chi^0)^T m_{\chi^0}\chi^0 + \text{h.c.}\,, \tag{3.87}$$

where m_{χ^0} is the 10×10 symmetric mass matrix. The neutral fermion mass matrix is given by

$$m_{\chi^0} = \begin{pmatrix}
0 & 0 & 0 & -\frac{g_1 v_{1L}}{2} & \frac{g_2 v_{1L}}{2} & 0 & \frac{v_{iR}Y^\nu_{1i}}{\sqrt{2}} \\
0 & 0 & 0 & -\frac{g_1 v_{2L}}{2} & \frac{g_2 v_{2L}}{2} & 0 & \frac{v_{iR}Y^\nu_{2i}}{\sqrt{2}} \\
0 & 0 & 0 & -\frac{g_1 v_{3L}}{2} & \frac{g_2 v_{3L}}{2} & 0 & \frac{v_{iR}Y^\nu_{3i}}{\sqrt{2}} \\
-\frac{g_1 v_{1L}}{2} & -\frac{g_1 v_{2L}}{2} & -\frac{g_1 v_{3L}}{2} & M_1 & 0 & -\frac{g_1 v_d}{2} & \frac{g_1 v_u}{2} \\
\frac{g_2 v_{1L}}{2} & \frac{g_2 v_{2L}}{2} & \frac{g_2 v_{3L}}{2} & 0 & M_2 & \frac{g_2 v_d}{2} & -\frac{g_2 v_u}{2} \\
0 & 0 & 0 & -\frac{g_1 v_d}{2} & \frac{g_2 v_d}{2} & 0 & -\mu \\
\frac{v_{iR}Y^\nu_{1i}}{\sqrt{2}} & \frac{v_{iR}Y^\nu_{2i}}{\sqrt{2}} & \frac{v_{iR}Y^\nu_{3i}}{\sqrt{2}} & \frac{g_1 v_u}{2} & -\frac{g_2 v_u}{2} & -\mu & 0 \\
\frac{v_u Y^\nu_{11}}{\sqrt{2}} & \frac{v_u Y^\nu_{21}}{\sqrt{2}} & \frac{v_u Y^\nu_{31}}{\sqrt{2}} & 0 & 0 & -\frac{v_u\lambda_1}{\sqrt{2}} & \frac{-v_d\lambda_1+v_{iL}Y^\nu_{i1}}{\sqrt{2}} \\
\frac{v_u Y^\nu_{12}}{\sqrt{2}} & \frac{v_u Y^\nu_{22}}{\sqrt{2}} & \frac{v_u Y^\nu_{32}}{\sqrt{2}} & 0 & 0 & -\frac{v_u\lambda_2}{\sqrt{2}} & \frac{-v_d\lambda_2+v_{iL}Y^\nu_{i2}}{\sqrt{2}} \\
\frac{v_u Y^\nu_{13}}{\sqrt{2}} & \frac{v_u Y^\nu_{23}}{\sqrt{2}} & \frac{v_u Y^\nu_{33}}{\sqrt{2}} & 0 & 0 & -\frac{v_u\lambda_3}{\sqrt{2}} & \frac{-v_d\lambda_3+v_{iL}Y^\nu_{i3}}{\sqrt{2}}
\end{pmatrix}
\begin{matrix} \cdots \\ \\ \\ \\ \\ \\ \\ \\ \\ \\ \end{matrix}
\begin{pmatrix}
\frac{v_u Y^\nu_{11}}{\sqrt{2}} & \frac{v_u Y^\nu_{12}}{\sqrt{2}} & \frac{v_u Y^\nu_{13}}{\sqrt{2}} \\
\frac{v_u Y^\nu_{21}}{\sqrt{2}} & \frac{v_u Y^\nu_{22}}{\sqrt{2}} & \frac{v_u Y^\nu_{23}}{\sqrt{2}} \\
\frac{v_u Y^\nu_{31}}{\sqrt{2}} & \frac{v_u Y^\nu_{32}}{\sqrt{2}} & \frac{v_u Y^\nu_{33}}{\sqrt{2}} \\
0 & 0 & 0 \\
0 & 0 & 0 \\
-\frac{v_u\lambda_1}{\sqrt{2}} & -\frac{v_u\lambda_2}{\sqrt{2}} & -\frac{v_u\lambda_3}{\sqrt{2}} \\
\frac{-v_d\lambda_1+v_{iL}Y^\nu_{i1}}{\sqrt{2}} & \frac{-v_d\lambda_2+v_{iL}Y^\nu_{i2}}{\sqrt{2}} & \frac{-v_d\lambda_3+v_{iL}Y^\nu_{i3}}{\sqrt{2}} \\
\sqrt{2}v_{iR}\kappa_{11i} & \sqrt{2}v_{iR}\kappa_{12i} & \sqrt{2}v_{iR}\kappa_{13i} \\
\sqrt{2}v_{iR}\kappa_{12i} & \sqrt{2}v_{iR}\kappa_{22i} & \sqrt{2}v_{iR}\kappa_{23i} \\
\sqrt{2}v_{iR}\kappa_{13i} & \sqrt{2}v_{iR}\kappa_{23i} & \sqrt{2}v_{iR}\kappa_{33i}
\end{pmatrix} \tag{3.88}$$

Because of the Majorana nature of the neutral fermions, we can diagonalize m_{χ^0} with the help of just a single - but complex - unitary matrix U^V_{ij},

$$U^{V^*}_{ik}(m_{\chi^0})_{kl}U^{V^*}_{jl} = (m_\nu)_{ij}\;, \tag{3.89}$$

with

$$\chi^0_i = U^{V^*}_{ji}\lambda^0_j\;, \tag{3.90}$$

where λ^0_i are the two-component spinors in the mass eigenstate basis. The eigenvalues of the diagonalized mass matrix m_ν are the masses of the neutral fermions. The mass matrix has a seesaw structure,

$$m_{\chi^0} = \begin{pmatrix} 0_{3\times 3} & m_{3\times 7} \\ m^T_{7\times 3} & M_{7\times 7}\end{pmatrix} \quad \text{with} \quad (m_{3\times 7})_{ij} \ll (M_{7\times 7})_{kl} \quad \text{for all} \quad i,j,k,l\;. \tag{3.91}$$

The scale of the elements of $m_{3\times7}$, mixing left- and right-handed neutrinos, is determined by the smallness of Y^ν_{ij} and v_{iL}. The scale of the elements of $M_{7\times7}$ are determined by the soft gaugino masses M_1 and M_2 and the vevs v_d, v_u and v_{iR}. The large hierarchy between the vevs, as shown in Eq. (3.33), assures that the three lightest eigenvalues will be very small, so that the mass eigenstates $\lambda^0_{1,2,3}$ can be identified with the SM left-handed neutrinos. Admixtures from the MSSM-like neutralinos and the right-handed neutrinos are negligible for the three lightest states due to the suppression by factors of Y^ν_{ij} and v_{il}. Thus, the left-handed neutrino mixing can for all practical purposes be expressed in the usual PMNS formalism [35, 36] by the three mixing angles θ_{12}, θ_{13} and θ_{23},

$$\begin{pmatrix} \lambda^0_1 \\ \lambda^0_2 \\ \lambda^0_3 \end{pmatrix} = \begin{pmatrix} c_{12}c_{13} & -s_{12}c_{23} - c_{12}s_{23}s_{13} & s_{12}s_{23} - c_{12}c_{23}s_{13} \\ s_{12}c_{13} & c_{12}c_{23} - s_{12}s_{23}s_{13} & -c_{12}s_{23} - s_{12}c_{23}s_{13} \\ s_{13} & s_{23}c_{13} & c_{23}c_{13} \end{pmatrix} \begin{pmatrix} \chi^0_1 \\ \chi^0_2 \\ \chi^0_3 \end{pmatrix} \tag{3.92}$$

$$= U^V_{ij} \begin{pmatrix} \chi^0_1 \\ \chi^0_2 \\ \chi^0_3 \end{pmatrix} , \tag{3.93}$$

with $i, j = \{1, 2, 3\}$, and we used the short-hand notation $c_x = \cos\theta_x$ and $s_x = \sin\theta_x$. Interestingly, non-diagonal Y^ν_{ij} are not necessary to generate a mixing of the three neutrino flavor state, because it is automatically present after the diagonalization of m_{χ^0}. It is induced by the mixing terms of the left-handed neutrino states with the gauginos, Higgsinos and right-handed neutrinos. This can be seen most easily in the simplified limit of universal parameters $\lambda := \lambda_i$, $v_R := v_{iR}$, $\kappa := \kappa_{iii}$, $Y^\nu_i := Y^\nu_{ii}$ and $\kappa_{ijk} = 0$, $Y^\nu_{ij} = 0$ otherwise, in which an analytical expression for the neutrino submatrix can be written as [28]

$$(m^{\text{eff}}_\nu)_{ij} \simeq \frac{Y^\nu_i Y^\nu_j v_u^2}{6\sqrt{2}\kappa v_R}(1 - 3\delta_{ij}) - \frac{v_{iL}v_{jL}}{4M^{\text{eff}}} - \frac{1}{4M^{\text{eff}}}\left[\frac{v_d\left(Y^\nu_i v_{jL} + Y^\nu_j v_{iL}\right)}{3\lambda} + \frac{Y^\nu_i Y^\nu_j v_d^2}{9\lambda^2}\right] , \tag{3.94}$$

with

$$M^{\text{eff}} \equiv \frac{M_1 M_2}{g_1^2 M_2 + g_2^2 M_1} - \frac{v^2}{2\sqrt{2}\left(\kappa v_R^2 + \lambda v_u v_d\right)\ 3\lambda v_R}\left(2\kappa v_R^2 \frac{v_u v_d}{v^2} + \frac{\lambda v^2}{2}\right) . \tag{3.95}$$

This formula demonstrates that substantial neutrino flavor mixing is practically unavoidable in the $\mu\nu$SSM. For moderate values of $\tan\beta$ and not to small values of λ, the first two terms in Eq. (3.94) are the dominant ones. They contain diagonal and non-diagonal contributions. The first term can be attributed to the mixing with the right-handed neutrinos and higgsinos, while the remaining terms also include the gaugino mixing. Note that the first term is exactly of the form of the Majorana masses arising from the effective Weinberg operator as shown in Eq. (3.4). In the denominator appears the Majorana mass term for the heavy right-handed neutrinos,

$$M^M_{\nu_R} \sim \sqrt{2}\kappa v_R , \tag{3.96}$$

which corresponds to the energy scale Λ_ν in Eq. (3.3), and which automatically is of the desired order (see Eq. (3.6)). The size of the nominator is determined by the neutrino

Yukawa couplings Y^{ν}_{ij} squared, such that the terms will be of the sub-eV size required to accommodate accurate neutrino masses. The second term stems from the mixing with the gauginos. The scale of new-physics Λ_ν consequently corresponds to the mass scale of the gauginos, defined by the soft gaugino masses M_1 and M_2. The smallness of the vevs v_{iL} provide contributions of the order of the measured neutrino mass differences. At the end of the day, the order of magnitudes of v_{iR}, M_1 and M_2 are fixed by the scale of EWSB and SUSY breaking. This proves the claim, made in the introduction of this chapter, that neutrino masses of the desired order of magnitude are evoked without the need to introduce further artificial energy scales. Surely, in scenarios in which the above simplifications of universal parameters are not satisfied, the precise values of the neutrino mixing angles can only be determined numerically. Nevertheless, the general statement above holds for all parameter configurations, granted that the neutrino Yukawa couplings are of the correct size, as shown in Eq. (3.7).

3.3.4 Charged fermions

The charged SM leptons, i.e., the electron, muon and tauon, form the charged fermion sector of the $\mu\nu$SSM together with the charged gauginos and the charged higgsinos. However, the mixing between the leptons and the MSSM-like charginos is suppressed, so that the leptons decouple. Following the notation of Ref. [11], we write the relevant part of the Lagrangian in terms of two-component spinors $(\chi^-)^T = \left((e_{iL})^{c^*}, \widetilde{W}^-, \widetilde{H}_d^-\right)$ and $(\chi^+)^T = \left((e_{jR})^c, \widetilde{W}^+, \widetilde{H}_u^+\right)$, such that

$$\mathcal{L}_{\chi^\pm} \;=\; -(\chi^-)^T m_{\chi^\pm}\chi^+ + \text{h.c.}\,. \tag{3.97}$$

The 5×5 tree-level mass matrix $m_{\chi^\pm}$ is defined by

$$m_{\chi^\pm} = \begin{pmatrix} \frac{v_d Y^e_{11}}{\sqrt{2}} & \frac{v_d Y^e_{12}}{\sqrt{2}} & \frac{v_d Y^e_{13}}{\sqrt{2}} & \frac{g_2 v_{1L}}{\sqrt{2}} & -\frac{v_{iR} Y^\nu_{i1}}{\sqrt{2}} \\ \frac{v_d Y^e_{21}}{\sqrt{2}} & \frac{v_d Y^e_{22}}{\sqrt{2}} & \frac{v_d Y^e_{23}}{\sqrt{2}} & \frac{g_2 v_{2L}}{\sqrt{2}} & -\frac{v_{iR} Y^\nu_{i2}}{\sqrt{2}} \\ \frac{v_d Y^e_{31}}{\sqrt{2}} & \frac{v_d Y^e_{32}}{\sqrt{2}} & \frac{v_d Y^e_{33}}{\sqrt{2}} & \frac{g_2 v_{3L}}{\sqrt{2}} & -\frac{v_{iR} Y^\nu_{i3}}{\sqrt{2}} \\ 0 & 0 & 0 & M_2 & \frac{g_2 v_u}{\sqrt{2}} \\ -\frac{v_{iL} Y^e_{1i}}{\sqrt{2}} & -\frac{v_{iL} Y^e_{2i}}{\sqrt{2}} & -\frac{v_{iL} Y^e_{3i}}{\sqrt{2}} & \frac{g_2 v_d}{\sqrt{2}} & \mu \end{pmatrix}. \tag{3.98}$$

The mass matrix is diagonalized by two unitary matrices U^L_{ij} and U^R_{ij},

$$U^{R^*}_{ik}\,(m_{\chi^\pm})_{kl} U^{L^*}_{jl} \;= (m_e)_{ij}\,, \tag{3.99}$$

where $(m_e)_{ii}$ give the masses of the charged fermions in the mass eigenstate basis

$$\chi^+_i = U^{L^*}_{ji}\,\lambda^+_j\,, \tag{3.100}$$

$$\chi^-_i = U^{R^*}_{ji}\,\lambda^-_j\,. \tag{3.101}$$

The decoupling of the leptons from the charged gaugino is assured by the smallness of v_{iL} in the non-diagonal elements of the fourth column of m_e. The decoupling from the charged Higgsino follows from the smallness of v_{iL} in the non-diagonal elements of the fifth row and the smallness of Y^ν_{ij} in the non-diagonal elements of the fifth column. Written in terms of the effective μ-term, the 2×2 submatrix of gaugino and Higgsino resembles the chargino mixing matrix of the MSSM.

3.3.5 Quarks and squarks

The work in the scope of this thesis deals with the calculation of radiative corrections to the neutral scalar potential. The numerically most important one-loop corrections to the scalar potential are expected to arise from the stop/top-sector, analogous to the (N)MSSM [37–42] due to the huge Yukawa coupling of the (scalar) top. Thus, the quark and the squark sector are particularly important.

The quark sector is unchanged w.r.t. the MSSM at tree level. Neglecting flavor mixing of quarks, as we will do throughout this thesis, the up- and down-type quark masses m_i^u and m_i^d are given by

$$m_i^u = \frac{v_u Y_i^u}{\sqrt{2}} \quad \text{and} \quad m_i^d = \frac{v_d Y_i^d}{\sqrt{2}} \,. \tag{3.102}$$

The squark sector, on the other hand, is modified compared to the MSSM. F-term contributions of the squark potential arise through the quartic coupling of up-type quarks and one left-handed and the right-handed sneutrinos after EWSB. Neglecting flavor mixing in the squark sector, one finds for the up-type squark mass matrix $M_i^{\widetilde{u}}$ of generation i,

$$\left(M_i^{\widetilde{u}}\right)_{11} = \left(m_{\widetilde{Q}}^2\right)_i + \frac{1}{24}(3g_2^2 - g_1^2)(v_d^2 + v_{jL}v_{jL} - v_u^2) + \frac{1}{2}v_u^2 Y_i^{u2} \,, \tag{3.103}$$

$$\left(M_i^{\widetilde{u}}\right)_{12} = \frac{1}{2}\left(\sqrt{2}v_u A_i^u + v_{jL}Y_{jk}^{\nu}v_{kR} - v_d v_{jR}\lambda_j\right) Y_i^u \,, \tag{3.104}$$

$$\left(M_i^{\widetilde{u}}\right)_{22} = \left(m_{\widetilde{u}}^2\right)_i + \frac{1}{6}g_1^2(v_d^2 + v_{jL}v_{jL} - v_u^2) + \frac{1}{2}v_u^2 Y_i^{u2} \,. \tag{3.105}$$

Note that neutrino Yukawa couplings Y_{ij}^{ν} explicitly appear the in the non-diagonal element. For numerical results, these contributions will have a negligible effect. However, if one wishes to calculate loop-corrections to the neutral scalar potential stemming from up-type squarks in the loops, these terms have to be properly taken into account for successfully renormalizing the potential. The mass eigenstates $\widetilde{u}_{i1}$ and $\widetilde{u}_{i2}$ are obtained by the unitary transformation

$$\begin{pmatrix}\widetilde{u}_{i1}\\ \widetilde{u}_{i2}\end{pmatrix} = U_i^{\widetilde{u}}\begin{pmatrix}\widetilde{u}_{iL}\\ \widetilde{u}_{iR}\end{pmatrix} \,, \qquad U_i^{\widetilde{u}}U_i^{\widetilde{u}\dagger} = \mathbb{1} \,. \tag{3.106}$$

For the down-type squarks the tree-level mass matrix $M_i^{\widetilde{d}}$ is given by

$$\left(M_i^{\widetilde{d}}\right)_{11} = \left(m_{\widetilde{Q}}^2\right)_i - \frac{1}{24}(3g_2^2 + g_1^2)(v_d^2 + v_{jL}v_{jL} - v_u^2) + \frac{1}{2}v_d^2 Y_i^{d2} \,, \tag{3.107}$$

$$\left(M_i^{\widetilde{d}}\right)_{12} = \frac{1}{2}\left(\sqrt{2}v_d A_i^d - v_u\lambda_j v_{jR}\right) Y_i^d \,, \tag{3.108}$$

$$\left(M_i^{\widetilde{d}}\right)_{22} = \left(m_{\widetilde{d}}^2\right)_i - \frac{1}{12}g_1^2(v_d^2 + v_{jL}v_{jL} - v_u^2) + \frac{1}{2}v_d^2 Y_i^{d2} \,. \tag{3.109}$$

The mass matrices $M_i^{\widetilde{d}}$ do not depend on Y_{ij}^{ν} explicitly. Neglecting terms proportional to v_{iL} and replacing $\lambda_i v_{iR}$ by the effective μ-term defined in Eq. (3.49), the mass matrix $M_i^{\widetilde{d}}$ is unchanged w.r.t. the MSSM. The mass eigenstates $\widetilde{d}_{i1}$ and $\widetilde{d}_{i2}$ are obtained by the unitary transformation

$$\begin{pmatrix}\widetilde{d}_{i1}\\ \widetilde{d}_{i2}\end{pmatrix} = U_i^{\widetilde{d}}\begin{pmatrix}\widetilde{d}_{iL}\\ \widetilde{d}_{iR}\end{pmatrix} \,, \qquad U_i^{\widetilde{d}}U_i^{\widetilde{d}\dagger} = \mathbb{1} \,. \tag{3.110}$$

3.3.6 Gravitino

Even though the $\mu\nu$SSM is an R-parity violating SUSY model, thus not featuring a stable LSP, it can still offer a dark matter candidate with a gravitino LSP having a lifetime longer than the age of the universe. Assuming that the gravitinos were produced during the reheating phase after inflation via the elastic scattering of particles in the thermal bath, the gravitino abundance can be estimated to be [43]

$$\Omega_{3/2}h^2 \sim 0.2 \left(\frac{T_R}{10^{10}\text{ GeV}}\right)\left(\frac{100\text{ GeV}}{m_{3/2}}\right)\left(\frac{m_{\widetilde{g}}}{1\text{ TeV}}\right) , \tag{3.111}$$

where $\Omega_{3/2}$ is the energy density of gravitino matter, h is the scale factor for the Hubble expansion rate, T_R is the reheating temperature, $m_{\widetilde{g}}$ the gluino mass and $m_{3/2}$ the gravitino mass. No direct information about the gravitino mass can be extracted from this relation, because there is a degeneracy due to the dependence on the reheating temperature.

The long lifetime of the gravitino LSP results from the suppression of its decays by the inverse of the Planck mass and by factors of Y^{ν}_{ij}. Nevertheless, the decays of the gravitinos lead to interesting experimental signatures. Depending on how much fraction of dark matter one assumes to be present in the form of gravitinos, bounds on the allowed mass window can be extracted. The most prominent decay channel of the gravitino is the two-body decay into a photon and a neutrino.[3] In the context of SUGRA the lifetime of the gravitino can be written as [26]

$$\tau_{3/2} \sim 3.8 \cdot 10^{27}\,\text{s} \left(\frac{10^{-16}}{|U_{\widetilde{\gamma}\nu}|^2}\right)\left(\frac{10\text{ GeV}}{m_{3/2}}\right)^3 , \tag{3.112}$$

where the suppression by Y^{ν}_{ij} is contained in the photino content of the neutrinos, given by

$$|U_{\widetilde{\gamma}\nu}|^2 = \sum_{i=1}^{3} |U^V_{i4}c_{\text{w}} + U^V_{i5}s_{\text{w}}|^2 . \tag{3.113}$$

Here c_{w} and s_{w} are the cosine and sin of the weak mixing angle, and U^V_{i4} and U^V_{i5} are the bino and the wino components of the neutrino ν_{iL}, respectively. This parameter takes on values of the order of [26]

$$|U_{\widetilde{\gamma}\nu}|^2 \sim 10^{-16}\text{–}10^{-12} , \tag{3.114}$$

so that the lifetime naturally is larger than the age of the universe of about 10^{17} s. This decay produces gamma rays that can be looked for by the FERMI satellite [44]. The resulting mass limits are briefly discussed in Sect. 3.4.

Regarding collider physics, the gravitino is only relevant for masses smaller than ~ 10 keV [45]. Otherwise, for larger gravitino masses, R-parity violating decays of SUSY particles directly into SM particles are much larger than decays into final states containing a gravitino. Thus, in the context of this thesis, the conclusions are independent of the presence of the gravitino. If we refer to a particle other than the gravitino as the LSP, it is implied that it actually might be the next-to LSP, because an even lighter, but for the Higgs sector irrelevant, gravitino can be present.

[3] Also three-body decays can be relevant for certain ranges of $m_{3/2}$ (see Sect. 3.4).

3.4 Current status

In this section we give a brief overview of the work that has already been done in the $\mu\nu$SSM. Some of the publications mentioned in this section were treating the simpler case of the $\mu\nu$SSM with one family of right-handed neutrinos. Nevertheless, general conclusions also valid for the full $\mu\nu$SSM can always be drawn.

The foundations of the model can be found in Ref. [1]. Therein the superpotential of the $\mu\nu$SSM was motivated and the idea of the electroweak seesaw mechanism in a SUSY context was formulated. Also, the gravitino as a dark matter candidate is already mentioned. The first discussions of the parameter space and general phenomenological conclusions can be found in Refs. [2, 29].

Several studies concentrated on the generation of appropriate neutrino masses and mixing angles. The neutrino Yukawa couplings act as Dirac mass parameters and, at the same time, are the parameters controlling the amount of R-parity violation in decays of LSPs other than the right-handed sneutrinos. Therefore, interesting correlations between the neutrino sector and the decay R-parity violating decays of the LSP were found [46]. Also the relations between the neutrino sector and the scalar sector in the context of spontaneous $\mathcal{CP}$-violation was investigated [28]. It was shown that at tree level the neutrino masses and mixing angles can be reproduced in agreement with experimental results [27, 28, 46]. Radiative corrections to the neutrino masses were determined in Refs. [47–49]. Corrections of the same order as the tree-level masses were found in the case of inverted mass ordering in which the overall mass scale of the neutrinos is smaller.

The collider phenomenology, in particular at the LHC, is probably the most studied topic in the context of the $\mu\nu$SSM. R-parity violating decays produce various distinct signals, in particular compared to the SM and other SUSY extensions of it [45, 47]. One immediate consequence of the smallness of Y^{ν}_{ij} is the possibility of displaced R-parity violating decays. Before the discovery of the SM-like Higgs boson, searches for unusual Higgs-boson decays containing displaced vertices were proposed [50]. Also after the discovery of the SM-like Higgs boson, the possibility of exotic Higgs-boson decays with [51] or without [30] displaced vertices was emphasized. Collider signals genuine to the $\mu\nu$SSM are also possible in processes unrelated to the SM-like Higgs boson. In Ref. [52] searches for novel prompt and displaced gauge-boson decays were proposed. The possibility of excluding parameter space containing gauge-singlet like scalars or fermions with masses below M_W with LHC data was discussed. Observable signatures of the prompt or displaced decay of a left-handed τ-sneutrino LSP were studied in Refs. [11, 53, 54]. Furthermore, electroweak fermions as the LSP were shown to be able to produce exotic multilepton signals together with missing energy from neutrinos [54, 55]. So far no direct evidence for SUSY particles that could be interpreted as a particle state of the $\mu\nu$SSM has been found.

Regarding cosmology, it was shown in Ref. [56] that the electroweak phase transition can be of first order, and that electroweak baryogenesis can be realized in the $\mu\nu$SSM. Further studies in the context of cosmology and astrophysics were treating the detection of gravitinos which were assumed to constitute the relic abundance of dark matter [57]. The gravitino decay into two-particle final states produces monochromatic γ-ray lines. The frequency of the γ-rays could provide direct information about the gravitino mass. So far, no experimental evidence for such γ-rays exists. Exclusion limits within the context of the $\mu\nu$SSM were extracted using data from the Fermi satellite [26, 58, 59]. In addition, broad regions of gravitino masses could be excluded by combining these results with exclusions from smooth spectral photon signatures stemming from three-

body decays of the gravitino [27]. Combining all these results, gravitino masses of a few GeV or larger are excluded assuming the gravitinos make up the total amount of dark matter in the universe.

Although already being a complicated model with a large amount of free parameter, even further extensions of the $\mu\nu$SSM were considered. In Ref. [60] the $\mu\nu$SSM was augmented with an extra U(1) gauge symmetry, where the charges of the fields are assigned to forbid baryon-number violating operators and therefore stabilize the proton. Also the domain wall problem can be avoided in this scenario, although exotic matter fields have to be introduced to obtain anomaly cancellation. In Ref. [61] a U(1) extension of the $\mu\nu$SSM was considered in order to restore an effective R-parity. In Ref. [12] the two Higgs fields were interpreted as a fourth family of leptons. In contrast to the three families of SM leptons, it is vector-like, since both Higgs fields are SU(2) doublets. In analogy, a fourth family of vector-like quarks was introduced to match the family structure in the lepton sector.

3.5 Aim of this work

The aim of the work done in the scope of this thesis in the framework of the $\mu\nu$SSM was to be able to make precise predictions for the Higgs-boson masses, with similar accuracy as already existing calculation for simpler SUSY models. This involves the calculation of radiative corrections to the propagators of the scalars. To incorporate the complete contributions at the one-loop level, which is necessary for SUSY-scales M_{Susy} of the order of ~ 1 TeV [62], the calculation was carried out in the Feynman-diagrammatic approach. This approach captures not only the leading logarithmic contributions, but also the subleading terms at each loop-order in perturbation theory being of

$$\mathcal{O}(\frac{v^2}{M_{\text{Susy}}^2}) \, . \tag{3.115}$$

Since bounds on the particle masses are usually way below the ones from the MSSM due to R-parity violation, the SUSY particles of the $\mu\nu$SSM can still be relatively light. Thus, it is crucial to take into account the subleading terms. In contrast to the effective potential approach, the diagrammatic method also includes the momentum-dependent contributions.

To obtain the radiative corrections to the scalar masses, we carried out the renormalization of the neutral scalar potential at the full one-loop level, at first in the $\mu\nu$SSM with one family of right-handed neutrinos [8], and afterwards in the $\mu\nu$SSM with three families of right-handed neutrinos [9]. The resulting mass corrections were numerically evaluated and the importance of different contributions were compared. Since a pure one-loop calculation contains a very large theory uncertainty regarding the prediction for the SM-like Higgs-boson mass, we supplemented the full one-loop corrections by available higher-order corrections from the MSSM. We explicitly checked that genuine one-loop corrections to the SM-like Higgs-boson mass from the $\mu\nu$SSM are subleading compared to the MSSM-like corrections. Hence, the higher-order contributions from the MSSM can be expected to cover the dominant fraction of missing higher-order contributions. The same was demonstrated for the genuine NMSSM-like contribution in Ref. [63]. We found numerical results for the SM-like Higgs-boson mass in agreement with the experiment value. The genuine $\mu\nu$SSM-like corrections compared to the ones from (N)MSSM-like couplings were found to be negligible concerning the SM-like Higgs-boson mass. This

indicates that the theory uncertainty of our Higgs-boson mass calculation is of the same level of accuracy as the one of the NMSSM [64].

To be able to match the one-loop corrections from the $\mu\nu$SSM with the higher-order corrections from the MSSM, it was essential to define a renormalization scheme as close as possible to the one used in the MSSM calculation. We therefore adopted a mixed on-shell-$\overline{\text{DR}}$ renormalization scheme in which some of the input parameters are directly identified with physical observables. Since on-shell conditions were used, the renormalization procedure adopted goes beyond automated calculations of fixed-order corrections available for a broad spectrum of SUSY models [65–67] using a pure $\overline{\text{DR}}$ scheme. Thus, they have the disadvantage that parameters cannot be directly related to observables.[4]

Consequently, the work of this thesis extends other, in principle automated, calculations of higher-order corrections in the $\mu\nu$SSM in a twofold way. Firstly, we included the full one-loop corrections, and not only leading terms that can be captured by effective field theory methods. Secondly, we adopted on-shell conditions, thus facilitating the interpretation of parameters. We will describe in detail the renormalization of the scalar potential for both versions of the $\mu\nu$SSM in Ch. 5 and Ch. 6. There also the numerical analysis can be found. Before that, we give a brief summary of technical details relevant for the renormalization of gauge theories in Ch. 4. We restrain ourselves to the relevant details needed to follow the discussion of the renormalization procedure adopted.

Bibliography

[1] D. E. Lopez-Fogliani and C. Muñoz, "Proposal for a Supersymmetric Standard Model", *Phys. Rev. Lett.* **97** (2006) 041801, arXiv:hep-ph/0508297.

[2] C. Muñoz, "Phenomenology of a New Supersymmetric Standard Model: The $\mu\nu$SSM", *AIP Conf. Proc.* **1200** (2010) 413–416, arXiv:0909.5140.

[3] **Planck** Collaboration, P. A. R. Ade *et al.*, "Planck 2015 results. XIII. Cosmological parameters", *Astron. Astrophys.* **594** (2016) A13, arXiv:1502.01589.

[4] C. Kraus *et al.*, "Final results from phase II of the Mainz neutrino mass search in tritium beta decay", *Eur. Phys. J.* **C40** (2005) 447–468, arXiv:hep-ex/0412056.

[5] **Troitsk** Collaboration, V. N. Aseev *et al.*, "An upper limit on electron antineutrino mass from Troitsk experiment", *Phys. Rev.* **D84** (2011) 112003, arXiv:1108.5034.

[6] S. A. Abel and C. Munoz, "Quark and lepton masses and mixing angles from superstring constructions", *JHEP* **02** (2003) 010, arXiv:hep-ph/0212258.

[7] S. Weinberg, "Baryon and Lepton Nonconserving Processes", *Phys. Rev. Lett.* **43** (1979) 1566–1570.

[8] T. Biekötter, S. Heinemeyer, and C. Muñoz, "Precise prediction for the Higgs-boson masses in the $\mu\nu$SSM", *Eur. Phys. J.* **C78** (2018), no. 6, 504, arXiv:1712.07475.

[4] It is not straight forward to compare the results of our mixed OS-$\overline{\text{DR}}$ calculation with the results of the automated spectrum generators. The latter suffer from the fact that it is technically challenging to take into account all the details given by the complexity of the $\mu\nu$SSM.

[9] T. Biekötter, S. Heinemeyer, and C. Muñoz, "Precise prediction for the Higgs-Boson Masses in the $\mu\nu$SSM with three right-handed neutrino superfields", arXiv:1906.06173.

[10] A. Brignole, L. E. Ibanez, and C. Munoz, "Soft supersymmetry breaking terms from supergravity and superstring models", *Adv. Ser. Direct. High Energy Phys.* **18** (1998) 125–148, arXiv:hep-ph/9707209.

[11] P. Ghosh, I. Lara, D. E. Lopez-Fogliani, C. Munoz, and R. Ruiz de Austri, "Searching for left sneutrino LSP at the LHC", *Int. J. Mod. Phys.* **A33** (2018), no. 18n19, 1850110, arXiv:1707.02471.

[12] D. E. Lopez-Fogliani and C. Muñoz, "On a reinterpretation of the Higgs field in supersymmetry and a proposal for new quarks", *Phys. Lett.* **B771** (2017) 136–141, arXiv:1701.02652.

[13] L. Girardello and M. T. Grisaru, "Soft Breaking of Supersymmetry", *Nucl. Phys.* **B194** (1982) 65.

[14] S. P. Martin, "A Supersymmetry primer", arXiv:hep-ph/9709356, [Adv. Ser. Direct. High Energy Phys.18,1(1998)].

[15] U. Ellwanger, "Nonrenormalizable interactions from supergravity, quantum corrections and effective low-energy theories", *Phys. Lett.* **133B** (1983) 187–191.

[16] Ya. B. Zeldovich, I. Yu. Kobzarev, and L. B. Okun, "Cosmological Consequences of the Spontaneous Breakdown of Discrete Symmetry", *Zh. Eksp. Teor. Fiz.* **67** (1974) 3–11, [Sov. Phys. JETP40,1(1974)].

[17] B. Rai and G. Senjanovic, "Gravity and domain wall problem", *Phys. Rev.* **D49** (1994) 2729–2733, arXiv:hep-ph/9301240.

[18] S. A. Abel, "Destabilizing divergences in the NMSSM", *Nucl. Phys.* **B480** (1996) 55–72, arXiv:hep-ph/9609323.

[19] J. M. Frere, D. R. T. Jones, and S. Raby, "Fermion Masses and Induction of the Weak Scale by Supergravity", *Nucl. Phys.* **B222** (1983) 11–19.

[20] M. Chemtob, "Phenomenological constraints on broken R parity symmetry in supersymmetry models", *Prog. Part. Nucl. Phys.* **54** (2005) 71–191, arXiv:hep-ph/0406029.

[21] H. K. Dreiner, K. Nickel, F. Staub, and A. Vicente, "New bounds on trilinear R-parity violation from lepton flavor violating observables", *Phys. Rev.* **D86** (2012) 015003, arXiv:1204.5925.

[22] **SINDRUM II** Collaboration, J. Kaulard *et al.*, "Improved limit on the branching ratio of mu- –> e+ conversion on titanium", *Phys. Lett.* **B422** (1998) 334–338.

[23] **SINDRUM II** Collaboration, W. H. Bertl *et al.*, "A Search for muon to electron conversion in muonic gold", *Eur. Phys. J.* **C47** (2006) 337–346.

[24] **MEG** Collaboration, J. Adam *et al.*, "New limit on the lepton-flavour violating decay $\mu^+ \to e^+\gamma$", *Phys. Rev. Lett.* **107** (2011) 171801, arXiv:1107.5547.

[25] **L3** Collaboration, M. Acciarri *et al.*, "Search for R-parity breaking sneutrino exchange at LEP", *Phys. Lett.* **B414** (1997) 373–381.

[26] K.-Y. Choi, D. E. Lopez-Fogliani, C. Muñoz, and R. Ruiz de Austri, "Gamma-ray detection from gravitino dark matter decay in the $\mu\nu$SSM", *JCAP* **1003** (2010) 028, arXiv:0906.3681.

[27] G. A. Gómez-Vargas, D. E. López-Fogliani, C. Muñoz, A. D. Perez, and R. Ruiz de Austri, "Search for sharp and smooth spectral signatures of $\mu\nu$SSM gravitino dark matter with Fermi-LAT", *JCAP* **1703** (2017), no. 03, 047, arXiv:1608.08640.

[28] J. Fidalgo, D. E. Lopez-Fogliani, C. Muñoz, and R. Ruiz de Austri, "Neutrino Physics and Spontaneous CP Violation in the $\mu\nu$SSM", *JHEP* **08** (2009) 105, arXiv:0904.3112.

[29] N. Escudero, D. E. Lopez-Fogliani, C. Muñoz, and R. Ruiz de Austri, "Analysis of the parameter space and spectrum of the $\mu\nu$SSM", *JHEP* **12** (2008) 099, arXiv:0810.1507.

[30] P. Ghosh, D. E. Lopez-Fogliani, V. A. Mitsou, C. Muñoz, and R. Ruiz de Austri, "Probing the $\mu\nu$SSM with light scalars, pseudoscalars and neutralinos from the decay of a SM-like Higgs boson at the LHC", *JHEP* **11** (2014) 102, arXiv:1410.2070.

[31] U. Ellwanger, C. Hugonie, and A. M. Teixeira, "The Next-to-Minimal Supersymmetric Standard Model", *Phys. Rept.* **496** (2010) 1–77, arXiv:0910.1785.

[32] S. Heinemeyer, "MSSM Higgs physics at higher orders", *Int. J. Mod. Phys.* **A21** (2006) 2659–2772, arXiv:hep-ph/0407244.

[33] S. Heinemeyer, W. Hollik, and G. Weiglein, "Electroweak precision observables in the minimal supersymmetric standard model", *Phys. Rept.* **425** (2006) 265–368, arXiv:hep-ph/0412214.

[34] A. Djouadi, "The Anatomy of electro-weak symmetry breaking. II. The Higgs bosons in the minimal supersymmetric model", *Phys. Rept.* **459** (2008) 1–241, arXiv:hep-ph/0503173.

[35] B. Pontecorvo, "Neutrino Experiments and the Problem of Conservation of Leptonic Charge", *Sov. Phys. JETP* **26** (1968) 984–988, [Zh. Eksp. Teor. Fiz.53,1717(1967)].

[36] Z. Maki, M. Nakagawa, and S. Sakata, "Remarks on the unified model of elementary particles", *Prog. Theor. Phys.* **28** (1962) 870–880, [,34(1962)].

[37] J. Ellis, G. Ridolfi, and F. Zwirner, "Radiative corrections to the masses of supersymmetric higgs bosons", *Physics Letters B* **257** (1991), no. 1, 83 – 91.

[38] U. Ellwanger, "Radiative corrections to the neutral Higgs spectrum in supersymmetry with a gauge singlet", *Phys. Lett.* **B303** (1993) 271–276, arXiv:hep-ph/9302224.

[39] T. Elliott, S. F. King, and P. L. White, "Supersymmetric Higgs bosons at the limit", *Phys. Lett.* **B305** (1993) 71–77, arXiv:hep-ph/9302202.

[40] T. Elliott, S. F. King, and P. L. White, "Squark contributions to Higgs boson masses in the next-to-minimal supersymmetric standard model", *Phys. Lett.* **B314** (1993) 56–63, arXiv:hep-ph/9305282.

[41] T. Elliott, S. F. King, and P. L. White, "Radiative corrections to Higgs boson masses in the next-to-minimal supersymmetric Standard Model", *Phys. Rev.* **D49** (1994) 2435–2456, arXiv:hep-ph/9308309.

[42] P. N. Pandita, "Radiative corrections to the scalar Higgs masses in a nonminimal supersymmetric Standard Model", *Z. Phys.* **C59** (1993) 575–584.

[43] M. Bolz, A. Brandenburg, and W. Buchmuller, "Thermal production of gravitinos", *Nucl. Phys.* **B606** (2001) 518–544, arXiv:hep-ph/0012052, [Erratum: Nucl. Phys.B790,336(2008)].

[44] **Fermi-LAT** Collaboration, W. B. Atwood *et al.*, "The Large Area Telescope on the Fermi Gamma-ray Space Telescope Mission", *Astrophys. J.* **697** (2009) 1071–1102, arXiv:0902.1089.

[45] J. Fidalgo, D. E. Lopez-Fogliani, C. Munoz, and R. Ruiz de Austri, "The Higgs sector of the $\mu\nu$SSM and collider physics", *JHEP* **10** (2011) 020, arXiv:1107.4614.

[46] P. Ghosh and S. Roy, "Neutrino masses and mixing, lightest neutralino decays and a solution to the μ problem in supersymmetry", *JHEP* **04** (2009) 069, arXiv:0812.0084.

[47] A. Bartl, M. Hirsch, A. Vicente, S. Liebler, and W. Porod, "LHC phenomenology of the $\mu\nu$SSM", *JHEP* **05** (2009) 120, arXiv:0903.3596.

[48] P. Ghosh, P. Dey, B. Mukhopadhyaya, and S. Roy, "Radiative contribution to neutrino masses and mixing in $\mu\nu$SSM", *JHEP* **05** (2010) 087, arXiv:1002.2705.

[49] S. Liebler and W. Porod, "On-shell renormalization of neutralino and chargino mass matrices in R-parity violating models - Correlation between LSP decays and neutrino mixing angles revisited", *Nucl. Phys.* **B855** (2012) 774–800, arXiv:1106.2921.

[50] P. Bandyopadhyay, P. Ghosh, and S. Roy, "Unusual Higgs boson signal in R-parity violating nonminimal supersymmetric models at the LHC", *Phys. Rev.* **D84** (2011) 115022, arXiv:1012.5762.

[51] P. Ghosh, D. E. Lopez-Fogliani, V. A. Mitsou, C. Munoz, and R. Ruiz de Austri, "Probing the μ-from-ν supersymmetric standard model with displaced multileptons from the decay of a Higgs boson at the LHC", *Phys. Rev.* **D88** (2013) 015009, arXiv:1211.3177.

[52] P. Ghosh, D. E. López-Fogliani, V. A. Mitsou, C. Muñoz, and R. Ruiz de Austri, "Hunting physics beyond the standard model with unusual $W^{\pm}$ and Z decays", *Phys. Rev.* **D91** (2015), no. 3, 035020, arXiv:1403.3675.

[53] I. Lara, D. E. López-Fogliani, C. Muñoz, N. Nagata, H. Otono, and R. Ruiz De Austri, "Looking for the left sneutrino LSP with displaced-vertex searches", *Phys. Rev.* **D98** (2018), no. 7, 075004, arXiv:1804.00067.

[54] I. Lara Pérez, "Probing the electroweak sector of the $\mu\nu$SSM at the LHC". https://repositorio.uam.es/handle/10486/686773, PhD thesis, 2019-01-22.

[55] I. Lara, D. E. López-Fogliani, and C. Muñoz, "Electroweak superpartners scrutinized at the LHC in events with multi-leptons", *Phys. Lett.* **B790** (2019) 176–183, arXiv:1810.12455.

[56] D. J. H. Chung and A. J. Long, "Electroweak Phase Transition in the munuSSM", *Phys. Rev.* **D81** (2010) 123531, arXiv:1004.0942.

[57] C. Munoz, "The mu nu SSM and gravitino dark matter", *AIP Conf. Proc.* **1178** (2009), no. 1, 1–7, arXiv:0909.4775.

[58] G. A. Gomez-Vargas, M. Fornasa, F. Zandanel, A. J. Cuesta, C. Muñoz, F. Prada, and G. Yepes, "CLUES on Fermi-LAT prospects for the extragalactic detection of munuSSM gravitino Dark Matter", *JCAP* **1202** (2012) 001, arXiv:1110.3305.

[59] **Fermi-LAT** Collaboration, A. Albert, G. A. Gomez-Vargas, M. Grefe, C. Muñoz, C. Weniger, E. D. Bloom, E. Charles, M. N. Mazziotta, and A. Morselli, "Search for 100 MeV to 10 GeV γ-ray lines in the Fermi-LAT data and implications for gravitino dark matter in $\mu\nu$SSM", *JCAP* **1410** (2014), no. 10, 023, arXiv:1406.3430.

[60] J. Fidalgo and C. Munoz, "The $\mu\nu$SSM with an Extra U(1)", *JHEP* **04** (2012) 090, arXiv:1111.2836.

[61] V. Martín-Lozano and S. Oviedo-Casado, "The non-Universal U(1) gauge extended $\mu\nu$SSM: anomalies cancellation and singular phenomenology", *JHEP* **09** (2018) 102, arXiv:1804.02378.

[62] P. Draper and H. Rzehak, "A Review of Higgs Mass Calculations in Supersymmetric Models", *Phys. Rept.* **619** (2016) 1–24, arXiv:1601.01890.

[63] P. Drechsel, L. Galeta, S. Heinemeyer, and G. Weiglein, "Precise Predictions for the Higgs-Boson Masses in the NMSSM", *Eur. Phys. J.* **C77** (2017), no. 1, 42, arXiv:1601.08100.

[64] P. Drechsel, "Precise Predictions for Higgs Physics in the Next-to-Minimal Supersymmetric Standard Model (NMSSM)", DESY-THESIS-2016-019, Hamburg, 2016

[65] F. Staub, "SARAH 4 : A tool for (not only SUSY) model builders", *Comput. Phys. Commun.* **185** (2014) 1773–1790, arXiv:1309.7223.

[66] M. D. Goodsell, K. Nickel, and F. Staub, "Two-Loop Higgs mass calculations in supersymmetric models beyond the MSSM with SARAH and SPheno", *Eur. Phys. J.* **C75** (2015), no. 1, 32, arXiv:1411.0675.

[67] P. Athron, M. Bach, D. Harries, T. Kwasnitza, J.-h. Park, D. Stöckinger, A. Voigt, and J. Ziebell, "FlexibleSUSY 2.0: Extensions to investigate the phenomenology of SUSY and non-SUSY models", *Comput. Phys. Commun.* **230** (2018) 145–217, arXiv:1710.03760.

Chapter 4

Ultraviolet divergences and renormalization

In Ch. 3 we introduced the neutral scalar potential of the $\mu\nu$SSM. However, the discussion was restricted to the tree level, meaning the lowest order of perturbation theory. In the context of SUSY the radiative corrections to the scalar potential are sizable (see the discussion in Sect. 4.4). In perturbation theory, these corrections are given by higher-order Feynman diagrams containing closed loops. The Higgs-boson masses, for instance, at leading order given by the squares of the eigenvalues of the tree-level mass matrix (see Eq. (3.34)), will receive quantum corrections by self-energy diagrams as the ones shown in Fig. 2.1. Regarding the amplitude of these kind of diagrams, each loop is associated with an integral

$$\int d^4q \, , \tag{4.1}$$

where q is the four-momentum of the particles running in the loop. In the limit of large momentum, these kind of integrals can diverge, so that so-called ultraviolet (UV) divergence arise. The S-matrix of a given quantum field theory (QFTs) would be ill defined without removing the UV divergences. With each order higher in perturbation theory, extra loops are present in the diagrams, leading to further UV divergences.

Fortunately, certain types of local QFTs can be cured from the appearance of UV divergences by a suitable subtraction procedure [1]. Such QFTs are referred to as (perturbatively) renormalizable. The basic idea consists of canceling the UV divergences stemming from closed loops within Feynman diagrams by introducing the same "amount" of divergence into the bare parameters of the Lagrangian, i.e., renormalizing them by multiplying an infinite renormalization constant Z. The bare parameters are then split into a renormalized parameter and a parameter counterterm by expanding the renormalization constant around one. We can write for the bare parameters of the Lagrangian, such as masses m_0, couplings g_0 and the fields ϕ_0 (neglecting spinor and Lorentz indices for fermions and vector bosons for the moment),

$$m_0 \to Z_m m \quad = m + \delta m \, , \tag{4.2}$$

$$g_0 \to Z_g g \quad = g + \delta g \, , \tag{4.3}$$

$$\phi_{0_i} \to Z^{1/2}_{\phi_i\phi_j}\phi_j = (\delta_{ij} + \frac{1}{2}\delta Z_{\phi_i\phi_j})\phi_j \, . \tag{4.4}$$

Then the Lagrangian can be expressed in terms of the renormalized parameters m, g and

ϕ, and the counterterm Lagrangian $\delta\mathcal{L}$,

$$\mathcal{L}(m_0, g_0, \phi_0) \to \mathcal{L}(m, g, \phi) + \delta\mathcal{L}(m, g, \phi, \delta m, \delta g, \delta Z_\phi) \; . \tag{4.5}$$

If the QFT is renormalizable the counterterm Lagrangian provides so-called counterdiagrams which cancel all UV divergences order by order in perturbation theory. This is the same as stating that all UV divergences can be absorbed into a finite number of parameters, namely the bare parameters appearing in $\mathcal{L}$. In Ref. [1] it was proven that the renormalizabilty of a local QFT is given by the absence of parameters with negative mass dimensions. This is true in spontaneously broken gauge theories like the SM. It follows that a SUSY model is renormalizable when the superpotential does not contain couplings with negative mass dimensions. Also models with softly broken SUSY, containing operators as shown in Eq. (2.51), were proven to be renormalizable [2]. Even though further operators not contained in $\mathcal{L}_{\text{soft}}$ are generated at loop-level, they are irrelevant for vertex-corrections, and can safely be neglected.

In principle, the subtraction of divergent contribution leads to an arbitrariness, as the results can yield an arbitrary finite number. To eliminate this degeneracy, the renormalization procedure has to be done following a proper definition of what one divergence is, and how it is extracted from loop integrals. This process is called regularization. There are several ways of doing this, but in the context of SUSY regularization by dimensional reduction is the most appropriate one. It conserves SUSY up to at least the three-loop level [3, 4]. We will explain dimensional reduction and how it relates to other regularization procedures in Sect. 4.1.

After having properly regularized the UV divergences, the Green's functions of the underlying QFT can be split into divergent and finite pieces. The divergent piece is canceled by the divergent pieces of the counterterm contributions by definition. The finite pieces of the counterterms, however, must be chosen, since adding or subtracting finite terms to the counterterms does not spoil the finiteness of the Green's function. One has to choose a so-called renormalization condition for each parameter counterterm, thus defining the meaning of the parameter. The compound of renormalization conditions is referred to as the renormalization scheme. In our case, the renormalization scheme applied to the Higgs potential of the $\mu\nu$SSM is a mixed one. Parameters that can directly be related to physical observables are renormalized by deploying on-shell (OS) conditions. They are defined in such a way that tree-level relations are not altered by radiative corrections. For parameters that cannot directly be related to a physical observable $\overline{\text{DR}}$ conditions are utilized. We will define the exact form of OS and $\overline{\text{DR}}$ conditions in Sect. 4.3.

Finally, when the divergent pieces of the Green's functions are canceled accurately, the finite Green's functions can be used to construct UV finite S-matrix elements.[1] We stress that renormalization at the level of Green's functions is not always necessary to obtain finite predictions for physical observables [5]. Even with UV divergent Green's functions finite S-matrix elements can be found following the LSZ reduction formula [6]. However, when the prime interests are the radiative corrections to the mass spectrum of a model, as in the case of this thesis, it is much more practical to work with properly renormalized Green's function. For instance, the mass corrections to the neutral scalars are given by the renormalized two-point Green's functions, i.e., the renormalized self-energies. We will state the general formula for renormalized one-, two- and three-point

[1] The problem of infrared divergences possibly present in S-matrix elements are not tackled by renormalization and do not play a role in the scope of this thesis.

Green's functions relevant for the discussions in Chs. 5 and 6 in Sect. 4.2. We will also show the relevant Feynman diagrams contributing to the radiative corrections of these quantities.

4.1 Regularization

A very naive regularization of UV divergences is achieved by introducing a momentum cutoff Λ on the momentum integrals, such that the divergences turn out to be of the form

$$\lim_{\Lambda\to\infty} \Lambda^2 = \infty \,, \quad \text{and} \quad \lim_{\Lambda\to\infty} \log\Lambda = \infty \,. \tag{4.6}$$

However, this approach has the disadvantage that it not only breaks Lorentz invariance, but also the gauge symmetries, thus violating the Ward identities [7]. A regularization prescription that maintains both Lorentz and gauge invariance is dimensional regularization (DREG) [1, 8, 9]. In DREG amplitudes are calculated in general D-dimensional spacetime, with

$$D = 4 - 2\epsilon \,. \tag{4.7}$$

The loop integrals are then converted to

$$\int d^4q \to \frac{1}{(2\pi\mu)^{D-4}} \int d^Dq \,, \tag{4.8}$$

such that for $\epsilon > 0$ the integrals are rendered finite in the UV. The divergences for $D = 4$ will appear as poles in ϵ. Also the γ^μ-matrices and the metric tensor $g^{\mu\nu}$ are treated as D-dimensional objects, and the vector fields are treated as fields in D dimensions. The parameter μ is by definition of mass dimension one. Then, the mass dimensions of the integrals, and thus of the coupling parameters of the underlying field theory, are preserved in D dimensions.

DREG is the most popular regularization prescription for SM calculations. However, it is not suitable for Susy models, because it explicitly breaks Susy by creating a mismatch between fermionic and bosonic degrees of freedom. In Susy, it is more convenient to work with regularization by dimensional reduction (DRED). In DRED the integrals are again evaluated in D dimensions. However, in contrast to DREG, the trace algebra of Lorentz and Dirac indices is done in four dimensions. Since the integrals are evaluated in D dimensions, the poles in ϵ will at the one-loop level be the same in DREG and DRED. The finite pieces, on the other hand, are potentially different already at the one-loop level, when diagrams contain non-scalar fields. In our case, the difference practically boils down to additional terms proportional to ϵ in DREG, stemming from traces like

$$g_{\mu\nu}g^{\mu\nu} = \begin{cases} D = 4 - 2\epsilon \,, & \text{in DREG} \\ 4 \,, & \text{in DRED} \end{cases} . \tag{4.9}$$

When this trace appears in coefficients of UV divergent terms, there will be an additional finite piece in DREG compared to DRED, since

$$g_{\mu\nu}g^{\mu\nu} \cdot \frac{1}{\epsilon} = \begin{cases} \frac{4}{\epsilon} - 2 \,, & \text{in DREG} \\ \frac{4}{\epsilon} \,, & \text{in DRED} \end{cases} . \tag{4.10}$$

In our calculation the finite differences are of minor numerical impact, since they arise from diagrams with gauge bosons in the loops, and are of $\mathcal{O}(\alpha_{\text{em}})$. This yields only

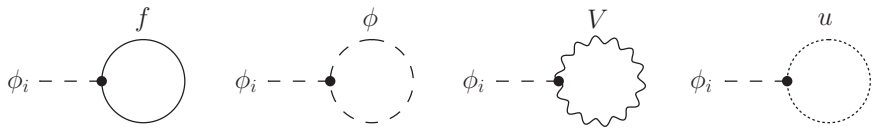

Figure 4.1: Generic one-loop diagrams contributing to to the tadpole coefficient T_i in the presence of fermions f, scalars ϕ, vector bosons V and ghosts u.

minor corrections to the scalar masses. Beyond the one-loop level, the differences described above can lead to contributions that are divergent in DREG, but finite in DRED calculations.

4.2 Renormalized Green's functions

For any process with n external particles, the higher-order corrections to the n-point Green's function Γ_n are obtained in perturbation theory by calculating the amplitudes of the one-particle irreducible Feynman-diagrams at a certain loop-order. To obtain the relevant parameter counterterms and field renormalization constants at the one-loop level, it is necessary to compute one-loop vertex-corrected Green's functions $\hat{\Gamma}_n^{(1)}$ (we denote renormalized quantities with a hat in the following). The unrenormalized quantities $\Gamma_n^{(1)}$ are defined by the Feynman diagrams constructed from the Feynman rules based on the initial Lagrangian expressed in terms of the renormalized parameters $\mathcal{L}(m, g, \phi)$ (see Eq. (4.5)). The renormalized Green's functions $\hat{\Gamma}_n^{(1)}$ are then obtained by subtracting the contributions from the counterdiagrams $\delta\hat{\Gamma}_n^{(1)}$, derived from the counterterm Lagrangian $\delta\mathcal{L}$. As already explained, the divergent parts of the parameter counterterms and the field renormalization counterterms can be determined by demanding that $\hat{\Gamma}_n^{(1)}$ is UV finite. The general formula for $\hat{\Gamma}_n^{(1)}$ depends on the number of external legs n and on the type of external fields. The counterterm $\delta\hat{\Gamma}_n^{(1)}$ is a function of the parameter counterterms δm and δg (see Eqs. (4.2) and (4.3)), whose form is defined by the tree-level expression $\Gamma_n^{(0)}$.

All counterterms required to renormalize the scalar potential of the $\mu\nu$SSM can be extracted by calculating renormalized one-, two- and three-point functions. This is related to the fact that in SUSY the quartic interactions are functions of the fundamental parameters of the theory, thus not containing further free parameters with independent counterterms. We will shortly summarize the general formulas for the renormalized Green's functions relevant for the discussion in Sect. 5.1 and Sect. 6.1. We also show the topologies of one-particle irreducibel Feynman diagrams contributing to the one-loop corrections. In some cases, we were only interested in the divergent parts of the one-loop amplitudes. Then, it can be more convenient to calculate the diagrams in the interaction basis instead of the mass eigenstate basis. We will show also the contributing topologies in the interaction basis for these cases.

Scalar 1-point functions: Tadpoles

A necessary conditions that the values used for the free parameters correspond to a minimum of the scalar potential is that the first derivatives of the Lagrangian w.r.t. fields vanish. At lowest order, this means that the tree-level tadpole coefficients defined by

$$T_i^{(0)} = \left.\frac{\partial\mathcal{L}}{\partial\phi_i}\right|_{\phi_j\to 0\ ,\ j=1,2,\ldots}\ , \tag{4.11}$$

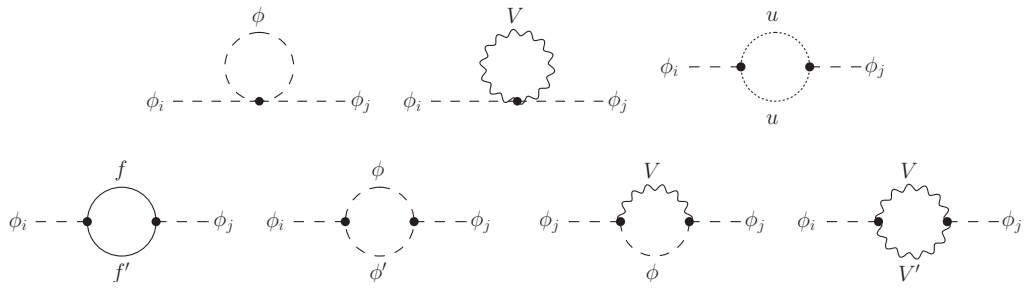

Figure 4.2: As in Fig. 4.1 for the scalar self-energies $\Sigma_{\phi_i\phi_j}$.

have to vanish. In principle, there will be a tree-level tadpole equation

$$T_i^{(0)} = 0 \,, \tag{4.12}$$

for each scalar field ϕ_i of the model. However, fields charged under an unbroken symmetry cannot have a linear term in $\mathcal{L}$, such that the total number of tadpole equations is given by the number of scalar fields that acquire a vev, or twice this number when $\mathcal{CP}$-violation is considered.

At the one-loop level, radiative corrections $T_i^{(1)}$ to the tadpole coefficients T_i are produced via tadpole diagrams as shown in Fig. 4.1. Since ϕ_i cannot be charged under an unbroken gauge group, only diagrams with gauge bosons and Faddeev-Popov ghosts belonging to spontaneously broken gauge groups in the loop can contribute to $T_i^{(1)}$. The renormalized tadpole coefficients $\hat{T}_i^{(1)}$ are then given by

$$\hat{T}_i^{(1)} = T_i^{(0)} + T_i^{(1)} + \delta T_i^{(1)} = T_i^{(1)} + \delta T_i^{(1)} \,. \tag{4.13}$$

Scalar 2-point functions: Self-energies

The inverse propagator matrix of mixing scalar fields ϕ_i is given at tree level by

$$\Gamma^{(0)}_{\phi_i\phi_j}(p^2) = \mathrm{i}\delta_{ij}\left(p^2 - m^2_{\phi_i\phi_j}\right) - \mathrm{i}\,(1-\delta_{ij})\, m^2_{\phi_i\phi_j} \,, \tag{4.14}$$

where p^2 is the momentum squared and $m^2_{\phi_i\phi_j}$ is the tree-level mass matrix of the scalars ϕ_i, defined by

$$m^2_{\phi_i\phi_j} = -\left.\frac{\partial^2\mathcal{L}}{\partial\phi_i\partial\phi_j^*}\right|_{\phi_k\to 0\,,\; k=1,2,\ldots} \,. \tag{4.15}$$

In the mass eigenstate basis, i.e., the basis in which $m^2_{\phi_i\phi_j}$ is diagonal, the second term in Eq. (4.14) vanishes and the diagonal elements are the scalar masses squared.

Radiative corrections are usually incorporated in terms of the renormalized self-energies $\hat{\Sigma}_{\phi_i\phi_j}$, such that

$$\begin{aligned}
\hat{\Gamma}^{(1)}_{\phi_i\phi_j}(p^2) &= \Gamma^{(0)}_{\phi_i\phi_j}(p^2) + \mathrm{i}\hat{\Sigma}^{(1)}_{\phi_i\phi_j}(p^2) \,, \\
\hat{\Sigma}^{(1)}_{\phi_i\phi_j}(p^2) &= \Sigma^{(1)}_{\phi_i\phi_j}(p^2) + \frac{1}{2}p^2\left(\delta Z_{\phi_j\phi_i} + \delta Z_{\phi_i\phi_j}\right) \\
&\quad - \frac{1}{2}\left(m^2_{\phi_k\phi_j}\delta Z_{\phi_k\phi_i} + m^2_{\phi_i\phi_k}\delta Z_{\phi_k\phi_j}\right) - \delta m^2_{\phi_i\phi_j} \,,
\end{aligned} \tag{4.16}$$

where in the second line the summation over the repeated index k is implied. We assumed that there is no $\mathcal{CP}$-violation, so that the mass matrix is real. The precise form of the

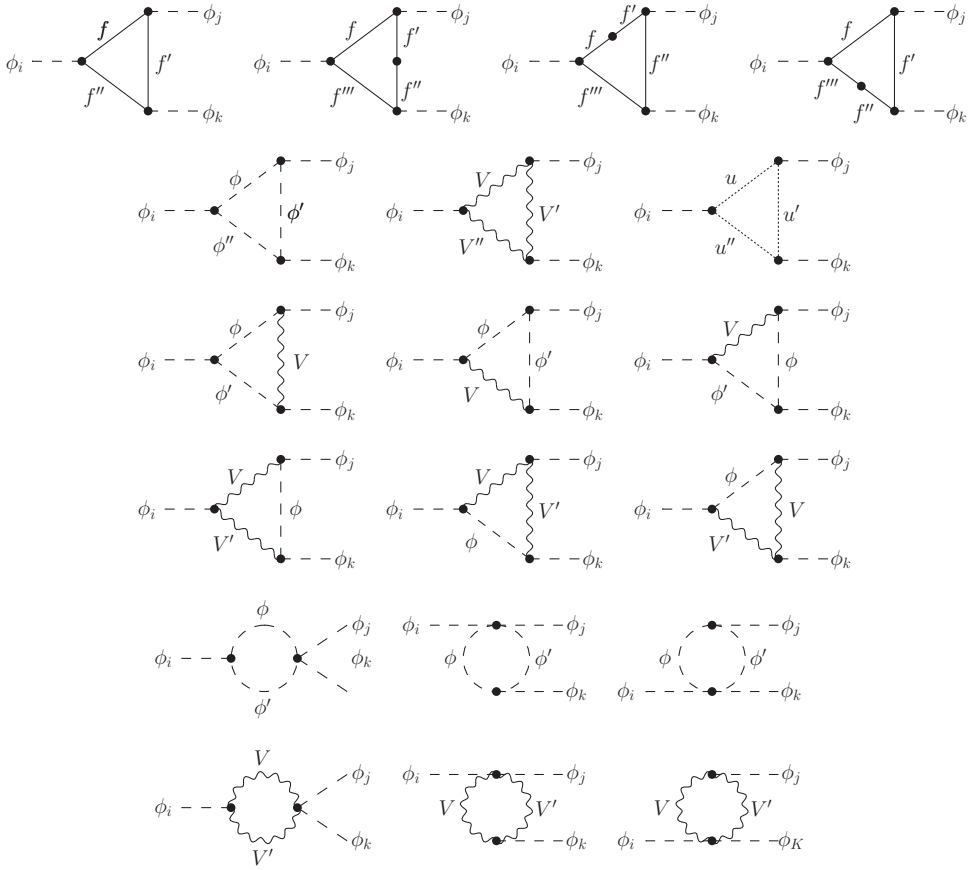

Figure 4.3: As in Fig. 4.1 for the divergent part of the scalar 3-point function $\Gamma_{\phi_i\phi_j\phi_k}$ in the interaction basis. The diagrams with a mass insertion (first row) are relevant in the interaction basis.

field renormalization counterterms $\delta Z_{\phi_i\phi_j}$ and the mass counterterms $\delta m^2_{\phi_i\phi_j}$ depends on the renormalization scheme applied. At the one-loop level, the radiative corrections $\Sigma^{(1)}_{\phi_i\phi_j}$ arise from self-energy diagrams shown in Fig. 4.2.

Scalar 3-point functions

The counterterms for some of the parameters of the Higgs potential of the $\mu\nu$SSM were extracted from radiative corrections to the scalar 3-point Green's functions $\Gamma_{\phi_i\phi_j\phi_k}$. At tree-level the vertices are simply given by

$$\Gamma^{(0)}_{\phi_i\phi_j\phi_k} = \left.\frac{\partial^3\mathcal{L}}{\partial\phi_i\partial\phi_j\partial\phi_k}\right|_{\phi_l\to 0\ ,\ l=1,2,\ldots} . \tag{4.17}$$

The general formula for the renormalized Green's function at the one-loop level is reads

$$\hat{\Gamma}^{(1)}_{\phi_i\phi_j\phi_k} = \Gamma^{(0)}_{\phi_i\phi_j\phi_k} + \Gamma^{(1)}_{\phi_i\phi_j\phi_k} - \frac{1}{2}\Big(\Gamma^{(0)}_{\phi_l\phi_j\phi_k}\delta Z_{\phi_l\phi_i} + \Gamma^{(0)}_{\phi_i\phi_l\phi_k}\delta Z_{\phi_l\phi_j} + \Gamma^{(0)}_{\phi_i\phi_j\phi_l}\delta Z_{\phi_l\phi_k}\Big) - \delta\Gamma^{(1)}_{\phi_i\phi_j\phi_k} . \tag{4.18}$$

The contribution in the bracket are the counterterms from the scalar field renormalization. It was assumed that $\Gamma^{(0)}_{\phi_i\phi_j\phi_k}$ does not depend on the momentum. The vertex

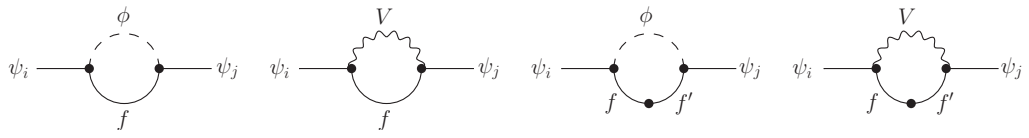

Figure 4.4: As in Fig. 4.1 for the divergent part of the fermionic self-energy $\Sigma_{\psi_i\psi_j}$. The diagrams with a mass insertion are relevant in the interaction basis.

counterterm $\delta\Gamma^{(1)}_{\phi_i\phi_j\phi_k}$ is a function of the counterterms of the fundamental parameters.

In our calculation, all parameters extracted from the radiative corrections to scalar 3-point functions were defined as $\overline{\text{DR}}$ parameters (see Sect. 4.3). Then, it is sufficient to compute only the divergent part $\Gamma^{(1)}_{\phi_i\phi_j\phi_k}|^{\text{div}}$. This can be done in the interaction basis, where diagrams with two-point vertices stemming from the non-diagonal elements of the mass matrices have to be included. While for the finite pieces one would have to calculate an infinite number of such diagrams with mass insertions, only a small amount contain UV divergences. Each mass insertion splits an internal line, so that an additional propagator is present in the amplitude. Each propagator contains inverse powers of the loop-momentum and the degree of divergence becomes smaller. It turns out that for scalar 3-point functions only diagrams with a mass insertion on an internal fermion line can potentially be UV divergent. In Fig. 4.3 we show the general form of all possibly UV divergent diagrams. The total number of diagrams that have to be calculated is usually much smaller in the interaction basis. Also, the corresponding amplitudes are much smaller, because the unrotated vertices can be used. Finally, the calculation of amplitudes in the interaction basis can be done purely analytically, because the vertices do not contain elements of mixing matrices of dimensions bigger than two, which have to be calculated numerically. Thus, it is possible to find compact analytical expressions for the parameter counterterms renormalized in the $\overline{\text{DR}}$ scheme.

Fermionic 2-point functions: Self-energies

As we saw in Ch. 3, the neutral scalar potential and the neutral fermion sector are highly connected in the $\mu\nu$SSM. A lot of parameters appear both in the scalar and the fermion mass matrices. We exploited this circumstance by extracting some of the $\overline{\text{DR}}$ parameters in the neutral fermion sector, where the number of potentially divergent diagrams in the interaction basis is drastically reduced. Apart from that, it is a good consistency check to apply the parameter counterterms to scalar and fermion self-energies, and check that the UV divergences cancel in both sectors.

At tree level the fermionic 2-point function reads

$$\Gamma^{(0)}_{\psi_i\psi_j}(p) = \mathrm{i}\delta_{ij}\left(\not{p} - m_{\psi_i\psi_j}\right) - \mathrm{i}(1-\delta_{ij})m_{\psi_i\psi_j} \ , \tag{4.19}$$

where the mass matrix for the mixing fermions ψ_i is given at tree level by

$$m_{\psi_i\psi_j} = -\left.\frac{\partial^2\mathcal{L}}{\partial\bar{\psi}_i\partial\psi_j}\right|_{\psi_k\to 0\ ,\ k=1,2,\ldots} \ , \tag{4.20}$$

and the second term is only present if one is not working in the mass eigenstate basis. At the one-loop level, the renormalized 2-point function can be written as

$$\begin{aligned}\hat{\Gamma}^{(1)}_{\psi_i\psi_j}(p) =& \Gamma^{(0)}_{\psi_i\psi_j}(p) + \mathrm{i}\hat{\Sigma}^{(1)}_{\psi_i\psi_j}(p) \ , \\ \hat{\Sigma}^{(1)}_{\psi_i\psi_j}(p) =& \not{p}\left(P_L\Sigma^{F_L(1)}_{\psi_i\psi_j}(p^2) + P_R\Sigma^{F_R(1)}_{\psi_i\psi_j}(p^2)\right) + P_L\Sigma^{S_L(1)}_{\psi_i\psi_j}(p^2) + P_R\Sigma^{S_R(1)}_{\psi_i\psi_j}(p^2)\end{aligned}$$

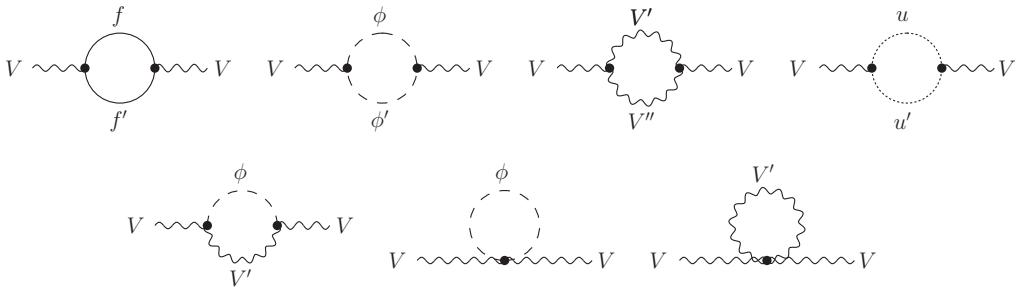

Figure 4.5: As in Fig. 4.1 for the vector boson self-energies Σ_{VV}.

$$+ \not{p}\left(P_L \delta Z^L_{\psi_i\psi_j} + P_R \delta Z^R_{\psi_i\psi_j}\right) - \frac{1}{2} P_L \left(m_{\psi_k\psi_j} \delta Z^L_{\psi_k\psi_j} + m_{\psi_i\psi_k} \delta Z^L_{\psi_k\psi_i}\right)$$
$$- \frac{1}{2} P_R \left(m_{\psi_k\psi_j} \delta Z^R_{\psi_k\psi_j} + m_{\psi_i\psi_k} \delta Z^R_{\psi_k\psi_i}\right) - \delta m_{\psi_i\psi_j} \; . \tag{4.21}$$

Here P_L and P_R are the left- and right-handed projectors, and $\Sigma^{F(1)}_{\psi_i\psi_j}$ and $\Sigma^{S(1)}_{\psi_i\psi_j}$ are the fermionic and scalar components of the self-energies, respectively. δZ^L and δZ^R are the field renormalization counterterms for the left- and right-handed components of the fermions. The mass counterterm $\delta m_{\psi_i\psi_j}$ is a function of the counterterms of the fundamental parameters. It renormalizes the scalar part of the self-energies. In the case of Majorana fermions, the self-energies are equal for left-handed and right-handed component, such that counterterms of fundamental parameters can be extracted from the scalar part of the self-energies at zero momentum,

$$\hat{\Sigma}^{S(1)}_{\psi_i\psi_j}(0) = \Sigma^{S(1)}_{\psi_i\psi_j}(0) - \frac{1}{2}\left(m_{\psi_k\psi_j} \delta Z_{\psi_k\psi_j} + m_{\psi_i\psi_k} \delta Z_{\psi_k\psi_i}\right) - \delta m_{\psi_i\psi_j} \; , \tag{4.22}$$

$$\text{with} \quad \delta Z_{\psi_i\psi_j} = \delta Z^L_{\psi_i\psi_j} = \delta Z^R_{\psi_i\psi_j} \; , \tag{4.23}$$

once the divergent parts of $\Sigma^{S(1)}_{\psi_i\psi_j}$ have been calculated. We show in Fig. 4.4 the potentially divergent generic diagrams in the interaction basis contributing to the fermion self-energies at the one-loop level.

Vector 2-point functions: Self-energies

In Chs. 5 and 6 we will make use of the masses M_W and M_Z of the SM gauge bosons as input parameters, because they are precisely measured observables. To renormalize the masses of vector fields, one needs to extract their counterterms from the 2-point Green's function which at the one-loop level can be written as

$$\hat{\Gamma}^{\mu\nu(1)}_{VV}(p) = -\mathrm{i} g^{\mu\nu} \delta_{ij} \left(p^2 - M_V^2\right) - \mathrm{i}\hat{\Sigma}^{\mu\nu(1)}_{VV}(p) \; , \quad V = Z, W \; ,$$
$$\hat{\Sigma}^{\mu\nu(1)}_{VV}(p) = \left(g^{\mu\nu} - \frac{p^\mu p^\nu}{p^2}\right) \hat{\Sigma}^{T(1)}_{VV}(p^2) + \frac{p^\mu p^\nu}{p^2} \hat{\Sigma}^{L(1)}_{VV}(p^2) \; . \tag{4.24}$$

$\hat{\Sigma}^T_{VV}$ and $\hat{\Sigma}^L_{VV}$ are the transverse and longitudinal parts of the renormalized self-energies, and we neglected effects from the mixing of the Z boson and the photon which has a numerically negligible impact on the scalar potential. Shifts to the pole of the vector bosons arise from the transverse part which appears with the coefficient $g^{\mu\nu}$ in the 2-point function. It reads at the one-loop level

$$\hat{\Sigma}^{T(1)}_{VV}(p^2) = \Sigma^{T(1)}_{VV}(p^2) + \delta Z_V \left(p^2 - M_V^2\right) - \delta M_V^2 \; . \tag{4.25}$$

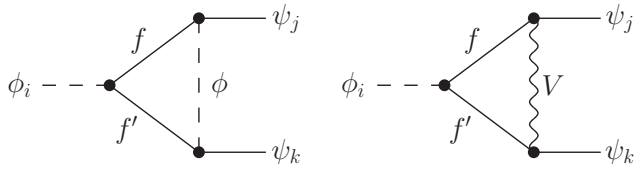

Figure 4.6: As in Fig. 4.1 for the divergent part of the fermion-scalar 3-point function $\Gamma_{\phi_i\psi_j\psi_k}$.

The diagrams contributing in the mass eigenstate basis to the self-energies $\Sigma_{VV}^{\mu\nu(1)}$ are shown in Fig. 4.5.

Fermion-scalar 3-point functions

The last renormalized Green's function that will be used is the 3-point function of a scalar coupled to a pair of Majorana fermions. In that case, the left- and right-handed projectors drop out and the relevant expression reduces to the same form as the ones for the trilinear scalar coupling shown in Eq. (4.18), except that the field renormalization constants of the fermion fields have to replace the ones of the scalar fields on the external legs. In the interaction basis, there is only one possibly divergent topology. We show the corresponding generic diagrams in Fig. 4.6.

4.3 Renormalization scheme

In the previous section, we stated the previous form of renormalized Green's functions from which counterterms of the fundamental parameters in the Lagrangian can be extracted. The divergent part of these counterterms is automatically fixed by demanding the finiteness of the renormalized Green's functions. The finite part, on the other hand, has to be fixed by renormalization conditions. Here we will explain the precise renormalization conditions used for the parameters appearing in the neutral scalar potential of the $\mu\nu$SSM.

4.3.1 $\overline{\text{DR}}$ conditions

Several parameters of the scalar potential cannot be directly related to a physical observable, such as a particle mass or a coupling strength. For practical purposes, we decided to renormalize these parameters using $\overline{\text{DR}}$ conditions. In the $\overline{\text{DR}}$ scheme a counterterm δX of a parameter X is defined by

$$\delta X = \Delta \cdot \text{const.} \,, \tag{4.26}$$

where Δ is defined by the UV poles expressed using DRED,

$$\Delta = \frac{1}{\epsilon} - \gamma_E + \ln 4\pi \,. \tag{4.27}$$

Here, the finite terms including the Euler-Mascharoni constant $\gamma_E = 0.5772\ldots$ are included by definition, because they always accompany the poles in ϵ when a loop integral is solved in D dimensions.

$\overline{\text{DR}}$ counterterms can thus be obtained by calculating just the divergent parts of unrenormalized n-point functions and extracting the component that has to be canceled by a certain parameter countertem. This is most easily done in the interaction basis.

Other advantages of $\overline{\text{DR}}$ conditions are that they can be given in compact analytical form, and that they are by definition process independent. At the one-loop level, a simple relation between a $\overline{\text{DR}}$ counterterm and the β-function of the corresponding parameter exists, because each pole in ϵ appears with a logarithm of the renormalization scale μ. We explicitly checked that our counterterms defined in the $\overline{\text{DR}}$ scheme fulfill the relation

$$\delta X = \frac{\beta_X^{(1)} \Delta}{32\pi^2} \,. \tag{4.28}$$

General formulas for $\beta_X^{(1)}$, i.e., the one-loop β-functions of the parameters X of local and renormalizable QFTs, exist in the literature [10–14]. In principle, these formulas could have been used directly to obtain counterterms of free parameters in the $\overline{\text{DR}}$ scheme. However, we decided to extract them independently from the renormalized Green's functions. By doing so, we perform an independent cross check of our results for the counterterms. Even more important, verifying the relation shown in Eq. (4.28) is an excellent test of the correct implementation of the mass matrices and tree-level couplings of the $\mu\nu$SSM which are huge expressions due to the complex particle mixings.

Furthermore, we will adopt $\overline{\text{DR}}$ conditions for the field renormalization constants Z_{ij}. The analog relation regarding the field renormalization counterterms is given by

$$\delta Z_{ij} = \left. \frac{\gamma_{ij}^{(1)} \Delta}{16\pi^2} \right|^{g_1, g_2 \to 0} \,, \tag{4.29}$$

where $\gamma_{ij}^{(1)}$ are the one-loop anomalous dimensions of the corresponding superfields. They are known at the one-loop level, also for theories with kinetic mixing [15, 16].

4.3.2 On-shell conditions

For a few parameters we will adopt so-called on-shell (OS) conditions. To be concrete, this will be the case for the tadpole coefficients and the SM gauge boson masses M_W and M_Z which are used as input parameters instead of the SM gauge couplings g_1 and g_2. OS conditions are defined in such a way, that the renormalized parameters have the same values as the parameters of the classical Lagrangian. Then, tree-level relations just involving parameters renormalized OS remain valid even at loop level.

For the renormalized tadpole coefficients $\hat{T}_i$ it is crucial to be still vanishing at loop level, since otherwise the values of the independent parameters in a certain benchmark point would not correspond anymore to a minimum of the scalar potential. Thus, the tadpole coefficients will be used as independent parameters. The OS renormalization conditions read

$$\hat{T}_i^{(1)} = 0 \,. \tag{4.30}$$

From Eq. (4.13) it then follows that the tadpole counterterms are given by

$$\delta T_i = -T_i^{(1)} \,. \tag{4.31}$$

For the gauge boson masses, the OS conditions are defined such that the radiative corrections to the poles of the propagators are absorbed into the mass counterterms δM_W^2 and δM_Z^2. From Eq. (4.24) and Eq. (4.25) the counterterms are then given by

$$\delta M_Z^2 = \text{Re}\left[\Sigma_{ZZ}^{T(1)}\left(M_Z^2\right)\right] \qquad \text{and} \qquad \delta M_W^2 = \text{Re}\left[\Sigma_{WW}^{T(1)}\left(M_W^2\right)\right] \,. \tag{4.32}$$

4.4 The SM-like Higgs-boson mass in SUSY

The discovery of the SM-like Higgs boson [17, 18] is of profound importance for extensions of the SM. Any BSM model has to accommodate a particle behaving according to the measured properties of the Higgs boson. In particular, its mass is already a precision observable, with an experimental uncertainty at the per-mille level [19–21].

SUSY relates the quartic scalar couplings to the gauge couplings and the superpotential parameters of the underlying theory. Therefore, within SUSY it is possible to make predictions for the scalar masses in terms of these model parameters. The prediction for the SM-like Higgs-boson mass in SUSY models is highly sensitive to radiative corrections [22, 23] which naturally implicates a theoretical uncertainty from missing higher-order contributions. Currently, the theory uncertainty of the SM-like Higgs-boson mass predictions are, depending on the parameter point considered, still an order of magnitude above the experimental uncertainty [24–26]. This is why a lot of effort goes towards a more precise Higgs-boson mass prediction [27].

If the SUSY-breaking scale is close to the electroweak scale, and thus SUSY particles are present with masses of the same order as the SM-like Higgs-boson mass, the complete radiative corrections at a certain order of perturbation theory can be computed by means of the Feynman-diagrammatic approach. If the SUSY-breaking scale is well above the TeV scale, effective field theory approaches yield more precise predictions [25, 28] by resumming the dominant logarithmic contributions to all orders of perturbation theory. In this thesis, the scalar masses of the $\mu\nu$SSM with one and three right-handed neutrinos were calculated at the full one-loop level (see Sect. 3.5), supplemented by dominant higher-order corrections taken over from the MSSM [29, 30]. Since our calculation is based on the previous work that was done in simpler SUSY models like the MSSM and the NMSSM, we give a brief summary of the status of calculation of the radiative corrections to the Higgs-boson masses in the MSSM and beyond.

In the MSSM the tree-level mass can be predicted by just two SUSY parameters, for instance, the ratio of the vevs of the Higgs doublets,

$$\tan\beta = \frac{v_u}{v_d} \,, \tag{4.33}$$

and either the mass of the $\mathcal{CP}$-odd Higgs boson M_A or the mass of the charged Higgs boson $M_{H^\pm}$. The tree-level mass is bounded from above by the Z-boson mass (see Sect. 2.5). Large loop corrections are required to achieve a Higgs-boson mass of ~ 125 GeV, where at the one-loop level the corrections of $\mathcal{O}(\alpha_t)$ (here we use $\alpha_f = (Y^f)^2/(4\pi)$, with Y^f denoting the fermion Yukawa coupling) are the largest contribution due to the huge top-Yukawa coupling. Beyond the one-loop level, the dominant two-loop corrections of $\mathcal{O}(\alpha_t\alpha_s)$ [31–36], $\mathcal{O}(\alpha_t^2)$ [37, 38], $\mathcal{O}(\alpha_b\alpha_s)$ [39, 40] and $\mathcal{O}(\alpha_t\alpha_b)$ [39] are known. These corrections, together with a resummation of leading and subleading logarithms from the top/stop sector [41] (see also [28, 42] for more details on this type of approach), a resummation of leading contributions from the bottom/sbottom sector [39, 40, 43–46] (see also [47, 48]) and momentum-dependent two-loop contributions [49, 50] (see also [51]) are included in the public code `FeynHiggs` [33, 41, 52–59]. The most recent version of `FeynHiggs` contains an improved effective field theory calculation relevant for large SUSY scales [58]. The complete two-loop QCD contributions in the $\mathcal{CP}$-violating MSSM were calculated in Ref. [60], but not yet included in `FeynHiggs`. A (nearly) full two-loop effective potential (EP) calculation, including even the leading three-loop corrections, has also been published [61, 62]. However, it is not publicly available as a computer

code. Furthermore, another leading three-loop calculation of $\mathcal{O}(\alpha_t\alpha_s^2)$, depending on the various SUSY mass hierarchies, has been performed [63, 64], resulting in the code `H3m` and is now available as a stand-alone code [65]. It was proven that regularization by dimensional reduction preserves supersymmetry at the required three-loop order [4]. A new calculation of the three-loop contributions of the $\mathcal{O}(\alpha_t\alpha_s^2)$ extends the validity of these corrections to the whole parameter space of the $\mathcal{CP}$-conserving MSSM [66]. Most recently, the leading terms of the $\mathcal{O}(\alpha_t\alpha_s^3)$ have been obtained by a resummation of terms at fourth logarithmic order. They are available through an updated version of the public code `Himalaya` [67]. The theoretical uncertainty on the lightest $\mathcal{CP}$-even Higgs-boson mass within the MSSM from unknown higher-order contributions is still at the level of about $2-3$ GeV for scalar top masses at the TeV-scale, where the actual uncertainty depends on the considered parameter region [24, 25, 54, 68, 69].

In the NMSSM the full one-loop calculation including the momentum dependence has been performed in the $\overline{\text{DR}}$ renormalization scheme in Ref. [70, 71], or in a mixed OS-$\overline{\text{DR}}$ scheme in Ref. [72–74]. Dominant two-loop contributions of $\mathcal{O}(\alpha_t\alpha_s, \alpha_t^2)$ have been calculated in the leading logarithmic approximation [75, 76], and of $\mathcal{O}(\alpha_t\alpha_s, \alpha_b\alpha_s)$ in the $\overline{\text{DR}}$ scheme in the EP approach [70]. The two-loop corrections involving only superpotential couplings were given in Ref. [77]. A two-loop calculation of the $\mathcal{O}(\alpha_t\alpha_s)$ corrections with the top/stop sector renormalized in the OS scheme or in the $\overline{\text{DR}}$ scheme was provided in Ref. [78], while the two-loop corrections of $\mathcal{O}(\alpha_t^2)$ in the $\mathcal{CP}$-violating NMSSM were calculated in a mixed OS-$\overline{\text{DR}}$ scheme [26]. These contributions are implemented in the public code `NMSSMCalc`. A consistent combination of a full one-loop calculation with all corrections beyond the one-loop level in the MSSM approximation was given in Ref. [74]. According to a comparison of the various two-loop contributions, at present the theoretical uncertainties from unknown higher-order corrections in the NMSSM are expected to be still larger than for the MSSM [26, 79, 80].

Beyond the MSSM and the NMSSM, only generic $\overline{\text{DR}}$ calculations of Higgs-boson mass corrections exist publicly available. An automated calculation of the full one-loop corrections, supplemented by partial two-loop corrections to neutral scalars [77] is implemented in the Mathematica package `SARAH` [81, 82]. It can be used to produce a spectrum generator based on the public code `SPheno` [83]. A hybrid Higgs-boson mass calculation combining effective field theory and fixed-order calculations for a generic class of SUSY models is publicly available in the code `FlexibleSUSY` [84], also using the expression for the renormalization group equations and fixed-order self-energies as they are calculated by `SARAH`.

Bibliography

[1] G. 't Hooft and M. J. G. Veltman, "Regularization and Renormalization of Gauge Fields", *Nucl. Phys.* **B44** (1972) 189–213.

[2] W. Hollik, E. Kraus, and D. Stockinger, "Renormalization of supersymmetric Yang-Mills theories with soft supersymmetry breaking", *Eur. Phys. J.* **C23** (2002) 735–747, arXiv:hep-ph/0007134.

[3] D. Stockinger, "Regularization by dimensional reduction: consistency, quantum action principle, and supersymmetry", *JHEP* **03** (2005) 076, arXiv:hep-ph/0503129.

[4] D. Stöckinger and J. Unger, "Three-loop MSSM Higgs-boson mass predictions and regularization by dimensional reduction", *Nucl. Phys.* **B935** (2018) 1–16, arXiv:1804.05619.

[5] M. D. Schwartz, "Quantum Field Theory and the Standard Model", Cambridge University Press, 2014.

[6] H. Lehmann, K. Symanzik, and W. Zimmermann, "On the formulation of quantized field theories", *Nuovo Cim.* **1** (1955) 205–225.

[7] M. E. Peskin and D. V. Schroeder, "An Introduction to quantum field theory", Addison-Wesley, Reading, USA, 1995.

[8] C. G. Bollini and J. J. Giambiagi, "Dimensional Renormalization: The Number of Dimensions as a Regularizing Parameter", *Nuovo Cim.* **B12** (1972) 20–26.

[9] J. F. Ashmore, "A Method of Gauge Invariant Regularization", *Lett. Nuovo Cim.* **4** (1972) 289–290.

[10] M. E. Machacek and M. T. Vaughn, "Two Loop Renormalization Group Equations in a General Quantum Field Theory. 2. Yukawa Couplings", *Nucl. Phys.* **B236** (1984) 221–232.

[11] S. P. Martin and M. T. Vaughn, "Two loop renormalization group equations for soft supersymmetry breaking couplings", *Phys. Rev.* **D50** (1994) 2282, arXiv:hep-ph/9311340, [Erratum: Phys. Rev.D78,039903(2008)].

[12] Y. Yamada, "Two loop renormalization group equations for soft SUSY breaking scalar interactions: Supergraph method", *Phys. Rev.* **D50** (1994) 3537–3545, arXiv:hep-ph/9401241.

[13] M.-x. Luo, H.-w. Wang, and Y. Xiao, "Two loop renormalization group equations in general gauge field theories", *Phys. Rev.* **D67** (2003) 065019, arXiv:hep-ph/0211440.

[14] M. Sperling, D. Stöckinger, and A. Voigt, "Renormalization of vacuum expectation values in spontaneously broken gauge theories", *JHEP* **07** (2013) 132, arXiv:1305.1548.

[15] M. E. Machacek and M. T. Vaughn, "Two Loop Renormalization Group Equations in a General Quantum Field Theory. 1. Wave Function Renormalization", *Nucl. Phys.* **B222** (1983) 83–103.

[16] R. M. Fonseca, M. Malinský, and F. Staub, "Renormalization group equations and matching in a general quantum field theory with kinetic mixing", *Phys. Lett.* **B726** (2013) 882–886, arXiv:1308.1674.

[17] **ATLAS** Collaboration, G. Aad *et al.*, "Observation of a new particle in the search for the Standard Model Higgs boson with the ATLAS detector at the LHC", *Phys. Lett.* **B716** (2012) 1–29, arXiv:1207.7214.

[18] **CMS** Collaboration, S. Chatrchyan *et al.*, "Observation of a new boson at a mass of 125 GeV with the CMS experiment at the LHC", *Phys. Lett.* **B716** (2012) 30–61, arXiv:1207.7235.

[19] **ATLAS, CMS** Collaboration, G. Aad *et al.*, "Combined Measurement of the Higgs Boson Mass in pp Collisions at $\sqrt{s} = 7$ and 8 TeV with the ATLAS and CMS Experiments", *Phys. Rev. Lett.* **114** (2015) 191803, arXiv:1503.07589.

[20] **ATLAS** Collaboration, M. Aaboud *et al.*, "Measurement of the Higgs boson mass in the $H \to ZZ^* \to 4\ell$ and $H \to \gamma\gamma$ channels with $\sqrt{s} = 13$ TeV pp collisions using the ATLAS detector", *Phys. Lett.* **B784** (2018) 345–366, arXiv:1806.00242.

[21] **CMS** Collaboration, A. M. Sirunyan *et al.*, "Measurements of properties of the Higgs boson decaying into the four-lepton final state in pp collisions at $\sqrt{s} = 13$ TeV", *JHEP* **11** (2017) 047, arXiv:1706.09936.

[22] Y. Okada, M. Yamaguchi, and T. Yanagida, "Upper bound of the lightest Higgs boson mass in the minimal supersymmetric standard model", *Prog. Theor. Phys.* **85** (1991) 1–6.

[23] J. R. Ellis, G. Ridolfi, and F. Zwirner, "Radiative corrections to the masses of supersymmetric Higgs bosons", *Phys. Lett.* **B257** (1991) 83–91.

[24] O. Buchmueller *et al.*, "Implications of Improved Higgs Mass Calculations for Supersymmetric Models", *Eur. Phys. J.* **C74** (2014), no. 3, 2809, arXiv:1312.5233.

[25] B. C. Allanach and A. Voigt, "Uncertainties in the Lightest CP Even Higgs Boson Mass Prediction in the Minimal Supersymmetric Standard Model: Fixed Order Versus Effective Field Theory Prediction", *Eur. Phys. J.* **C78** (2018), no. 7, 573, arXiv:1804.09410.

[26] T. N. Dao, R. Gröber, M. Krause, M. Mühlleitner, and H. Rzehak, "Two-Loop $\mathcal{O}(\alpha_t^2)$ Corrections to the Neutral Higgs Boson Masses in the CP-Violating NMSSM", arXiv:1903.11358.

[27] See: http://sites.google.com/site/kutsmh/home.

[28] P. Draper, G. Lee, and C. E. M. Wagner, "Precise estimates of the Higgs mass in heavy supersymmetry", *Phys. Rev.* **D89** (2014), no. 5, 055023, arXiv:1312.5743.

[29] T. Biekötter, S. Heinemeyer, and C. Muñoz, "Precise prediction for the Higgs-boson masses in the $\mu\nu$SSM", *Eur. Phys. J.* **C78** (2018), no. 6, 504, arXiv:1712.07475.

[30] T. Biekötter, S. Heinemeyer, and C. Muñoz, "Precise prediction for the Higgs-Boson Masses in the $\mu\nu$SSM with three right-handed neutrino superfields", arXiv:1906.06173.

[31] S. Heinemeyer, W. Hollik, and G. Weiglein, "QCD corrections to the masses of the neutral CP - even Higgs bosons in the MSSM", *Phys. Rev.* **D58** (1998) 091701, arXiv:hep-ph/9803277.

[32] S. Heinemeyer, W. Hollik, and G. Weiglein, "Precise prediction for the mass of the lightest Higgs boson in the MSSM", *Phys. Lett.* **B440** (1998) 296–304, arXiv:hep-ph/9807423.

[33] S. Heinemeyer, W. Hollik, and G. Weiglein, "The Masses of the neutral CP - even Higgs bosons in the MSSM: Accurate analysis at the two loop level", *Eur. Phys. J.* **C9** (1999) 343–366, arXiv:hep-ph/9812472.

[34] R.-J. Zhang, "Two loop effective potential calculation of the lightest CP even Higgs boson mass in the MSSM", *Phys. Lett.* **B447** (1999) 89–97, arXiv:hep-ph/9808299.

[35] J. R. Espinosa and R.-J. Zhang, "MSSM lightest CP even Higgs boson mass to O(alpha(s) alpha(t)): The Effective potential approach", *JHEP* **03** (2000) 026, arXiv:hep-ph/9912236.

[36] G. Degrassi, P. Slavich, and F. Zwirner, "On the neutral Higgs boson masses in the MSSM for arbitrary stop mixing", *Nucl. Phys.* **B611** (2001) 403–422, arXiv:hep-ph/0105096.

[37] J. R. Espinosa and R.-J. Zhang, "Complete two loop dominant corrections to the mass of the lightest CP even Higgs boson in the minimal supersymmetric standard model", *Nucl. Phys.* **B586** (2000) 3–38, arXiv:hep-ph/0003246.

[38] A. Brignole, G. Degrassi, P. Slavich, and F. Zwirner, "On the O(alpha(t)**2) two loop corrections to the neutral Higgs boson masses in the MSSM", *Nucl. Phys.* **B631** (2002) 195–218, arXiv:hep-ph/0112177.

[39] A. Brignole, G. Degrassi, P. Slavich, and F. Zwirner, "On the two loop sbottom corrections to the neutral Higgs boson masses in the MSSM", *Nucl. Phys.* **B643** (2002) 79–92, arXiv:hep-ph/0206101.

[40] S. Heinemeyer, W. Hollik, H. Rzehak, and G. Weiglein, "High-precision predictions for the MSSM Higgs sector at O(alpha(b) alpha(s))", *Eur. Phys. J.* **C39** (2005) 465–481, arXiv:hep-ph/0411114.

[41] T. Hahn, S. Heinemeyer, W. Hollik, H. Rzehak, and G. Weiglein, "High-Precision Predictions for the Light CP -Even Higgs Boson Mass of the Minimal Supersymmetric Standard Model", *Phys. Rev. Lett.* **112** (2014), no. 14, 141801, arXiv:1312.4937.

[42] G. Lee and C. E. M. Wagner, "Higgs bosons in heavy supersymmetry with an intermediate m_A", *Phys. Rev.* **D92** (2015), no. 7, 075032, arXiv:1508.00576.

[43] R. Hempfling, "Yukawa coupling unification with supersymmetric threshold corrections", *Phys. Rev.* **D49** (1994) 6168–6172.

[44] L. J. Hall, R. Rattazzi, and U. Sarid, "The Top quark mass in supersymmetric SO(10) unification", *Phys. Rev.* **D50** (1994) 7048–7065, arXiv:hep-ph/9306309.

[45] M. Carena, M. Olechowski, S. Pokorski, and C. E. M. Wagner, "Electroweak symmetry breaking and bottom - top Yukawa unification", *Nucl. Phys.* **B426** (1994) 269–300, arXiv:hep-ph/9402253.

[46] M. Carena, D. Garcia, U. Nierste, and C. E. M. Wagner, "Effective Lagrangian for the $\bar{t}bH^+$ interaction in the MSSM and charged Higgs phenomenology", *Nucl. Phys.* **B577** (2000) 88–120, arXiv:hep-ph/9912516.

[47] D. Noth and M. Spira, "Higgs Boson Couplings to Bottom Quarks: Two-Loop Supersymmetry-QCD Corrections", *Phys. Rev. Lett.* **101** (2008) 181801, arXiv:0808.0087.

[48] D. Noth and M. Spira, "Supersymmetric Higgs Yukawa Couplings to Bottom Quarks at next-to-next-to-leading Order", *JHEP* **06** (2011) 084, arXiv:1001.1935.

[49] S. Borowka, T. Hahn, S. Heinemeyer, G. Heinrich, and W. Hollik, "Momentum-dependent two-loop QCD corrections to the neutral Higgs-boson masses in the MSSM", *Eur. Phys. J.* **C74** (2014), no. 8, 2994, arXiv:1404.7074.

[50] S. Borowka, T. Hahn, S. Heinemeyer, G. Heinrich, and W. Hollik, "Renormalization scheme dependence of the two-loop QCD corrections to the neutral Higgs-boson masses in the MSSM", *Eur. Phys. J.* **C75** (2015), no. 9, 424, arXiv:1505.03133.

[51] G. Degrassi, S. Di Vita, and P. Slavich, "Two-loop QCD corrections to the MSSM Higgs masses beyond the effective-potential approximation", *Eur. Phys. J.* **C75** (2015), no. 2, 61, arXiv:1410.3432.

[52] S. Heinemeyer, W. Hollik, and G. Weiglein, "FeynHiggs: A Program for the calculation of the masses of the neutral CP even Higgs bosons in the MSSM", *Comput. Phys. Commun.* **124** (2000) 76–89, arXiv:hep-ph/9812320.

[53] T. Hahn, S. Heinemeyer, W. Hollik, H. Rzehak, and G. Weiglein, "FeynHiggs: A program for the calculation of MSSM Higgs-boson observables - Version 2.6.5", *Comput. Phys. Commun.* **180** (2009) 1426–1427.

[54] G. Degrassi, S. Heinemeyer, W. Hollik, P. Slavich, and G. Weiglein, "Towards high precision predictions for the MSSM Higgs sector", *Eur. Phys. J.* **C28** (2003) 133–143, arXiv:hep-ph/0212020.

[55] M. Frank, T. Hahn, S. Heinemeyer, W. Hollik, H. Rzehak, and G. Weiglein, "The Higgs Boson Masses and Mixings of the Complex MSSM in the Feynman-Diagrammatic Approach", *JHEP* **02** (2007) 047, arXiv:hep-ph/0611326.

[56] H. Bahl and W. Hollik, "Precise prediction for the light MSSM Higgs boson mass combining effective field theory and fixed-order calculations", *Eur. Phys. J.* **C76** (2016), no. 9, 499, arXiv:1608.01880.

[57] H. Bahl, S. Heinemeyer, W. Hollik, and G. Weiglein, "Reconciling EFT and hybrid calculations of the light MSSM Higgs-boson mass", *Eur. Phys. J.* **C78** (2018), no. 1, 57, arXiv:1706.00346.

[58] H. Bahl, T. Hahn, S. Heinemeyer, W. Hollik, S. Paßehr, H. Rzehak, and G. Weiglein, "Precision calculations in the MSSM Higgs-boson sector with FeynHiggs 2.14", arXiv:1811.09073.

[59] See: http://www.feynhiggs.de.

[60] S. Borowka, S. Paßehr, and G. Weiglein, "Complete two-loop QCD contributions to the lightest Higgs-boson mass in the MSSM with complex parameters", *Eur. Phys. J.* **C78** (2018), no. 7, 576, arXiv:1802.09886.

[61] S. P. Martin, "Two-loop scalar self-energies and pole masses in a general renormalizable theory with massless gauge bosons", *Phys. Rev.* **D71** (2005) 116004, arXiv:hep-ph/0502168.

[62] S. P. Martin, "Three-loop corrections to the lightest Higgs scalar boson mass in supersymmetry", *Phys. Rev.* **D75** (2007) 055005, arXiv:hep-ph/0701051.

[63] R. V. Harlander, P. Kant, L. Mihaila, and M. Steinhauser, "Higgs boson mass in supersymmetry to three loops", *Phys. Rev. Lett.* **100** (2008) 191602, arXiv:0803.0672, [Erratum: Phys. Rev. Lett.101,039901(2008)].

[64] P. Kant, R. V. Harlander, L. Mihaila, and M. Steinhauser, "Light MSSM Higgs boson mass to three-loop accuracy", *JHEP* **08** (2010) 104, arXiv:1005.5709.

[65] R. V. Harlander, J. Klappert, and A. Voigt, "Higgs mass prediction in the MSSM at three-loop level in a pure $\overline{\text{DR}}$ context", *Eur. Phys. J.* **C77** (2017), no. 12, 814, arXiv:1708.05720.

[66] A. R. Fazio and E. A. Reyes R., "The Lightest Higgs Boson Mass of the MSSM at Three-Loop Accuracy", *Nucl. Phys.* **B942** (2019) 164–183, arXiv:1901.03651.

[67] R. V. Harlander, J. Klappert, A. D. Ochoa Franco, and A. Voigt, "The light CP-even MSSM Higgs mass resummed to fourth logarithmic order", *Eur. Phys. J.* **C78** (2018), no. 10, 874, arXiv:1807.03509.

[68] S. Heinemeyer, W. Hollik, and G. Weiglein, "Electroweak precision observables in the minimal supersymmetric standard model", *Phys. Rept.* **425** (2006) 265–368, arXiv:hep-ph/0412214.

[69] H. Bahl and W. Hollik, "Precise prediction of the MSSM Higgs boson masses for low M_A", *JHEP* **07** (2018) 182, arXiv:1805.00867.

[70] G. Degrassi and P. Slavich, "On the radiative corrections to the neutral Higgs boson masses in the NMSSM", *Nucl. Phys.* **B825** (2010) 119–150, arXiv:0907.4682.

[71] F. Staub, W. Porod, and B. Herrmann, "The Electroweak sector of the NMSSM at the one-loop level", *JHEP* **10** (2010) 040, arXiv:1007.4049.

[72] K. Ender, T. Graf, M. Muhlleitner, and H. Rzehak, "Analysis of the NMSSM Higgs Boson Masses at One-Loop Level", *Phys. Rev.* **D85** (2012) 075024, arXiv:1111.4952.

[73] T. Graf, R. Grober, M. Muhlleitner, H. Rzehak, and K. Walz, "Higgs Boson Masses in the Complex NMSSM at One-Loop Level", *JHEP* **10** (2012) 122, arXiv:1206.6806.

[74] P. Drechsel, L. Galeta, S. Heinemeyer, and G. Weiglein, "Precise Predictions for the Higgs-Boson Masses in the NMSSM", *Eur. Phys. J.* **C77** (2017), no. 1, 42, arXiv:1601.08100.

[75] G. K. Yeghian, "Upper bound on the lightest Higgs mass in supersymmetric theories", *Acta Phys. Slov.* **49** (1999) 823, arXiv:hep-ph/9904488.

[76] U. Ellwanger and C. Hugonie, "Masses and couplings of the lightest Higgs bosons in the (M+1) SSM", *Eur. Phys. J.* **C25** (2002) 297–305, arXiv:hep-ph/9909260.

[77] M. D. Goodsell, K. Nickel, and F. Staub, "Two-loop corrections to the Higgs masses in the NMSSM", *Phys. Rev.* **D91** (2015) 035021, arXiv:1411.4665.

[78] M. Mühlleitner, D. T. Nhung, H. Rzehak, and K. Walz, "Two-loop contributions of the order $\mathcal{O}(\alpha_t\alpha_s)$ to the masses of the Higgs bosons in the CP-violating NMSSM", *JHEP* **05** (2015) 128, arXiv:1412.0918.

[79] F. Staub, P. Athron, U. Ellwanger, R. Gröber, M. Mühlleitner, P. Slavich, and A. Voigt, "Higgs mass predictions of public NMSSM spectrum generators", *Comput. Phys. Commun.* **202** (2016) 113–130, arXiv:1507.05093.

[80] P. Drechsel, R. Gröber, S. Heinemeyer, M. M. Muhlleitner, H. Rzehak, and G. Weiglein, "Higgs-Boson Masses and Mixing Matrices in the NMSSM: Analysis of On-Shell Calculations", *Eur. Phys. J.* **C77** (2017), no. 6, 366, arXiv:1612.07681.

[81] F. Staub, "SARAH 4 : A tool for (not only SUSY) model builders", *Comput. Phys. Commun.* **185** (2014) 1773–1790, arXiv:1309.7223.

[82] M. D. Goodsell and F. Staub, "The Higgs mass in the CP violating MSSM, NMSSM, and beyond", *Eur. Phys. J.* **C77** (2017), no. 1, 46, arXiv:1604.05335.

[83] W. Porod and F. Staub, "SPheno 3.1: Extensions including flavour, CP-phases and models beyond the MSSM", *Comput. Phys. Commun.* **183** (2012) 2458–2469, arXiv:1104.1573.

[84] P. Athron, M. Bach, D. Harries, T. Kwasnitza, J.-h. Park, D. Stöckinger, A. Voigt, and J. Ziebell, "FlexibleSUSY 2.0: Extensions to investigate the phenomenology of SUSY and non-SUSY models", *Comput. Phys. Commun.* **230** (2018) 145–217, arXiv:1710.03760.

Chapter 5

Higgs potential of the $\mu\nu$SSM with one right-handed neutrino

In this chapter we present the renormalization of the neutral scalar potential of the $\mu\nu$SSM with one right-handed neutrino superfield at the full one-loop level [1]. This model is already capable of reproducing the measured values for the neutrino masses and mixing angles. Due to the presence of the right-handed neutrino, one light left-handed neutrino masses is accounted for at tree level. Two more neutrino masses are generated by means of quantum corrections, which however lies beyond the scope of this thesis. From the renormalized scalar potential we derive the radiative corrections to the neutral scalar Higgs bosons, and supplement these corrections with higher-order contributions from the MSSM. In the numerical analyses we show benchmark points (BPs) with additional light scalars with masses close to the SM-like Higgs-boson mass. In such BPs the corrections are of particular importance. Afterwards, we extended our renormalization procedure to the $\mu\nu$SSM with three right-handed neutrino superfields [2]. The results for this more complete version of the $\mu\nu$SSM are presented in Ch. 6.

When one instead of three right-handed superfields are considered to be present in the $\mu\nu$SSM, the neutral scalar potential simplifies because of the smaller number of parameters. The parameters of the general superpotential and soft Lagrangian shown in Eq. (3.8) and Eq. (3.9) reduce to

$$Y^{\nu}_{ij} \to Y^{\nu}_{i} \,, \quad \lambda_i \to \lambda \,, \qquad \kappa_{ijk} \to \kappa \,, \tag{5.1}$$

$$T^{\nu}_{ij} \to T^{\nu}_{i} \,, \quad T^{\lambda}_{i} \to T^{\lambda} \,, \quad T^{\kappa}_{ijk} \to T^{\kappa} \,, \quad \left(m^2_{\widetilde{\nu}}\right)_{ij} \to m_{\widetilde{\nu}} \,, \tag{5.2}$$

and there will only be a single right-handed sneutrino vev v_R. The neutral scalar potential at tree-level reads in the one-generation case

$$V^{(0)} = V_{\text{soft}} + V_F + V_D \,, \tag{5.3}$$

with

$$\begin{aligned} V_{\text{soft}} = \quad & \left(T^{\nu}_{i} \, H^0_u \, \widetilde{\nu}_{iL} \, \widetilde{\nu}^*_R - T^{\lambda} \, \widetilde{\nu}^*_R \, H^0_d H^0_u + \frac{1}{3} T^{\kappa} \, \widetilde{\nu}^*_R \widetilde{\nu}^*_R \widetilde{\nu}^*_R \; + \text{h.c.} \right) \\ + \quad & \left(m^2_{\widetilde{L}} \right)_{ij} \widetilde{\nu}^*_{iL} \widetilde{\nu}_{jL} + \left(m^2_{H_d \widetilde{L}} \right)_i H^{0*}_d \widetilde{\nu}_{iL} + m^2_{\widetilde{\nu}} \widetilde{\nu}^*_R \widetilde{\nu}_R + m^2_{H_d} H^{0^*}_d H^0_d + m^2_{H_u} H^{0^*}_u H^0_u \,, \end{aligned} \tag{5.4}$$

$$\begin{aligned} V_F = \quad & \lambda^2 H^0_d H^{0^*}_d H^0_u H^{0^*}_u + \lambda^2 \tilde{\nu}^*_R \tilde{\nu}_R H^0_d H^{0*}_d + \lambda^2 \tilde{\nu}^*_R \tilde{\nu}_R H^0_u H^{0*}_u \\ + \quad & \kappa^2 \left(\tilde{\nu}^*_R \right)^2 \left(\tilde{\nu}_R \right)^2 - \Big(\kappa \lambda \left(\tilde{\nu}^*_R \right)^2 H^{0*}_d H^{0*}_u - Y^{\nu}_i \kappa \tilde{\nu}_{iL} \left(\tilde{\nu}_R \right)^2 H^0_u \end{aligned}$$

$$
\begin{aligned}
&+ \quad Y_i^\nu \lambda \tilde{\nu}_{iL} H_d^{0*} H_u^{0*} H_u^0 + Y_i^\nu \lambda \tilde{\nu}_{iL}^* \tilde{\nu}_R \tilde{\nu}_R^* H_d^0 + \text{h.c.}\big) \\
&+ \quad Y_i^\nu Y_i^\nu \tilde{\nu}_R^* \tilde{\nu}_R H_u^0 H_u^{0*} + Y_i^\nu Y_j^\nu \tilde{\nu}_{iL} \tilde{\nu}_{jL}^* \tilde{\nu}_R^* \tilde{\nu}_R + Y_i^\nu Y_j^\nu \tilde{\nu}_i \tilde{\nu}_j^* H_u^0 H_u^{0*} \,, \qquad (5.5)
\end{aligned}
$$

$$
V_D = \quad \frac{1}{8}\left(g_1^2 + g_2^2\right)\left(\widetilde{\nu}_{iL}\widetilde{\nu}_{iL}^* + H_d^0 H_d^{0*} - H_u^0 H_u^{0*}\right)^2 . \qquad (5.6)
$$

We also explicitly state the tadpole equations for the one-generation case, because the tadpole coefficients will be used as independent parameters,

$$
\begin{aligned}
T_{H_d^\mathcal{R}} =& - m_{H_d}^2 v_d - \left(m_{H_d\widetilde{L}}^2\right)_i v_{iL} - \frac{1}{8}\left(g_1^2 + g_2^2\right) v_d \left(v_d^2 + v_{iL} v_{iL} - v_u^2\right) \\
& - \frac{1}{2}\lambda \left(v_R^2 + v_u^2\right)\left(\lambda v_d - v_{iL} Y_i^\nu\right) + \frac{1}{\sqrt{2}} T^\lambda v_R v_u + \frac{1}{2}\kappa\lambda v_R^2 v_u \,, \qquad (5.7)
\end{aligned}
$$

$$
\begin{aligned}
T_{H_u^\mathcal{R}} =& - m_{H_u}^2 v_u + \frac{1}{8}\left(g_1^2 + g_2^2\right) v_u \left(v_d^2 + v_{iL} v_{iL} - v_u^2\right) \\
& - \frac{1}{2}\lambda^2 \left(v_d^2 + v_R^2\right) + \frac{1}{\sqrt{2}} T^\lambda v_d v_R + \lambda v_d v_u v_{iL} Y_i^\nu + \frac{1}{2}\kappa\lambda v_d v_R^2 - \frac{1}{2}\kappa v_R^2 v_{iL} Y_i^\nu \\
& - \frac{1}{2} v_u \left(v_{iL} Y_i^\nu\right)^2 - \frac{1}{\sqrt{2}} v_R v_{iL} T_i^\nu - \frac{1}{2} v_R^2 v_u Y_i^\nu Y_i^\nu \,, \qquad (5.8)
\end{aligned}
$$

$$
\begin{aligned}
T_{\widetilde{\nu}_R^\mathcal{R}} =& - m_{\widetilde{\nu}}^2 v_R - \frac{1}{\sqrt{2}} T^\kappa v_R^2 - \kappa^2 v_R^3 + \frac{1}{\sqrt{2}} T^\lambda v_d v_u - \frac{1}{2}\lambda^2 v_R \left(v_d^2 + v_u^2\right) \\
& + \lambda v_d v_R v_{iL} Y_i^\nu + \kappa\lambda v_d v_R v_u - \kappa v_R v_u v_{iL} Y_i^\nu - \frac{1}{2} v_R \left(v_{iL} Y_i^\nu\right)^2 \\
& - \frac{1}{\sqrt{2}} v_u v_{iL} T_i^\nu - \frac{1}{2} v_R v_u^2 Y_i^\nu Y_i^\nu \,, \qquad (5.9)
\end{aligned}
$$

$$
\begin{aligned}
T_{\widetilde{\nu}_{iL}^\mathcal{R}} =& - \left(m_{\widetilde{L}}^2\right)_{ij} v_{jL} - \left(m_{H_d\widetilde{L}}^2\right)_i v_d - \frac{1}{8}\left(g_1^2 + g_2^2\right) v_{iL} \left(v_d^2 + v_{jL} v_{jL} - v_u^2\right) \\
& + \frac{1}{2}\lambda v_d v_R^2 Y_i^\nu - \frac{1}{\sqrt{2}} v_R v_u T_i^\nu - \frac{1}{2}\kappa v_R^2 v_u Y_i^\nu + \frac{1}{2}\lambda v_d v_u^2 Y_i^\nu \\
& - \frac{1}{2} v_R^2 Y_i^\nu v_{jL} Y_j^\nu - \frac{1}{2} v_u^2 Y_i^\nu v_{jL} Y_j^\nu \,. \qquad (5.10)
\end{aligned}
$$

The mass matrices for the neutral scalars in the one-generation case can be found in Ref. [1]. Therein, we also give the precise form of the mass matrices of the other sectors of the model. Since they are trivial simplifications of the general formulas given in Sects. 3.3.2–3.3.6, we do not state them explicitly here.

One conceptual difference to the complete $\mu\nu$SSM with three right-handed neutrino superfields is that only one light neutrino mass is generated at tree level via the electroweak seesaw mechanism. Two more light neutrino masses are radiatively generated via loop-corrections to the fermion propagators (see Eq. (4.21)). Calculating these loop-corrections is beyond the scope of this thesis, as we are primarily interested in the corrections to the scalar sector. Also, the presence of tiny neutrino masses has a negligible impact on the SM-like Higgs-boson mass. Therefore, a precise discussion of BPs in agreement with neutrino oscillation data was left for the three generation case [2]. Nevertheless, the values we picked for the free parameters here provide realistic scenarios, i.e., neutrino Yukawas Y_i^ν have values between 10^{-7} and 10^{-6}, to generate neutrino masses of the order less than 1 eV. For the left-handed sneutrino vevs, which are used as input parameters (see below) this directly implies $v_{iL} \ll v_d, v_u$ so that the tadpole coefficients shown in Eq. (3.31) vanish.

5.1 Renormalization at the one-loop level

The first step in renormalizing the neutral scalar potential is to choose the set of independent parameters. The coefficients of the Lagrangian are functions of the this set of parameters. When the parameters are renormalized, their counterterms are defined in such a way that all UV divergences appearing in higher-order Green's functions are canceled by the them.

Our final aim is to obtain the quantum corrections to the pole masses of the neutral $\mathcal{CP}$-even scalars. The relevant part of the Higgs potential is given by the linear tadpole coefficients and the $\mathcal{CP}$-even and $\mathcal{CP}$-odd mass matrix elements. The following parameters appear in the Higgs potential:

- Scalar soft masses: $m^2_{H_d}$, $m^2_{H_u}$, $m^2_{\widetilde{\nu}}$, $\left(m^2_{\widetilde{L}}\right)_{ij}$, $\left(m^2_{H_d\widetilde{L}}\right)_i$ (12 parameters)
- Vacuum expectation values: v_d, v_u, v_R, v_{iL} (6 parameters)
- Gauge couplings: g_1, g_2 (2 parameters)
- Superpotential parameters: λ, κ, Y^ν_i (5 parameters)
- Soft trilinear couplings: T^λ, T^κ, T^ν_i (5 parameters)

The complexity of the $\mu\nu$SSM scalar sector becomes evident when one compares the numbers of free parameters (30) with the one in the real MSSM (7) [3] and the NMSSM (12) [4]. Non of the initial parameters stated above can be directly related to a physical observable.

Hence, we replace the soft masses $m^2_{H_d}$, $m^2_{H_u}$, $m^2_{\widetilde{\nu}}$, and the diagonal elements of the matrix $m^2_{\widetilde{L}}$ by the tadpole coefficients shown in Eqs. (3.28)–(3.31), for which OS conditioned can be conveniently applied (see Sect. 4.3.2), such that

$$\delta T_{\varphi_i^{\mathcal{R}}} = -T^{(1)}_{\varphi_i^{\mathcal{R}}} \quad \text{with} \quad \varphi^T = (H_d^{\mathcal{R}}, H_u^{\mathcal{R}}, \widetilde{\nu}_R^{\mathcal{R}}, \widetilde{\nu}_{1L}^{\mathcal{R}}, \widetilde{\nu}_{2L}^{\mathcal{R}}, \widetilde{\nu}_{3L}^{\mathcal{R}}) \, . \tag{5.11}$$

By doing so we guarantee that the true vacuum of the theory is not spoiled by the higher-order corrections. The tadpole diagrams contributing to $T^{(1)}_{\varphi_i^{\mathcal{R}}}$ are calculated in the mass eigenstate basis h_i. The one-loop tadpole contributions in the interaction basis φ_i are then obtained by the rotation

$$T^{(1)}_{\varphi_i^{\mathcal{R}}} = U^H_{ji} T^{(1)}_{h_i} \, . \tag{5.12}$$

Note that, alternatively, the tadpole coefficients could have been introduced as independent parameters by replacing the vevs of the scalar fields, and keeping the soft mass parameters written above as input parameters. However, solving the tadpole equations for the soft masses, given the vevs as input, is computationally much more eligible. Solving the tadpole equations for the vevs, given the soft mass parameters, yields a system of polynomial equations that can only be solved numerically, and the solutions are not unique.

In addition, we replace the Higgs doublet vevs v_d and v_u by the MSSM-like parameters $\tan\beta$ and v according to

$$\tan\beta = \frac{v_u}{v_d} \qquad \text{and} \qquad v^2 = v_d^2 + v_u^2 + v_{iL} v_{iL} \, . \tag{5.13}$$

The definition of v^2 differs from the one in the MSSM by the term $v_{iL}v_{iL}$. This allows to maintain the relations between v^2 and the gauge boson masses as they are in the SM and

Soft masses	vevs	Gauge cpls.	Superpot.	Soft trilinears
$m^2_{H_d}$, $m^2_{H_u}$, $m^2_{\widetilde{\nu}}$, $m^2_{\widetilde{L}ij}$, $m^2_{H_d\widetilde{L}_i}$	v_d, v_u, v_R, v_{iL}	g_1, g_2	λ, κ, Y^ν_i	T^λ, T^κ, T^ν_i
$\downarrow$	$\downarrow$	$\downarrow$	$\downarrow$	$\downarrow$
$T_{H^{\mathcal{R}}_d}$, $T_{H^{\mathcal{R}}_u}$, $T_{\widetilde{\nu}^{\mathcal{R}}_R}$, $T_{\widetilde{\nu}^{\mathcal{R}}_{iL}}$, $m^2_{\widetilde{L}i\neq j}$, $m^2_{H_d\widetilde{L}_i}$	$\tan\beta$, v, μ, v_{iL}	M_W, M_Z	λ, κ, Y^ν_i	A^λ, A^κ, A^ν_i

Table 5.1: Set of independent parameters initially entering the tree-level Higgs potential of the $\mu\nu$SSM in the first row, and final choice of free parameters after the substitutions mentioned in the text.

the MSSM. Numerically, the difference in the definition of v^2 is negligible, since the v_{iL} are of the order of 10^{-4} GeV in realistic scenarios. Analytically, however, maintaining the functional form of $\tan\beta$ as it is in the (N)MSSM is convenient to facilitate the comparison of the quantum corrections in the $\mu\nu$SSM and the NMSSM. In particular, we can still express the one-loop counterterm of $\tan\beta$ (see below) without having to include the counterterms for the left-handed sneutrino vevs.

When the right-handed sneutrino obtains a vev, the μ-term of the MSSM is dynamically generated. We substitute the vev by the effective μ-parameter, such that

$$\mu = \frac{v_R\lambda}{\sqrt{2}} \,, \tag{5.14}$$

again facilitating the comparison between the $\mu\nu$SSM and the (N)MSSM in which the μ-parameter appears as well.

The gauge couplings g_1 and g_2 will be replaced by the gauge boson masses M_W and M_Z, given by

$$M_W^2 = \frac{1}{4}g_2^2v^2 \qquad \text{and} \qquad M_Z^2 = \frac{1}{4}\left(g_1^2+g_2^2\right)v^2 \,. \tag{5.15}$$

By employing OS conditions for M_W and M_Z (see Sect. 4.3.2), so that

$$\delta M_Z^2 = \mathrm{Re}\left[\Sigma^T_{ZZ}\left(M_Z^2\right)\right] \qquad \text{and} \qquad \delta M_W^2 = \mathrm{Re}\left[\Sigma^T_{WW}\left(M_W^2\right)\right] \,. \tag{5.16}$$

we make sure that the renormalized gauge boson masses can be set to the experimentally measured values. Radiative corrections are absorbed into the counterterms and the pole mass predictions will not be modified.

Finally, the soft trilinear couplings are set to be proportional to the corresponding superpotential couplings,

$$T^\lambda = A^\lambda\lambda \,, \qquad T^\kappa = A^\kappa\kappa \,, \qquad T^\nu_i = A^\nu_i Y^\nu_i \,, \tag{5.17}$$

and the parameters $A^{\lambda,\kappa,\nu}$ are used as input parameters. The reparametrization from the initial to the physical set of independent parameters is summarized in Tab. 5.1.

The entries of the neutral scalar mass matrices are functions of the final set of parameters,

$$m^2_\varphi = m^2_\varphi\left(M_Z^2, v^2, \tan\beta, \lambda, \dots\right) \,, \tag{5.18}$$

$$m^2_\sigma = m^2_\sigma\left(M_Z^2, v^2, \tan\beta, \lambda, \dots\right) \,, \tag{5.19}$$

and we define their renormalization as

$$m_\varphi^2 \to m_\varphi^2 + \delta m_\varphi^2 \,, \tag{5.20}$$
$$m_\sigma^2 \to m_\sigma^2 + \delta m_\sigma^2 \,. \tag{5.21}$$

The mass counterterms δm_φ^2 and δm_σ^2 enter the renormalized one-loop scalar self-energies. We define the one-loop renormalization of the independent parameters by

$$\begin{aligned}
T_{H_d^\mathcal{R}} &\to T_{H_d^\mathcal{R}} + \delta T_{H_d^\mathcal{R}} \,, & \tan\beta &\to \tan\beta + \delta\tan\beta \,, & \lambda &\to \lambda + \delta\lambda \,, \\
T_{H_u^\mathcal{R}} &\to T_{H_u^\mathcal{R}} + \delta T_{H_u^\mathcal{R}} \,, & v^2 &\to v^2 + \delta v^2 \,, & \kappa &\to \kappa + \delta\kappa \,, \\
T_{\widetilde{\nu}_R^\mathcal{R}} &\to T_{\widetilde{\nu}_R^\mathcal{R}} + \delta T_{\widetilde{\nu}_R^\mathcal{R}} \,, & \mu &\to \mu + \delta\mu \,, & Y_i^\nu &\to Y_i^\nu + \delta Y_i^\nu \,, \\
T_{\widetilde{\nu}_{iL}^\mathcal{R}} &\to T_{\widetilde{\nu}_{iL}^\mathcal{R}} + \delta T_{\widetilde{\nu}_{iL}^\mathcal{R}} \,, & v_{iL}^2 &\to v_{iL}^2 + \delta v_{iL}^2 \,, & A^\lambda &\to A^\lambda + \delta A^\lambda \,, \\
m^2_{\widetilde{L}i\neq j} &\to m^2_{\widetilde{L}i\neq j} + \delta m^2_{\widetilde{L}i\neq j} \,, & M_W^2 &\to M_W^2 + \delta M_W^2 \,, & A^\kappa &\to A^\kappa + \delta A^\kappa \,, \\
m^2_{H_d\widetilde{L}_i} &\to m^2_{H_d\widetilde{L}_i} + \delta m^2_{H_d\widetilde{L}_i} \,, & M_Z^2 &\to M_Z^2 + \delta M_Z^2 \,, & A_i^\nu &\to A_i^\nu + \delta A_i^\nu \,.
\end{aligned} \tag{5.22}$$

Apart from the tadpole coefficients and the gauge boson masses, the remaining parameters lack a direct relation to a physical observable. Thus, they will be renormalized as $\overline{\text{DR}}$ parameters. The precise definition of the renormalization conditions, from which the counterterms were extracted, will be given in the following. The dependence of the mass counterterms δm_φ^2 and δm_σ^2 on the counterterms of the free parameters is given at one-loop level by

$$(\delta m_\varphi^2)_{ij} = \sum_{X\in\text{Free param.}} \left(\frac{\partial}{\partial X}(m_\varphi^2)_{ij}\right)\delta X \,, \qquad (\delta m_\sigma^2)_{ij} = \sum_{X\in\text{Free param.}} \left(\frac{\partial}{\partial X}(m_\sigma^2)_{ij}\right)\delta X \,. \tag{5.23}$$

The mixing matrices U^H and U^A (see Eqs. (3.46) and (3.66)) diagonalize the renormalized mass matrices, so they do not have to be renormalized, because they are defined exclusively by renormalized quantities. The counterterms of the scalar mass matrices in the mass eigenstate basis then read

$$(\delta m_h^2)_{ij} = U^H_{ik}(\delta m_\varphi^2)_{kl}U^H_{jl} \,, \qquad (\delta m_A^2)_{ij} = U^A_{ik}(\delta m_\sigma^2)_{kl}U^A_{jl} \,. \tag{5.24}$$

We stress that this rotation does not leave the mass counterterms in the mass eigenstate basis δm_h^2 and δm_A^2 diagonal, as they would be in a purely OS renormalization procedure which is often used in theories with flavor mixing [5]. This approach, however, is not possible in SUSY models, where there are not enough independent parameters to renormalize each particle OS.

As can be seen in Eq. (4.16), the momentum-dependent self-energy contributions of renormalized scalar Green's functions are renormalized by the field renormalization counterterms. We write the renormalization of the scalar components of the neutral chiral superfields $\phi = (H_d, H_u, \widetilde{\nu}_R, \widetilde{\nu}_{1L}, \widetilde{\nu}_{2L}, \widetilde{\nu}_{3L})$ as

$$\phi_i \to Z^{1/2}_{\phi_i\phi_j}\phi_j = \left(\mathbb{1} + \frac{1}{2}\delta Z_{\phi_i\phi_j}\right)\phi_j \,, \tag{5.25}$$

where $Z^{1/2}_{\phi_i\phi_j}$ and $\delta Z_{\phi_i\phi_j}$ are 6×6 dimensional matrices and the equal sign is valid at the one-loop level. For the field renormalization in the mass eigenstate basis,

$$h_i \to \left(\mathbb{1} + \frac{1}{2}\delta Z_{h_ih_j}\right)h_j \,, \qquad A_i \to \left(\mathbb{1} + \frac{1}{2}\delta Z_{A_iA_j}\right)A_j \,, \tag{5.26}$$

we then find

$$\delta Z_{h_i h_j} = U^H_{ik}\, \delta Z_{\phi_k\phi_l}\, U^H_{jl} \qquad \text{and} \qquad \delta Z_{A_i A_j} = U^A_{ik}\, \delta Z_{\phi_k\phi_l}\, U^A_{jl}\,. \tag{5.27}$$

We adopted $\overline{\text{DR}}$ conditions for the field renormalization counterterms. We calculate the UV-divergent part of the derivative of the scalar $\mathcal{CP}$-even self-energies in the interaction basis and extract the field renormalization counterterms from demanding finiteness of the renormalized scalar 2-point function given in Eq. (4.16). Thus, the $\overline{\text{DR}}$ renormalization condition read

$$\delta Z_{\phi_i\phi_j} = -\left.\frac{d}{dp^2}\Sigma^{(1)}_{\varphi_i\varphi_j}\right|^{\text{div}}\,, \tag{5.28}$$

where $\varphi^T = (H_d^{\mathcal{R}}, H_u^{\mathcal{R}}, \widetilde{\nu}_R^{\mathcal{R}}, \widetilde{\nu}_{1L}^{\mathcal{R}}, \widetilde{\nu}_{2L}^{\mathcal{R}}, \widetilde{\nu}_{3L}^{\mathcal{R}})$ are the $\mathcal{CP}$-even neutral scalar fields. We find the following field renormalization counterterms:

$$\delta Z_{H_d H_d} = -\frac{\Delta}{16\pi^2}\left(\lambda^2 + Y^e_{ij}Y^e_{ij} + 3\left(Y^d_i Y^d_i\right)\right)\,, \tag{5.29}$$

$$\delta Z_{H_d\widetilde{\nu}_{iL}} = \frac{\Delta}{16\pi^2}\lambda Y^\nu_i\,, \tag{5.30}$$

$$\delta Z_{H_u H_u} = -\frac{\Delta}{16\pi^2}\left(\lambda^2 + Y^\nu_i Y^\nu_i + 3\left(Y^u_i Y^u_i\right)\right)\,, \tag{5.31}$$

$$\delta Z_{\widetilde{\nu}_R\widetilde{\nu}_R} = -\frac{\Delta}{16\pi^2}\left(\lambda^2 + \kappa^2 + Y^\nu_i Y^\nu_i\right)\,, \tag{5.32}$$

$$\delta Z_{\widetilde{\nu}_{iL}\widetilde{\nu}_{jL}} = -\frac{\Delta}{16\pi^2}\left(Y^e_{ki}Y^e_{kj} + Y^\nu_i Y^\nu_j\right)\,. \tag{5.33}$$

In contrast to the (N)MSSM, the $\overline{\text{DR}}$ field renormalization in the Higgs sector of the $\mu\nu$SSM contains off-diagonal counterterms in the interaction basis, induced by the neutrino Yukawa couplings Y^ν_i (see Eq. (5.30)). The off-diagonal contributions appear relating the down-type Higgs field H_d and the left-handed sneutrino fields $\widetilde{\nu}_{iL}$ which have exactly the same quantum numbers due to the breaking of R-parity and lepton-number conservation, so that mixed kinetic terms are allowed by the symmetries.[1] In the limit $Y^\nu_i \to 0$ we find the field renormalization constants of the NMSSM.

Having found the field renormalization counterterms, and applying OS conditions to the tadpole coefficients and the gauge-boson masses, the remaining problem in renormalizing the Higgs potential consists of extracting the counterterms for the parameters renormalized using $\overline{\text{DR}}$ conditions. In the following paragraphs, we state the precise renormalization condition applied to each parameter and the exact form of the resulting counterterm. They were obtained by calculating the divergent parts of one-loop corrections to different scalar and fermionic two- and three-point functions. We state the determination of the counterterms in the (possible) order in which they can be successively derived. We start with the counterterms that were obtained by renormalizing certain neutral fermion self-energies.

Renormalization of μ

The μ-parameter appears isolated in the Majorana-type mass matrix of the neutral fermions

$$\left(m_{\chi^0}\right)_{\widetilde{H}^0_d\widetilde{H}^0_u} = -\frac{\lambda v_R}{\sqrt{2}} = -\mu\,. \tag{5.34}$$

[1] As was argued in Ref. [6], non-diagonal field renormalization constants are not necessary if one only demands physical quantities to be UV finite, permitting UV divergences in non-diagonal 2-point Green's functions to remain. These would then be canceled by the additional mixing effects on the outer legs of S-matrix elements following the LSZ theorem.

It is the element mixing the down-type and the up-type Higgsinos $\widetilde{H}_d^0$ and $\widetilde{H}_u^0$. Hence, the mass counterterm simply reads

$$\delta\left(m_{\chi^0}\right)_{\widetilde{H}_d^0\widetilde{H}_u^0} = -\delta\mu \ . \tag{5.35}$$

We extract $\delta\mu$ following the general formula given in Eq. (4.22) by substituting the explicit mass-matrix elements into the renormalized scalar part of the self-energy $\Sigma_{\widetilde{H}_d^0\widetilde{H}_u^0}$ and demanding that $\hat{\Sigma}^S_{\widetilde{H}_d^0\widetilde{H}_u^0}$ is finite. This yields

$$\delta\mu = \frac{1}{2}\mu\left(-\left(\delta Z_{\widetilde{H}_d^0\widetilde{H}_d^0} + \delta Z_{\widetilde{H}_u^0\widetilde{H}_u^0}\right) + \frac{1}{\lambda}\delta Z_{\nu_{iL}\widetilde{H}_d^0}Y_i^\nu\right) - \Sigma^{S(1)}_{\widetilde{H}_d^0\widetilde{H}_u^0}\Big|^{\text{div}} \ , \tag{5.36}$$

where $\delta Z_{\chi_i^0\chi_j^0}$ are the field renormalization counterterms for the neutral fermions. In the $\overline{\text{DR}}$ scheme they can be obtained from the fermionic part of the self-energies (see Eq. (4.21)), such that for Majorana fermions we find

$$\delta Z_{\chi_i^0\chi_j^0} = -\left.\Sigma^{F_L(1)}_{\chi_i^0\chi_j^0}\right|^{\text{div}} = -\left.\Sigma^{F_R(1)}_{\chi_i^0\chi_j^0}\right|^{\text{div}} = -\left.\Sigma^{F(1)}_{\chi_i^0\chi_j^0}\right|^{\text{div}} \ . \tag{5.37}$$

In Eq. (5.36) we already made us of the fact that the counterterms $\delta Z_{\chi_i^0\chi_j^0}$ are real and symmetric in i and j, and that components mixing left-handed neutrinos ν_{iL} and the down-type Higgsino $\widetilde{H}_d^0$ are the only non-diagonal elements contributing. After calculating the UV divergent parts of the neutral fermion self-energies by means of the one-loop diagrams in the interaction basis (see Fig. 4.4), the explicit expression for $\delta\mu$ in the $\overline{\text{DR}}$ scheme is found to be

$$\delta\mu = \frac{\Delta}{32\pi^2}\mu\left(-\frac{4\pi\alpha\left(s_{\text{w}}^2+3c_{\text{w}}^2\right)}{s_{\text{w}}^2c_{\text{w}}^2} + 2\lambda^2 + 3\left(Y_i^uY_i^u + Y_i^dY_i^d\right) + Y_{ij}^eY_{ij}^e + 2Y_i^\nu Y_i^\nu\right) \ , \tag{5.38}$$

where s_{w} is the sine of the weak mixing angle given by $s_{\text{w}} = \sqrt{1-c_{\text{w}}^2}$ with $c_{\text{w}} = M_W/M_Z$, and $\alpha = e/(4\pi)$ with $e = g_1c_{\text{w}}$ is the electromagnetic coupling constant.

Renormalization of κ

The parameter κ appears isolated at tree level in the three-point vertex that couples the right-handed neutrino to the right-handed $\mathcal{CP}$-even sneutrino,

$$\Gamma^{(0)}_{\nu_R\nu_R\widetilde{\nu}_R^{\mathcal{R}}} = -\sqrt{2}\kappa \ . \tag{5.39}$$

The UV divergences induced to this coupling at the one-loop level have to be absorbed by the field renormalization of the right-handed neutrino and sneutrino and the counterterm for κ. From the form of the general renormalized 3-point function shown in Eq. (4.18) we therefore find the renormalization condition

$$\delta\kappa = \frac{1}{\sqrt{2}}\left.\Gamma^{(1)}_{\nu_R\nu_R\widetilde{\nu}_R^{\mathcal{R}}}\right|^{\text{div}} - \frac{1}{2}\kappa\left(\delta Z_{\widetilde{\nu}_R\widetilde{\nu}_R} + 2\,\delta Z_{\nu_R\nu_R}\right) \ . \tag{5.40}$$

It turns out that the one-loop vertex corrections are finite, so that $\delta\kappa$ is given by the field renormalization counterterms. Using the $\overline{\text{DR}}$ conditions Eq. (5.28) and Eq. (5.37), one finds

$$\delta\kappa = \frac{3\Delta}{16\pi^2}\kappa\left(\kappa^2 + \lambda^2 + Y_i^\nu Y_i^\nu\right) \ . \tag{5.41}$$

Renormalization of $\boldsymbol{\lambda}$

Having calculated $\delta\mu$ and $\delta\kappa$, we can extract the counterterm for λ in the neutral fermion sector given the mass matrix element

$$\left(m_{\chi^0}\right)_{\nu_R\nu_R} = \sqrt{2}\kappa v_R = \frac{2\kappa\mu}{\lambda} \,. \tag{5.42}$$

Expanding the mass counterterm $\delta\left(m_{\chi^0}\right)_{\nu_R\nu_R}$ in terms of $\delta\lambda$, $\delta\kappa$ and $\delta\mu$ and again using Eq. (4.22), the renormalization condition for λ reads

$$\delta\lambda = \lambda\left(\delta Z_{\nu_R\nu_R} + \frac{\delta\kappa}{\kappa} + \frac{\delta\mu}{\mu}\right) - \frac{\lambda^2}{2\mu\kappa}\,\Sigma^{S(1)}_{\nu_R\nu_R}\Big|^{\text{div}} \,. \tag{5.43}$$

This yields the expression

$$\begin{aligned}\delta\lambda = \frac{\Delta}{32\pi^2}\lambda\Bigg(&- \frac{4\pi\alpha\left(s_{\text{w}}^2 + 3c_{\text{w}}^2\right)}{s_{\text{w}}^2 c_{\text{w}}^2} + 4\lambda^2 + 2\kappa^2 + 3\big(Y_i^u Y_i^u + Y_i^d Y_i^d\big) \\ &+ Y_{ij}^e Y_{ij}^e + 4Y_i^\nu Y_i^\nu\Bigg) \,.\end{aligned} \tag{5.44}$$

Renormalization of $\boldsymbol{A^\kappa}$

Now that $\delta\kappa$, $\delta\lambda$ and $\delta\mu$ are fixed, the counterterm for A_κ can be extracted from the one-loop corrections to the scalar 3-point vertex of $\mathcal{CP}$-even right-handed sneutrinos. The tree-level vertex is given by

$$\Gamma^{(0)}_{\widetilde{\nu}_R^{\mathcal{R}}\widetilde{\nu}_R^{\mathcal{R}}\widetilde{\nu}_R^{\mathcal{R}}} = -\sqrt{2}\kappa\left(A^\kappa + \frac{6\kappa\mu}{\lambda}\right) \,. \tag{5.45}$$

Demanding that the renormalized 3-point Green's function is finite provides the renormalization condition

$$\delta A^\kappa = \frac{1}{\sqrt{2}\kappa}\left(\Gamma^{(1)}_{\widetilde{\nu}_R^{\mathcal{R}}\widetilde{\nu}_R^{\mathcal{R}}\widetilde{\nu}_R^{\mathcal{R}}}\Big|^{\text{div}} + \frac{3}{2}\delta Z_{\widetilde{\nu}_R\widetilde{\nu}_R}\Gamma^{(0)}_{\widetilde{\nu}_R^{\mathcal{R}}\widetilde{\nu}_R^{\mathcal{R}}\widetilde{\nu}_R^{\mathcal{R}}}\right) - A^\kappa\frac{\delta\kappa}{\kappa} - \frac{6\kappa\mu}{\lambda}\left(2\frac{\delta\kappa}{\kappa} + \frac{1}{2}\delta Z_{\widetilde{\nu}_R\widetilde{\nu}_R}\right) \,, \tag{5.46}$$

where $\delta\mu$ and $\delta\lambda$ were eliminated using the relation

$$\left[\frac{\delta\mu}{\mu} - \frac{\delta\lambda}{\lambda}\right]^{\text{div}} = \frac{1}{2}\delta Z_{\widetilde{\nu}_R\widetilde{\nu}_R}\Big|^{\text{div}} \,. \tag{5.47}$$

We find the counterterm

$$\delta A^\kappa = \frac{3\Delta}{8\pi^2}\left(A^\kappa\kappa^2 + A^\lambda\lambda^2 + A_i^\nu Y_i^{\nu 2}\right) \,. \tag{5.48}$$

Note that, in contrast to the superpotential parameters, the counterterms for soft parameters are not proportional to the parameter itself. This is related to the fact that they break SUSY, such that the non-renormalization theorems do not apply [7–9].

Renormalization of A^λ

Similarly, the counterterm for A^λ can be fixed by renormalizing the scalar 3-point vertex

$$\Gamma^{(0)}_{H_d^{\mathcal{R}} H_u^{\mathcal{R}} \widetilde{\nu}_R^{\mathcal{R}}} = \frac{A^\lambda \lambda}{\sqrt{2}} + \sqrt{2}\kappa\mu \,, \tag{5.49}$$

such that the renormalization condition reads

$$\begin{aligned}\delta A^\lambda = &-\frac{\sqrt{2}}{\lambda}\,\Gamma^{(1)}_{H_d^{\mathcal{R}} H_u^{\mathcal{R}} \widetilde{\nu}_R^{\mathcal{R}}}\Big|^{\text{div}} - \frac{1}{\sqrt{2}\lambda}\Bigg(\delta Z_{H_d H_d}\Gamma^{(0)}_{H_d^{\mathcal{R}} H_u^{\mathcal{R}} \widetilde{\nu}_R^{\mathcal{R}}} + \delta Z_{H_d \widetilde{\nu}_{1L}}\Gamma^{(0)}_{\widetilde{\nu}_{1L}^{\mathcal{R}} H_u^{\mathcal{R}} \widetilde{\nu}_R^{\mathcal{R}}} \\ &+\delta Z_{H_d \widetilde{\nu}_{2L}}\Gamma^{(0)}_{\widetilde{\nu}_{2L}^{\mathcal{R}} H_u^{\mathcal{R}} \widetilde{\nu}_R^{\mathcal{R}}} + \delta Z_{H_d \widetilde{\nu}_{3L}}\Gamma^{(0)}_{\widetilde{\nu}_{3L}^{\mathcal{R}} H_u^{\mathcal{R}} \widetilde{\nu}_R^{\mathcal{R}}} + \delta Z_{H_u H_u}\Gamma^{(0)}_{H_d^{\mathcal{R}} H_u^{\mathcal{R}} \widetilde{\nu}_R^{\mathcal{R}}} + \delta Z_{\widetilde{\nu}_R \widetilde{\nu}_R}\Gamma^{(0)}_{H_d^{\mathcal{R}} H_u^{\mathcal{R}} \widetilde{\nu}_R^{\mathcal{R}}}\Bigg) \\ &-\frac{A^\lambda}{\lambda}\delta\lambda - \frac{2\kappa}{\lambda}\delta\mu - \frac{2\mu}{\lambda}\delta\kappa \,,\end{aligned} \tag{5.50}$$

with

$$\Gamma^{(0)}_{\widetilde{\nu}_{iL}^{\mathcal{R}} H_u^{\mathcal{R}} \widetilde{\nu}_R^{\mathcal{R}}} = \frac{-Y_i^\nu \left(A_i^\nu + \frac{2\kappa\mu}{\lambda}\right)}{\sqrt{2}} \,. \tag{5.51}$$

The condition for δA^λ is more complicated due to the contributions arising from the off-diagonal field renormalization constants. After calculating $\Gamma^{(1)}_{H_d^{\mathcal{R}} H_u^{\mathcal{R}} \widetilde{\nu}_R^{\mathcal{R}}}|^{\text{div}}$ and inserting the field renormalization constants and the tree-level expression from Eq. (5.51), we find

$$\begin{aligned}\delta A^\lambda = &\frac{\Delta}{32\pi^2}\Bigg(\frac{8\pi\alpha\left(3c_{\text{w}}^2 M_2 + s_{\text{w}}^2 M_1\right)}{c_{\text{w}}^2 s_{\text{w}}^2} + 4A^\kappa\kappa^2 + A^\lambda\left(8\lambda^2 + Y_i^\nu Y_i^\nu\right) \\ &+ 6\left(A_i^u Y_i^{u2} + A_i^d Y_i^{d2}\right) + 7A_i^\nu Y_i^{\nu 2} + 2A_{ij}^e Y_{ij}^{e2}\Bigg) \,,\end{aligned} \tag{5.52}$$

where the soft gaugino mass parameter M_1 and M_2 appear in the term proportional to α.

Renormalization of v^2

The counterterm for the SM vev v is expressed in terms of the OS counterterms of the gauge boson masses δM_W^2 and δM_Z^2 and the counterterm δZ_e that renormalizes the electromagnetic coupling, such that

$$e \to e\,(1 + \delta Z_e) \,. \tag{5.53}$$

δZ_e can be calculated via [10]

$$\delta Z_e = \frac{1}{2}\left(\frac{\partial \Sigma_{\gamma\gamma}^{T(1)}}{\partial p^2}(0)\right) + \frac{s_{\text{w}}}{c_{\text{w}} M_Z^2}\Sigma_{\gamma Z}^{T(1)}(0) \,, \tag{5.54}$$

where $\Sigma_{\gamma\gamma}^{T(1)}(0)$ is the transverse part of the one-loop photon self-energy and $\Sigma_{\gamma Z}^{T(1)}$ is the transverse part of the mixed one-loop γ-Z boson self-energy. Making use of the fact that v^2 and e are related by

$$v^2 = \frac{2 s_{\text{w}}^2 M_W^2}{e^2} \,. \tag{5.55}$$

the counterterm δv^2 can be obtained through

$$\delta v^2 = \frac{4 s_{\rm w}^2 M_W^2}{e^2} \left(\frac{\delta s_{\rm w}^2}{s_{\rm w}^2} + \frac{\delta M_W^2}{M_W^2} - 2\delta Z_e \right) \Bigg|^{\rm div} , \tag{5.56}$$

where

$$s_{\rm w}^2 \to s_{\rm w}^2 + \delta s_{\rm w}^2 , \quad \text{with} \quad \delta s_{\rm w}^2 = -c_{\rm w}^2 \left(\frac{\delta M_W^2}{M_W^2} - \frac{\delta M_Z^2}{M_Z^2} \right) . \tag{5.57}$$

We stress that taking only the divergent part in Eq. (5.56) explicitly defines v^2 as $\overline{\rm DR}$ parameter, such that δZ_e is not an independent counterterm anymore. It was just calculated as such to obtain the UV divergences that contribute to δv^2 in Eq. (5.56). Extracting the divergent parts from δM_W^2, δM_Z^2 and δZ_e, the counterterm for v^2 can be written as

$$\begin{aligned} \delta v^2 =& \frac{\Delta}{32\pi^2} \Bigg(\frac{4\pi\alpha v^2 \left(s_{\rm w}^2 + 3c_{\rm w}^2\right)}{s_{\rm w}^2 c_{\rm w}^2} - 2 \Big(v_d^2 \left(3 Y_i^d Y_i^d + Y_{ij}^e Y_{ij}^e \right) + v_u^2 \left(3 Y_i^u Y_i^u + Y_i^\nu Y_i^\nu \right) \\ &+ Y_{ij}^e Y_{ik}^e v_{jL} v_{kL} \Big) + 2 v_{iL} Y_i^\nu \left(2\lambda v_d - v_{jL} Y_j^\nu \right) \Bigg) . \end{aligned} \tag{5.58}$$

Renormalization of v_{iL}^2

The counterterms δv_{iL}^2 can be extracted from the divergent part of the one-loop self-energies $\Sigma^{(1)}_{\widetilde{B}\nu_{iL}}$ between the bino and each left-handed neutrino. The tree-level mass matrix entries mixing both fields are given by

$$\left(m_{\chi^0}\right)_{\widetilde{B}\nu_{iL}} = -\frac{g_1 v_{iL}}{2} . \tag{5.59}$$

The counterterm of the gauge coupling g_1, whose renormalization we define as $g_1 \to g_1 + \delta g_1$, can be obtained from δM_W^2, δM_Z^2 and δv^2 through the definitions of the gauge boson masses in Eq. (5.15), so that

$$\delta g_1 = \frac{2}{g_1 v^2} \left(\delta M_Z^2 - \delta M_W^2 \right) - \frac{g_1}{2} \frac{\delta v^2}{v^2} . \tag{5.60}$$

Renormalizing the self-energies $\Sigma^{S(1)}_{\widetilde{B}\nu_{iL}}$ using Eq. (4.22), we find the renormalization condition

$$\delta v_{iL}^2 = \frac{4 v_{iL}}{g_1} \Sigma^{S(1)}_{\widetilde{B}\nu_{iL}} \Big|^{\rm div} - v_{iL} \left(\delta Z_{\widetilde{B}\widetilde{B}} v_{iL} + \delta Z_{\nu_{iL}\nu_{iL}} v_{jL} + \delta Z_{\nu_{iL}\widetilde{H}_d^0} v_d \right) - 2 v_{iL}^2 \frac{\delta g_1}{g_1} \Bigg|^{\rm div} , \tag{5.61}$$

which yields

$$\delta v_{iL}^2 = \frac{\Delta}{32\pi^2} v_{iL} \left(\frac{4\pi\alpha v_{iL} \left(s_{\rm w}^2 + 3c_{\rm w}^2\right)}{s_{\rm w}^2 c_{\rm w}^2} + 2 \left(v_d \lambda Y_i^\nu - v_{kL} Y_{ji}^e Y_{jk}^e - v_{jL} Y_i^\nu Y_j^\nu \right) \right) . \tag{5.62}$$

Renormalization of Y_i^ν

We decide to use the renormalization of the element

$$\left(m_{\chi^0}\right)_{\nu_{iL}\widetilde{H}_u^0} = \frac{\mu Y_i^\nu}{\lambda} , \tag{5.63}$$

of the neutral fermion mass matrix, mixing the left-handed neutrinos and the up-type Higgsino, to extract the counterterms δY_i^ν. From the expression for the renormalized scalar part of the self-energies $\Sigma^{S(1)}_{\nu_{iL}\widetilde{H}_u}$, we find the renormalization conditions

$$\delta Y_i^\nu = \frac{1}{2}\left(\delta Z_{\nu_{iL}\widetilde{H}_d^0}\lambda - \delta Z_{\widetilde{H}_u^0\widetilde{H}_u^0} Y_i^\nu - \delta Z_{\nu_{iL}\nu_{iL}} Y_j^\nu\right) - \left(\frac{\delta\mu}{\mu} - \frac{\delta\lambda}{\lambda}\right) + \frac{\lambda}{\mu}\,\Sigma^{S(1)}_{\nu_{iL}\widetilde{H}_u}\Big|^{\text{div}} \ , \tag{5.64}$$

from which we obtain

$$\delta Y_i^\nu = \frac{\Delta}{32\pi^2}\Bigg(- \frac{4\pi\alpha Y_i^\nu\left(s_{\rm w}^2 + 3c_{\rm w}^2\right)}{s_{\rm w}^2 c_{\rm w}^2} + Y_i^\nu\left(3Y_i^u Y_i^u + 2\kappa^2 + 4\lambda^2 + 4Y_j^\nu Y_j^\nu\right) + Y_{ji}^e Y_{jk}^e Y_k^\nu\Bigg) \ . \tag{5.65}$$

Renormalization of $\tan\beta$

We adopted the usual definition for $\tan\beta$ as in the MSSM (see Eq. (5.13)). If we define the renormalization for the vevs of the doublet fields as

$$v_d^2 \to v_d^2 + \delta v_d^2 \ , \quad v_u^2 \to v_u^2 + \delta v_u^2 \ , \tag{5.66}$$

the counterterm for $\tan\beta$ can be written at the one-loop level as a linear combination of the counterterms for the vevs of the doublet Higgses,

$$\delta\tan\beta = \frac{1}{2}\tan\beta\left(\frac{\delta v_u^2}{v_u^2} - \frac{\delta v_d^2}{v_d^2}\right) \ . \tag{5.67}$$

Note that our renormalization of v_u^2 and v_d^2 in Eq. (5.66) includes the contributions from the field renormalization constants inside the counterterms δv_u^2 and δv_d^2. This approach is equivalent to defining

$$v_d \to Z_{H_dH_d}^{1/2}\left(v_d + \delta\hat{v}_d\right) \ , \quad v_u \to Z_{H_uH_u}^{1/2}\left(v_u + \delta\hat{v}_u\right) \ , \tag{5.68}$$

and writing the counterterm of $\tan\beta$ as

$$\delta\tan\beta = \frac{1}{2}\tan\beta\left(\delta Z_{H_uH_u} - \delta Z_{H_dH_d}\right) + \tan\beta\left(\frac{\delta\hat{v}_u}{v_u} - \frac{\delta\hat{v}_d}{v_d}\right) \ . \tag{5.69}$$

This notation was convenient in the MSSM and the NMSSM, because the second bracket in Eq. (5.69) is finite at the one-loop level [4, 11–13], and can be neglected in the $\overline{\rm DR}$ scheme. Then, $\delta\tan\beta$ is expressed exclusively by the field renormalization constants. In contrast, in the $\mu\nu$SSM we find

$$\left(\frac{\delta\hat{v}_u}{v_u} - \frac{\delta\hat{v}_d}{v_d}\right)\Bigg|^{\text{div}} = -\frac{\Delta\lambda v_{iL} Y_i^\nu}{32\pi^2 v_d} \ . \tag{5.70}$$

There are several possibilities to extract the counterterms δv_d^2 and δv_u^2. A convenient choice is to extract δv_d^2 from the renormalization of the entry of the neutral fermion mass matrix mixing the up-type Higgsino and the right-handed neutrino,

$$\left(m_{\chi^0}\right)_{\widetilde{H}_u^0\nu_R} = \frac{1}{\sqrt{2}}\left(-\lambda v_d + v_{iL} Y_i^\nu\right) \ , \tag{5.71}$$

because in this case no off-diagonal field renormalization counterterms appear. The renormalization condition for v_d^2 then reads

$$\begin{aligned}\delta v_d^2 =& -\frac{2\sqrt{2}v_d}{\lambda}\,\Sigma^{S(1)}_{\widetilde{H}_u^0 v_R}\Big|^{\text{div}} + \frac{v_d}{\lambda}\left(\delta Z_{\widetilde{H}_u^0\widetilde{H}_u^0} + \delta Z_{\nu_R\nu_R}\right)(-v_d\lambda + v_{iL}Y_i^\nu) - 2v_d^2\frac{\delta\lambda}{\lambda}\\ &+ \frac{v_d}{\lambda}Y_i^\nu\delta_{ij}\frac{\delta v_{iL}^2}{v_{jL}} + \frac{2v_d}{\lambda}v_{iL}\delta Y_i^\nu\ .\end{aligned} \tag{5.72}$$

There are now two ways to determine δv_u^2. Firstly, we could similarly to δv_d^2 extract the counterterm δv_u^2 by renormalizing the scalar part of the up-type Higgsino self-energy $\Sigma^{S(1)}_{\widetilde{H}_u\widetilde{H}_u}$. Alternatively, we can deduce δv_u^2 from the definition of v^2 in Eq. (5.13) and simply write

$$\delta v_u^2 = \delta v^2 - \delta v_d^2 - \delta v_{1L}^2 - \delta v_{2L}^2 - \delta v_{3L}^2\ . \tag{5.73}$$

We verified that both options yield the same result, which constitutes a consistency test for the counterterms δv_{iL}^2 being unique for the $\mu\nu$SSM. Inserting δv_d^2 from Eq. (5.72) and δv_u^2 from Eq. (5.73) into Eq. (5.67) finally gives

$$\delta\tan\beta = \frac{\Delta}{32\pi^2}\tan\beta\left(3\left(Y_i^dY_i^d - Y_i^uY_i^u\right) + Y_{ij}^eY_{ij}^e - Y_i^\nu Y_i^\nu - \frac{v_{iL}}{v_d}\lambda Y_i^\nu\right)\ . \tag{5.74}$$

The renormalization of $\tan\beta$ in the $\overline{\text{DR}}$ scheme is manifestly process-independent and has shown to give stable numerical results in the MSSM [14, 15] and the NMSSM [4, 13].

Renormalization of A_i^ν

The tree-level expression for the interaction between the up-type Higgs, one left-handed sneutrinos and the right-handed sneutrino is given by

$$\Gamma^{(0)}_{H_u^{\mathcal{R}}\widetilde{\nu}_R^{\mathcal{R}}\widetilde{\nu}_{iL}^{\mathcal{R}}} = -\left(\frac{A_i^\nu}{\sqrt{2}} + \frac{\sqrt{2}\kappa\mu}{\lambda}\right)Y_i^\nu\ . \tag{5.75}$$

In this expression the parameters A_i^ν are the only ones whose counterterms are not yet fixed. Applying the general formula for the renormalized scalar 3-point functions shown in Eq. (4.18) to $\Gamma^{(1)}_{H_u^{\mathcal{R}}\widetilde{\nu}_R^{\mathcal{R}}\widetilde{\nu}_{iL}^{\mathcal{R}}}$, the renormalization condition for the A_i^ν read

$$\begin{aligned}\delta A_i^\nu =& \frac{\sqrt{2}}{Y_i^\nu}\,\Gamma^{(1)}_{H_u^{\mathcal{R}}\widetilde{\nu}_R^{\mathcal{R}}\widetilde{\nu}_{iL}^{\mathcal{R}}}\Big|^{\text{div}} + \frac{1}{\sqrt{2}Y_i^\nu}\Big(\left(\delta Z_{H_uH_u} + \delta Z_{\widetilde{\nu}_R\widetilde{\nu}_R}\right)\Gamma^{(0)}_{H_u^{\mathcal{R}}\widetilde{\nu}_R^{\mathcal{R}}\widetilde{\nu}_{iL}^{\mathcal{R}}} + \delta Z_{H_d\widetilde{\nu}_{iL}}\Gamma^{(0)}_{H_u^{\mathcal{R}}\widetilde{\nu}_R^{\mathcal{R}}H_d^{\mathcal{R}}}\\ &+\delta Z_{\widetilde{\nu}_{jL}\widetilde{\nu}_{iL}}\Gamma^{(0)}_{H_u^{\mathcal{R}}\widetilde{\nu}_R^{\mathcal{R}}\widetilde{\nu}_{jL}^{\mathcal{R}}}\Big) - \frac{A_i^\nu}{Y_i^\nu}\delta Y_i^\nu - \frac{2\mu}{\lambda}\delta\kappa - \frac{2\kappa}{\lambda}\delta\mu - \frac{2\kappa\mu}{\lambda Y_i^\nu}\delta Y_i^\nu + \frac{2\kappa\mu}{\lambda^2}\delta\lambda\ ,\end{aligned} \tag{5.76}$$

with

$$\Gamma^{(0)}_{H_u^{\mathcal{R}}\widetilde{\nu}_R^{\mathcal{R}}H_d^{\mathcal{R}}} = \frac{\lambda A^\lambda}{\sqrt{2}} + \sqrt{2}\kappa\mu\ . \tag{5.77}$$

As in the case of the renormalization of A^λ, the non-diagonal field renormalization counterterms lead to additional terms, in this case proportional to the tree-level vertices $\Gamma^{(0)}_{H_u^{\mathcal{R}}\widetilde{\nu}_R^{\mathcal{R}}H_d^{\mathcal{R}}}$ that compared to the original vertex in Eq. (5.75) have $H_d^{\mathcal{R}}$ instead of $\widetilde{\nu}_{iL}^{\mathcal{R}}$ on an external leg. Putting everything together we find

$$\begin{aligned}\delta A_i^\nu =& \frac{\Delta}{32\pi^2Y_i^\nu}\Bigg(\frac{8\pi\alpha Y_i^\nu\left(M_1s_{\text{w}}^2 + 3M_2c_{\text{w}}^2\right)}{s_{\text{w}}^2c_{\text{w}}^2} + Y_{ji}^eY_{jk}^eT_k^\nu + 2T_{ji}^eY_{jk}^eY_k^\nu + Y_i^\nu\left(7Y_j^\nu T_j^\nu\right.\end{aligned}$$

$$+\ 6Y^u_{ij}T^u_{ij} + 4\kappa^2 A^\kappa + 7\lambda^2 A^\lambda\Big) + A^\nu_i\left(\left(\lambda^2 + Y^\nu_j Y^\nu_j\right) Y^\nu_i - Y^e_{ji}Y^e_{jk}Y^\nu_k\right)\Bigg) \ . \quad (5.78)$$

Renormalization of $m^2_{H_d\widetilde{L}_i}$

The soft scalar masses appear in the bilinear terms of the Higgs potential. Their counterterms can be found by calculating radiative corrections to scalar self-energies. However, calculating scalar self-energy diagrams in the interaction basis is particularly difficult, because also diagrams with more than one mass insertion are potentially UV divergent. To extract $\delta m^2_{H_d\widetilde{L}_i}$ we therefore calculate the $\mathcal{CP}$-odd scalar self-energies in the mass eigenstate basis, and then rotate the self-energies back to the interaction basis. From the form of the renormalized self-energies shown in Eq. (4.16) we can obtain the mass counterterm corresponding to a particular self-energy $\Sigma^{(1)}_{A_iA_j}$ in the mass eigenstate basis from

$$\delta\left(m^2_A\right)_{ij}\Big|^{\text{div}} = \Sigma^{(1)}_{A_iA_j}(0)\Big|^{\text{div}} - \frac{1}{2}\left(\delta Z_{A_iA_j} m^2_{A_j} + m^2_{A_i}\delta Z_{A_iA_j}\right) \ , \quad (5.79)$$

where the field counterterms in the mass eigenstate basis $Z_{A_iA_j}$ were defined in Eq. (5.27), and $m^2_{A_i}$ are the masses squared of the $\mathcal{CP}$-odd scalars. Now inverting the rotation in Eq. (5.24) we can get the mass counterterms for the $\mathcal{CP}$-odd self-energies in the interaction basis via

$$\delta(m^2_\sigma)_{ij}\big|^{\text{div}} = U^A_{ki}\,\delta(m^2_A)_{kl}\big|^{\text{div}}\,U^A_{lj} \ , \quad (5.80)$$

In particular, we recognize that the mass counterterm for the self-energy $\Sigma^{(1)}_{\widetilde{\nu}^{\mathcal{I}}_{iL}H^{\mathcal{I}}_d}$ is defined by the counterterm of the corresponding mass matrix element

$$\left(\delta m^2_\sigma\right)_{\widetilde{\nu}^{\mathcal{I}}_{iL}H^{\mathcal{I}}_d} = \delta m^2_{\widetilde{\nu}^{\mathcal{I}}_{iL}H^{\mathcal{I}}_d} \ , \quad (5.81)$$

where $m^2_{\widetilde{\nu}^{\mathcal{I}}_{iL}H^{\mathcal{I}}_d}$ is given by

$$m^2_{\widetilde{\nu}^{\mathcal{I}}_{iL}H^{\mathcal{I}}_d} = \left(m^2_{H_d\widetilde{L}}\right)_i - \frac{1}{2}v_R^2\lambda Y^\nu_i - \frac{1}{2}v_u^2\lambda Y^\nu_i \ , \quad (5.82)$$

Thus, we find for the parameters $(m^2_{H_d\widetilde{L}})_i$ the renormalization conditions

$$\begin{aligned}\delta\left(m^2_{H_d\widetilde{L}}\right)_i = &\left(\delta m^2_\sigma\right)_{\widetilde{\nu}^{\mathcal{I}}_{iL}H^{\mathcal{I}}_d}\Big|^{\text{div}} + \frac{2\mu Y^\nu_i}{\lambda}\delta\mu + \lambda\left(v_d^2 + v_u^2\right)Y^\nu_i\cos^3\beta\sin\beta\,\delta\tan\beta \\ &+ \frac{1}{2}\lambda Y^\nu_i\sin^2\beta\,\delta v^2 - \frac{1}{2}\lambda\sin^2\beta Y^\nu_i\left(\delta v^2_{1L} + \delta v^2_{2L} + \delta v^2_{3L}\right) \\ &+ \left(\frac{\mu^2}{\lambda} + \frac{1}{2}\lambda\left(v_d^2 + v_u^2\right)\sin^2\beta\right)\delta Y^\nu_i \\ &- \left(\frac{\mu^2 Y^\nu_i}{\lambda^2} - \frac{1}{2}\left(v_d^2 + v_u^2\right)Y^\nu_i\sin^2\beta\right)\delta\lambda \ . \end{aligned} \quad (5.83)$$

The disadvantage of this approach is that we cannot obtain a compact analytical expression for the counterterms $\delta m^2_{H_d\widetilde{L}_i}$, because the couplings in the mass eigenstate, and therefore the self-energies, depend on the mixing matrix elements of all fields that can only be calculated numerically. Also, we are forced to calculate the complete set of self-energies for the $\mathcal{CP}$-odd sector to be able to make the rotation in Eq. (5.80).

Renormalization of $m^2_{\widetilde{L}i\neq j}$

Since we neglect $\mathcal{CP}$-violation the hermitian matrix $m^2_{\widetilde{L}}$ is symmetric, and there are only three independent off-diagional elements. We can extract the counterterms for them in the same way as the ones for $m^2_{H_d\widetilde{L}_i}$ in the $\mathcal{CP}$-odd scalar sector. They appear in the tree-level mass matrix in

$$m^2_{\widetilde{\nu}^{\mathcal{I}}_{iL}\widetilde{\nu}^{\mathcal{I}}_{jL}} = \left(m^2_{\widetilde{L}}\right)_{ij} + \frac{1}{2}\left(v_R^2 + v_u^2\right) Y_i^\nu Y_j^\nu \quad \text{for } i \neq j \,. \tag{5.84}$$

Hence, the renormalization conditions for the counterterms $\delta(m^2_{\widetilde{L}})_{ij}$ for $i \neq j$ can be written in terms of the other independent parameter counterterms as

$$\begin{aligned}\delta\left(m^2_{\widetilde{L}_L}\right)_{ij} = {} & \left(\delta m^2_\sigma\right)_{\widetilde{\nu}^{\mathcal{I}}_{iL}\widetilde{\nu}^{\mathcal{I}}_{jL}}\Big|^{\text{div}} - \frac{1}{2}\left(v_R^2 + v_u^2\right)\left(Y_i^\nu \delta Y_j^\nu - Y_j^\nu \delta Y_i^\nu\right) \\ & - \frac{2\mu Y_i^\nu Y_j^\nu}{\lambda^2}\left(\frac{\delta\mu}{\mu} - \frac{\delta\lambda}{\lambda}\right) - \frac{1}{2}Y_i^\nu Y_j^\nu \sin^2\beta\, \delta v^2 \\ & - \left(v_d^2 + v_u^2\right) Y_i^\nu Y_j^\nu \cos^3\beta \sin\beta\, \delta\tan\beta + \frac{1}{2}Y_i^\nu Y_j^\nu \sin^2\beta\left(\delta v_{1L}^2 + \delta v_{3L}^2 + \delta v_{3L}^2\right) \,.\end{aligned} \tag{5.85}$$

`FeynArts` modelfile

The diagrams and their amplitudes that had to be calculated to obtain the counterterms (as described for each parameter above) were generated using the Mathematica package `FeynArts` [16] and further evaluated with the package `FormCalc` [17] and `LoopTools` [17, 18]. The `FeynArts` model file for the $\mu\nu$SSM was initially created with the Mathematica program `SARAH` [19]. We modified the model file to neglect $\mathcal{CP}$-violation by choosing all relevant parameters to be real. We also neglected flavor mixing in the squark and the quark sector in this work. Certain expressions for the tree-level vertices were modified by hand to improve the numerical performance, and to avoid memory problems caused by too large expressions when using `FormCalc`. The `FeynArts` model file can be provided by the authors upon request. It contains the counterterms as they are defined in the scope of this thesis. The calculation of renormalized two- and three-point functions of the neutral scalars of the $\mu\nu$SSM at one-loop accuracy is thereby fully automated (as it is in the MSSM [20]).

In the following, we will present our predictions for the Higgs-boson masses in the $\mu\nu$SSM. We compared our results to the ones of the NMSSM. To be able to make this comparison, we calculated the NMSSM predictions in the same renormalization scheme and using the same conventions as were used in the $\mu\nu$SSM. This is why we calculated the one-loop self-energies in the NMSSM with our own NMSSM model file for `FeynArts`/`FormCalc` created with `SARAH`, using the same procedure as for the $\mu\nu$SSM. We verified that the results calculated in the NMSSM with our model file are equal to the results calculated with the model file presented in Ref. [21], which was a good check that the generation of the model files for the NMSSM and the $\mu\nu$SSM was correct.

5.2 Loop-corrected Higgs-boson masses

In the previous section we have derived an OS-$\overline{\text{DR}}$ renormalization scheme for the $\mu\nu$SSM Higgs sector. It can be applied (via the `FeynArts` model file) to any higher-order correction in the $\mu\nu$SSM. As a first application, we evaluate the full one-loop corrections to

the $\mathcal{CP}$-even scalar sector in the $\mu\nu$SSM. The corrections to the scalar pole masses are given by the renormalized self-energies in the mass eigenstate basis,

$$\hat{\Sigma}^{(1)}_{h_i h_j}\left(p^2\right) = \Sigma^{(1)}_{h_i h_j}\left(p^2\right) + \delta Z_{h_i h_j}\left(p^2 - \frac{1}{2}\left(m^2_{h_i} + m^2_{h_j}\right)\right) - \left(\delta m^2_h\right)_{ij} \ , \tag{5.86}$$

where $\delta Z_{h_i h_j}$ are the field renormalization counterterms in the mass eigenstate basis (see Eq. (5.27)), and $(\delta m^2_h)_{ij}$ are the mass counterterms defined in Eq. (5.24). The tree-level masses squared $m^2_{h_i}$ are the eigenvalues of the $\mathcal{CP}$-even scalar mass matrix, i.e, the diagonal elements of m^2_h. The self-energy diagrams were calculated in the 't Hooft-Feynman gauge in which the Goldstone bosons G^0 and $G^\pm$ and the ghost fields $u^{W^\pm}$ and u^Z have the same masses as the corresponding gauge bosons. In this gauge the gauge-fixing terms do not yield counterterm contributions in the Higgs sector at the one-loop level. The loop integrals were regularized using DRED [22, 23] and numerically evaluated for arbitrary real momentum using `LoopTools` [17]. The contributions from complex values of p^2 were approximated using a Taylor expansion with respect to the imaginary part of p^2 up to first order.

The self-energies enter the inverse propagator matrix

$$\hat{\Gamma}_h = \mathrm{i}\left[p^2\,\mathbb{1} - \left(m^2_h - \hat{\Sigma}_h\left(p^2\right)\right)\right] \ , \qquad \text{with } \left(\hat{\Sigma}_h\right)_{ij} = \hat{\Sigma}_{h_i h_j} \ . \tag{5.87}$$

The loop-corrected scalar masses squared are the zeroes of the determinant of the inverse propagator matrix. The determination of corrected masses has to be done numerically when one wants to account for the momentum-dependence of the renormalized self-energies. This is done by an iterative method that has to be carried out for each of the six loop-corrected eigenvalues [24].

In Eq. (5.87) we did not include the superscript $^{(1)}$ for the self-energies. Restricting the numerical evaluation to a pure one-loop calculation would lead to very large theoretical uncertainties. We therefore supplement the full one-loop corrections by partial contribtuins beyond the one-loop level. Here, we follow the approach of Ref. [25] and supplement the $\mu\nu$SSM one-loop results by higher-order corrections in the MSSM limit as provided by `FeynHiggs` (version 2.13.0) [3, 26–32]. In this way the leading and subleading two-loop corrections (2) are included, as well as a resummation of large logarithmic terms $^{\text{resum}}$ (see the discussion in Sect. 4.4),

$$\hat{\Sigma}_{h_i h_j}\left(p^2\right) = \hat{\Sigma}^{(1)}_{h_i h_j}\left(p^2\right) + \hat{\Sigma}^{(2)}_{h_i h_j} + \hat{\Sigma}^{\text{resum}}_{h_i h_j} \ . \tag{5.88}$$

In the partial two-loop contributions $\hat{\Sigma}^{(2)}_h$ we take over the corrections of $\mathcal{O}(\alpha_s\alpha_t, \alpha_s\alpha_b, \alpha_t^2, \alpha_t\alpha_b)$, assuming that the MSSM-like corrections are also valid in the $\mu\nu$SSM. This assumption is reasonable, since the only difference between the squark sector of the $\mu\nu$SSM in comparison to the MSSM are the terms proportional to $Y^\nu_i v_{iL}$ in the non-diagonal element of the up-type squark mass matrices (see Eq. (3.104)) and the terms proportional to $v_{iL}v_{iL}$ in the diagonal elements of the up- and down-type squark mass matrices (see Eq. (3.103), Eq. (3.105), Eq. (3.107) and Eq. (3.109)). These terms are negligible in realistic scenarios, since $v_{iL} \ll v_d, v_u, v_R$. Furthermore, in Ref. [4] the quality of the MSSM approximation was tested in the NMSSM, showing that the genuine NMSSM contributions are in most cases sub-leading. Due to the sizes of the neutrino Yukawa couplings Y^ν_i in the $\mu\nu$SSM, also genuine $\mu\nu$SSM contributions are subleading. The same is expected for the contributions stemming from the resummation of large logarithmic terms given by $\hat{\Sigma}^{\text{resum}}_h$.

$v_{iL}/\sqrt{2}$	Y_i^ν	A_i^ν	λ	$\tan\beta$	μ	A^λ	κ	A^κ	
10^{-4}	10^{-6}	-1000	$[0.026; 0.3]$	8	125	897.61	0.2	-300	
M_1	M_2	M_3	$m^2_{\widetilde{Q}_{iL},\widetilde{u}_{iR},\widetilde{d}_{iR}}$	A_3^u	$A_{1,2}^u$	$A_{1,2,3}^d$	$(m^2_{\widetilde{e}})_{ii}$	A_{33}^e	$A_{11,22}^e$
143	300	1500	1500^2	-2000	-1500	-1500	200^2	-1500	-100

Table 5.2: Input parameters for the NMSSM-like crossing point scenario. Dimensionful parameters are given in GeV.

5.3 Numerical analysis

In the following we present the full one-loop corrections to the scalar masses in the $\mu\nu$SSM with one generation of right-handed neutrinos, obtained in the Feynman-diagrammtic approach in a mixed OS-$\overline{\text{DR}}$ renormalization scheme. We take into account all parameters of the model and the dependence on the external momentum. Our results extend the calculations in the MSSM and the NMSSM to a model which has a rich and unique phenomenology through explicit R-parity breaking. The one-loop results are supplemented by known higher-loop results from the MSSM (see the previous section) to reproduce the Higgs-boson mass value of ~ 125 GeV [33]. Here, the theory uncertainty must be kept in mind. In the MSSM it is estimated to be at the level of ~ 2 to 3 GeV [34, 35], and in extended models it is naturally slightly larger [36, 37].

We will present results in several different scenarios, in all of which one scalar with the correct SM-like Higgs-boson mass is reproduced. To get an estimation of the significance of quantum corrections to the SM-like Higgs-boson mass that are unique for the $\mu\nu$SSM, we compare the results to the corresponding ones in the NMSSM. Due to the smallness of Y_i^ν we only find negligible differences. For the left-handed sneutrinos, however, we will see that loop corrections can be become very large, so that it is crucial to control the full set of $\mu\nu$SSM parameters.

The BPs used in the following were not tested in detail against experimental bounds including the R-parity violating effects of the $\mu\nu$SSM. They have been chosen to exemplify the potential magnitude of unique $\mu\nu$SSM-like corrections. Nevertheless, the values we picked for the free parameters should be close to realistic and experimentally allowed scenarios. The parameters in the scalar sector are taken over from calculations in the NMSSM [4] (see Sect. 5.3.1), or from previous studies in the $\mu\nu$SSM with one right-handed neutrino [38] (see Sect. 5.3.2). Unique $\mu\nu$SSM parameters are chosen in a range to reproduce neutrino masses of the correct order of magnitude. That means that for the neutrino Yukawas we chose values of $Y_i^\nu \lesssim 10^{-6}$ and also $v_{iL} \lesssim 10^{-4}$ to generate neutrino masses smaller than 1 eV.

5.3.1 NMSSM-like crossing point scenario

The first scenario we analyze is a BP already studied in the NMSSM taken from Ref. [4]. This scenario was tested therein against the experimental limits from direct searches for BSM Higgs bosons implemented in `HiggsBounds 4.1.3` [39–43]. The scenario features a crossing point in the neutral $\mathcal{CP}$-even scalar sector when $\lambda \approx \kappa$ in which the masses of the singlet (or right-handed sneutrino in our case) and the SM-like Higgs boson become

$m_t^{\overline{\rm MS}}$	m_b	m_c	m_s	m_u	m_d
167.48	4.2	1.286	0.095	0.003	0.006
m_τ	m_μ	m_e	M_W	M_Z	v
1.7792	0.105 658	$5.109\,98 \cdot 10^{-4}$	80.385	91.1875	246.2196

Table 5.3: Values for the SM parameters, i.e., fermion and gauge boson masses and the vev, in GeV.

degenerate, and loop corrections beyond the MSSM become sizable.

In Tab. 5.2 we list the values chosen for the parameters. The SM parameters from the electroweak sector and the lepton and quark masses are given in Tab. 5.3. The parameters present in the $\mu\nu$SSM and the NMSSM, that is all parameters except v_{iL}, Y_i^ν and A_i^ν, are chosen as in the NMSSM calculation [4]. The value for A^λ corresponds to a mass of $m_{H^\pm} = 1000$ GeV for the charged Higgs boson in the NMSSM with $m_{H^\pm}$ renormalized OS, which was the renormalization condition applied in Ref. [4] instead of a $\overline{\rm DR}$ condition for A^λ. A^κ is chosen to be negative and κ positive to avoid tachyons in the pseudoscalar sector (see Eq. (3.68) and the discussion below).

It should be kept in mind that the diagonal soft scalar masses in the neutral sector are extracted from the values for v_{iL}, $\tan\beta$ and μ via the tadpole equations. This is of crucial importance for the comparison of the scalar masses in the $\mu\nu$SSM and the NMSSM, since in the NMSSM the soft slepton masses $m^2_{\widetilde{L}}$ are independent parameters, while in the $\mu\nu$SSM the diagonal elements are dependent parameters fixed by the tadpole equations in Eqs. (3.31), when the vevs are used as input. Consequently, for an accurate comparison, for each BP calculated in the $\mu\nu$SSM, the corresponding values for $m^2_{\widetilde{L}}$ in the NMSSM have to be adjusted accordingly to the same value.

In Fig. 5.1 we show the resulting spectrum of the $\mathcal{CP}$-even scalars at tree level and including the full one-loop and two-loop contributions as a function of λ.[2] The region $\lambda < 0.026$ is excluded because the left-handed sneutrinos become tachyonic at tree-level. The SM-like Higgs-boson mass is reproduced accurately when the quantum corrections are included. The heavy MSSM-like Higgs H and the left-handed sneutrinos $\widetilde{\nu}^{\mathcal{R}}_{iL}$ are at the TeV-scale due to the values chosen for A_i^ν and A^λ. The three $\widetilde{\nu}^{\mathcal{R}}_{iL}$ are degenerate because the $\mu\nu$SSM-like parameters are set equal for all flavors. Their mixings with the doublet Higgs fields $H^{\mathcal{R}}_{d,u}$ and the $\mathcal{CP}$-even right-handed sneutrino $\widetilde{\nu}^{\mathcal{R}}_R$ are suppressed by the size of Y_i^ν, such that they do not play a role in the discussion of this BP.

The mass of $\widetilde{\nu}^{\mathcal{R}}_R$ strongly depends on λ, because when μ is fixed, increasing λ leads to a smaller value for v_R (see Eq. (5.14)). As was observed in Ref. [4], the loop-corrected mass of the singlet becomes smaller than the SM-like Higgs boson mass at about $\lambda \approx \kappa$. We observe large loop corrections to $\widetilde{\nu}^{\mathcal{R}}_R$ in the region of λ where the singlet is the lightest neutral scalar.

Due to the similarity of the Higgs sectors of the NMSSM and the $\mu\nu$SSM, the masses of the doublet-like Higgs bosons and the right-handed sneutrino will be of comparable size as the masses predicted for the doublet-like Higgses and the singlet in the NMSSM. We explicitly checked that genuine $\mu\nu$SSM-like corrections stemming from the additional neutrino Yukawa term and its soft counterpart do have a negligible effect on the Higgs-

[2] Here and in the following we denote with "two-loop" result the one-loop plus partial two-loop plus resummation corrected masses, as described in Sect. 5.3.

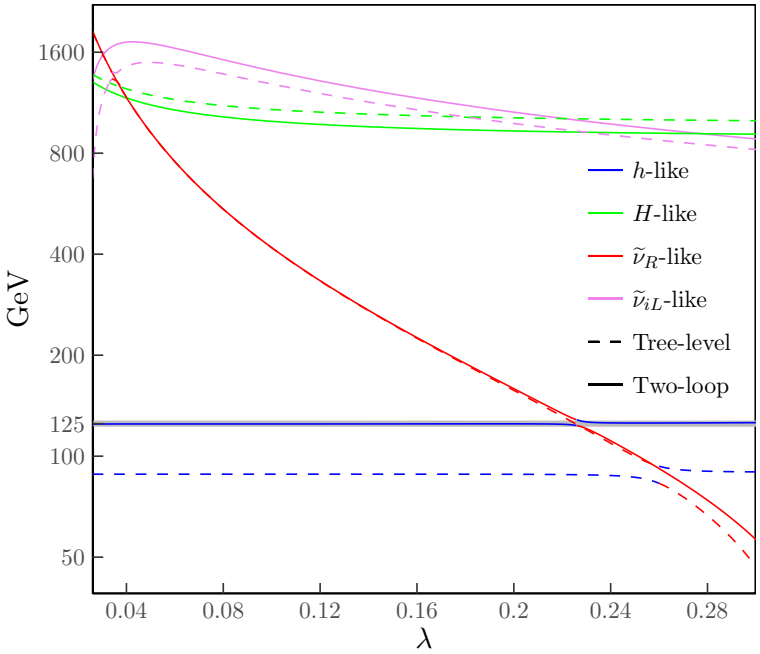

Figure 5.1: Spectrum of $\mathcal{CP}$-even scalar masses in NMSSM-like crossing point scenario. The three left-handed sneutrinos $\widetilde{\nu}_{iL}$ are degenerate. The colors indicate the main composition of the mass eigenstates at tree level (*dashed*) and at two-loop level (*solid*).[3]

boson masses and the mass of $\widetilde{\nu}_R^{\mathcal{R}}$. This is expected, because the values of Y_i^ν are six orders of magnitude smaller than the top Yukawa coupling, and also much smaller than the values for the NMSSM parameters λ and κ. However, in Sect. 5.3.2 we will encounter that the additional parameters of the $\mu\nu$SSM do have a sizable impact on the radiative corrections to the $\mathcal{CP}$-even left-handed sneutrinos.

In Fig. 5.2 we show the tree-level and the one- and two-loop corrected mass of the SM-like Higgs boson in the crossing-point scenario. One can see that the two-loop corrections are crucial to predict a SM-like Higgs-boson mass of 125 GeV. We confirmed that differences between $\mu\nu$SSM and NMSSM predictions of the SM-like Higgs-boson mass are negligible compared to the current experimental uncertainty [33] and the anticipated experimental accuracy of the ILC of about $\lesssim 50$ MeV [44]. Apart from that, they are clearly exceeded by the (future) parametric uncertainties in the Higgs-boson mass calculations, for instance, arising from the uncertainty of the mass of the top quark. Consequently, the Higgs sector alone will not be sufficient to distinguish the $\mu\nu$SSM from the NMSSM. On the other hand, we can regard the theoretical uncertainties in the NMSSM and the $\mu\nu$SSM to be at the same level of accuracy.

5.3.2 Light left-handed τ-sneutrino scenario

In the previous scenario, we observed that in a scenario where the left-handed sneutrinos $\widetilde{\nu}_{iL}^{\mathcal{R}}$ were much heavier than the SM-like Higgs boson, the unique $\mu\nu$SSM-like corrections do not account for a substantial deviation of the SM-like Higgs-boson mass prediction compared to the NMSSM. In this section, we investigate a scenario in which one of the $\widetilde{\nu}_{iL}^{\mathcal{R}}$ has a small mass close to SM Higgs-boson mass. The phenomenology of such a

[3] All plots in this chapter have been produced using `ggplot2` [45] and `tikzDevice` [46] in `R` [47].

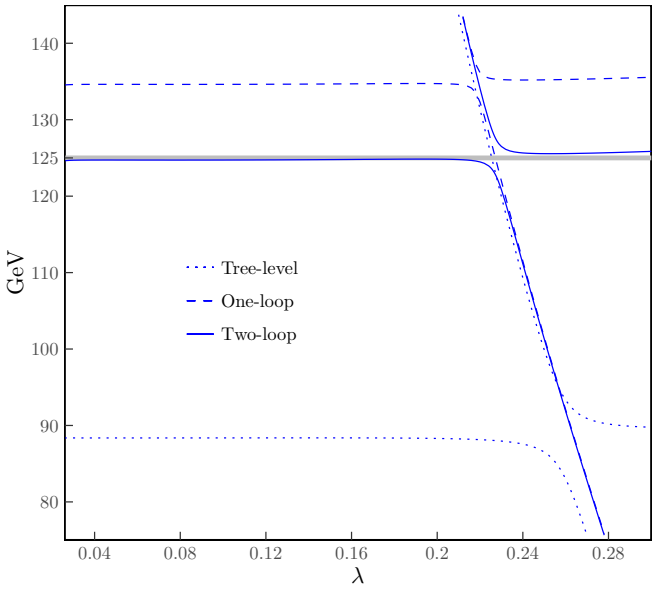

Figure 5.2: Tree-level, one-loop and two-loop corrected masses of the SM-like Higgs boson in the $\mu\nu$SSM in the NMSSM-like crossing point scenario.

spectrum was studied in detail, including a comparison of its predictions with the LHC searches [38, 48]. It was found that a light left-handed sneutrino as the LSP can give rise to distinct signals for the $\mu\nu$SSM (for instance, final states with diphoton plus missing energy, diphoton plus leptons and multileptons).[4]

In Tab. 5.4 we list the relevant parameters that were chosen such that a light $\mathcal{CP}$-even left-handed τ-sneutrino $\widetilde{\nu}^{\mathcal{R}}_{\tau L}$ is present. The parameters not shown are chosen to be the same as in the previous BP, shown in Tab. 5.2. The vev v_{3L} (corresponding to $\widetilde{\nu}^{\mathcal{R}}_{\tau L}$) was increased w.r.t. the NMSSM-like scenario, leading to a reduced tree-level mass of $\widetilde{\nu}^{\mathcal{R}}_{\tau L}$, scaling with the inverse of v_{3L}, as can be seen from the approximate formula

$$m^2_{\widetilde{\nu}^{\mathcal{R}}_{iL}\widetilde{\nu}^{\mathcal{R}}_{iL}} \approx \frac{Y^\nu_i v_R v_u}{2 v_{iL}} \left(-\sqrt{2} A^\nu_i - \kappa v_R + \frac{\sqrt{2}\mu}{\tan\beta} \right) , \tag{5.89}$$

which follows from the general expression shown in Eq. (3.48) when only one right-handed neutrino superfield is considered. We also decreased the absolute value of A^ν_3 in comparison to the previous BP, keeping it negative, so that it is of order κv_R and the the sum in the brackets of Eq. (5.89) becomes small.

In Fig. 5.3 we show the tree-level and loop-corrected spectrum of the scalars in the region of λ, where there are no tachyons at tree level. For too small λ the tree-level mass of $\widetilde{\nu}^{\mathcal{R}}_{\tau L}$ becomes tachyonic, because, for fixed μ, v_R has to grow when λ becomes smaller. At some point the second term in the bracket of Eq. (5.89) will grow larger than the sum of the first and the third term. For too large λ, i.e., when v_R becomes small, the tree-level mass of the right-handed $\mathcal{CP}$-even sneutrino becomes tachyonic, because the first term in Eq. (3.53) is negative when $A^\kappa < 0$.

The value of ~ 125 GeV for the SM-like Higgs-boson mass is reproduced in this BP up to values of $\lambda \leq 0.22$. However, considering the theoretical uncertainty, even higher

[4]Due to the R-parity breaking it is a slight abuse of terminology to refer to the left-handed sneutrino as the LSP. However, the R-parity violating decays and the mixing of the $\widetilde{\nu}^{\mathcal{R}}_{iL}$ with SM particles are suppressed by the smallness of Y^ν_i, so that they can practically be identified as Susy particles.

$v_{1,2L}/\sqrt{2}$	$v_{3L}/\sqrt{2}$	Y_i^ν	A_i^ν	$\tan\beta$	μ	λ	A^λ	κ	A^κ
10^{-5}	$4 \cdot 10^{-4}$	$5 \cdot 10^{-7}$	-400	10	270	$[0.19; 0.3]$	1000	0.3	-1000

Table 5.4: Input parameters for the light τ-sneutrino scenario. Dimensionful parameters are given in GeV.

values of λ can be viable. For $\lambda = 0.236$ the prediction for the SM-like Higgs-boson mass decreases below $m_{h_1}^{(2)} \approx 122$ GeV. As discussed in the introduction, we assume a theory uncertainty of ~ 3 GeV on the mass evaluation, so we consider in this scenario the region $\lambda \leq 0.236$ to be valid regarding the SM-like Higgs-boson mass.

An interesting observation is that the mass of $\widetilde{\nu}_{\tau L}^{\mathcal{R}}$ is mainly induced via quantum corrections, while the tree-level mass approaches zero for small values of λ. Since the partial two-loop corrections are purely MSSM-like contributions, and since the $\widetilde{\nu}_{iL}^{\mathcal{R}}$ do not mix significantly with the Higgs doublet fields $H_{d,u}^{\mathcal{R}}$, the loop-corrections to $\widetilde{\nu}_{\tau L}^{\mathcal{R}}$ can be entirely attributed to the one-loop corrections from the $\mu\nu$SSM. They increase the mass of $\widetilde{\nu}_{\tau L}^{\mathcal{R}}$ roughly by a factor of two over the whole region of λ. In other words, for light left-handed sneutrinos the radiative corrections at the one-loop level can be of the same size as the tree-level masses themselves. This indicates that a consistent treatment of quantum corrections to light left-handed sneutrino masses is of crucial importance in the $\mu\nu$SSM.

The large upward shift of the mass of $\widetilde{\nu}_{\tau L}^{\mathcal{R}}$ through the one-loop corrections is due to the fact that in the $\mu\nu$SSM the sneutrino fields are part of the Higgs potential, each with an associated tadpole coefficient $T_{\widetilde{\nu}_{iL}^{\mathcal{R}}}$ (see Eq. (5.10)). To ensure the stability of the vacuum w.r.t. quantum corrections, the tadpoles are renormalized OS, absorbing all finite corrections into the counterterms $\delta T_{\widetilde{\nu}_{iL}^{\mathcal{R}}}$. In the mass counterterms for the left-handed sneutrinos the finite parts $\delta T_{\widetilde{\nu}_{iL}^{\mathcal{R}}}^{\text{fin}}$ introduce a contribution of the form

$$\delta m^{2\,\text{fin}}_{\widetilde{\nu}_{iL}^{\mathcal{R}}\widetilde{\nu}_{iL}^{\mathcal{R}}} = -\frac{\delta T^{\text{fin}}_{\widetilde{\nu}_{iL}^{\mathcal{R}}}}{v_{iL}} + \cdots \,, \tag{5.90}$$

which is enhanced by the inverse of the vev of ν_{iL}. Precisely these terms inside the counterterms of the renormalized self-energies $\hat{\Sigma}^{(1)}_{\widetilde{\nu}_{iL}^{\mathcal{R}}\widetilde{\nu}_{iL}^{\mathcal{R}}}$ shift the poles of the propagator matrix and increase the masses of the left-handed sneutrinos, especially in cases where the tree-level masses are small.

This behavior is a peculiarity of the $\mu\nu$SSM in which the leptonic sector and the Higgs sector are mixed due the breaking of R-parity. The relations between the vevs v_{iL} and the soft masses $m^2_{\widetilde{L}}$ via the tadpole equations automatically lead to dependences between the sneutrino masses and, for instance, the neutrino or the Higgs sector. In the NMSSM, on the other hand, the sneutrinos are not part of the Higgs potential, since the fields are protected by lepton-number conservation. Hence, the soft masses $m^2_{\widetilde{L}}$ are, without further assumptions, free parameters that can be chosen without taking into account any leptonic observable (such as neutrino masses and mixings). In principle, the additional dependences of the $\mu\nu$SSM scalar masses on parameters related to the neutrino sector, such as Y_i^ν and v_{iL}, could be used (e.g. when all neutrino masses and mixing angles will be known with sufficient experimental accuracy) to restrict the possible range of $m^2_{\widetilde{L}}$, and thus the possible values for the left-handed sneutrino masses. However, with our current experimental knowledge on the neutrino masses, the possible values for the vevs v_{iL}, and hence the possible range of left-handed sneutrino masses, are effectively not yet

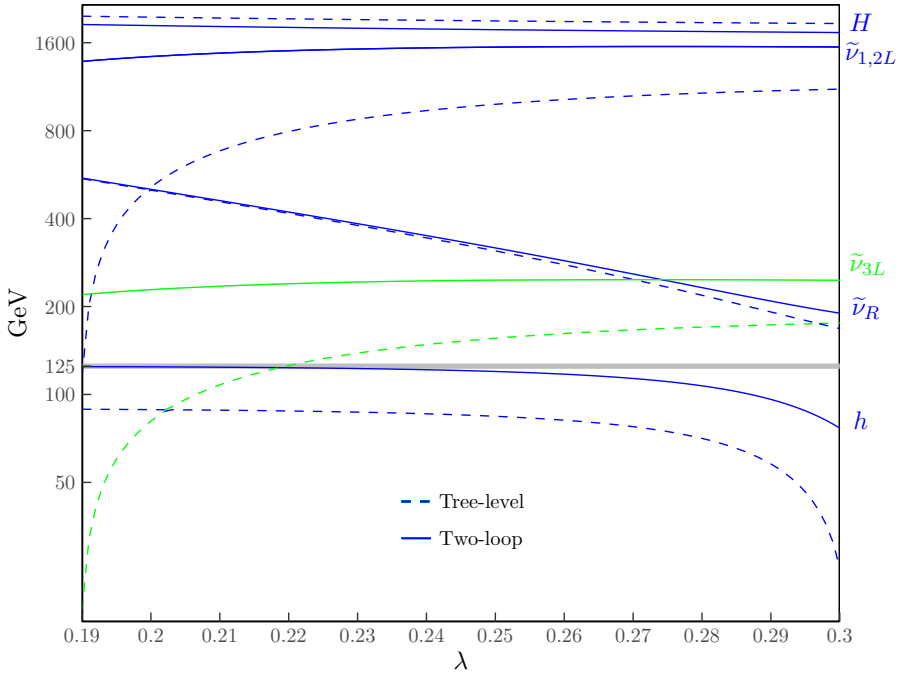

Figure 5.3: $\mathcal{CP}$-even scalar mass spectrum of the $\mu\nu$SSM in the light τ-sneutrino scenario at tree level (*dashed*) and at two-loop level (*solid*). On the right side we state the dominant composition of the mass eigenstates. The lines corresponding to $\widetilde{\nu}^{\mathcal{R}}_{\tau L}$ are highlighted in green.

constrained. Apart from that, the soft trilinears A^{ν}_{i} constitute a further independent parameter to adjust the masses of the $\widetilde{\nu}^{\mathcal{R}}_{iL}$, which is not directly related to the fermion sector.

It should be noted as well, that the soft masses $m^2_{\widetilde{L}}$ also appear in the mass matrix of the charged scalars and the pseudoscalars. In many cases, they are the dominant term in the tree-level masses of the left-handed sleptons and sneutrinos, so the values of the masses of charged sleptons and sneutrino of the same family will be close (see also Eq. (3.86)). Thus, a precise treatment of quantum corrections of the size observed in Fig. 5.3 is extremely important, since they might easily change the relative sign of the mass differences of left-handed sleptons and sneutrinos of the same family. This can result in a complete change of the phenomenology of the corresponding BP, for instance, when the neutral (pseudo)scalar is the LSP [38, 48].

In Fig. 5.4 we compare the light $\mathcal{CP}$-even scalar spectrum of the $\mu\nu$SSM to the corresponding Higgs sector in the NMSSM. We show the tree-level and one-loop corrected masses of the light $\mathcal{CP}$-even scalars in the $\mu\nu$SSM, and the masses of the SM-like Higgs boson and the singlet-like Higgs boson in the NMSSM on the right, with parameters set accordingly. We shade in gray the region of λ in which the prediction for the SM-like Higgs-boson mass is below 122 GeV at the two-loop level. As expected, the SM-like Higgs-boson mass and the mass of the singlet-like states turn out to be equal in both models. Even where the SM-like Higgs boson is degenerate with the left-handed sneutrinos, such that a mixing of both states theoretically can become sizable, the differences between the predictions for the SM-like Higgs-boson mass in both models are not larger than a few keV.

It is rather surprising that the predictions for the SM-like Higgs-boson mass coincide this precisely in both models, considering the fact that in the $\mu\nu$SSM a substantial

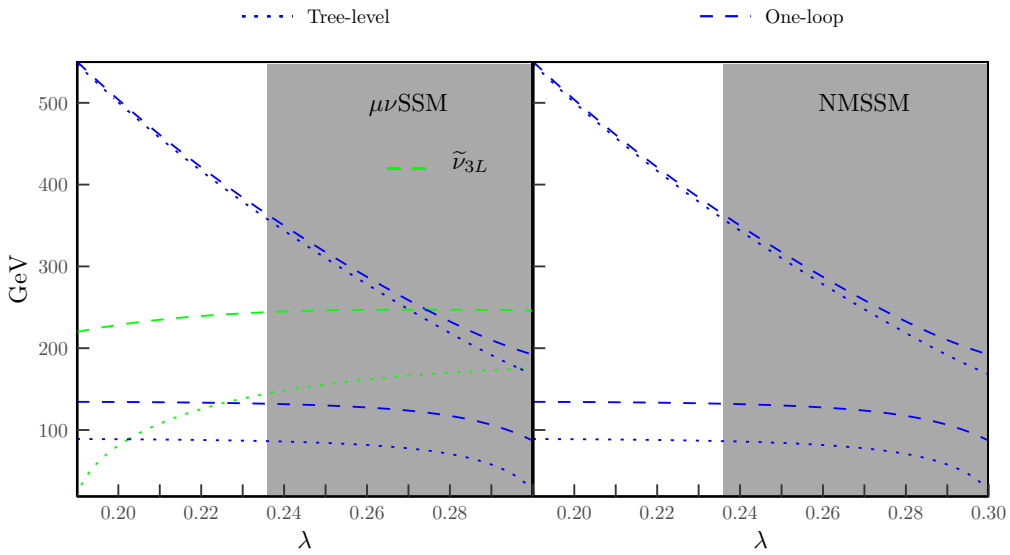

Figure 5.4: Comparison of Higgs-boson masses in the light τ-sneutrino scenario. In the shaded region the prediction for the SM-like Higgs-boson mass is below 122 GeV at the two-loop level. *Left:* Masses of the SM-like Higgs-boson, the left-handed τ-sneutrino (*green*) and the right-handed sneutrino in the $\mu\nu$SSM at tree level (*dotted*) and one-loop level (*dashed*). *Right:* Masses of the SM-like Higgs-boson and the singlet-like Higgs boson in the NMSSM at tree-level and one-loop level.

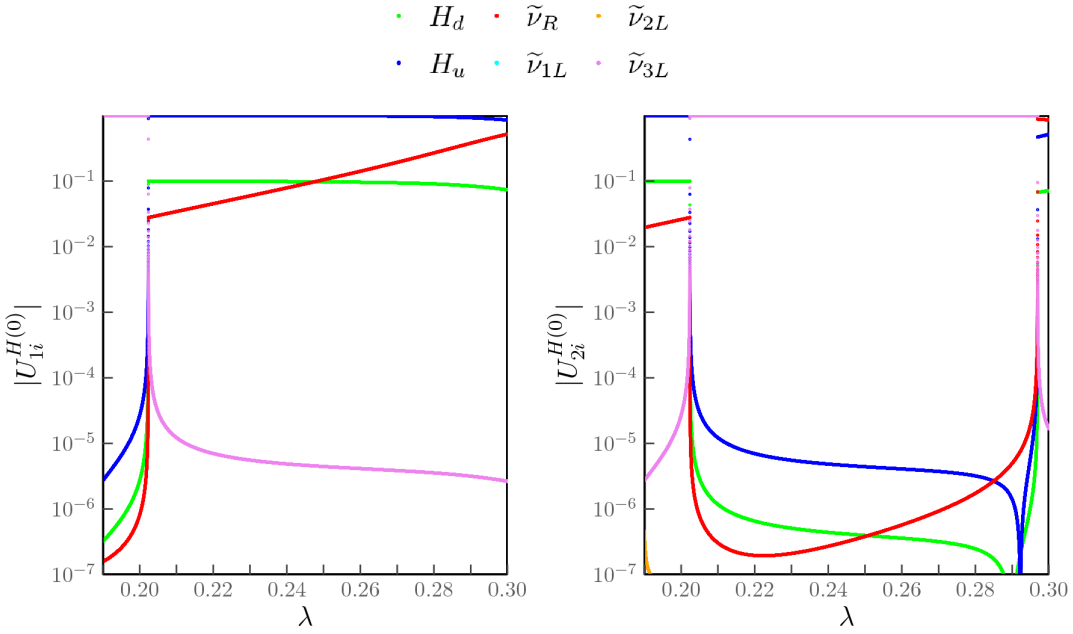

Figure 5.5: Absolute values of the mixing matrix elements at tree level $|U_{1i}^{H(0)}|$ (*left*) and $|U_{2i}^{H(0)}|$ (*right*), whose squared values define the admixture of the two-lightest $\mathcal{CP}$-even scalar mass eigenstate $h_{1,2}$ with the fields $\varphi_i = (H_d^{\mathcal{R}}, H_u^{\mathcal{R}}, \widetilde{\nu}_R^{\mathcal{R}}, \widetilde{\nu}_{1L}^{\mathcal{R}}, \widetilde{\nu}_{2L}^{\mathcal{R}}, \widetilde{\nu}_{3L}^{\mathcal{R}})$ in the interaction basis. A substantial admixture of $\widetilde{\nu}_{\tau L}^{\mathcal{R}}$ (*pink*) with the SM-like Higgs boson h^{125} and with the singlet $\widetilde{\nu}_R$ is present in the narrow region where the corresponding tree-level masses are degenerate, i.e., at $\lambda \sim 0.20237$ and $\lambda \sim 0.29692$.

mixing with the left-handed sneutrino is possible at tree level, as we show in Fig. 5.5. We individually plot the elements of the first two rows of the tree-level mixing matrix $U^{H(0)}$, whose squared values define the composition of the two lightest $\mathcal{CP}$-even mass eigenstate $h_1^{(0)}$ and $h_2^{(0)}$ at tree level. In the left plot we see that in the cross-over point in which the masses of the τ-sneutrino and the SM-like Higgs boson become degenerate, the lightest scalar results to be a mixture of $\widetilde{\nu}_{\tau L}^{\mathcal{R}}$ and the doublet-components $H_u^{\mathcal{R}}$ and $H_d^{\mathcal{R}}$. For example, if we fine-tune $\lambda = 0.20237$ we find that the lightest Higgs boson is composed of approximately

$$H_d \quad \rightarrow \quad |U_{11}^{H(0)}|^2 \sim 1\% \,, \tag{5.91}$$

$$H_u \quad \rightarrow \quad |U_{12}^{H(0)}|^2 \sim 80\% \,, \tag{5.92}$$

$$\widetilde{\nu}_{3L} \quad \rightarrow \quad |U_{16}^{H(0)}|^2 \sim 19\% \,. \tag{5.93}$$

Nevertheless, due to the upward shift of the mass of $\widetilde{\nu}_{\tau L}^{\mathcal{R}}$ caused by the finite loop corrections, as explained before, the one-loop corrections break the degeneracy and no trace on the SM-like Higgs-boson mass remains which would deviate its prediction from the one in the NMSSM.

Bibliography

[1] T. Biekötter, S. Heinemeyer, and C. Muñoz, "Precise prediction for the Higgs-boson masses in the $\mu\nu$SSM", *Eur. Phys. J.* **C78** (2018), no. 6, 504, arXiv:1712.07475.

[2] T. Biekötter, S. Heinemeyer, and C. Muñoz, "Precise prediction for the Higgs-Boson Masses in the $\mu\nu$SSM with three right-handed neutrino superfields", arXiv:1906.06173.

[3] M. Frank, T. Hahn, S. Heinemeyer, W. Hollik, H. Rzehak, and G. Weiglein, "The Higgs Boson Masses and Mixings of the Complex MSSM in the Feynman-Diagrammatic Approach", *JHEP* **02** (2007) 047, arXiv:hep-ph/0611326.

[4] P. Drechsel, "Precise Predictions for Higgs Physics in the Next-to-Minimal Supersymmetric Standard Model (NMSSM)", DESY-THESIS-2016-019, Hamburg, 2016

[5] W. Grimus and M. Löschner, "Revisiting on-shell renormalization conditions in theories with flavor mixing", *Int. J. Mod. Phys.* **A31** (2017), no. 24, 1630038, arXiv:1606.06191, [Erratum: Int. J. Mod. Phys.A32,no.13,1792001(2017)].

[6] J. Bijnens, J. Oredsson, and J. Rathsman, "Scalar Kinetic Mixing and the Renormalization Group", arXiv:1810.04483.

[7] A. Salam and J. A. Strathdee, "On Superfields and Fermi-Bose Symmetry", *Phys. Rev.* **D11** (1975) 1521–1535.

[8] M. T. Grisaru, W. Siegel, and M. Rocek, "Improved Methods for Supergraphs", *Nucl. Phys.* **B159** (1979) 429.

[9] S. P. Martin, "A Supersymmetry primer", arXiv:hep-ph/9709356, [Adv. Ser. Direct. High Energy Phys.18,1(1998)].

[10] W. Hollik, "Electroweak theory", in "5th Hellenic School and Workshops on Elementary Particle Physics (CORFU 1995) Corfu, Greece, September 3-24, 1995". 1995. arXiv:hep-ph/9602380.

[11] P. H. Chankowski, S. Pokorski, and J. Rosiek, "Complete on-shell renormalization scheme for the minimal supersymmetric Higgs sector", *Nucl. Phys.* **B423** (1994) 437–496, arXiv:hep-ph/9303309.

[12] A. Dabelstein, "The One loop renormalization of the MSSM Higgs sector and its application to the neutral scalar Higgs masses", *Z. Phys.* **C67** (1995) 495–512, arXiv:hep-ph/9409375.

[13] K. Ender, T. Graf, M. Muhlleitner, and H. Rzehak, "Analysis of the NMSSM Higgs Boson Masses at One-Loop Level", *Phys. Rev.* **D85** (2012) 075024, arXiv:1111.4952.

[14] M. Frank, S. Heinemeyer, W. Hollik, and G. Weiglein, "FeynHiggs1.2: Hybrid MS-bar / on-shell renormalization for the CP even Higgs boson sector in the MSSM", arXiv:hep-ph/0202166.

[15] A. Freitas and D. Stockinger, "Gauge dependence and renormalization of tan beta in the MSSM", *Phys. Rev.* **D66** (2002) 095014, arXiv:hep-ph/0205281.

[16] T. Hahn, "Generating Feynman diagrams and amplitudes with FeynArts 3", *Comput. Phys. Commun.* **140** (2001) 418–431, arXiv:hep-ph/0012260.

[17] T. Hahn and M. Perez-Victoria, "Automatized one loop calculations in four-dimensions and D-dimensions", *Comput. Phys. Commun.* **118** (1999) 153–165, arXiv:hep-ph/9807565.

[18] G. J. van Oldenborgh and J. A. M. Vermaseren, "New Algorithms for One Loop Integrals", *Z. Phys.* **C46** (1990) 425–438.

[19] F. Staub, "From Superpotential to Model Files for FeynArts and CalcHep/CompHep", *Comput. Phys. Commun.* **181** (2010) 1077–1086, arXiv:0909.2863.

[20] T. Fritzsche, T. Hahn, S. Heinemeyer, F. von der Pahlen, H. Rzehak, and C. Schappacher, "The Implementation of the Renormalized Complex MSSM in FeynArts and FormCalc", *Comput. Phys. Commun.* **185** (2014) 1529–1545, arXiv:1309.1692.

[21] S. Paßehr, "FeynArts model file with counterterms for the NMSSM with complex parameters", FeynHiggs workshop, Hamburg (Germany), 30 Mar 2015 - 1 Apr 2015. Mar 2015.

[22] W. Siegel, "Supersymmetric dimensional regularization via dimensional reduction", *Physics Letters B* **84** (1979), no. 2, 193 – 196.

[23] D. Capper, D. Jones, and P. V. Nieuwenhuizen, "Regularization by dimensional reduction of supersymmetric and non-supersymmetric gauge theories", *Nuclear Physics B* **167** (1980), no. 3, 479 – 499.

[24] E. Fuchs, "Interference effects in new physics processes at the LHC", DESY-THESIS-2015-037, U. Hamburg, Dept. Phys., Hamburg, 2015

[25] P. Drechsel, L. Galeta, S. Heinemeyer, and G. Weiglein, "Precise Predictions for the Higgs-Boson Masses in the NMSSM", *Eur. Phys. J.* **C77** (2017), no. 1, 42, arXiv:1601.08100.

[26] S. Heinemeyer, W. Hollik, and G. Weiglein, "FeynHiggs: A Program for the calculation of the masses of the neutral CP even Higgs bosons in the MSSM", *Comput. Phys. Commun.* **124** (2000) 76–89, arXiv:hep-ph/9812320.

[27] T. Hahn, S. Heinemeyer, W. Hollik, H. Rzehak, and G. Weiglein, "FeynHiggs: A program for the calculation of MSSM Higgs-boson observables - Version 2.6.5", *Comput. Phys. Commun.* **180** (2009) 1426–1427.

[28] S. Heinemeyer, W. Hollik, and G. Weiglein, "The Masses of the neutral CP - even Higgs bosons in the MSSM: Accurate analysis at the two loop level", *Eur. Phys. J.* **C9** (1999) 343–366, arXiv:hep-ph/9812472.

[29] G. Degrassi, S. Heinemeyer, W. Hollik, P. Slavich, and G. Weiglein, "Towards high precision predictions for the MSSM Higgs sector", *Eur. Phys. J.* **C28** (2003) 133–143, arXiv:hep-ph/0212020.

[30] T. Hahn, S. Heinemeyer, W. Hollik, H. Rzehak, and G. Weiglein, "High-Precision Predictions for the Light CP -Even Higgs Boson Mass of the Minimal Supersymmetric Standard Model", *Phys. Rev. Lett.* **112** (2014), no. 14, 141801, arXiv:1312.4937.

[31] H. Bahl and W. Hollik, "Precise prediction for the light MSSM Higgs boson mass combining effective field theory and fixed-order calculations", *Eur. Phys. J.* **C76** (2016), no. 9, 499, arXiv:1608.01880.

[32] See: http://www.feynhiggs.de.

[33] **ATLAS, CMS** Collaboration, G. Aad *et al.*, "Combined Measurement of the Higgs Boson Mass in pp Collisions at $\sqrt{s} = 7$ and 8 TeV with the ATLAS and CMS Experiments", *Phys. Rev. Lett.* **114** (2015) 191803, arXiv:1503.07589.

[34] H. Bahl, S. Heinemeyer, W. Hollik, and G. Weiglein, "Reconciling EFT and hybrid calculations of the light MSSM Higgs-boson mass", *Eur. Phys. J.* **C78** (2018), no. 1, 57, arXiv:1706.00346.

[35] B. C. Allanach and A. Voigt, "Uncertainties in the Lightest CP Even Higgs Boson Mass Prediction in the Minimal Supersymmetric Standard Model: Fixed Order Versus Effective Field Theory Prediction", *Eur. Phys. J.* **C78** (2018), no. 7, 573, arXiv:1804.09410.

[36] P. Drechsel, R. Gröber, S. Heinemeyer, M. M. Muhlleitner, H. Rzehak, and G. Weiglein, "Higgs-Boson Masses and Mixing Matrices in the NMSSM: Analysis of On-Shell Calculations", *Eur. Phys. J.* **C77** (2017), no. 6, 366, arXiv:1612.07681.

[37] T. N. Dao, R. Gröber, M. Krause, M. Mühlleitner, and H. Rzehak, "Two-Loop $\mathcal{O}(\alpha_t^2)$ Corrections to the Neutral Higgs Boson Masses in the CP-Violating NMSSM", arXiv:1903.11358.

[38] P. Ghosh, I. Lara, D. E. Lopez-Fogliani, C. Munoz, and R. Ruiz de Austri, "Searching for left sneutrino LSP at the LHC", *Int. J. Mod. Phys.* **A33** (2018), no. 18n19, 1850110, arXiv:1707.02471.

[39] P. Bechtle, O. Brein, S. Heinemeyer, G. Weiglein, and K. E. Williams, "HiggsBounds: Confronting Arbitrary Higgs Sectors with Exclusion Bounds from LEP and the Tevatron", *Comput. Phys. Commun.* **181** (2010) 138–167, arXiv:0811.4169.

[40] P. Bechtle, O. Brein, S. Heinemeyer, G. Weiglein, and K. E. Williams, "HiggsBounds 2.0.0: Confronting Neutral and Charged Higgs Sector Predictions with Exclusion Bounds from LEP and the Tevatron", *Comput. Phys. Commun.* **182** (2011) 2605–2631, arXiv:1102.1898.

[41] P. Bechtle, O. Brein, S. Heinemeyer, O. Stal, T. Stefaniak, G. Weiglein, and K. Williams, "Recent Developments in HiggsBounds and a Preview of HiggsSignals", *PoS* **CHARGED2012** (2012) 024, arXiv:1301.2345.

[42] P. Bechtle, O. Brein, S. Heinemeyer, O. Stål, T. Stefaniak, G. Weiglein, and K. E. Williams, "HiggsBounds – 4: Improved Tests of Extended Higgs Sectors against Exclusion Bounds from LEP, the Tevatron and the LHC", *Eur. Phys. J.* **C74** (2014), no. 3, 2693, arXiv:1311.0055.

[43] P. Bechtle, S. Heinemeyer, O. Stal, T. Stefaniak, and G. Weiglein, "Applying Exclusion Likelihoods from LHC Searches to Extended Higgs Sectors", *Eur. Phys. J.* **C75** (2015), no. 9, 421, arXiv:1507.06706.

[44] A. Arbey *et al.*, "Physics at the e+ e- Linear Collider", *Eur. Phys. J.* **C75** (2015), no. 8, 371, arXiv:1504.01726.

[45] H. Wickham, "ggplot2: Elegant graphics for data analysis", Springer-Verlag New York, 2009.

[46] C. Sharpsteen and C. Bracken, *tikzDevice: R Graphics Output in LaTeX Format*, 2018. R package version 0.10-1.2.

[47] R Core Team, *R: A Language and Environment for Statistical Computing*. R Foundation for Statistical Computing, Vienna, Austria, 2018.

[48] I. Lara, D. E. López-Fogliani, C. Muñoz, N. Nagata, H. Otono, and R. Ruiz De Austri, "Looking for the left sneutrino LSP with displaced-vertex searches", *Phys. Rev.* **D98** (2018), no. 7, 075004, arXiv:1804.00067.

Chapter 6

Higgs potential of the $\mu\nu$SSM with three right-handed neutrinos

In this chapter we apply our renormalization procedure to the $\mu\nu$SSM with three right-handed neutrino superfields [1], instead of just one as in Ch. 5. Since three right-handed neutrinos are present, a total number of three neutrino masses are generated already at tree level via the electroweak seesaw mechanism. The scalar Susy partners of the additional right-handed neutrinos extend the $\mathcal{CP}$-even and $\mathcal{CP}$-odd neutral scalar sector by two additional particles, respectively. Consequently, the renormalization at the one-loop level will be more complicated. Also the numbers of free parameters in the scalar potential increases dramatically. For instance, there will be three different λ_i-terms, and a total of ten κ_{ijk}-terms (see Eq. (3.8)), considering that κ_{ijk} must be symmetric under the exchange of indices. The complete set of independent parameters utilized to define the renormalization scheme is stated in Sect. 6.1. In analogy to the previous discussion for the one-generation case, we give the precise form of the renormalization condition for each parameter, again deploying OS conditions when this is eligible. Conceptual differences to the discussion in Sect. 5.1 are emphasized. Afterwards, we describe the incorporation of the loop corrections to the neutral scalar masses in Sect. 6.2. Because neutrino masses and mixings can be accounted for at tree level in the three-generation case, we are able to present BPs in the numerical discussion in Sect. 6.3 in which, in addition to the properties of the SM-like Higgs boson, the neutrino sector is described in agreement with experimental results. We focus in particular on scenarios incorporating light right-handed neutrinos with masses close to the SM-like Higgs-boson mass.

6.1 Renormalization at the one-loop level

We already described the neutral scalar potential for the $\mu\nu$SSM with three right-handed neutrino superfields in Sect. 3.3.1. The relevant part for the radiative corrections to the masses of the neutral scalars is given by the tadpole equations shown in Eqs. (3.28)-(3.31), and by the $\mathcal{CP}$-even and $\mathcal{CP}$-odd scalar mass matrices in Eq. (3.34) and Eq. (3.35), where the vevs of the scalar components are defined via the decomposition in Eqs. (3.23)-(3.25).

As in the one-generation case, we substitute some of the parameters of the scalar potential. To facilitate the comparison to calculations in the (N)MSSM, we again use the parameters

$$\tan\beta = \frac{v_u}{v_d} \qquad \text{and} \qquad v^2 = v_d^2 + v_u^2 + v_{iL} v_{iL} \ , \tag{6.1}$$

Soft masses	vevs	Gauge cpl.	Superpot.	Soft trilinears
$m^2_{H_d}$, $m^2_{H_u}$, $m^2_{\widetilde{\nu}_R ij}$	v_d, v_u, v_{iR}, v_{iL}	g_1, g_2	λ_i, κ_{ijk}, Y^ν_{ij}	T^λ_i, T^κ_{ijk}, T^ν_{ij}
$m^2_{\widetilde{L}ij}$, $m^2_{H_d\widetilde{L}_i}$				
$\downarrow$	$\downarrow$	$\downarrow$		
$T_{H_d^{\mathcal{R}}}$, $T_{H_u^{\mathcal{R}}}$, $T_{\widetilde{\nu}^{\mathcal{R}}_{iR}}$, $T_{\widetilde{\nu}^{\mathcal{R}}_{iL}}$,	$\tan\beta$, v, v_{iR}, v_{iL}	M_W, M_Z		
$m^2_{\widetilde{\nu}i\neq j}$, $m^2_{\widetilde{L}i\neq j}$, $m^2_{H_d\widetilde{L}_i}$				

Table 6.1: Set of independent parameters initially entering the tree-level Higgs potential of the $\mu\nu$SSM on top, and final choice of free parameters after the substitutions defined in the text.

instead of the vevs v_d and v_u as input parameters. v corresponds to the SM vev, such that the SM gauge boson masses are given by

$$M_W^2 = \frac{1}{4} g_2^2 v^2 \qquad \text{and} \qquad M_Z^2 = \frac{1}{4}\left(g_1^2 + g_2^2\right) v^2 \,. \tag{6.2}$$

We eliminate the gauge couplings g_1 and g_2 using the above formulas and instead use the SM gauge boson masses as independent parameters. Hence, we can define OS conditions for M_W^2 and M_Z^2, in total analogy to the was already explained in Sect. 5.1. Furthermore, the scalar soft masses $m^2_{H_d}$ and $m^2_{H_u}$ and the diagonal elements of the soft slepton mass matrices $(m^2_{\widetilde{L}})_{ii}$ and $(m^2_{\widetilde{\nu}})_{ii}$ are replaced by the tadpole coefficient in which they appear. Again, this is the same approach as was used in the one-generation case. The only difference is that due to the presence of three $\mathcal{CP}$-even right-handed sneutrinos, the soft mass $m^2_{\widetilde{\nu}}$ becomes a 3×3 dimensional matrix. There are a total of eight tadpole equations. The three coefficients $T_{\widetilde{\nu}^{\mathcal{R}}_{iL}}$ shown in Eq. (3.30) are used to replace the elements $(m^2_{\widetilde{\nu}})_{ii}$. As explained before, the tadpole coefficients will be treated as OS parameters to ensure the stability of the vacuum of the scalar potential at the one-loop level.

The remaining parameter appearing in the potential will be kept as independent parameters. They cannot be directly related to any physical observable yielding appropriate OS conditions. Thus, they all are renormalized using $\overline{\text{DR}}$ renormalization conditions. The complete set of independent parameters is summarized in Tab. 6.1 Accordingly, we define the renormalized parameters as

$$\begin{aligned}
T_{H_d^{\mathcal{R}}} &\to T_{H_d^{\mathcal{R}}} + \delta T_{H_d^{\mathcal{R}}} \,, \\
T_{H_u^{\mathcal{R}}} &\to T_{H_u^{\mathcal{R}}} + \delta T_{H_u^{\mathcal{R}}} \,, \\
T_{\widetilde{\nu}^{\mathcal{R}}_{iR}} &\to T_{\widetilde{\nu}^{\mathcal{R}}_{iR}} + \delta T_{\widetilde{\nu}^{\mathcal{R}}_{iR}} \,, \\
T_{\widetilde{\nu}^{\mathcal{R}}_{iL}} &\to T_{\widetilde{\nu}^{\mathcal{R}}_{iL}} + \delta T_{\widetilde{\nu}^{\mathcal{R}}_{iL}} \,, \\
m^2_{\widetilde{\nu}i\neq j} &\to m^2_{\widetilde{\nu}i\neq j} + \delta m^2_{\widetilde{\nu}i\neq j} \,, \\
m^2_{\widetilde{L}i\neq j} &\to m^2_{\widetilde{L}i\neq j} + \delta m^2_{\widetilde{L}i\neq j} \,, \\
m^2_{H_d\widetilde{L}_i} &\to m^2_{H_d\widetilde{L}_i} + \delta m^2_{H_d\widetilde{L}_i} \,,
\end{aligned}
\qquad
\begin{aligned}
\tan\beta &\to \tan\beta + \delta\tan\beta \,, \\
v^2 &\to v^2 + \delta v^2 \,, \\
v_{iR}^2 &\to v_{iR}^2 + \delta v_{iR}^2 \,, \\
v_{iL}^2 &\to v_{iL}^2 + \delta v_{iL}^2 \,, \\
M_W^2 &\to M_W^2 + \delta M_W^2 \,, \\
M_Z^2 &\to M_Z^2 + \delta M_Z^2 \,,
\end{aligned}
\qquad
\begin{aligned}
\lambda_i &\to \lambda_i + \delta\lambda_i \,, \\
\kappa_{ijk} &\to \kappa_{ijk} + \delta\kappa_{ijk} \,, \\
Y^\nu_{ij} &\to Y^\nu_{ij} + \delta Y^\nu_{ij} \,, \\
T^\lambda_i &\to T^\lambda_i + \delta T^\lambda_i \,, \\
T^\kappa_{ijk} &\to T^\kappa_{ijk} + \delta T^\kappa_{ijk} \,, \\
T^\nu_{ij} &\to T^\nu_{ij} + \delta T^\nu_{ij} \,.
\end{aligned}
\tag{6.3}$$

We give the precise renormalization conditions used to define the counterterms of the $\overline{\text{DR}}$ parameters in the following subsections. Once they are extracted, all vertex counter-

terms of n-point functions are given as a linear combination of the counterterms of the independent parameter shown above.

Also the field renormalization of the scalar fields, required to renormalize the momentum-dependent parts of the self-energies, is defined (as in the one-generation case) by $\overline{\text{DR}}$ renormalization conditions. We write the field renormalization as

$$\phi_i \to Z^{1/2}_{\phi_i\phi_j}\phi_j = \left(\mathbb{1} + \frac{1}{2}\delta Z_{\phi_i\phi_j}\right)\phi_j \ , \tag{6.4}$$

with $\phi = (H_d, H_u, \widetilde{\nu}_{1R}, \widetilde{\nu}_{3R}, \widetilde{\nu}_{3R}, \widetilde{\nu}_{1L}, \widetilde{\nu}_{2L}, \widetilde{\nu}_{3L})$. $\delta Z_{\phi_i\phi_j}$ is now an 8×8 dimensional matrix. The $\overline{\text{DR}}$ conditions is as shown in Eq. (5.27), and the rotation to obtain the field renormalization counterterms in the mass eigenstate basis $\delta Z_{h_ih_j}$ can be found in Eq. (5.26). Calculating the one-loop self-energies for the $\mathcal{CP}$-even fields $\Sigma^{(1)}_{\varphi_i\varphi_j}$ we find

$$\delta Z_{H_dH_d} = -\frac{\Delta}{16\pi^2}\left(\lambda_i\lambda_i + Y^e_{ij}Y^e_{ij} + 3\left(Y^d_iY^d_i\right)\right) \ , \tag{6.5}$$

$$\delta Z_{H_d\widetilde{\nu}_{iL}} = \frac{\Delta}{16\pi^2}\lambda_jY^\nu_{ij} \ , \tag{6.6}$$

$$\delta Z_{H_uH_u} = -\frac{\Delta}{16\pi^2}\left(\lambda_i\lambda_i + Y^\nu_{ij}Y^\nu_{ij} + 3\left(Y^u_iY^u_i\right)\right) \ , \tag{6.7}$$

$$\delta Z_{\widetilde{\nu}_{iR}\widetilde{\nu}_{jR}} = -\frac{\Delta}{8\pi^2}\left(\lambda_i\lambda_j + \kappa_{ikl}\kappa_{jkl} + Y^\nu_{ki}Y^\nu_{kj}\right) \ , \tag{6.8}$$

$$\delta Z_{\widetilde{\nu}_{iL}\widetilde{\nu}_{jL}} = -\frac{\Delta}{16\pi^2}\left(Y^e_{ki}Y^e_{kj} + Y^\nu_{ik}Y^\nu_{jk}\right) \ . \tag{6.9}$$

We verified that the coefficients of the divergent part of the field renormalization counterterms are equal to the one-loop anomalous dimensions of the corresponding superfields $\gamma^{(1)}_{ij}$, neglecting the terms proportional to the gauge couplings g_1 and g_2, i.e.,

$$\delta Z_{\phi_i\phi_j} = \left.\frac{\gamma^{(1)}_{ij}\Delta}{16\pi^2}\right|^{g1,g2\to 0} \ , \tag{6.10}$$

which is the same relation that holds in the (N)MSSM. Note that due to the presence of three $\widetilde{\nu}_{iR}$, all sharing the same quantum numbers, a second source of off-diagonal field renormalization counterterms is present. Unfortunately, this complicates the expressions for renormalized Green's functions that contain a sum over one of the indices of the field renormalization counterterms of each external field. Therefore, also the $\overline{\text{DR}}$ conditions will be more complicated. We briefly summarize the renormalization of each parameter in the following. Since the general strategy for finding the parameter counterterms is the same as was used in Ch. 5, where we described more detailed how they can be extracted from demanding the finiteness of renormalized 2- and 3-point Green's functions, we here only state the renormalization condition and the resulting counterterm in the $\overline{\text{DR}}$ scheme for each parameter. The order in which the counterterms are extracted (and given here) is relevant because some renormalization conditions contain counterterms of other parameters that necessarily have to be extracted before. The general strategy is illustrated in Fig. 6.1.

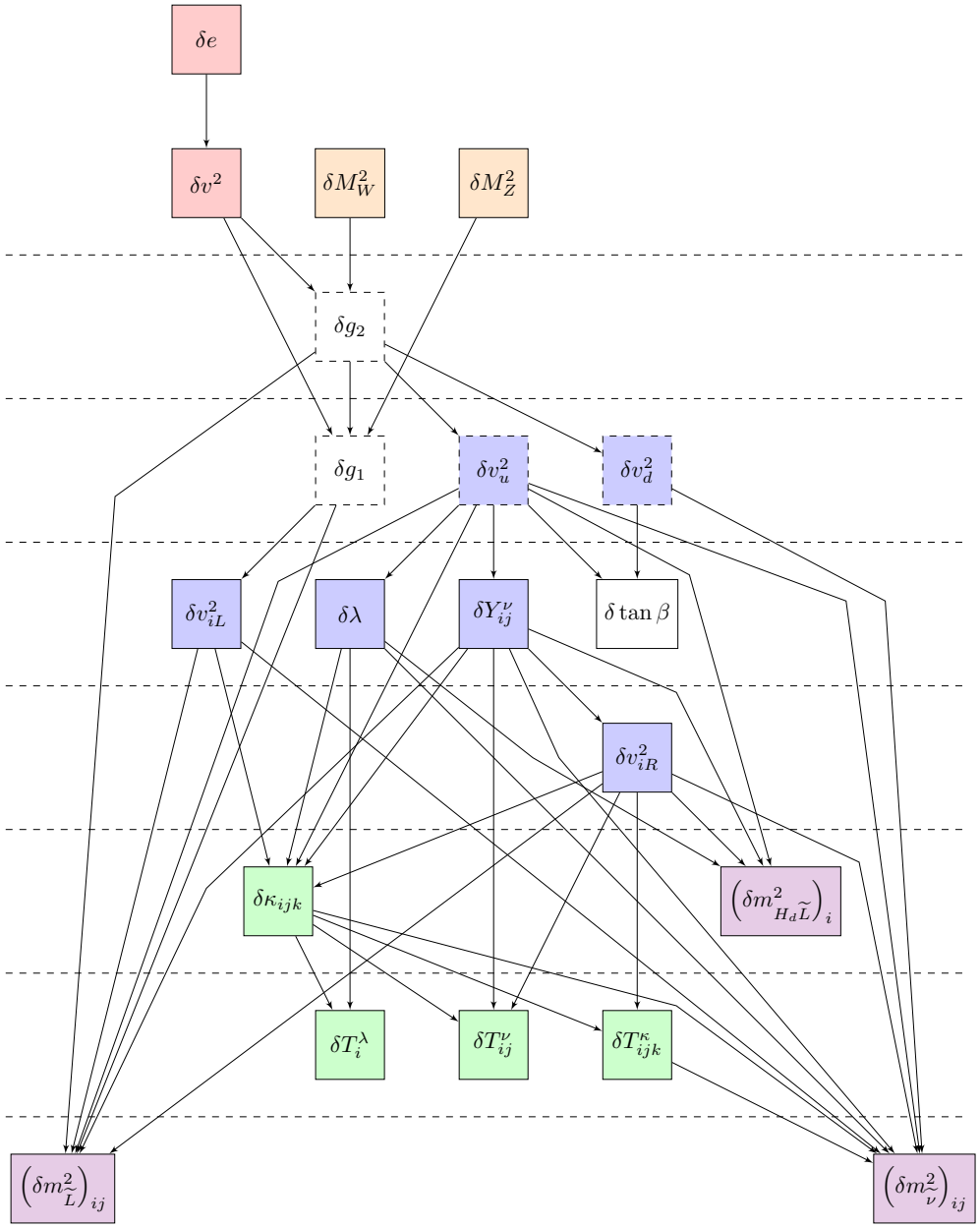

Figure 6.1: Strategy for extracting the counterterms required for renormalizing the neutral scalar potential. The arrows indicate the order in which the counterterms were obtained, while the colors stand for the sector that was used to extract the counterterms. *Red*: Renormalization of electromagnetic coupling. *Violet*: Renormalization of $\mathcal{CP}$-odd self-energies. *Yellow*: Renormalization of gauge boson self-energies. *Blue*: Renormalization of neutral fermion self-energies. *Green*: Renormalization of $\mathcal{CP}$-even scalar trilinear couplings. *White*: Completely fixed by the dependence on other counterterms. The counterterms in the dashed boxes do not belong to the set of independent parameters, but their counterterms were calculated as an intermediate step. The counterterms below one of the horizontal dashed lines could be extracted only after the counterterms above the same horizontal line were determined.

Renormalization of $\tan\beta$

Using the renormalization shown in Eq. (5.66) for v_d and v_u, their counterterms can be extracted in the neutral fermion sector, such that

$$\delta v_d^2 = \frac{4v_d}{g_2}\left(\Sigma^{S(1)}_{\widetilde{W}^0\widetilde{H}_d^0}\Big|^{\text{div}} - \frac{g_2}{4}\left(v_d\big(\delta Z_{\widetilde{W}^0\widetilde{W}^0} + \delta Z_{\widetilde{H}_d^0\widetilde{H}_d^0}\big) + v_{iL}\delta Z_{\nu_{iL}\widetilde{H}_d^0}\right) - \frac{v_d}{2}\,\delta g_2|^{\text{div}}\right), \tag{6.11}$$

$$\delta v_u^2 = \frac{4v_u}{g_2}\left(-\Sigma^{S(1)}_{\widetilde{W}^0\widetilde{H}_u^0}\Big|^{\text{div}} - \frac{g_2 v_u}{4}\left(\delta Z_{\widetilde{W}^0\widetilde{W}^0} + \delta Z_{\widetilde{H}_u^0\widetilde{H}_u^0}\right) - \frac{v_u}{2}\,\delta g_2|^{\text{div}}\right), \tag{6.12}$$

where the $\overline{\text{DR}}$ field renormalization constants for the neutral fermions were defined in Eq. (5.37). The counterterms δg_1 and δg_2 are related to the OS counterterms δM_W^2 and δM_Z^2, and given by

$$\delta g_2 = \frac{g_2}{2}\left(\frac{\delta M_W^2}{M_W^2} - \frac{\delta v^2}{v^2}\right), \tag{6.13}$$

$$\delta g_1 = \frac{2}{g_1 v^2}\left(\delta M_Z^2 - \delta M_W^2\right) - \frac{g_1}{2}\frac{\delta v^2}{v^2}\,. \tag{6.14}$$

Here, the counterterm for the SM vev δv^2 is defined as in the one-generation case (see Eq. (5.56)). Then the counterterm $\delta\tan\beta$ follows from Eq. (5.67). We find

$$\delta\tan\beta = \frac{\Delta}{32\pi^2}\tan\beta\left(3\left(Y_i^d Y_i^d - Y_i^u Y_i^u\right) + Y_{ij}^e Y_{ij}^e - Y_{ij}^\nu Y_{ij}^\nu - \frac{1}{v_d}\lambda_i Y_{ji}^\nu v_{jL}\right). \tag{6.15}$$

Renormalization of Y_{ij}^ν

Given δv_u^2, the counterterms for the neutrino Yukawa couplings Y_{ij}^ν can be extracted from the renormalized self-energy $\hat{\Sigma}^{(1)}_{\nu_{iL}\nu_{iR}}$. The renormalization condition reads

$$\delta Y_{ij}^\nu = \frac{\sqrt{2}}{v_u}\,\Sigma^{S(1)}_{\nu_{iL}\nu_{jR}}\Big|^{\text{div}} - \frac{1}{2}\left(\delta Z_{\nu_{iL}\nu_{kL}} Y_{kj}^\nu - \delta Z_{\nu_{iL}\widetilde{H}_d^0}\lambda_j + \delta Z_{\nu_{kR}\nu_{jR}} Y_{ik}^\nu\right) - \frac{Y_{ij}^\nu}{2}\frac{\delta v_u^2}{v_u^2}\,, \tag{6.16}$$

and we find

$$\begin{aligned}\delta Y_{ij}^\nu = \frac{\Delta}{32\pi^2}\Bigg(&\left(-\frac{4\pi\alpha Y_i^\nu\left(s_{\text{w}}^2 + 3c_{\text{w}}^2\right)}{c_{\text{w}}^2 s_{\text{w}}^2} + \lambda_k\lambda_k + 3Y_k^u Y_k^u + Y_{kl}^\nu Y_{kl}^\nu\right)Y_{ij}^\nu + Y_{ki}^e Y_{kl}^e Y_{lj}^\nu \\ &+ 3Y_{ik}^\nu Y_{lk}^\nu Y_{lj}^\nu + 2Y_{ik}^\nu\kappa_{klm}\kappa_{jlm} + 3Y_{ik}^\nu\lambda_k\lambda_j\Bigg)\,.\end{aligned} \tag{6.17}$$

Renormalization of λ_i

Similarly, from the form of $\hat{\Sigma}^{(1)}_{\widetilde{H}_d^0\nu_{iR}}$ we can find the condition

$$\delta\lambda_i = -\frac{\sqrt{2}}{v_u}\,\Sigma^{S(1)}_{\widetilde{H}_d^0\nu_{iR}}\Big|^{\text{div}} + \frac{1}{2}\left(\delta Z_{\nu_{jL}\widetilde{H}_d^0} Y_{ji}^\nu - \delta Z_{\widetilde{H}_d^0\widetilde{H}_d^0}\lambda_i - \delta Z_{\nu_{iR}\nu_{jR}}\lambda_j\right) - \frac{\lambda_i}{2}\frac{\delta v_u^2}{v_u^2}\,, \tag{6.18}$$

which yields

$$\delta\lambda_i = \frac{\Delta}{32\pi^2}\Bigg(\Bigg(-\frac{4\pi\alpha(s_{\rm w}^2+3c_{\rm w}^2)}{c_{\rm w}^2 s_{\rm w}^2} + 4\lambda_j\lambda_j + 3(Y_j^d Y_j^d + Y_j^u Y_j^u) + Y_{jk}^e Y_{jk}^e + Y_{jk}^\nu Y_{jk}^\nu\Bigg)\lambda_i + 3Y_{ji}^\nu Y_{jk}^\nu \lambda_k + 2\kappa_{ijk}\kappa_{jkl}\lambda_l\Bigg) . \tag{6.19}$$

Renormalization of v_{iL}

Using the fact that δg_1 is fixed by the relation shown in Eq. (6.14), we can define for $\delta v_{iL}^2 = 2v_{iL}\,\delta v_{iL}$ the renormalization condition

$$\delta v_{iL} = -\frac{2}{g_1}\,\Sigma^{S(1)}_{\nu_{iL}\widetilde{B}}\Big|^{\rm div} - \frac{1}{2}\left(\delta Z_{\nu_{iL}\nu_{jL}} v_{jL} + \delta Z_{\nu_{iL}\widetilde{H}_d^0} v_d + \delta Z_{\widetilde{B}\widetilde{B}} v_{iL}\right) - v_{iL}\frac{\delta g_1}{g_1} , \tag{6.20}$$

from which we obtain

$$\delta v_{iL}^2 = \frac{\Delta}{16\pi^2} v_{iL}\delta_{ij}\left(\frac{2\pi\alpha\left(s_{\rm w}^2+3c_{\rm w}^2\right)v_{jL}}{s_{\rm w}^2 c_{\rm w}^2} + v_d Y_{jk}^\nu\lambda_k - \left(Y_{kj}^e Y_{kl}^e - Y_{jk}^\nu Y_{lk}^\nu\right)v_{lL}\right) . \tag{6.21}$$

Renormalization of v_{iR}

The last counterterms obtained in the neutral fermion sector are the ones for the vevs of the right-handed sneutrinos $\delta v_{iR}^2 = 2v_{iR}\,\delta v_{iR}$. Their extraction was more complicated due to the fact that there is no tree-level quantity in which only one of the three v_{iR} appears separately. They always appear in sums over the family index. Therefore, we calculated loop corrections to the three mass matrix elements

$$\left(m_{\chi^0}\right)_{\nu_{iL}\widetilde{H}_u^0} = -\frac{Y_{ij}^\nu v_{jR}}{\sqrt{2}} . \tag{6.22}$$

This provides us with a linear system of three independent equations,

$$Y_{ij}^\nu\delta v_{jR} = \sqrt{2}\,\Sigma^{S(1)}_{\nu_{iL}\widetilde{H}_u^0}\Big|^{\rm div} - \frac{1}{2}\left(\delta Z_{\nu_{iL}\nu_{jL}} v_{kR}Y_{jk}^\nu - \delta Z^\chi_{i6} v_{jR}\lambda_j + \delta Z^\chi_{77} v_{jR}Y_{ij}^\nu\right) - v_{jR}\delta Y_{ij}^\nu , \tag{6.23}$$

that can be solved analytically for δv_{jR}. This gives

$$\delta v_{iR}^2 = -\frac{\Delta}{8\pi^2} v_{iR}\delta_{ij}\left(Y_{kj}^\nu Y_{kl}^\nu v_{lR} + \kappa_{jkm}\kappa_{klm}v_{lR} + v_{kR}\lambda_k\lambda_j\right) . \tag{6.24}$$

Renormalization of κ_{ijk}

The first counterterms extracted in the scalar sector are the counterterms for κ_{ijk} (see Fig. 6.1). Similarly to the vevs v_{iR}, they never appear isolated, except for the parameter κ_{123}. However, using the renormalized expression in Eq. (4.18) for the vertex

$$\Gamma^{(0)}_{\widetilde{\nu}_{iR}^{\mathcal{R}}\widetilde{\nu}_{kR}^{\mathcal{R}}\widetilde{\nu}_{jL}^{\mathcal{R}}} = \frac{1}{2}v_d\lambda_k Y_{ji}^\nu + \frac{1}{2}v_d\lambda_i Y_{jk}^\nu - \frac{1}{2}v_{lL}Y_{li}^\nu Y_{jk}^\nu - \frac{1}{2}v_{lL}Y_{lk}^\nu Y_{ji}^\nu - v_u\kappa_{ikl}Y_{jl}^\nu , \tag{6.25}$$

we can extract the counterterms for the three subsets $(\delta\kappa_{11j}, \delta\kappa_{22j}, \delta\kappa_{33j})$ by renormalizing the subset of vertices $(\Gamma_{\widetilde{\nu}_{1R}^{\mathcal{R}}\widetilde{\nu}_{1R}^{\mathcal{R}}\widetilde{\nu}_{jL}^{\mathcal{R}}}, \Gamma_{\widetilde{\nu}_{2R}^{\mathcal{R}}\widetilde{\nu}_{2R}^{\mathcal{R}}\widetilde{\nu}_{jL}^{\mathcal{R}}}, \Gamma_{\widetilde{\nu}_{3R}^{\mathcal{R}}\widetilde{\nu}_{3R}^{\mathcal{R}}\widetilde{\nu}_{jL}^{\mathcal{R}}})$. Thus, for each subset

(κ_{iij}; $i = 1,2,3$) we obtain a linear system of three ($j = 1,2,3$) equations to extract the counterterms $\delta\kappa_{iij}$ from the condition that the renormalized one-loop 3-point function is finite. The renormalization conditions for the subsets κ_{ijj} then read

$$\begin{aligned}-v_u Y^\nu_{jk}\delta\kappa_{iij} = \Gamma^{(1)}_{\widetilde{\nu}^{\mathcal{R}}_{iR}\widetilde{\nu}^{\mathcal{R}}_{iR}\widetilde{\nu}^{\mathcal{R}}_{jL}}\Big|^{\text{div}} - \frac{1}{2}\Bigg(2\delta Z_{\widetilde{\nu}_{kR}\widetilde{\nu}_{iR}}\Gamma^{(0)}_{\widetilde{\nu}^{\mathcal{R}}_{kR}\widetilde{\nu}^{\mathcal{R}}_{iR}\widetilde{\nu}^{\mathcal{R}}_{jL}} + \delta Z_{H_d\widetilde{\nu}_{jL}}\Gamma^{(0)}_{\widetilde{\nu}^{\mathcal{R}}_{iR}\widetilde{\nu}^{\mathcal{R}}_{iR}H^{\mathcal{R}}_d}\\ + \delta Z_{\widetilde{\nu}_{kL}\widetilde{\nu}_{jL}}\Gamma^{(0)}_{\widetilde{\nu}^{\mathcal{R}}_{iR}\widetilde{\nu}^{\mathcal{R}}_{iR}\widetilde{\nu}^{\mathcal{R}}_{kL}}\Bigg) - \Bigg(\lambda_i Y^\nu_{ji}\delta v_d + v_d Y^\nu_{ji}\delta\lambda_i + v_d\lambda_i\delta Y^\nu_{32} - v_u\kappa_{iik}\delta Y^\nu_{jk}\\ - \kappa_{iik}Y^\nu_{jk}\delta v_u - v_u Y^\nu_{jk}\delta\kappa_{iik} - v_{kL}Y^\nu_{ki}\delta Y^\nu_{ji} - v_{kL}Y^\nu_{ji}\delta Y^\nu_{ki} - Y^\nu_{ji}Y^\nu_{ki}\delta v_{kL}\Bigg)\,,\end{aligned} \tag{6.26}$$

where

$$\Gamma^{(0)}_{\widetilde{\nu}^{\mathcal{R}}_{iR}\widetilde{\nu}^{\mathcal{R}}_{kR}\widetilde{\nu}^{\mathcal{R}}_{jL}} = \frac{1}{2}v_d\lambda_k Y^\nu_{ji} + \frac{1}{2}v_d\lambda_i Y^\nu_{jk} - \frac{1}{2}v_{lL}Y^\nu_{li}Y^\nu_{jk} - \frac{1}{2}v_{lL}Y^\nu_{lk}Y^\nu_{ji} - v_u\kappa_{ikl}Y^\nu_{jl}\,, \tag{6.27}$$

$$\Gamma^{(0)}_{\widetilde{\nu}^{\mathcal{R}}_{iR}\widetilde{\nu}^{\mathcal{R}}_{jR}H^{\mathcal{R}}_d} = -v_d\lambda_i\lambda_j + v_u\kappa_{ijk}\lambda_k + \frac{1}{2}\left(Y^\nu_{ki}\lambda_j v_{kL} + Y^\nu_{kj}\lambda_i v_{kL}\right)\,, \tag{6.28}$$

When the counterterms $\delta\kappa_{iij}$ are fixed by the above condition, the last missing counterterm $\delta\kappa_{123}$ can be derived from the renormalization condition

$$\begin{aligned}\delta\kappa_{123} = \frac{\sqrt{2}}{v_{1R}}\,\Sigma^{S(1)}_{\nu_{2R}\nu_{3R}}\Big|^{\text{div}} - \frac{1}{2v_{1R}}\Bigg(\delta Z_{\nu_{2R}\nu_{iR}}v_{jR}\kappa_{i3j} + v_{jR}\kappa_{i2j}\delta Z_{\nu_{iR}\nu_{3R}}\Bigg)\\ - \frac{1}{v_{1R}}\Bigg(v_{2R}\delta\kappa_{223} + v_{3R}\delta\kappa_{233} + \kappa_{i23}\delta v_{iR}\Bigg)\,.\end{aligned} \tag{6.29}$$

Evaluating the above system of equations we find

$$\begin{aligned}\delta\kappa_{ijk} = \frac{\Delta}{16\pi^2}\Big(Y^\nu_{lk}Y^\nu_{lm}\kappa_{ijm} + Y^\nu_{lj}Y^\nu_{lm}\kappa_{ikm} + Y^\nu_{li}Y^\nu_{lm}\kappa_{jkm} + \kappa_{ikl}\kappa_{lmn}\kappa_{jmn} + \kappa_{ijl}\kappa_{lmn}\kappa_{kmn}\\ + \kappa_{ilm}\kappa_{lmn}\kappa_{jkn} + \kappa_{jkl}\lambda_l\lambda_i + \kappa_{ikl}\lambda_l\lambda_j + \kappa_{ijl}\lambda_l\lambda_k\Big)\,.\end{aligned} \tag{6.30}$$

Renormalization of T^λ_i

The counterterms for the soft trilinear parameters were most conveniently obtained by renormalizing scalar 3-point functions. The parameters T^λ_i are contained in the vertex

$$\Gamma^{(0)}_{H^{\mathcal{R}}_d H^{\mathcal{R}}_u\widetilde{\nu}^{\mathcal{R}}_{iR}} = \frac{T^\lambda_i}{\sqrt{2}} + \kappa_{ijk}\lambda_j v_{kR}\,, \tag{6.31}$$

so that we can derive the renormalization condition

$$\begin{aligned}\delta T^\lambda_i = \sqrt{2}\,\Gamma^{(1)}_{H^{\mathcal{R}}_d H^{\mathcal{R}}_u\widetilde{\nu}^{\mathcal{R}}_{iR}}\Big|^{\text{div}} - \frac{1}{\sqrt{2}}\Bigg(\delta Z_{H_dH_d}\Gamma_{H^{\mathcal{R}}_d H^{\mathcal{R}}_u\widetilde{\nu}^{\mathcal{R}}_{iR}} + \delta Z_{\widetilde{\nu}_{jL}H_d}\Gamma_{\widetilde{\nu}^{\mathcal{R}}_{jL}H^{\mathcal{R}}_u\widetilde{\nu}^{\mathcal{R}}_{iR}} + \delta Z_{H_uH_u}\Gamma_{H^{\mathcal{R}}_d H^{\mathcal{R}}_u\widetilde{\nu}^{\mathcal{R}}_{iR}}\\ + \delta Z_{\widetilde{\nu}_{jR}\widetilde{\nu}_{iR}}\Gamma_{H^{\mathcal{R}}_d H^{\mathcal{R}}_u\widetilde{\nu}^{\mathcal{R}}_{jR}}\Bigg) - \sqrt{2}\Bigg(\kappa_{ijk}\lambda_j\delta v_{kR} + \kappa_{ijk}v_{kR}\delta\lambda_j + \lambda_j v_{kR}\delta\kappa_{ijk}\Bigg)\,,\end{aligned} \tag{6.32}$$

with

$$\Gamma^{(0)}_{H^{\mathcal{R}}_u\widetilde{\nu}^{\mathcal{R}}_{iL}\widetilde{\nu}^{\mathcal{R}}_{jR}} = -\frac{T^\nu_{ij}}{\sqrt{2}} - Y^\nu_{ik}\kappa_{jkl}v_{lR}\,. \tag{6.33}$$

This gives

$$\delta T_i^\lambda = \frac{\Delta}{32\pi^2}\Bigg(\Bigg(-\frac{4\pi\alpha(s_\mathrm{w}^2+3c_\mathrm{w}^2)}{c_\mathrm{w}^2 s_\mathrm{w}^2}+6\lambda_j\lambda_j+3(Y_j^d Y_j^d+Y_j^u Y_j^u)+Y_{jk}^e Y_{jk}^e+Y_{jk}^\nu Y_{jk}^\nu\Bigg)T_i^\lambda$$
$$+\Bigg(\frac{8\pi\alpha(M_1 s_\mathrm{w}^2+3M_2 c_\mathrm{w}^2)}{c_\mathrm{w}^2 s_\mathrm{w}^2}+6\lambda_j T_j^\lambda+6Y_j^d T_j^d+2Y_{jk}^e T_{jk}^e+6Y_j^u T_j^u+2Y_{jk}^\nu T_{jk}^\nu\Bigg)\lambda_i$$
$$+5Y_{kj}^\nu\lambda_j T_{ki}^\nu+4Y_{ji}^\nu Y_{jk}^\nu T_k^\lambda+4\kappa_{jkl}\lambda_j T_{ikl}^\kappa+2\kappa_{ijk}\kappa_{jkl}T_l^\lambda\Bigg)\,. \tag{6.34}$$

Renormalization of T_{ij}^ν

In the same way, the counterterms for T_{ij}^ν can be derived from the tree-level vertex shown in Eq. (6.33), such that the renormalization conditions read

$$\delta T_{ij}^\nu = -\sqrt{2}\,\Gamma^{(1)}_{H_u^\mathcal{R}\widetilde{\nu}_{iL}^\mathcal{R}\widetilde{\nu}_{jR}^\mathcal{R}}\Big|^{\mathrm{div}}+\frac{1}{\sqrt{2}}\Bigg(\delta Z_{H_u H_u}\Gamma^{(0)}_{H_u^\mathcal{R}\widetilde{\nu}_{iL}^\mathcal{R}\widetilde{\nu}_{jR}^\mathcal{R}}+\delta Z_{\widetilde{\nu}_{kR}\widetilde{\nu}_{jR}}\Gamma^{(0)}_{H_u^\mathcal{R}\widetilde{\nu}_{iL}^\mathcal{R}\widetilde{\nu}_{kR}^\mathcal{R}}$$
$$+\delta Z_{H_d\widetilde{\nu}_{iL}}\Gamma^{(0)}_{H_u^\mathcal{R}H_d^\mathcal{R}\widetilde{\nu}_{jR}^\mathcal{R}}+\delta Z_{\widetilde{\nu}_{kL}\widetilde{\nu}_{iL}}\Gamma^{(0)}_{H_u^\mathcal{R}\widetilde{\nu}_{kL}^\mathcal{R}\widetilde{\nu}_{jR}^\mathcal{R}}\Bigg)-\sqrt{2}\Bigg(Y_{ik}^\nu\kappa_{jkl}\delta v_{lR}+\kappa_{jkl}v_{lR}\delta Y_{ik}^\nu$$
$$+Y_{ik}^\nu v_{lR}\delta\kappa_{jkl}\Bigg)\,, \tag{6.35}$$

yielding

$$\delta T_{ij}^\nu = \frac{\Delta}{32\pi^2}\Bigg(\Bigg(-\frac{4\pi\alpha(s_\mathrm{w}^2+3c_\mathrm{w}^2)}{c_\mathrm{w}^2 s_\mathrm{w}^2}+\lambda_k\lambda_k+3Y_k^u Y_k^u+Y_{kl}^\nu\Bigg)T_{ij}^\nu+\Bigg(\frac{8\pi\alpha(M_1 s_\mathrm{w}^2+3M_2 c_\mathrm{w}^2)}{c_\mathrm{w}^2 s_\mathrm{w}^2}$$
$$+2\lambda_k T_k^\lambda+6Y_k^u T_k^u+2Y_{kl}^\nu T_{kl}^\nu\Bigg)Y_{ij}^\nu+2Y_{lk}^e Y_{kj}^\nu T_{li}^e+4Y_{kj}^\nu Y_{kl}^\nu T_{il}^\nu+Y_{ki}^e Y_{kl}^e T_{lj}^\nu$$
$$+5Y_{ik}^\nu Y_{lk}^\nu T_{lj}^\nu+4Y_{ik}^\nu\kappa_{klm}T_{jlm}^\kappa+2\kappa_{jkl}\kappa_{klm}T_{im}^\nu+4\lambda_k T_{ik}^\nu\lambda_j+5Y_{ik}^\nu\lambda_k T_j^\lambda\Bigg)\,. \tag{6.36}$$

Renormalization of T_{ijk}^κ

The most complicated renormalization condition results for the counterterms of T_{ijk}^κ. We use that at tree-level the corresponding vertex is given by

$$\Gamma^{(0)}_{\widetilde{\nu}_{iR}^\mathcal{R}\widetilde{\nu}_{jR}^\mathcal{R}\widetilde{\nu}_{kR}^\mathcal{R}} = -\sqrt{2}T_{ijk}^\kappa-2\big(\kappa_{ijl}\kappa_{klm}v_{mR}+\kappa_{ilm}\kappa_{jkl}v_{mR}+\kappa_{ikl}\kappa_{jlm}v_{mR}\big)\,. \tag{6.37}$$

The renormalization condition for the T_{ijk}^κ then read

$$\delta T_{ijk}^\kappa = -\frac{1}{\sqrt{2}}\,\Gamma^{(1)}_{\widetilde{\nu}_{iR}^\mathcal{R}\widetilde{\nu}_{jR}^\mathcal{R}\widetilde{\nu}_{kR}^\mathcal{R}}\Big|^{\mathrm{div}}$$
$$+\frac{1}{2\sqrt{2}}\Bigg(\delta Z_{\widetilde{\nu}_{lR}\widetilde{\nu}_{iR}}\Gamma^{(0)}_{\widetilde{\nu}_{lR}^\mathcal{R}\widetilde{\nu}_{jR}^\mathcal{R}\widetilde{\nu}_{kR}^\mathcal{R}}+\delta Z_{\widetilde{\nu}_{lR}\widetilde{\nu}_{jR}}\Gamma^{(0)}_{\widetilde{\nu}_{iR}^\mathcal{R}\widetilde{\nu}_{lR}^\mathcal{R}\widetilde{\nu}_{kR}^\mathcal{R}}+\delta Z_{\widetilde{\nu}_{lR}\widetilde{\nu}_{kR}}\Gamma^{(0)}_{\widetilde{\nu}_{iR}^\mathcal{R}\widetilde{\nu}_{jR}^\mathcal{R}\widetilde{\nu}_{lR}^\mathcal{R}}\Bigg)$$
$$-2\big(\kappa_{klm}v_{mR}\delta\kappa_{ijl}+\kappa_{ijl}v_{mR}\delta\kappa_{klm}+\kappa_{ijl}\kappa_{klm}\delta v_{mR}+\kappa_{jkl}v_{mR}\delta\kappa_{ilm}$$
$$+\kappa_{ilm}v_{mR}\delta\kappa_{jkl}+\kappa_{ilm}\kappa_{jkl}\delta v_{mR}+\kappa_{jlm}v_{mR}\delta\kappa_{ikl}+\kappa_{ikl}v_{mR}\delta\kappa_{jlm}$$
$$+\kappa_{ikl}\kappa_{jlm}\delta v_{mR}\big)\,, \tag{6.38}$$

and we find for the counterterms

$$\begin{aligned}\delta T^{\kappa}_{ijk} = \frac{\Delta}{16\pi^2}\Big(&2Y^{\nu}_{ml}\kappa_{jkl}T^{\nu}_{mi} + 2Y^{\nu}_{ml}\kappa_{ikl}T^{\nu}_{mj} + 2Y^{\nu}_{ml}\kappa_{ijl}T^{\nu}_{mk} + Y^{\nu}_{lk}Y^{\nu}_{lm}T^{\kappa}_{ijm} + Y^{\nu}_{lj}Y^{\nu}_{lm}T^{\kappa}_{ikm}\\ &+ Y^{\nu}_{li}Y^{\nu}_{lm}T^{\kappa}_{jkm} + 2\kappa_{jkl}\kappa_{lmn}T^{\kappa}_{imn} + 2\kappa_{ikl}\kappa_{lmn}T^{\kappa}_{jmn} + 2\kappa_{ijl}\kappa_{lmn}T^{\kappa}_{kmn} + \kappa_{klm}\kappa_{lmn}T^{\kappa}_{ijn}\\ &+ \kappa_{jlm}\kappa_{lmn}T^{\kappa}_{ikn} + \kappa_{ilm}\kappa_{lmn}T^{\kappa}_{jkn} + \lambda_l T^{\kappa}_{jkl}\lambda_i + \lambda_l T^{\kappa}_{ikl}\lambda_j + \lambda_l T^{\kappa}_{ijl}\lambda_k + 2\kappa_{jkl}\lambda_l T^{\lambda}_{i}\\ &+ 2\kappa_{ikl}\lambda_l T^{\lambda}_{j} + 2\kappa_{ijl}\lambda_l T^{\lambda}_{k}\Big)\,. \end{aligned} \tag{6.39}$$

Renormalization of $m^2_{H_d\widetilde{L}_i}$

The remaining independent parameters that have to be renormalized are the soft scalar mass parameters. As in the one-generation case, we decided to extract their counterterms in the $\mathcal{CP}$-odd scalar sector.

The parameters $(m^2_{H_d\widetilde{L}})_i$ appear in the element $m^2_{\widetilde{\nu}^{\mathcal{I}}_{iL}H^{\mathcal{I}}_d}$ shown in Eq. (3.62). From the renormalization of this expression we obtain the renormalization condition

$$\begin{aligned}\delta\left(m^2_{H_d\widetilde{L}}\right)_i = \left(\delta m^2_{\sigma}\right)_{\widetilde{\nu}^{\mathcal{I}}_{iL}H^{\mathcal{I}}_d}\Big|^{\text{div}} + \frac{1}{2}\Big(&Y^{\nu}_{ij}\lambda_j\delta v_u^2 + v_u^2\lambda_j\delta Y^{\nu}_{ij} + v_u^2 Y^{\nu}_{ij}\delta\lambda_j + \lambda_j v_{kR}Y^{\nu}_{ik}\delta_{jR}\\ &+ v_{jR}v_{kR}Y^{\nu}_{ik}\delta\lambda_j + v_{jR}\lambda_j Y^{\nu}_{ik}\delta v_{kR} + v_{jR}\lambda_j v_{kR}\delta Y^{\nu}_{ik}\Big)\,, \end{aligned} \tag{6.40}$$

The mass counterterm $(\delta m^2_{\sigma})_{\widetilde{\nu}^{\mathcal{I}}_{iL}H^{\mathcal{I}}_d}$ renormalizes the scalar self-energy $\Sigma^{(1)}_{\widetilde{\nu}^{\mathcal{I}}_{iL}H^{\mathcal{I}}_d}$. We already explained in Sect. 5.1 how these contributions can be obtained by calculating all self-energy diagrams in the mass eigenstate basis, and rotating them back to the interaction basis (see Eq. (5.79) and Eq. (5.80)).

Renormalization of $m^2_{\widetilde{L}i\neq j}$

The three independent off-diagonal parameters of $m^2_{\widetilde{L}}$ appear in the tree-level mass matrix in $m^2_{\widetilde{\nu}^{\mathcal{I}}_{iL}\widetilde{\nu}^{\mathcal{I}}_{jL}}$ (see Eq. (3.65)). Hence, the renormalization conditions for the counterterms $\delta(m^2_{\widetilde{L}})_{ij}$ for $i \neq j$ can be written as

$$\begin{aligned}\delta\left(m^2_{\widetilde{L}}\right)_{ij} = \left(\delta m^2_{\sigma}\right)_{\widetilde{\nu}^{\mathcal{I}}_{iL}\widetilde{\nu}^{\mathcal{I}}_{jL}}\Big|^{\text{div}} - \frac{1}{2}\Big(&Y^{\nu}_{ik}Y^{\nu}_{jk}\delta v_u^2 + v_u^2 Y^{\nu}_{jk}\delta Y^{\nu}_{ik} + v_u^2 Y^{\nu}_{ik}\delta Y^{\nu}_{jk} + Y^{\nu}_{ik}v_{lR}Y^{\nu}_{jl}\delta v_{kR}\\ &+ v_{kR}v_{lR}Y^{\nu}_{jl}\delta Y^{\nu}_{ik} + v_{kR}Y^{\nu}_{ik}Y^{\nu}_{jl}\delta v_{lR} + v_{kR}Y^{\nu}_{ik}v_{lR}\delta Y^{\nu}_{jl}\Big)\,. \end{aligned} \tag{6.41}$$

Renormalization of $m^2_{\widetilde{\nu}i\neq j}$

The off-diagonal elements of $(m^2_{\widetilde{\nu}})_{ij}$, not present in the one-generation case where $m^2_{\widetilde{\nu}}$ is just a single parameter, are contained in the mass matrix elements mixing the different generations of right-handed sneutrinos. In the $\mathcal{CP}$-odd sector we find from $m^2_{\widetilde{\nu}^{\mathcal{I}}_{iR}\widetilde{\nu}^{\mathcal{I}}_{jR}}$ given in Eq. (3.61) the renormalization condition

$$\delta\left(m^2_{\widetilde{\nu}}\right)_{ij} = \left(\delta m^2_{\sigma}\right)_{\widetilde{\nu}^{\mathcal{I}}_{iR}\widetilde{\nu}^{\mathcal{I}}_{jR}}\Big|^{\text{div}} - \frac{1}{2}\Big(Y^{\nu}_{ki}Y^{\nu}_{kj}\delta v_u^2 + v_u^2 Y^{\nu}_{kj}\delta Y^{\nu}_{ki} + v_u^2 Y^{\nu}_{ki}\delta Y^{\nu}_{kj}\Big) - v_u\kappa_{ijk}\lambda_k\delta v_d$$

$$
\begin{aligned}
&- v_d\kappa_{ijk}\lambda_k\delta v_u - v_d v_u\lambda_k\delta\kappa_{ijk} - v_d v_d\kappa_{ijk}\delta\lambda_k + \sqrt{2}\left(T^{\kappa}_{ijk}\delta v_{kR} + v_{kR}\delta T^{\kappa}_{ijk}\right)\\
&+ Y^{\nu}_{lk}\kappa_{ijk}v_{lL}\delta v_u + v_u\kappa_{ijk}v_{lL}\delta Y^{\nu}_{lk} + v_u Y^{\nu}_{lk}v_{lL}\delta\kappa_{ijk} + v_u Y^{\nu}_{lk}\kappa_{ijk}\delta v_{lL}\\
&- \frac{1}{2}\left(Y^{\nu}_{ki}v_{lL}Y^{\nu}_{lj}\delta v_{kL} + v_{kL}v_{lL}Y^{\nu}_{lj}\delta Y^{\nu}_{ki} + v_{kL}Y^{\nu}_{ki}Y^{\nu}_{lj}\delta v_{lL} + v_{kL}Y^{\nu}_{ki}v_{lL}\delta Y^{\nu}_{lj}\right)\\
&- \kappa_{jkl}v_{lR}v_{mR}\delta\kappa_{ikm} - \kappa_{ikm}v_{lR}v_{mR}\delta\kappa_{jkl} - \kappa_{ikm}\kappa_{jkl}v_{mR}\delta v_{lR} - \kappa_{ikm}\kappa_{jkl}v_{lR}\delta v_{mR}\\
&+ \kappa_{klm}v_{lR}v_{mR}\delta\kappa_{ijk} + \kappa_{ijk}v_{lR}v_{mR}\delta\kappa_{klm} + \kappa_{ijk}\kappa_{klm}v_{mR}\delta v_{lR} + \kappa_{ijk}\kappa_{klm}v_{lR}\delta v_{mR}\\
&+ \frac{1}{2}\left(v_{kL}Y^{\nu}_{kj}\lambda_i\delta v_d + v_d Y^{\nu}_{kj}\lambda_i\delta v_{kL} + v_d v_{kL}\lambda_i\delta Y^{\nu}_{kj} + v_d v_{kL}Y^{\nu}_{kj}\delta\lambda_i\right)\\
&+ \frac{1}{2}\left(v_{kL}Y^{\nu}_{ki}\lambda_j\delta v_d + v_d Y^{\nu}_{ki}\lambda_j\delta v_{kL} + v_d v_{kL}\lambda_j\delta Y^{\nu}_{ki} + v_d v_{kL}Y^{\nu}_{ki}\delta\lambda_j\right)\\
&- \frac{1}{2}\left(\lambda_i\lambda_j\delta v_d^2 + \lambda_i\lambda_j\delta v_u^2 + v_d^2\lambda_j\delta\lambda_i + v_d^2\lambda_i\delta\lambda_j + v_u^2\lambda_j\delta\lambda_i\right.\\
&\left.+ v_u^2\lambda_i\delta\lambda_j\right) . \qquad (6.42)
\end{aligned}
$$

`FeynArts` model file

The calculation of the one-loop n-point vertex corrections was done by using the same tools as in the one-generation case. We generated the Feynman diagrams using our `FeynArts` [2] model file. It was initially created with `SARAH` version 4.12.0 [3, 4]. We obtained the one-loop amplitudes regularized in DRED utilizing `FormCalc` [5] and `LoopTools` [5, 6]. Because of the huge expressions for the tree-level couplings, we modified the `FeynArts` model file by substituting these expressions by generic functions. They are only evaluated explicitly if the user decides to do so. The same was done for the counterterms defined above, which are all included in our private model file. Therefore, the calculation of the one-loop scalar self-energies is fully automated. Apart from that, also the counterterm diagrams for the neutral fermion self-energies and the scalar trilinear vertices with three $\mathcal{CP}$-even Higgs bosons on the external legs can be generated in terms of the counterterms shown above.

We used the `FeynArts` model file to do several consistency checks on the proper renormalization of the scalar potential, i.e., that all UV divergences in one-loop Greens's functions are canceled by our counterterms:

- The field renormalization counterterms are related to the anomalous dimensions as shown in Eq. (4.29)
- The parameter counterterms are related to the one-loop β-functions as shown in Eq. (4.28).[1]
- All neutral scalar self-energies are finite.[2]
- All $\mathcal{CP}$-even scalar 3-point functions are finite
- All neutral fermion self-energies are finite. For this check the two additional counterterms δM_1 and δM_2 were extracted. However, they do not appear in the scalar

[1] The β-functions and anomalous dimensions γ_{ij} at the one-loop level can be calculated with `SARAH`, which evaluates the general expressions found in Refs. [7–12].

[2] To check the finiteness of a certain expression, `LoopTools` allows for calculating loop integrals for arbitrary values of Δ as defined in Eq. (4.27). If the one-loop amplitudes are properly renormalized, the terms containing Δ cancel each other, such that renormalized quantities should be independent of Δ. This can be checked numerically by varying Δ over several orders of magnitude and verifying that the results are unchanged.

potential, and thus are not relevant for the discussion here.
- In the limit $Y^\nu_{i1} = Y^\nu_i$ and vanishing otherwise the counterterms for the one-generation case are recovered, which in turn reduce to the NMSSM counterterms in the limit $Y^\nu_i \to 0$.

6.2 Loop-corrected Higgs-boson masses

In analogy to the one-generation case, we applied our OS-$\overline{\text{DR}}$ renormalization prescription to the neutral scalar spectrum. The radiative corrections to the pole masses are contained in the renormalized self-energies

$$\hat{\Sigma}_{h_i h_j}\left(p^2\right) = \hat{\Sigma}^{(1)}_{h_i h_j}\left(p^2\right) + \hat{\Sigma}^{(2')}_{h_i h_j} + \hat{\Sigma}^{\text{resum}}_{h_i h_j}\,, \tag{6.43}$$

where we again supplemented our full one-loop corrections $\hat{\Sigma}^{(1)}_{h_i h_j}$ by higher-order corrections from the MSSM (see Sect. 5.2 for details). Inserting these contributions into the inverse propagator matrix as shown in Eq. (5.87) yields the radiatively corrected pole masses and mixing matrices U^H after diagonalizing $\hat{\Gamma}_h$.

Due to the presence of three scalar gauge-singlet fields $\widetilde{\nu}_{iR}$, $\hat{\Gamma}_h$ is a matrix of dimension 8, instead of 6 like in the one-generation case. Because we neglect $\mathcal{CP}$-violation, $\hat{\Gamma}_h$ remains symmetric, so that a total number of 36 self-energies have to be calculated for each BP. Each self-enregy is a very large function of the momentum. Therefore, the numerical evaluation of the radiative corrections is rather time-consuming in the $\mu\nu$SSM with three right-handed neutrino superfields, having in mind that the diagonalization of $\hat{\Gamma}_h$ is done iteratively, such that the self-energies have to be evaluated several times for different momenta. Consequently, our numerical analysis is restricted to a set of BPs illustrating the importance of accurately taking into account the radiative corrections, particular when the mixing of the SM-like Higgs boson with the $\widetilde{\nu}^{\mathcal{R}}_{iR}$ is sizable.

6.3 Numerical analysis

As already emphasized in Sect. 6.2, in the numerical analysis we concentrate on BP in which a right-handed sneutrino is substantially mixed with the SM-like Higgs boson. To achieve that only a single right-handed sneutrino mixes with the SM-like Higgs boson, we set $\kappa_{ijk} = \kappa\ \delta_{ij}\delta_{jk}$ in the following (see Eq. (3.51)) [13]. Naturally, the mass scale of the right-handed sneutrinos will be of the order of ~ 125 GeV in BPs yielding large mixing between $\widetilde{\nu}^{\mathcal{R}}_{iR}$ and the SM-like Higgs boson. However, scenarios in which the decay of the SM-like Higgs boson into two right-handed sneutrinos is kinematically allowed are experimentally very constrained [13].

In contrast to most of the previous studies of the $\mu\nu$SSM with three generations of right-handed neutrinos [13–17], we do not make the simplifying assumption that all genuine low-energy $\mu\nu$SSM-parameters have universal values independent of the family index. In Sect. 6.3.3 we elaborate on the effect of non-universal λ_i on the SM-like Higgs-boson mass, while keeping $\boldsymbol{\lambda}^2 = \lambda_i\lambda_i$ constant. Since we know from Eq. (3.54) that the tree-level mass of the SM-like Higgs boson primarily depends on $\boldsymbol{\lambda}^2$, it will be discussed whether the loop corrections increase the dependence on the individual values λ_i.

Experimental constraints

We use the public code `HiggsBounds v.5.2.0` [18–22] to determine whether a BP has been excluded by cross-section limits from Higgs searches at LEP, LHC or Tevatron. These searches are mostly sensitive to the heavy Higgs and the right-handed sneutrinos, if the latter are substantially mixed with the SM-like Higgs boson. The production of the left-handed sneutrinos is much smaller at the LHC, and signals from their decay usually demand dedicated searches [23], especially if the left-handed sneutrino is the LSP [24, 25].

The properties of the SM-like Higgs boson, i.e., its mass and signal rates at LHC and Tevatron, are checked using the public code `HiggsSignals v.2.2.1` [26–28]. Here, we assume a theoretical mass uncertainty of 3 GeV. `HiggsSignals` provides us with a χ^2-analysis of $n_{\rm obs} = 106$ observables in the 7+8 TeV data package and $n_{\rm obs} = 101$ observables in the 13 TeV data package. In our plots we show the reduced $\chi^2_{\rm red} = \chi^2/n_{\rm obs}$, where a value of $\chi^2_{\rm red} = 1$ means that, on average, the signal rates of the SM-like Higgs boson are at the level of the $\pm 1\sigma$ range of the measurements.

For the necessary input of `HiggsBounds` and `HiggsSignals` we compute the decay widths of the scalars at leading order, but with the loop-corrected mixing matrix elements inserted in the expressions of the scalar couplings. In the limit of vanishing external momentum, which we used in the determination of the mixing matrix elements for the couplings, this method corresponds to include the finite wave-function renormalization factors (Z-factors) for each external scalar [29, 30]. For loop-induced decays and off-shell decays to vector bosons we implemented analytic results from the MSSM well known in the literature [31–35]. We scaled the expressions with effective couplings defined by the mixing matrix elements and $\tan\beta$ to obtain the result for the scalars in the $\mu\nu$SSM. For the coupling to b-quarks we included the running bottom mass and for the decay to gluons the running of α_s from M_Z to the mass of the decaying scalar, and finally add leading higher-order QCD corrections [33, 36].

The properties of the neutrino sector were verified to be in agreement with the measurements of the mass-squared differences and the mixing angles from the PMNS matrix (see Eq. (3.92)), which are given in the $\mu\nu$SSM by

$$s^2_{13} = |U^V_{31}|^2 \,, \qquad s^2_{12} = \frac{|U^V_{21}|^2}{1 - s^2_{13}} \,, \qquad s^2_{23} = \frac{|U^V_{32}|^2}{1 - s^2_{13}} \,, \tag{6.44}$$

$$\delta m^2_{12} = m^2_{\lambda^0_2} - m^2_{\lambda^0_1} \,, \qquad \Delta m^2_{13} \sim \Delta m^2_{23} = m^2_{\lambda^0_3} - m^2_{\lambda^0_{1,2}} \tag{6.45}$$

These equations are valid as long as Y^e_{ij} is chosen to be diagonal. We check that our predictions are within the $\pm 3\sigma$ bands published by the NuFit collaboration [37, 38],

$$6.80\ \text{eV}^2 \leq \delta m^2_{12}/10^{-5} \leq 8.02\ \text{eV}^2 \,, \quad 2.399\ \text{eV}^2 \leq \Delta m^2_{13}/10^{-3} \leq 2.593\ \text{eV}^2 \,, \tag{6.46}$$

$$0.0198 \leq s^2_{13} \leq 0.0244 \,, \quad 0.272 \leq s^2_{12} \leq 0.346 \,, \quad 0.418 \leq s^2_{23} \leq 0.613 \,, \tag{6.47}$$

where we considered the normal mass ordering which is now favored by experiments [39]. A genetic algorithm was used to find parameter points that minimize the sum of squared deviations between theoretical prediction and experimental values specified above [40]. Even though the $\mu\nu$SSM allows for flavor-violating decays of leptons, the existing experimental bounds (for instance on $\mu \to e\gamma$) are automatically fulfilled when the constrains on neutrino masses are taken into account [41].

We use the left-handed vevs v_{iL}, the soft gaugino masses M_1 and M_2, and the neutrino Yukawa couplings Y^ν_{ij} to fit the neutrino masses and mixings accurately, making use of the fact that they can be modified without spoiling the properties of the SM-like Higgs

$\tan\beta$	λ	κ	$v_{1,3R}$	v_{2R}	A^λ	A^κ	A^ν
5	$[0.13, 0.18]$	0.5	1000	765	1000	-1000	-1000
A^u_3	$A^u_{1,2}$	$A^{d,e}$	$m_{\widetilde{Q},\widetilde{u},\widetilde{d}}$	$m_{\widetilde{e}}$	M_3		
-2000	-1500	-1500	1500	200	2700		
$v_{1L}/10^{-4}$	$v_{2L}/10^{-4}$	$v_{3L}/10^{-4}$	$Y^\nu_{11}/10^{-7}$	$Y^\nu_{22}/10^{-7}$	$Y^\nu_{33}/10^{-7}$	M_1	M_2
1.390	6.215	4.912	4.181	1.756	6.306	1228	2814

Table 6.2: Low-energy values for the parameters, as defined in the text, in the light $\widetilde{\nu}^{\mathcal{R}}_{\mu R}$ scenario. Dimensionful parameters are given in GeV. The parameters in the last row are fitted to neutrino oscillation data.

boson, whose dependence on these parameters is mild. In this chapter it will be sufficient to just consider diagonal non-zero elements of Y^ν_{ij}.

We concentrate here on the scalar sector of the $\mu\nu$SSM. Since the fitting to neutrino data has to be done numerically, which takes a quit amount of time, we do the fitting in our scans just in one particular point for each scenario. By varying a parameter, the prediction for the neutrino properties can be outside the experimentally allowed range in some points. We indicate in our plots when this is the case. Since the neutral fermion mass matrix is of dimension 10, with large hierarchies between the neutrino sector and the remaining part, including one-loop corrections is time-consuming and numerically very challenging. Therefore, we stick to a tree-level analysis for the neutrinos. However, we checked for several points that the one-loop corrections are sub-leading and can in principle be compensated by a slight change of the parameters.[3]

6.3.1 Light right-handed μ-sneutrino scenario

The first scenario we present is one with a light right-handed μ-sneutrino that mixes substantially with the SM-like Higgs boson. We show the chosen parameters in Tab. 6.2. The values for SM parameters are chosen as in the one-generation case, as shown in Tab. 5.3. To simplify the notation we define $\lambda = \lambda_i$, $A^\lambda = A^\lambda_i$, $A^\nu = A^\nu_{ii}$, $\kappa = \kappa_{iii}$ and $A^\kappa = A^\kappa_{iii}$ and vanishing otherwise. The soft parameters are given in terms of $A^d = A^d_i$, $A^e = A^e_{ii}$, $m_{\widetilde{Q}} = m_{\widetilde{Q}_i}$, $m_{\widetilde{u}} = m_{\widetilde{u}_i}$, $m_{\widetilde{d}} = m_{\widetilde{d}_i}$, and $m_{\widetilde{e}} = m_{\widetilde{e}_{ii}}$ and vanishing otherwise. We vary over a small range of the universal parameter λ, while keeping the remaining parameters fixed. For the right-handed e- and τ-sneutrino vevs we chose $v_{1,3R} = 1$ TeV, but set a smaller value of $v_{2R} = 765$ GeV for the μ-sneutrino vev to decrease the mass of the $\mathcal{CP}$-even μ-sneutrino to the range around the SM-like Higgs-boson mass. It is of no relevance that $\widetilde{\nu}^{\mathcal{R}}_{\mu R}$ was picked as the light right-handed sneutrino. The large value of $\kappa = 0.5$ assures that the other two right-handed sneutrinos will have masses between 300 and 400 GeV, well above 125 GeV. Because the SM-like Higgs-boson mass will get additional contributions from the mixing with $\widetilde{\nu}^{\mathcal{R}}_{\mu R}$, $\tan\beta$ can be chosen rather low.

We fit the properties of the neutrinos in the BP with $\lambda = 0.168$, leading to the values of v_{iL}, Y^ν_{ii}, M_1 and M_2 shown in Tab. 6.2. We emphasize that this effectively leaves just the trilinear parameters A^ν_{ii} to adjust the masses of the left-handed sneutrinos. For the prediction of the masses of the right-handed sneutrinos and the SM-like Higgs boson, the fitted parameters only play a minor role.

[3]See also Ref. [17] for a detailed discussion of radiative corrections to the neutrino masses.

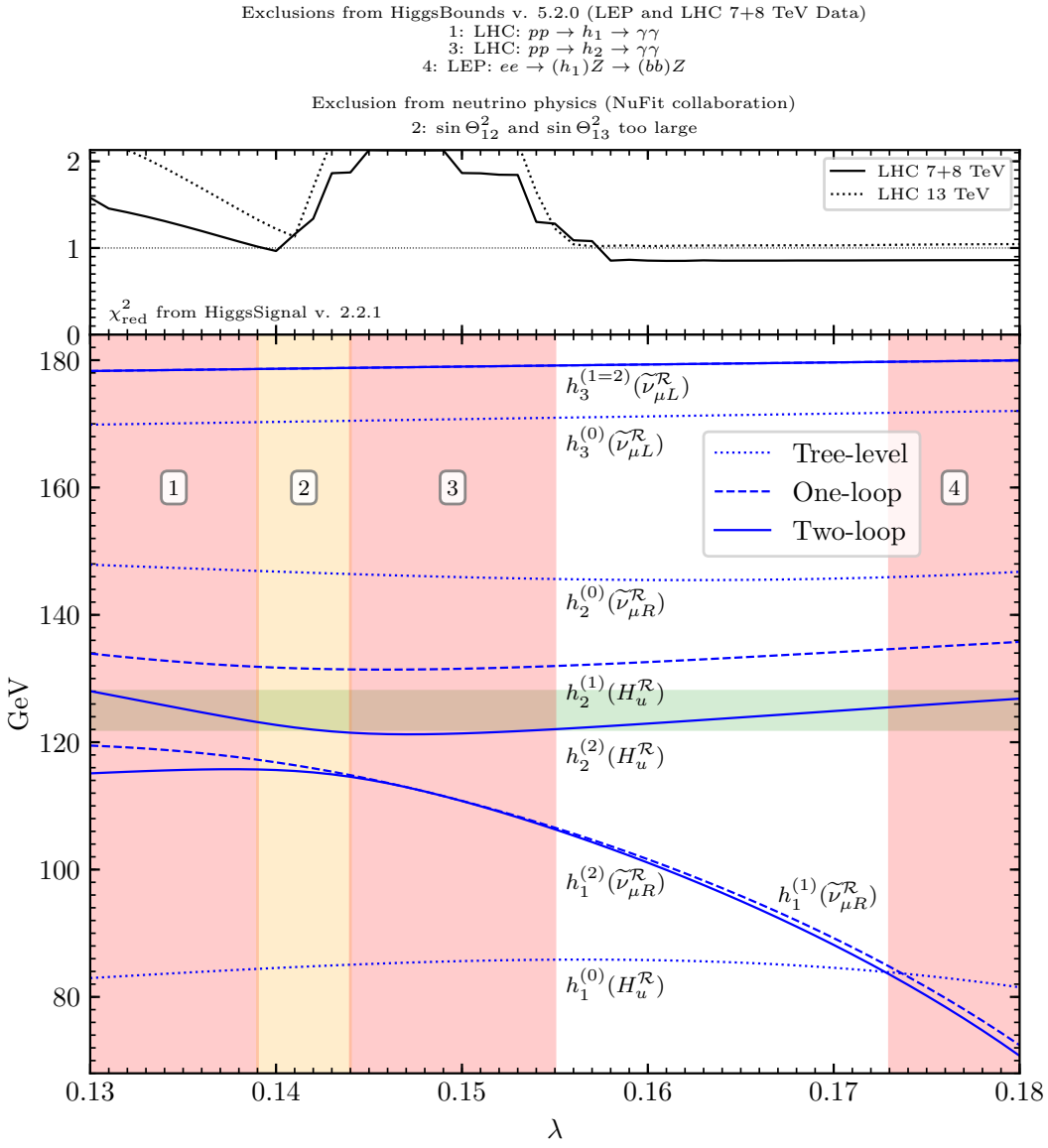

Figure 6.2: $\mathcal{CP}$-even scalar spectrum in the light $\widetilde{\nu}^{\mathcal{R}}_{\mu R}$ scenario at tree level, one-loop level and partial two-loop level. We show in the brackets the dominant composition of the tree-level, one-loop and two-loop mass eigenstates $h^{(0)}$, $h^{(1)}$ and $h^{(2)}$, in the experimentally allowed region of the plot. The desired SM-like Higgs-boson mass is indicated with the horizontal green band, assuming a theory uncertainty of 3 GeV. The red regions are excluded by direct searches for additional scalars. In the yellow region the prediction for the mixing angles of the neutrinos lies outside of the 3σ band of the experimental measurement. On top we show $\chi^2_{\rm red}$ for various Higgs-boson signal-strength measurements at LHC.

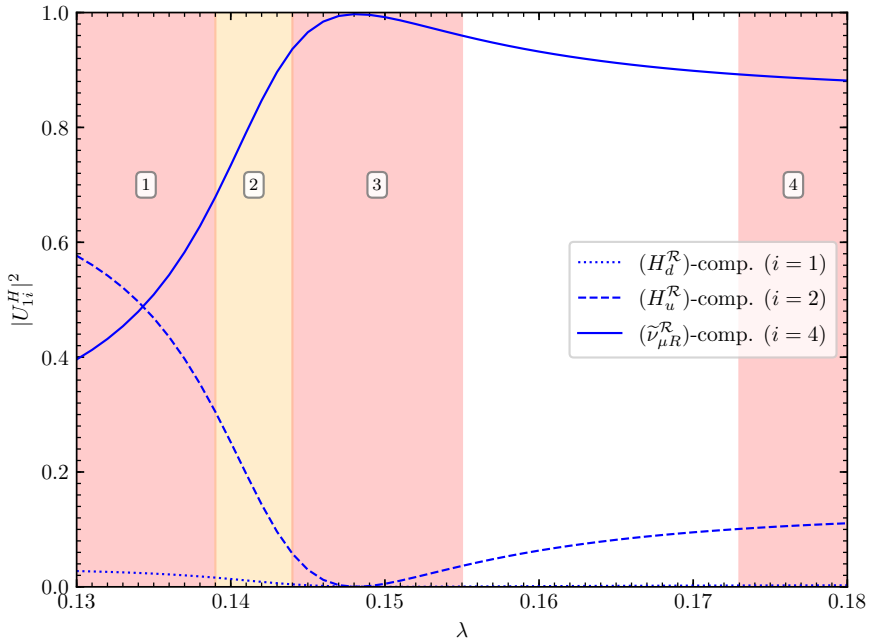

Figure 6.3: Doublet components ($H_d^{\mathcal{R}}$, $H_u^{\mathcal{R}}$) and the right-handed μ-sneutrino component ($\widetilde{\nu}_{\mu R}^{\mathcal{R}}$) of the lightest $\mathcal{CP}$-even mass eigenstate $h_1^{(2)}$. The components are defined by $|U_{1i}^{H(2)}|^2$ with $i = 1, 2$ and $i = 4$ respectively.

In Fig. 6.2 we show the resulting spectrum of the light $\mathcal{CP}$-even scalars.[4] The remaining $\mathcal{CP}$-even scalars not shown in the plot have masses above 300 GeV and do not play a role in the following discussion. The dotted lines represent the tree-level masses $m_{h_i}^{(0)}$, the dashed lines the masses including the full one-loop corrections $m_{h_i}^{(1)}$, and the solid lines the one-loop + partial two-loop + resummed corrected masses $m_{h_i}^{(2)}$ (referred to as two loop in the following, as was done in Ch. 5). We mark the regions in the plot which are excluded experimentally, either by `HiggsBounds` (red), or by not being in agreement with the neutrino oscillation data (yellow). We stress that region 2 is just excluded for the precise choice of parameters shown in Tab. 6.2. A new fit of the neutrino properties for each value of λ could accommodate predictions for the properties of the neutrinos in agreement with experiments. However, since this would exclusively affect the phenomenology of the heavier left-handed sneutrinos in the scalar sector, we do not apply the fit for each value of λ.

The spectrum is characterized by the interplay between the light $\widetilde{\nu}_{\mu R}^{\mathcal{R}}$ and the SM-like Higgs boson. For small λ the two lightest loop-corrected mass eigenstates h_1 and h_2 have roughly an equal amount of $H_u^{\mathcal{R}}$- and $\widetilde{\nu}_{\nu R}^{\mathcal{R}}$-admixture (see also Fig. 6.3). Region 1 is excluded by direct searches at the LHC, because there both h_1 and h_2 share a substantial Higgs-doublet admixture, such that via the diphoton signal strength of h_1 this region is excluded by LHC constraints [43]. At $\lambda \sim 0.14$ the point is reached where the mass of h_1 drops well below 125 GeV. Thus, beyond that point h_1 can be identified with $\widetilde{\nu}_{\mu R}^{\mathcal{R}}$, as the doublet-component of h_1 shrinks to values of roughly $\sim 10\%$. h_2, on the other hand, sheds its sneutrino admixture, so that it can identified as the SM-like Higgs boson, and the large quantum corrections from the top/stop sector dominantly contribute to

[4] Plots in this chapter have been produced using `Matplotlib` [42] in `Python`.

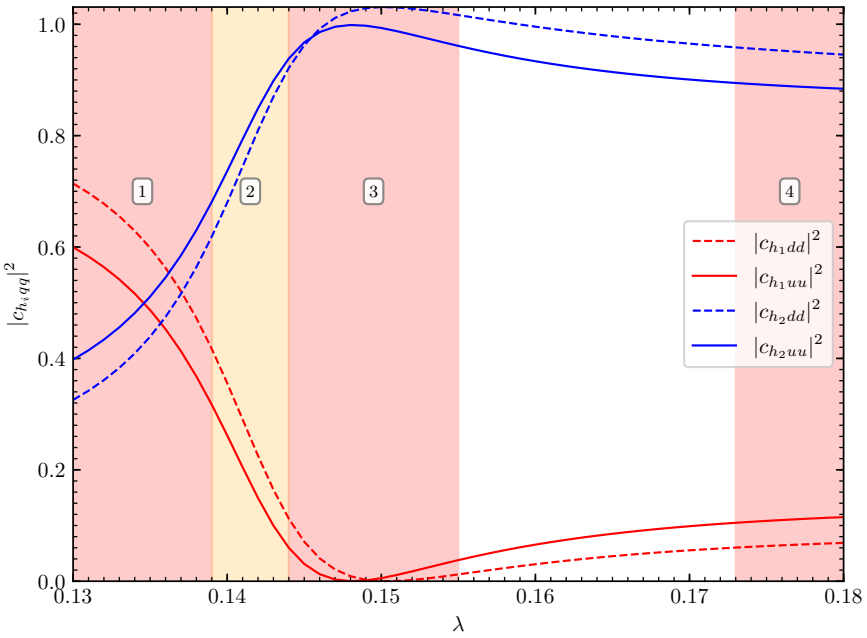

Figure 6.4: Effective couplings of the two light $\mathcal{CP}$-even scalar mass eigenstates $h_1^{(2)}$ (*red*) and $h_2^{(2)}$ (*blue*) to up-type quarks (*solid*) and down-type quarks (*dashed*), normalized to the SM prediction.

the mass of h_2. This yields an increase of the SM-like Higgs boson mass of several GeV, so that beyond region 3 it agrees with the experimental value, assuming a theoretical uncertainty of 3 GeV.

An interesting observation is that in the allowed region of λ the large one-loop corrections change the order of $\widetilde{\nu}_{\mu R}^{\mathcal{R}}$ and the SM-like Higgs boson. While the large shift of the SM-like Higgs-boson mass from $\sim$ 83 GeV at tree level to $\sim$ 125 GeV at two-loop level are familiar from the MSSM, the large one-loop corrections to $\widetilde{\nu}_{\mu R}^{\mathcal{R}}$, with a tree-level mass of $\sim$ 147 GeV and a two-loop mass below 100 GeV, emphasize the importance of accurately taking into account the radiative corrections to the Higgs-boson masses in the $\mu\nu$SSM.

In the allowed region, the doublet component of $\widetilde{\nu}_{\mu R}^{\mathcal{R}}$ reaches values of approximately 10%, which can be seen in Fig. 6.3, where we plot the down- and up-type doublet component $H_d^{\mathcal{R}}$ and $H_u^{\mathcal{R}}$, and the $\widetilde{\nu}_{\mu R}^{\mathcal{R}}$-component of the lightest $\mathcal{CP}$-even scalar mass eigenstates $h_1^{(2)}$. Naturally, this mixing will also affect the SM-like Higgs-boson properties. In this way, scenarios like the one shown here will be tested by experiments in two different and complementary ways, both caused by the mixing of $\widetilde{\nu}_{\mu R}^{\mathcal{R}}$ and the SM-like Higgs boson. Firstly, direct searches for additional Higgs bosons can look for $\widetilde{\nu}_{\mu R}^{\mathcal{R}}$, because it is directly coupled to SM particles. Secondly, precise measurements of the SM-like Higgs-boson couplings can detect (or exclude) possible variations from SM predictions.

To illustrate the possible modifications, we show in Fig. 6.4 the effective couplings of the two light $\mathcal{CP}$-even scalar mass eigenstates to up- and down-type quarks normalized to the SM-prediction which in good approximation can be expressed via the loop-corrected mixing matrix elements $U_{ij}^{H(2)}$ and β;

$$c_{h_i dd} = \frac{U_{i1}^{H(2)}}{\cos\beta} \,, \qquad c_{h_i uu} = \frac{U_{i2}^{H(2)}}{\sin\beta} \,. \tag{6.48}$$

$\tan\beta$	λ	κ	v_R	A^λ	A^κ	A^ν	
9.0	0.08	0.3	$[1210, 1270]$	1000	-1000	-1000	
$A^{u,d,e}$	$m_{\widetilde{Q},\widetilde{u},\widetilde{d}}$	$m_{\widetilde{e}}$	M_3				
-1000	1000	200	2700				
$v_{1L}/10^{-5}$	$v_{2L}/10^{-5}$	$v_{3L}/10^{-4}$	$Y^\nu_{11}/10^{-7}$	$Y^\nu_{22}/10^{-7}$	$Y^\nu_{33}/10^{-8}$	M_1	M_2
1.466	8.520	1.855	2.963	5.337	5.902	175.6	188.0

Table 6.3: Same as in Tab. 6.2 for the scenario with three light $\widetilde{\nu}^{\mathcal{R}}_{iR}$.

In the experimentally allowed region the effective coupling of the SM-like Higgs boson to up-type quarks shows deviations of roughly 10%. This is of the order of precision expected by measurements of the SM Higgs-boson couplings at the High-Luminosity LHC [44], and (depending on the center-of-mass energy deployed) an order of magnitude larger than the uncertainty expected for these kind of measurements at a possible future e^+e^- collider like the ILC [45–47]. Comparing to Fig. 6.2 (top) we can see that the region where the effective couplings are closest to one, meaning equal to the SM prediction, does not coincide with the region where the χ^2_{red} from `HiggsSignals` is minimized. This is because the mass of the SM-like Higgs boson is slightly too small in this range of λ, so even including a theoretical uncertainty of 3 GeV some signal strength measurements implemented in `HiggsSignals` are not accounted for by $h_2^{(2)}$, so that χ^2_{red} is worse.

6.3.2 Three right-handed sneutrinos below 125 GeV

In Sect. 6.3.1 we demonstrated how BPs with light right-handed sneutrinos give rise to interesting experimental signatures due to the mixing with the SM-like Higgs boson. Using data of direct searches for additional Higgs bosons and measurements of the couplings of the SM-like Higgs boson, the parameter space of the $\mu\nu$SSM can be constrained effectively. In this section we present a scenario in which all three of the $\mathcal{CP}$-even right-handed sneutrinos will have masses below 125 GeV. We choose the parameters appearing in the mass terms of the $\widetilde{\nu}^{\mathcal{R}}_{iR}$ to be universal, i.e., $\lambda := \lambda_i$, $v_R := v_{iR}$, $\kappa := \kappa_{iii}$, $A^\lambda := A^\lambda_i$, $A^\nu := A^\nu_{ii}$, $A^\kappa := A^\kappa_{iii}$, and vanishing otherwise. As explained in Sect. 3.3.1, this assures that only one of the $\widetilde{\nu}^{\mathcal{R}}_{iR}$ mixes substantially with the SM-like Higgs boson, while the other two are practically decoupled. This helps to control the total admixture of the doublet components of the $\widetilde{\nu}^{\mathcal{R}}_{iR}$. A parameter scan including scenarios with all three $\widetilde{\nu}^{\mathcal{R}}_{iR}$ possibly mixed with the SM-like Higgs boson is left for a future work.

The complete set of free parameters is shown in Tab. 6.3. In this scenario we vary v_R, because the vevs appear linearly in the Majorana-like mass terms of the $\widetilde{\nu}^{\mathcal{R}}_{iR}$. Thus, they are convenient parameters to control the masses. By decreasing λ compared to the BP in Sect. 6.3.1 the overall behavior of the SM-like Higgs boson is aligned more to the SM predictions. Consequently, because at tree level the additional contribution to the SM-like Higgs-boson mass proportional $\boldsymbol{\lambda}^2$ is smaller (see Eq. (3.54)), $\tan\beta$ is larger to increase the quantum corrections. Also the value for κ is decreased, so that the masses of the $\widetilde{\nu}^{\mathcal{R}}_{iR}$ are smaller. As before, the parameters in the last row of Tab. 6.3 were fitted to accurately predict the left-handed neutrino masses and mixings. The fit was done in the point $v_R = 1226$ GeV, but in this case the neutrino data is described in agreement with experimental data over the whole range of v_R at tree level.

We show the resulting light $\mathcal{CP}$-even scalar spectrum in Fig. 6.5. In the experimen-

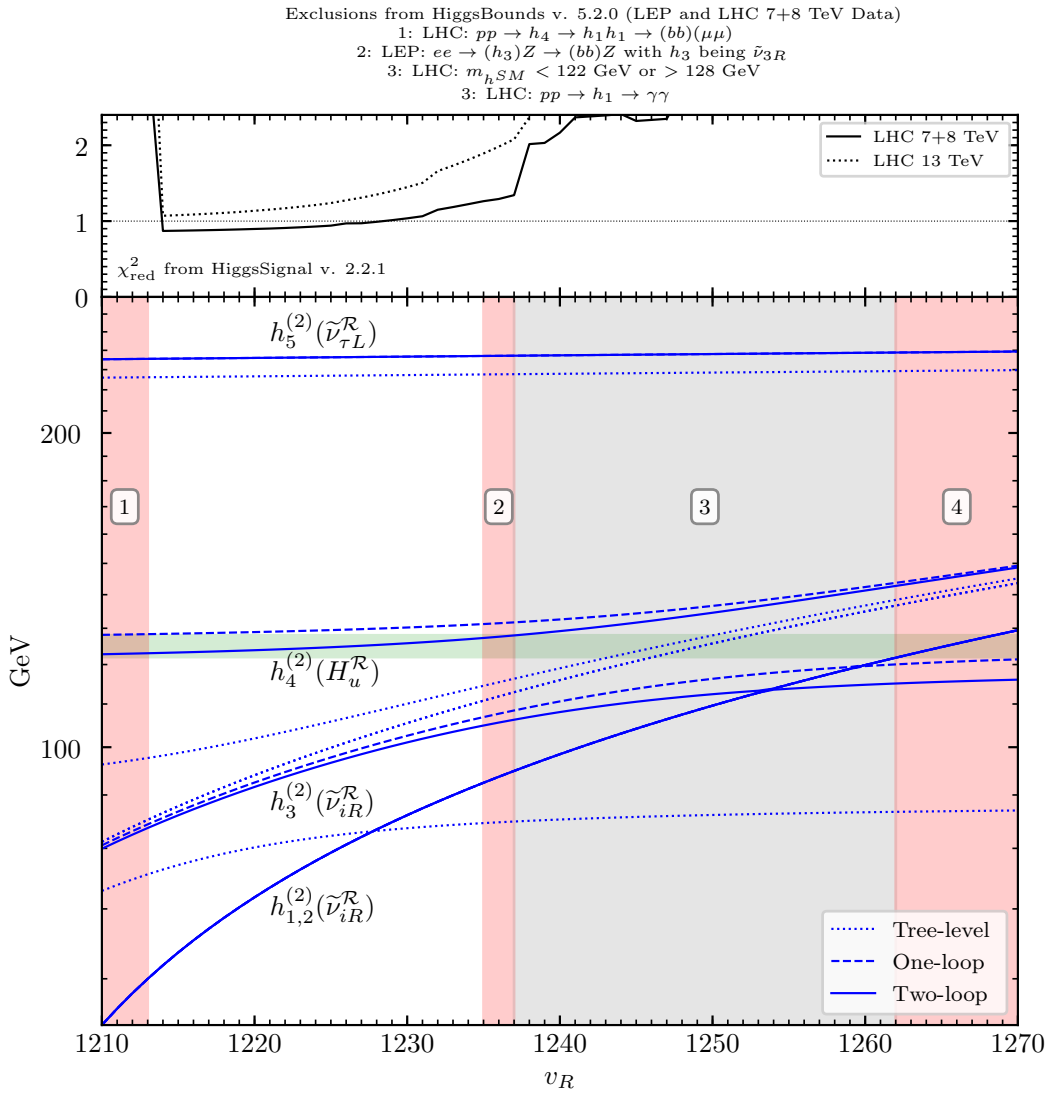

Figure 6.5: Light $\mathcal{CP}$-even scalar spectrum in the in the scenario with three light $\widetilde{\nu}_{iR}^{\mathcal{R}}$. Shown are the masses at tree level (*dotted*), at the one-loop level (*dashed*) and at the partial two-loop level (*solid*). We show in the brackets the dominant composition of the loop-corrected mass eigenstates $h^{(2)}$ in the experimentally allowed region of v_R. The desired SM-like Higgs-boson mass is indicated with the horizontal green band, assuming a theory uncertainty of 3 GeV. The red regions are excluded by direct searches for additional scalars. In the gray region the SM-like Higgs-boson mass is not predicted accurately. On top we show χ^2_{red} for various Higgs-boson signal-strength measurements at LHC.

tally allowed region (1213 GeV $\leq v_R \leq$ 1235 GeV) the lightest mass eigenstates $h_{1,2}$ are two almost degenerate right-handed sneutrinos. The third right-handed sneutrino corresponds to h_3. It is is roughly 20 GeV heavier and acquires substantial mixing with the SM-like Higgs boson h_4. Naturally, the right-handed sneutrinos increase their masses when v_R becomes larger, but also the SM-like Higgs-boson mass increases, because the mixing with the heavier $\widetilde{\nu}_{iR}^{\mathcal{R}}$ gives additional contributions.

The BP is excluded experimentally for small values of v_R in region 1 by searches for the decay of the SM-like Higgs boson into two lighter scalars, that subsequently decay into two b-jets and a pair of μ-leptons [48]. There the two lightest mass eigenstates $h_{1,2}$ become lighter than half the mass of h_4, so the decays $h_4 \to h_{1,2}h_{1,2}$ are kinematically allowed. These additional decay channels are also the reason why the χ^2_{red} from `HiggsSignals` rapidly increases in region 1, because it suppresses ordinary SM-like decays of h_4.

When v_R increases above 1235 GeV further constrains from direct searches for additional Higgs bosons and measurement of the properties of the SM-like Higgs boson become relevant. χ^2_{red} quickly increases above 2 at $v_R \sim 1237$ GeV. Already at $v_R \sim 1235$ GeV the scenario is excluded by LEP searches [49], yielding the red region 2. Here, the mixing of h_3 and h_4 enlarges, while h_3 is kinematically still in reach of being produced at LEP via Higgsstrahlung production. At $v_R \sim 1235$ GeV the doublet admixture of h_3 is so large that the channel $ee \to (h_3)Z \to (b\bar{b})Z$ can exclude this interval. Interestingly, in the experimentally allowed region, where the mass of h_3 is even smaller, LEP data cannot rule out this scenario. The reasons for this is not only the smaller mixing of h_3 and the SM-like Higgs boson h_4, but also that in the mass range below 100 GeV LEP saw an excess over the SM background in the decay channel written above (see Ch. 8) [49].

In region 3 the BP is excluded because the SM-like Higgs-boson mass is not predicted accurately, even including a theoretical uncertainty of 3 GeV. Beyond that, the BP is excluded by the LHC cross-section measurement of the process $pp \to h_1 \to \gamma\gamma$ [50]. In region 3 the cross-over point is reached in which the masses of the $\widetilde{\nu}_{iR}^{\mathcal{R}}$ become larger than the SM-like Higgs-boson mass. Through the interference effects the SM-like Higgs-boson mass is pushed to lower values beyond that point. In region 4 the mass eigenstate corresponding to the SM-like Higgs boson is the lightest one at just about 118 GeV. Even though there are two scalars in the mass range of the experimentally measured Higgs-boson mass in region 4, there is no contribution to any signal-strength measurement at the LHC, reflected by the fact that the χ^2_{red} is huge there. The reason is that these two mass-degenerate states correspond to the practically singlet-like right-handed sneutrino states. The third right-handed sneutrino carrying the doublet admixture taken from the SM-like Higgs boson has a mass of over 140 GeV. Hence, it also does not contribute to signal-strength measurements of the SM-like Higgs boson.

On a side note we briefly discuss the remaining light scalar h_5 in Fig. 6.5, corresponding to the left-handed τ-sneutrino at roughly 235–240 GeV. This particular fit to the neutrino oscillation data generated a hierarchy between the vevs of the left-handed sneutrinos, with v_{3L} being the largest. Since dominant tree-level contributions to the masses of the $\widetilde{\nu}_{iL}^{\mathcal{R}}$ scale with inverse of v_{iL} (see Eq. (3.48)), the $\widetilde{\nu}_{\tau L}^{\mathcal{R}}$ is the lightest $\mathcal{CP}$-even left-handed sneutrino. It is difficult to detect such a $\widetilde{\nu}_{\tau L}^{\mathcal{R}}$ by usual searches for additional Higgs bosons at colliders. A dedicated analysis of LHC data was proposed to search for light left-handed sneutrinos in the framework of the $\mu\nu$SSM [23]. However, that analysis concentrated on τ-sneutrinos as the LSP, whereas here there are even lighter SUSY particles in the spectrum. For a detailed discussion of distinct signatures at the LHC related to left-handed sneutrinos within the $\mu\nu$SSM we refer to the literature [23–25].

$\tan\beta$	$\boldsymbol{\lambda}^2$	κ	$v_{1,3R}$	v_{2R}	A^λ	A^κ_{iii}	A^ν_{ii}
5	$3 \cdot 0.168^2$	0.5	1000	765	1000	-1000	-1000

A^u_3	$A^u_{1,2}$	$A^{(d,e)}$	$m_{\widetilde{Q},\widetilde{u},\widetilde{d}}$	$m_{\widetilde{e}}$	M_3
-2000	-1500	-1500	1500	200	2700

$v_{1L}/10^{-4}$	$v_{2L}/10^{-4}$	$v_{3L}/10^{-4}$	$Y^\nu_{11}/10^{-7}$	$Y^\nu_{22}/10^{-7}$	$Y^\nu_{33}/10^{-7}$	M_1	M_2
1.497	6.179	4.946	4.388	1.759	6.258	1228	2814

Table 6.4: Same as in Tab. 6.2 for the scan over λ_i while $\boldsymbol{\lambda}^2 = \text{const}$.

6.3.3 Scan over $\boldsymbol{\lambda_i}$ while $\boldsymbol{\lambda^2 = \lambda_i\lambda_i = \text{const}}$.

As already explained in Sect. 6.3, without further assumptions there is no theoretical reason for the $\mu\nu$SSM-like parameters to be universal w.r.t. the family indices. In this section we investigate if that can have consequences for the prediction of the SM-like Higgs-boson mass. In particular, we try to estimate the significance of non-universal values for the three parameters λ_i. At tree level (see Eq. (3.54)) the mass dominantly depends on the term $\boldsymbol{\lambda}^2 = \lambda_i\lambda_i$, and not on the individual values for λ_i. However, as soon as mixing effects between the $\mathcal{CP}$-even right-handed sneutrinos and the SM-like Higgs boson become sizable, this is not anymore the case. This effects can enter at tree level, or via radiative corrections proportional to λ_i. These radiative corrections depend on the masses and the mixing of each of the right-handed sneutrino. Since it is not the case that all three $\widetilde{\nu}_{iR}$ are degenerate, the radiative corrections are expected to depend strongly on the individual values of λ_i. Also, when $\boldsymbol{\lambda}^2$ is fixed, the μ-term which is dynamically generated after EWSB and linearly dependent on λ_i cannot be constant when the λ_i are varied. This can be another source of corrections to the SM-like Higgs-boson mass that explicitly depend on the individual values of the λ_i.

Yet, in experimentally allowed BPs, the loop corrections proportional to λ_i are always subleading regarding the corrections to the SM-like Higgs-boson mass, owing to the limitation on the $\widetilde{\nu}^{\mathcal{R}}_{iR}$-admixture it can possibly account for. We give here an idea of how large the remnant effect of non-universal λ_i on the SM-like Higgs-boson mass can be by varying the values for the three λ_i under the conditions that $\boldsymbol{\lambda}^2$ remains the same. We performed a small scan over all possible values of the λ_i in a scenario in which $\widetilde{\nu}^{\mathcal{R}}_{\mu R}$ has a mass between 92 and 115 GeV and mixes substantially with the SM-like Higgs boson. The free parameters were set to the values shown in Tab. 6.4.

The scenario is very similar to the one in Sect. 6.3.1. When the λ_i are chosen uniformly we recover the BP at $\lambda = 0.168$ in Fig. 6.2, which is in the middle of the experimentally allowed parameter region. In Fig. 6.6 we illustrate the dependence of the SM-like Higgs-boson mass on the individual values of λ_i. We show ternary plots [51] with the values of λ_i^2 on the axes. The colors of the points encode the mass of the SM-like Higgs boson at tree level (top left), at one-loop level (top right), the difference of the SM-like Higgs-boson mass at tree level and one-loop level (bottom left), and the one-loop mass of the right-handed μ-sneutrino (bottom right). We do not show the two-loop mass of the SM-like Higgs boson, because the two-loop corrections supplemented from `FeynHiggs` are purely MSSM-like corrections independent of λ_i, thus not playing a role here.

The one-loop mass of the SM-like Higgs boson is the largest in the central point in which all λ_i are equal. The tree-level mass, on the other hand, shows the opposite behavior. It has its maximum value in the corners of the plot in which one of the λ_i

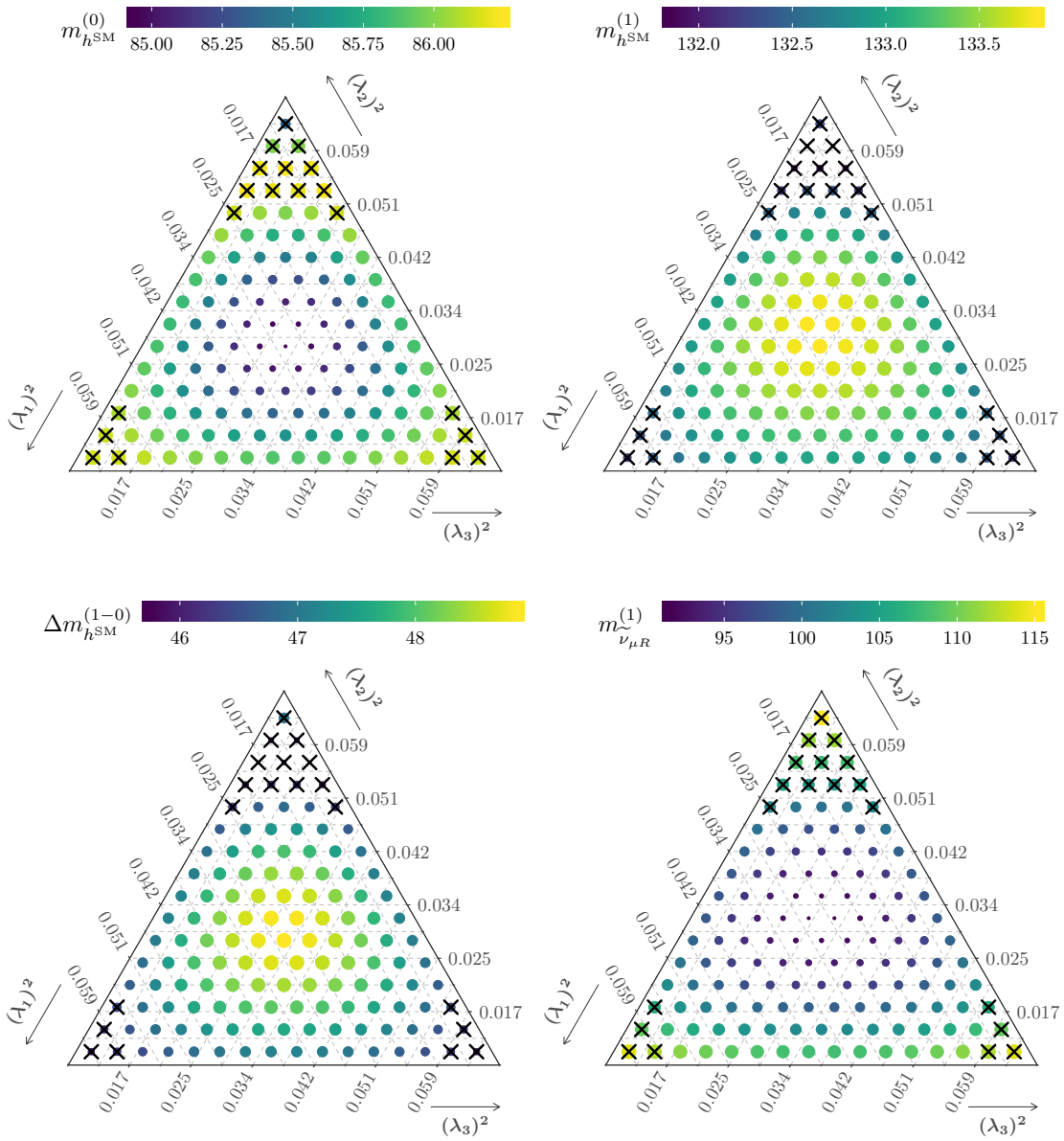

Figure 6.6: SM-like Higgs-boson mass at tree level $m^{(0)}_{h^{\rm SM}} = m_{h_1^{(0)}}$ (*top left*), and at one-loop level $m^{(1)}_{h^{\rm SM}} = m_{h_2^{(1)}}$ (*top right*), and their difference $\Delta m^{(1-0)}_{h^{\rm SM}} = m^{(1)}_{h^{\rm SM}} - m^{(0)}_{h^{\rm SM}}$ (*bottom left*), and the one-loop mass of $\widetilde{\nu}_{\mu R}$ (*bottom right*) for fixed $\boldsymbol{\lambda}^2$ but varying λ_i. Crossed points are excluded by either `HiggsBounds`, `HiggsSignals` with $\chi^2_{red} \geq 150/101 = 1.485$ for the 13 TeV data set, or because the SM-like Higgs boson mass including the two-loop corrections is smaller than 123 GeV or larger than 127 GeV.

is practically zero. The one-loop mass of the SM-like Higgs boson varies in the experimentally allowed region by more than 1 GeV. This demonstrates that for an accurate prediction it is crucial to include the independent contributions of all three λ_i to the radiative corrections, when mixing effects between the right-handed sneutrinos and the SM-like Higgs boson are sizable.

Note that the variation of the one-loop mass would be even larger if we neglect the experimental constrains. In these BPs, the main exclusion limit is the requirement to have the SM-like Higgs-boson mass above 123 GeV at two-loop. Thus, in other BPs in which the experimental constraints are respected while potentially having an even larger $\widetilde{\nu}^{\mathcal{R}}_{iR}$-component in the SM-like Higgs boson, the dependence on the values of λ_i might be even stronger. Regarding the constraints, the problem in the scenario shown here is that in the corners of the plots the mass of $\widetilde{\nu}^{\mathcal{R}}_{\mu R}$ increases to values very close to ~ 125 GeV. This increases the mixing between both scalars, yielding a reduction of the radiative corrections to the mass of the SM-like Higgs boson. Practically speaking, parts of the loop corrections "are lost" to $\widetilde{\nu}^{\mathcal{R}}_{\mu R}$. This is why the difference between the tree-level and the one-loop mass of the SM-like Higgs boson is the smallest when the mass of $\widetilde{\nu}^{\mathcal{R}}_{\mu R}$ is the largest.

We finally note that the variation of the difference between tree-level and one-loop mass, as a measure for the size of genuine one-loop corrections, is more than twice as large as the variation of the one-loop mass of the SM-like Higgs boson itself. This indicates a cancellation of λ_i-dependence between tree-level mass and the radiative corrections, owing to the fact that the mass eigenstates at tree-level corresponding to the SM-like Higgs boson can have a larger $\widetilde{\nu}^{\mathcal{R}}_{\mu R}$-component. The loop-corrected mass eigenstate, on the other hand, cannot have an arbitrary large $\widetilde{\nu}^{\mathcal{R}}_{\mu R}$-component, because it has to fulfill the experimental constraints.

Bibliography

[1] T. Biekötter, S. Heinemeyer, and C. Muñoz, "Precise prediction for the Higgs-Boson Masses in the $\mu\nu$SSM with three right-handed neutrino superfields", arXiv:1906.06173.

[2] T. Hahn, "Generating Feynman diagrams and amplitudes with FeynArts 3", *Comput. Phys. Commun.* **140** (2001) 418–431, arXiv:hep-ph/0012260.

[3] F. Staub, "From Superpotential to Model Files for FeynArts and CalcHep/CompHep", *Comput. Phys. Commun.* **181** (2010) 1077–1086, arXiv:0909.2863.

[4] F. Staub, "SARAH 4 : A tool for (not only SUSY) model builders", *Comput. Phys. Commun.* **185** (2014) 1773–1790, arXiv:1309.7223.

[5] T. Hahn and M. Perez-Victoria, "Automatized one loop calculations in four-dimensions and D-dimensions", *Comput. Phys. Commun.* **118** (1999) 153–165, arXiv:hep-ph/9807565.

[6] G. J. van Oldenborgh and J. A. M. Vermaseren, "New Algorithms for One Loop Integrals", *Z. Phys.* **C46** (1990) 425–438.

[7] S. P. Martin and M. T. Vaughn, "Two loop renormalization group equations for soft supersymmetry breaking couplings", *Phys. Rev.* **D50** (1994) 2282, arXiv:hep-ph/9311340, [Erratum: Phys. Rev.D78,039903(2008)].

[8] Y. Yamada, "Two loop renormalization group equations for soft SUSY breaking scalar interactions: Supergraph method", *Phys. Rev.* **D50** (1994) 3537–3545, arXiv:hep-ph/9401241.

[9] M. E. Machacek and M. T. Vaughn, "Two Loop Renormalization Group Equations in a General Quantum Field Theory. 2. Yukawa Couplings", *Nucl. Phys.* **B236** (1984) 221–232.

[10] M.-x. Luo, H.-w. Wang, and Y. Xiao, "Two loop renormalization group equations in general gauge field theories", *Phys. Rev.* **D67** (2003) 065019, arXiv:hep-ph/0211440.

[11] M. E. Machacek and M. T. Vaughn, "Two Loop Renormalization Group Equations in a General Quantum Field Theory. 1. Wave Function Renormalization", *Nucl. Phys.* **B222** (1983) 83–103.

[12] R. M. Fonseca, M. Malinský, and F. Staub, "Renormalization group equations and matching in a general quantum field theory with kinetic mixing", *Phys. Lett.* **B726** (2013) 882–886, arXiv:1308.1674.

[13] P. Ghosh, D. E. Lopez-Fogliani, V. A. Mitsou, C. Muñoz, and R. Ruiz de Austri, "Probing the $\mu\nu$SSM with light scalars, pseudoscalars and neutralinos from the decay of a SM-like Higgs boson at the LHC", *JHEP* **11** (2014) 102, arXiv:1410.2070.

[14] N. Escudero, D. E. Lopez-Fogliani, C. Muñoz, and R. Ruiz de Austri, "Analysis of the parameter space and spectrum of the $\mu\nu$SSM", *JHEP* **12** (2008) 099, arXiv:0810.1507.

[15] P. Ghosh and S. Roy, "Neutrino masses and mixing, lightest neutralino decays and a solution to the μ problem in supersymmetry", *JHEP* **04** (2009) 069, arXiv:0812.0084.

[16] J. Fidalgo, D. E. Lopez-Fogliani, C. Muñoz, and R. Ruiz de Austri, "Neutrino Physics and Spontaneous CP Violation in the $\mu\nu$SSM", *JHEP* **08** (2009) 105, arXiv:0904.3112.

[17] P. Ghosh, P. Dey, B. Mukhopadhyaya, and S. Roy, "Radiative contribution to neutrino masses and mixing in $\mu\nu$SSM", *JHEP* **05** (2010) 087, arXiv:1002.2705.

[18] P. Bechtle, O. Brein, S. Heinemeyer, G. Weiglein, and K. E. Williams, "HiggsBounds: Confronting Arbitrary Higgs Sectors with Exclusion Bounds from LEP and the Tevatron", *Comput. Phys. Commun.* **181** (2010) 138–167, arXiv:0811.4169.

[19] P. Bechtle, O. Brein, S. Heinemeyer, G. Weiglein, and K. E. Williams, "HiggsBounds 2.0.0: Confronting Neutral and Charged Higgs Sector Predictions with Exclusion Bounds from LEP and the Tevatron", *Comput. Phys. Commun.* **182** (2011) 2605–2631, arXiv:1102.1898.

[20] P. Bechtle, O. Brein, S. Heinemeyer, O. Stal, T. Stefaniak, G. Weiglein, and K. Williams, "Recent Developments in HiggsBounds and a Preview of HiggsSignals", *PoS* **CHARGED2012** (2012) 024, arXiv:1301.2345.

[21] P. Bechtle, O. Brein, S. Heinemeyer, O. Stål, T. Stefaniak, G. Weiglein, and K. E. Williams, "HiggsBounds – 4: Improved Tests of Extended Higgs Sectors against Exclusion Bounds from LEP, the Tevatron and the LHC", *Eur. Phys. J.* **C74** (2014), no. 3, 2693, arXiv:1311.0055.

[22] P. Bechtle, S. Heinemeyer, O. Stal, T. Stefaniak, and G. Weiglein, "Applying Exclusion Likelihoods from LHC Searches to Extended Higgs Sectors", *Eur. Phys. J.* **C75** (2015), no. 9, 421, arXiv:1507.06706.

[23] I. Lara, D. E. López-Fogliani, C. Muñoz, N. Nagata, H. Otono, and R. Ruiz De Austri, "Looking for the left sneutrino LSP with displaced-vertex searches", *Phys. Rev.* **D98** (2018), no. 7, 075004, arXiv:1804.00067.

[24] I. Lara, D. E. López-Fogliani, and C. Muñoz, "Electroweak superpartners scrutinized at the LHC in events with multi-leptons", *Phys. Lett.* **B790** (2019) 176–183, arXiv:1810.12455.

[25] P. Ghosh, I. Lara, D. E. Lopez-Fogliani, C. Munoz, and R. Ruiz de Austri, "Searching for left sneutrino LSP at the LHC", *Int. J. Mod. Phys.* **A33** (2018), no. 18n19, 1850110, arXiv:1707.02471.

[26] P. Bechtle, S. Heinemeyer, O. Stål, T. Stefaniak, and G. Weiglein, "*HiggsSignals*: Confronting arbitrary Higgs sectors with measurements at the Tevatron and the LHC", *Eur. Phys. J.* **C74** (2014), no. 2, 2711, arXiv:1305.1933.

[27] O. Stål and T. Stefaniak, "Constraining extended Higgs sectors with HiggsSignals", *PoS* **EPS-HEP2013** (2013) 314, arXiv:1310.4039.

[28] P. Bechtle, S. Heinemeyer, O. Stål, T. Stefaniak, and G. Weiglein, "Probing the Standard Model with Higgs signal rates from the Tevatron, the LHC and a future ILC", *JHEP* **11** (2014) 039, arXiv:1403.1582.

[29] M. D. Goodsell, S. Liebler, and F. Staub, "Generic calculation of two-body partial decay widths at the full one-loop level", *Eur. Phys. J.* **C77** (2017), no. 11, 758, arXiv:1703.09237.

[30] M. Frank, T. Hahn, S. Heinemeyer, W. Hollik, H. Rzehak, and G. Weiglein, "The Higgs Boson Masses and Mixings of the Complex MSSM in the Feynman-Diagrammatic Approach", *JHEP* **02** (2007) 047, arXiv:hep-ph/0611326.

[31] A. Djouadi, J. Kalinowski, and P. M. Zerwas, "Two and three-body decay modes of SUSY Higgs particles", *Z. Phys.* **C70** (1996) 435–448, arXiv:hep-ph/9511342.

[32] A. Djouadi, "The Anatomy of electro-weak symmetry breaking. I: The Higgs boson in the standard model", *Phys. Rept.* **457** (2008) 1–216, arXiv:hep-ph/0503172.

[33] M. Spira, "Higgs Boson Production and Decay at Hadron Colliders", *Prog. Part. Nucl. Phys.* **95** (2017) 98–159, arXiv:1612.07651.

[34] A. Djouadi, "Decays of the Higgs bosons", in "Quantum effects in the minimal supersymmetric standard model. Proceedings, International Workshop, MSSM, Barcelona, Spain, September 9-13, 1997", pp. 197–222. 1997. arXiv:hep-ph/9712334.

[35] T. G. Rizzo, "Decays of heavy higgs bosons", *Phys. Rev. D* **22** Aug (1980) 722–726.

[36] M. Spira, Memorandum, https://twiki.cern.ch/twiki/pub/LHCPhysics/LHCHXSWGSMInputParameter/Higgs_coupling.pdf.

[37] I. Esteban, M. C. Gonzalez-Garcia, M. Maltoni, I. Martinez-Soler, and T. Schwetz, "Updated fit to three neutrino mixing: exploring the accelerator-reactor complementarity", *JHEP* **01** (2017) 087, arXiv:1611.01514.

[38] NuFIT 3.2 (2018), www.nu-fit.org.

[39] I. Esteban, M. C. Gonzalez-Garcia, A. Hernandez-Cabezudo, M. Maltoni, and T. Schwetz, "Global analysis of three-flavour neutrino oscillations: synergies and tensions in the determination of $\theta_2 3, \delta_C P$, and the mass ordering", *JHEP* **01** (2019) 106, arXiv:1811.05487.

[40] F.-A. Fortin, F.-M. De Rainville, M.-A. Gardner, M. Parizeau, and C. Gagné, "DEAP: Evolutionary algorithms made easy", *Journal of Machine Learning Research* **13** jul (2012) 2171–2175.

[41] A. Bartl, M. Hirsch, A. Vicente, S. Liebler, and W. Porod, "LHC phenomenology of the $\mu\nu$SSM", *JHEP* **05** (2009) 120, arXiv:0903.3596.

[42] J. D. Hunter, "Matplotlib: A 2d graphics environment", *Computing in Science & Engineering* **9** (2007), no. 3, 90–95.

[43] **CMS** Collaboration, "Combination of standard model Higgs boson searches and measurements of the properties of the new boson with a mass near 125 GeV", CMS-PAS-HIG-12-045, 2012

[44] **Physics of the HL-LHC Working Group** Collaboration, M. Cepeda *et al.*, "Higgs Physics at the HL-LHC and HE-LHC", arXiv:1902.00134.

[45] S. Dawson *et al.*, "Working Group Report: Higgs Boson", in "Proceedings, 2013 Community Summer Study on the Future of U.S. Particle Physics: Snowmass on the Mississippi (CSS2013): Minneapolis, MN, USA, July 29-August 6, 2013". 2013. arXiv:1310.8361.

[46] K. Fujii *et al.*, "Physics Case for the 250 GeV Stage of the International Linear Collider", DESY-17-155, KEK-PREPRINT-2017-31, LAL-17-059, SLAC-PUB-17161, 2017 arXiv:1710.07621.

[47] P. Bambade *et al.*, "The International Linear Collider: A Global Project", DESY 19-037, FERMILAB-FN-1067-PPD, IFIC/19-10, JLAB-PHY-19-2854, KEK Preprint 2018-92, LAL/RT 19-001, SLAC-PUB-17412, 2019 arXiv:1903.01629.

[48] **CMS** Collaboration, V. Khachatryan *et al.*, "Search for light bosons in decays of the 125 GeV Higgs boson in proton-proton collisions at $\sqrt{s} = 8$ TeV", *JHEP* **10** (2017) 076, arXiv:1701.02032.

[49] **OPAL, DELPHI, LEP Working Group for Higgs boson searches, ALEPH, L3** Collaboration, R. Barate *et al.*, "Search for the standard model Higgs boson at LEP", *Phys. Lett.* **B565** (2003) 61–75, arXiv:hep-ex/0306033.

[50] **CMS** Collaboration, "Updated measurements of the Higgs boson at 125 GeV in the two photon decay channel", CMS-PAS-HIG-13-001, 2013

[51] N. E. Hamilton and M. Ferry, "ggtern: Ternary diagrams using ggplot2", *Journal of Statistical Software, Code Snippets* **87** (2018), no. 3, 1–17.

Chapter 7

The Next-to 2 Higgs doublet model

Susy extensions of the SM necessarily need to be constructed with the help of a second Higgs doublet. This is one reason why so-called 2 Higgs Doublet Models (2HDM) are well established BSM scenarios. However, there are several other motivations to consider extended scalar sectors. For instance, in an extended scalar sector with two scalar doublet fields the hierarchy between fermion masses of up- and down-type can be attributed to a hierarchy between the vevs of the different neutral components [1, 2]. The solution of the strong $\mathcal{CP}$-problem via a Peccei-Quinn symmetry requires additional scalar fields [3–5]. These solutions predict a physical Goldstone boson called axion which until now could not be detected experimentally. Further SU(2) singlet scalar fields can help to relax experimental constraints [6]. Another motivation to consider models with more than one Higgs doublet comes from the matter-antimatter asymmetry of the universe. One solution to this problem, called baryogenesis [7], requires additional sources of $\mathcal{CP}$-violation that cannot be accounted for in the SM [8–10]. In models with two or more Higgs doublets, additional explicit or spontaneous sources of $\mathcal{CP}$-violation can be present. However, the possible amount is constrained, because the breaking of $\mathcal{CP}$-conservation is strongly related to the appearance of flavor-changing neutral currents (FCNC) at tree level [11]. The precisely measured value of the ρ-parameter [12],

$$\rho = \frac{M_W^2}{M_Z^2 c_{\mathrm{w}}^2} = 1.00039 \pm 0.00019 \,, \tag{7.1}$$

where c_{w} is the weak mixing angle, being very close to the SM prediction $\rho = 1$ at tree level, constrains the possible structure of weak isospin and hypercharge attributed to additional scalar fields. Models in which additional Higgs bosons transform as SU(2) doublets or gauge singlets do not modify the tree-level prediction of ρ, and are therefore particularly motivated [11].

In the $\mathcal{CP}$-conserving case the scalar sector of the 2HDM consists of two $\mathcal{CP}$-even, one $\mathcal{CP}$-odd and two charged Higgs bosons. Both the lighter or the heavier $\mathcal{CP}$-even Higgs boson can be identified with the SM-like Higgs boson at $\sim 125\,\mathrm{GeV}$. One refers to the 2HDM in which the particle content is further enhanced by a real scalar singlet as the next-to 2 Higgs doublet model (N2HDM) [13]. There the physical spectrum additionally incorporates a third $\mathcal{CP}$-even Higgs boson that, being a gauge singlet, is characterized by reduced couplings to SM particles. The addition of a singlet scalar to the spectrum has several motivations depending on the global symmetries applied on the scalar sector. We will briefly summarize a few of them in the following.

The NMSSM is a Susy model that, in addition to the field content of the MSSM, features a gauge singlet superfield (see Sect. 2.5). Thus, as in the N2HDM, the scalar

spectrum is enhanced by a third $\mathcal{CP}$-even Higgs boson that mixes with the two doublet-like Higgs bosons. The NMSSM further contains a second physical $\mathcal{CP}$-odd Higgs boson which, however, does not have a corresponding particle in the N2HDM. Certain types of the N2HDM can be regarded as an effective theory of the NMSSM at low energies in case the sparticles are heavy enough that they can be integrated out. In our case, however, a Z_2 symmetry, only softly broken in the scalar sector, forbids trilinear terms in the scalar potential that are required to entirely map the NMSSM on the N2HDM.

Models with additional singlet scalars are also prominently studied in the context of dark matter [14–20], and in some cases can be realized within the N2HDM. If one scalar field, either the singlet or one of the doublet fields, is prevented from obtaining a vev [21, 22], the field is stable and can contribute to the relic abundance of dark matter. These kind of scenarios are in one of the so-called dark phases of the N2HDM. In our case there is no exact Z_2 symmetry to stabilize one of the scalar fields, and no scalar particle is stable.

We study the case in which all three physical $\mathcal{CP}$-even Higgs bosons acquire a vev and mix with each other [23] which is called the broken phase of the N2HDM. The broken phase is the one with the most general mixing in the $\mathcal{CP}$-even sector, such that couplings both to up- and down-type quarks can be realized for any mass eigenstate. In Sect. 7.1 we describe in detail the scalar potential of the N2HDM in the broken phase. Afterwards we introduce in Sect. 7.2 the different types of the N2HDM which differ in the way the doublet Higgs fields couple to the SM fermions. Subsequently, we illustrate general phenomenological considerations in Sect. 7.3, such as possible exotic signals and experimental constraints. The numerical analysis done in the scope of this thesis was aimed to explain two experimental excesses for which we give details in Ch. 8 [23]. Consequently, we postpone the discussion of our numerical results to the end of that chapter.

7.1 Higgs potential

The scalar potential of the $\mathcal{CP}$-conserving N2HDM is given by [24]

$$\begin{aligned} V &= m_{11}^2|\Phi_1|^2 + m_{22}^2|\Phi_2|^2 - m_{12}^2(\Phi_1^\dagger\Phi_2 + \text{h.c.}) + \frac{\lambda_1}{2}(\Phi_1^\dagger\Phi_1)^2 + \frac{\lambda_2}{2}(\Phi_2^\dagger\Phi_2)^2 \\ &\quad + \lambda_3(\Phi_1^\dagger\Phi_1)(\Phi_2^\dagger\Phi_2) + \lambda_4(\Phi_1^\dagger\Phi_2)(\Phi_2^\dagger\Phi_1) + \frac{\lambda_5}{2}[(\Phi_1^\dagger\Phi_2)^2 + h.c.] \\ &\quad + \frac{1}{2}m_S^2\Phi_S^2 + \frac{\lambda_6}{8}\Phi_S^4 + \frac{\lambda_7}{2}(\Phi_1^\dagger\Phi_1)\Phi_S^2 + \frac{\lambda_8}{2}(\Phi_2^\dagger\Phi_2)\Phi_S^2 \,, \end{aligned} \tag{7.2}$$

where Φ_1 and Φ_2 are the two $SU(2)_L$ doublets and Φ_S is a real scalar singlet. The scalar potential is constructed respecting a global Z_2 symmetry, under which the fields transform as

$$\Phi_1 \to \Phi_1 \,, \quad \Phi_2 \to -\Phi_2 \,, \quad \Phi_S \to \Phi_S \,, \tag{7.3}$$

which is only softly broken by the bilinear term

$$m_{12}^2(\Phi_1^\dagger\Phi_2 + h.c.) \,. \tag{7.4}$$

The breaking of the global Z_2 symmetry also allows for $\mathcal{CP}$-violating phases in the scalar potential which, however, are assumed to be absent in the following discussion. The

extension of the Z_2 symmetry to the Yukawa sector forbids FCNC at tree level. There is no unique choice for the corresponding charges of the SM fermions under this symmetry. Depending on this choice, one obtains four different types of the N2HDM, whose differences will be explained in Sect. 7.2. They are analogues to the different types of the 2HDM.

Assuming $\mathcal{CP}$-conservation and that the global minimum of the scalar potential is not electromagnetically charged, the scalar fields can be parametrized as

$$\Phi_1 = \begin{pmatrix} \phi_1^+ \\ \frac{1}{\sqrt{2}}(v_1 + \rho_1 + i\eta_1) \end{pmatrix} , \quad \Phi_2 = \begin{pmatrix} \phi_2^+ \\ \frac{1}{\sqrt{2}}(v_2 + \rho_2 + i\eta_2) \end{pmatrix} , \quad \Phi_S = v_S + \rho_S \, . \tag{7.5}$$

In contrast to SUSY models, the doublet-fields Φ_1 and Φ_2 are defined as carrying the same hypercharge. That is why for both fields the neutral component appears in the bottom column. The neutral components obtain the vacuum expectation values

$$\langle \Phi_1 \rangle = \frac{1}{\sqrt{2}} \begin{pmatrix} 0 \\ v_1 \end{pmatrix} , \quad \langle \Phi_2 \rangle = \frac{1}{\sqrt{2}} \begin{pmatrix} 0 \\ v_2 \end{pmatrix} , \quad \langle \Phi_S \rangle = v_S \, . \tag{7.6}$$

In analogy to SUSY models, one defines

$$\tan\beta = \frac{v_2}{v_1} \, , \tag{7.7}$$

however, without implying that Φ_1 and Φ_2 can be interpreted as down- and up-type fields, respectively. The singlet field Φ_S is by definition real and has no imaginary component. Therefore, the charged and the $\mathcal{CP}$-odd scalar sector are unchanged compared to the 2HDM. On the contrary, the $\mathcal{CP}$-even scalar sector features significant changes due to the presence of the additional particle state, leading to a total of three $\mathcal{CP}$-even Higgs bosons that in general will be mixed states composed out of the real components ρ_1, ρ_2 and ρ_S. The rotation from the interaction basis to the physical mass basis can be written as

$$\begin{pmatrix} h_1 \\ h_2 \\ h_3 \end{pmatrix} = R \begin{pmatrix} \rho_1 \\ \rho_2 \\ \rho_S \end{pmatrix} , \tag{7.8}$$

where R is an orthogonal three-dimensional rotation matrix, and we use the convention $m_{h_1} < m_{h_2} < m_{h_3}$. In principle, each of the three mass eigenstates h_i can be identified with the SM-like Higgs boson at 125 GeV. The rotation matrix can be expressed in terms of the three mixing angles $\alpha_{1,2,3}$ as

$$R = \begin{pmatrix} c_{\alpha_1} c_{\alpha_2} & s_{\alpha_1} c_{\alpha_2} & s_{\alpha_2} \\ -(c_{\alpha_1} s_{\alpha_2} s_{\alpha_3} + s_{\alpha_1} c_{\alpha_3}) & c_{\alpha_1} c_{\alpha_3} - s_{\alpha_1} s_{\alpha_2} s_{\alpha_3} & c_{\alpha_2} s_{\alpha_3} \\ -c_{\alpha_1} s_{\alpha_2} c_{\alpha_3} + s_{\alpha_1} s_{\alpha_3} & -(c_{\alpha_1} s_{\alpha_3} + s_{\alpha_1} s_{\alpha_2} c_{\alpha_3}) & c_{\alpha_2} c_{\alpha_3} \end{pmatrix} , \tag{7.9}$$

where we used the short-hand notation $s_x = \sin x$, $c_x = \cos x$. The mixing angles can by definition take values in the range

$$-\frac{\pi}{2} \leq \alpha_i \leq \frac{\pi}{2} \, . \tag{7.10}$$

An important quantity is the singlet admixture of each mass eigenstate h_i that can be computed by

$$\Sigma_{h_i} = |R_{i3}|^2 \, . \tag{7.11}$$

The larger the singlet admixture of the Higgs boson, the smaller are its couplings to SM fermions and vector bosons.

The scalar potential given in Eq. (7.2) contains 12 independent parameters;

$$m_{11}^2\,, \quad m_{22}^2\,, \quad m_{12}^2\,, \quad m_S^2\,, \quad \lambda_{i=1,8}\,. \tag{7.12}$$

The scalar potential of the N2HDM can be renormalized in an OS scheme. Therefore, it is convenient to trade as much parameters of the Lagrangian as possible for physical quantities, i.e., parameters that are directly related to physical observables. The quartic couplings λ_i can be replaced by the physical scalar masses and mixing angles, via [24]

$$\lambda_1 = \frac{1}{v^2 c_\beta^2}\left(-\tilde{\mu}^2 s_\beta^2 + \sum_{i=1}^{3} m_{h_i}^2 R_{i1}^2\right)\,, \tag{7.13}$$

$$\lambda_2 = \frac{1}{v^2 s_\beta^2}\left(-\tilde{\mu}^2 c_\beta^2 + \sum_{i=1}^{3} m_{h_i}^2 R_{i2}^2\right)\,, \tag{7.14}$$

$$\lambda_3 = \frac{1}{v^2}\left(-\tilde{\mu}^2 + \frac{1}{s_\beta c_\beta}\sum_{i=1}^{3} m_{h_i}^2 R_{i1} R_{i2} + 2m_{H^\pm}^2\right)\,, \tag{7.15}$$

$$\lambda_4 = \frac{1}{v^2}\left(\tilde{\mu}^2 + m_A^2 - 2m_{H^\pm}^2\right)\,, \tag{7.16}$$

$$\lambda_5 = \frac{1}{v^2}\left(\tilde{\mu}^2 - m_A^2\right)\,, \tag{7.17}$$

$$\lambda_6 = \frac{1}{v_S^2}\sum_{i=1}^{3} m_{h_i}^2 R_{i3}^2\,, \tag{7.18}$$

$$\lambda_7 = \frac{1}{v v_S c_\beta}\sum_{i=1}^{3} m_{h_i}^2 R_{i1} R_{i3}\,, \tag{7.19}$$

$$\lambda_8 = \frac{1}{v v_S s_\beta}\sum_{i=1}^{3} m_{h_i}^2 R_{i2} R_{i3}\,, \tag{7.20}$$

$$\text{with} \quad \tilde{\mu}^2 = \frac{m_{12}^2}{s_\beta c_\beta}\,. \tag{7.21}$$

m_A and $M_{H^\pm}$ denote the masses of the physical $\mathcal{CP}$-odd and charged Higgs bosons, respectively. Apart from that, one can use the three minimization conditions [24]

$$\frac{v_2}{v_1} m_{12}^2 - m_{11}^2 = \frac{1}{2}(v_1^2\lambda_1 + v_2^2\,(\lambda_3 + \lambda_4 + \lambda_5) + v_S^2\lambda_7) \tag{7.22}$$

$$\frac{v_1}{v_2} m_{12}^2 - m_{22}^2 = \frac{1}{2}(v_1^2\,(\lambda_3 + \lambda_4 + \lambda_5) + v_2^2\lambda_2 + v_S^2\lambda_8) \tag{7.23}$$

$$-m_S^2 = \frac{1}{2}(v_1^2\lambda_7 + v_2^2\lambda_8 + v_S^2\lambda_6)\,, \tag{7.24}$$

to substitute the bilinears m_{11}^2, m_{22}^2 and m_S^2 for the SM vev

$$v = \sqrt{v_1^2 + v_2^2}\,, \tag{7.25}$$

$\tan\beta$ and the singlet vev v_S [24]. This leads to the physical parameter set

$$\alpha_{1,2,3}\,, \quad \tan\beta\,, \quad v\,, \quad v_S\,, \quad m_{h_{1,2,3}}\,, \quad m_A\,, \quad M_{H^\pm}\,, \quad m_{12}^2\,. \tag{7.26}$$

	u-type	d-type	leptons
type I	Φ_2	Φ_2	Φ_2
type II	Φ_2	Φ_1	Φ_1
type III (lepton-specific)	Φ_2	Φ_2	Φ_1
type IV (flipped)	Φ_2	Φ_1	Φ_2

Table 7.1: Allowed fermion couplings in the four types of N2HDM.

7.2 Yukawa structures

The doublet fields Φ_1 and Φ_2 carry charges appropriate to write gauge-invariant Yukawa couplings for the SM fermions. They are equal to the Yukawa terms of the 2HDM and read

$$-\mathcal{L}_{\text{Yuk}} = \sum_{i=1}^{2} \left[Y_i^u \overline{Q}_L \widetilde{\Phi}_i u_R + Y_i^d \overline{Q}_L \Phi_i d_R + Y_i^e \overline{L}_L \Phi_i e_R + \text{h.c.} \right] , \tag{7.27}$$

where $\widetilde{\Phi}_i = \mathrm{i}\sigma_2 \Phi_i$ and Y^f are the 3×3 Yukawa matrices in flavor space for each fermion type $f = u, d, e$ and Higgs doublet Φ_i. The Yukawa matrices Y_i can only be non-zero for one Higgs field per fermion type due to the Z_2 symmetry under which Φ_1 and Φ_2 carry opposite charge. Hence, only one of them can couple to each type of fermions, i.e, up-type quarks, down-type qaurks and leptons. Depending on the charge assignment of the Z_2 symmetry to the SM fermions, there are four different variants of the N2HDM, each of them different in the way which of the doublet field couples to which fermion type. In Tab. 7.1 we show the resulting four types of the N2HDM.

The type II N2HDM resembles the familiar Yukawa pattern of SUSY models. One field couples to up-type quarks, and the other one to down-type quarks and charged leptons. The type IV is referred to as the flipped scenario, because the leptons are coupled to the same field as the up-type quarks instead of the down-type quarks. Type I and type III are distinct, because only one scalar field is coupled to quarks. In the type I N2HDM the second scalar field has no coupling to the fermions at all, while in the lepton-specific it is at least allowed to couple to the leptons.

In principle, the different types of coupling patterns in the N2HDM are totally analogues to the types of the 2HDM. However, in the N2HDM the Higgs-boson couplings are further modified w.r.t. the SM predictions due to the more complex mixing in the Higgs sector. It is convenient to express the couplings of the scalar mass eigenstates h_i normalized to the corresponding SM couplings, given by the coupling coefficients $c_{h_i f\bar{f}}$. After rotating the terms in Eq. (7.27) to the mass eigenstate basis of the fermions and the Higgs bosons, one can express the Yukawa Lagrangian as

$$-\mathcal{L}_{\text{Yuk}} = \sum_{i=1}^{2} \frac{\sqrt{2} m_f}{v} c_{h_i f\bar{f}} \overline{\Psi}_f \Psi_f h_i , \tag{7.28}$$

with m_f being the fermion mass, and Ψ_f the four-component Dirac spinor of each fermion. Then, the couplings of the Higgs bosons to the SM fermions are given by

$$g_{h_i f\bar{f}} = \frac{\sqrt{2} m_f}{v} \left(c_{h_i f\bar{f}} \right) , \tag{7.29}$$

Similarly, we can express the couplings of the Higgs bosons to massive vector bosons in terms of the coupling coefficient $c_{h_i VV}$, such that

$$\left(g_{h_i WW}\right)_{\mu\nu} = \mathrm{i} g_{\mu\nu} \left(c_{h_i VV}\right) g M_W \quad \text{and} \quad \left(g_{h_i ZZ}\right)_{\mu\nu} = \mathrm{i} g_{\mu\nu} \left(c_{h_i VV}\right) \frac{g M_Z}{c_{\text{w}}} . \tag{7.30}$$

	u-type ($c_{h_i t\bar{t}}$)	d-type ($c_{h_i b\bar{b}}$)	leptons ($c_{h_i \tau\bar{\tau}}$)
type I	R_{i2}/s_β	R_{i2}/s_β	R_{i2}/s_β
type II	R_{i2}/s_β	R_{i1}/c_β	R_{i1}/c_β
type III (lepton-specific)	R_{i2}/s_β	R_{i2}/s_β	R_{i1}/c_β
type IV (flipped)	R_{i2}/s_β	R_{i1}/c_β	R_{i2}/s_β

Table 7.2: Coupling factors of the Yukawa couplings of the N2HDM Higgs bosons h_i w.r.t. their SM values.

They are the same in all four types of N2HDM. In Tab. 7.2 we list the coupling coefficients for the coupling of each $\mathcal{CP}$-even Higgs boson to fermions. The same for the couplings to the gauge bosons is shown in Tab. 7.3.

From the form of the mixing matrix R in Eq. (7.9) it becomes apparent that in the limit

$$\alpha_2 \to 0 \quad \text{and} \quad \alpha_3 \to 0\,, \tag{7.31}$$

the singlet state decouples from the other two states. This limit corresponds to the 2HDM with the mass eigenstates h and H and the decoupled singlet not interacting whatsoever with the SM particles. Matching the the N2HDM and the 2HDM with mixing angle α requires the shift

$$\alpha_1 \to \alpha + \frac{\pi}{2}\,, \tag{7.32}$$

because of different conventions for the mixing angels.

Besides the interactions of each Higgs boson with SM particles, there are also vertices with more than one Higgs boson present in the N2HDM. The expressions can be quite lengthy due to the mixing of the scalar fields, and our numerical analysis aimed to accommodate specific experimental anomalies primarily depends on the couplings to the SM particles. We therefore do not list the expressions for the couplings involving multiple scalars here, and instead refer to Ref. [24]. There, besides the trilinear self-couplings, also the expressions for the couplings of the h_i to the pseudoscalar A and a Z boson and to the charged Higgs bosons $H^\pm$ and the W bosons are given.

Since the $\mathcal{CP}$-odd and the charged scalar sector are unchanged compared to the 2HDM, the couplings of A and $H^\pm$ to the SM particles are identical to the ones in the 2HDM. They can be found in the literature as well [25, 26]. The complete Lagrangian of the 2HDM and the Feynman rules incorporating the interactions of A and $H^\pm$ can be found in Ref. [2].

7.3 Phenomenological aspects

In this section we present a few general phenomenological aspects that are valid for all four types of the N2HDM.

One of the most important consequences of models containing more than one Higgs doublet is that they necessarily predict a physical charged Higgs boson. The behavior of the charged Higgs boson in the N2HDM is very similar to the one of the 2HDM, except when couplings to the $\mathcal{CP}$-even scalar sector are involved. There are two possibilities in which the presence of the charged Higgs boson can be made manifest. Firstly, it can be produced at colliders and searched for in various final states. Secondly, indirect effects via quantum corrections to electroweak precision observables or flavor physics observables can be sizable. A recent review on the status of the charged Higgs boson confronted with collider constraints and flavor physics observables can be found in Ref. [26]. The charged

	$c_{h_iVV} = c_\beta R_{i1} + s_\beta R_{i2}$
h_1	$c_{\alpha_2} c_{\beta-\alpha_1}$
h_2	$-c_{\beta-\alpha_1} s_{\alpha_2} s_{\alpha_3} + c_{\alpha_3} s_{\beta-\alpha_1}$
h_3	$-c_{\alpha_3} c_{\beta-\alpha_1} s_{\alpha_2} - s_{\alpha_3} s_{\beta-\alpha_1}$

Table 7.3: Coupling factors of the neutral $\mathcal{CP}$-even Higgs bosons h_i to the massive gauge bosons $V = W, Z$ in the N2HDM.

scalar sector can be described at tree level by just two parameters, namely the charged Higgs-boson mass $M_{H^\pm}$ and $\tan\beta$.

Regarding collider searches, the charged Higgs boson can be produced at the LHC via several different processes. If it is heavier than the top quark, the most important production mode is usually

$$pp \to H^\pm tb \,, \tag{7.33}$$

with subsequent decay modes [27–32]

$$H^\pm \to tb \quad \text{and} \quad H^\pm \to \tau\nu \,. \tag{7.34}$$

The hadronic decay is important for low values of $\tan\beta$, while the leptonic decay is enhanced when $\tan\beta$ is large. For $M_{H^\pm} \gtrsim 200$ GeV the production in the vector-boson fusion mode with subsequent decay

$$H^\pm \to W^\pm Z \,, \tag{7.35}$$

can become relevant [33, 34]. For very light charged Higgs bosons, exclusion limits from LEP are important. At e^+e^- colliders the charged Higgs can be produced pairwise,

$$e^+e^- \to Z/\gamma \to H^+H^- \,. \tag{7.36}$$

This process does not depend on the value of $\tan\beta$, so that a lower limit of $M_{H^\pm} \gtrsim 70$ GeV could be obtained [35–41]. For type II and type IV, however, the reach of LEP is ruled out anyway by constraints from flavor physics (see below).

Through loop effects the charged Higgs boson also has a crucial effect on electroweak precision observables (EWPO). Constraints from EWPO can in a simple approximation be expressed in terms of the oblique parameters S, T and U [42, 43]. Deviations to these parameters are significant if new physics beyond the SM enters mainly through gauge boson self-energies, as it is the case for the N2HDM. The corrections to the oblique parameters are very sensitive to the relative mass squared differences of the scalars. They become small when either the non SM-like doublet Higgs boson or the pseudoscalar A has a mass close to the mass of the charged Higgs boson [44, 45].

Regarding flavor physics observables, the charged Higgs boson can induce sizable deviations from the SM prediction, in some cases even at tree level. Constraints from flavor physics observables can provide exclusion limits beyond the reach of colliders, but they can also be compatible or even stronger for relatively low charged Higgs-boson masses. Most of the observables, like rare B-meson decays, Z partial decay widths and ΔM_{B_s} from neutral B-meson mixing, only have a subleading dependence on the neutral scalar sector. Thus, corresponding experimental bounds in the $\tan\beta$-$M_{H^\pm}$ plane [26] can be taken over directly from the 2HDM to a very good approximation. Since in the type I and type III scenario only one Higgs doublet couples to quarks, while in the type II and type IV scenario each doublet field couples to either up- or down-type quarks, constraints

from flavor physics are conceptually different in both cases. In type II and type IV a lower limit of

$$M_{H^\pm} \gtrsim 600 \text{ GeV} \tag{7.37}$$

could be obtained from experimental limits on $\text{BR}(B \to X_s\gamma)$ [26]. For type I and type III no such $\tan\beta$-independent limit exists. For $\tan\beta \lesssim 1$ also bounds from the measurement of $\text{BR}(B_s \to \mu^+\mu^-)$ become important [26]. Unlike the above mentioned observables, $\text{BR}(B_s \to \mu^+\mu^-)$ can get contributions from the neutral scalar sector of the model as well [46, 47]. Thus, in principle the value of $\text{BR}(B_s \to \mu^+\mu^-)$ in the N2HDM may differ from that of the 2HDM. However, genuine contributions from the N2HDM are expected to be small, since the additional scalar field is a gauge singlet. Furthermore, as mentioned before, the constraints from direct LHC searches for $H^\pm$ already provide fairly strong exclusion limits. Also the constraint from ΔM_{B_s} covers the region of very small $\tan\beta$ and in the 2HDM is always stronger than the bound from $\text{BR}(B_s \to \mu^+\mu^-)$. Keeping the above facts in mind, we assume that the bounds from $\text{BR}(B \to X_s\gamma)$ and ΔM_{B_s} as obtained in Ref. [26] still remain to be the dominant constraints in the N2HDM.

Finally, we shortly discuss the phenomenological impact of the additional neutral Higgs bosons. Direct searches for additional neutral Higgs bosons can exclude parameter points, mainly when the second Higgs doublet-like $\mathcal{CP}$-even Higgs boson H or the $\mathcal{CP}$-odd Higgs boson A are rather light. Depending on the type and the value of $\tan\beta$, the resonant decay of extra scalars or the pseudoscalar to a pair of quarks [48–50, 50–52] or leptons [53–61] can be searched for. Searches for diphoton resonances, the golden channel proving the existence of the SM-like Higgs boson [62, 63], are used to constrain the $\mathcal{CP}$-even Higgs-boson sector [64–68]. For small values of $\tan\beta$ also searches for additional Higgs bosons decaying into a pair of massive gauge bosons which then decay either hadronically or leptonically, are relevant [69–77]. Very interesting experimental signatures result from the decay of Higgs bosons into each other, even more so in the N2HDM, where these kind of signals might help to distinguish the N2HDM from the 2HDM. For instance, a heavy scalar was searched for via the decay into different pairings of a gauge-boson and a SM-like Higgs boson [78–80], and additional Higgs bosons can contribute to the pair production of the SM-like Higgs boson [81–87]. Heavy pseudoscalars can decay into a gauge boson and a scalar, where the latter can be the SM-like Higgs boson [88–90] or not [91]. Very light Higgs bosons might be detectable in exotic decays of the SM-like Higgs boson [92–95].

7.4 Aim of this work

Our numerical analysis was aimed to accommodate two experimental excesses which hint to the existence of a second Higgs boson lighter than the SM-like Higgs boson. In the following chapter we give details about these two excesses, and explain the general properties a Higgs boson possibly causing them should have. Subsequently, we give example benchmark scenarios within the context of the $\mu\nu$SSM with one or three families of right-handed neutrinos, that contain such a scalar particle, accommodating the excesses at the 1σ level. Finally we show with the help of an extensive parameter scan that in the N2HDM in which the scalar potential does not have to obey Susy relations a light singlet-like Higgs boson can further improve the explication of both excesses, being in perfect agreement with the experimental data. All the relevant details of the scans, i.e., the parameter ranges, the theoretical and experimental constraints, and the results are depicted in Sect. 8.2. The numerical analysis is focused on the type II and type IV sce-

narios in which both excesses could actually be explained simultaneously. We also give experimental prospects on how our explanation of the excesses can (and will) be probed by the LHC and future colliders.

Bibliography

[1] C. D. Froggatt, I. G. Knowles, and R. G. Moorhouse, "Third generation masses from a two Higgs model fixed point", *Phys. Lett.* **B249** (1990) 273–280.

[2] C. D. Froggatt, R. G. Moorhouse, and I. G. Knowles, "Two scalar doublet models with softly broken symmetries", *Nucl. Phys.* **B386** (1992) 63–114.

[3] R. D. Peccei and H. R. Quinn, "Constraints Imposed by CP Conservation in the Presence of Instantons", *Phys. Rev.* **D16** (1977) 1791–1797.

[4] S. Weinberg, "A New Light Boson?", *Phys. Rev. Lett.* **40** (1978) 223–226.

[5] F. Wilczek, "Problem of Strong P and T Invariance in the Presence of Instantons", *Phys. Rev. Lett.* **40** (1978) 279–282.

[6] J. E. Kim, "Weak Interaction Singlet and Strong CP Invariance", *Phys. Rev. Lett.* **43** (1979) 103.

[7] A. D. Sakharov, "Violation of CP Invariance, C asymmetry, and baryon asymmetry of the universe", *Pisma Zh. Eksp. Teor. Fiz.* **5** (1967) 32–35, [Usp. Fiz. Nauk161,no.5,61(1991)].

[8] P. Huet and E. Sather, "Electroweak baryogenesis and standard model CP violation", *Phys. Rev.* **D51** (1995) 379–394, arXiv:hep-ph/9404302.

[9] M. B. Gavela, M. Lozano, J. Orloff, and O. Pene, "Standard model CP violation and baryon asymmetry. Part 1: Zero temperature", *Nucl. Phys.* **B430** (1994) 345–381, arXiv:hep-ph/9406288.

[10] M. B. Gavela, P. Hernandez, J. Orloff, O. Pene, and C. Quimbay, "Standard model CP violation and baryon asymmetry. Part 2: Finite temperature", *Nucl. Phys.* **B430** (1994) 382–426, arXiv:hep-ph/9406289.

[11] M. Sher, "Electroweak Higgs Potentials and Vacuum Stability", *Phys. Rept.* **179** (1989) 273–418.

[12] **Particle Data Group** Collaboration, M. Tanabashi *et al.*, "Review of Particle Physics", *Phys. Rev.* **D98** (2018), no. 3, 030001.

[13] C.-Y. Chen, M. Freid, and M. Sher, "Next-to-minimal two Higgs doublet model", *Phys. Rev.* **D89** (2014), no. 7, 075009, arXiv:1312.3949.

[14] N. G. Deshpande and E. Ma, "Pattern of Symmetry Breaking with Two Higgs Doublets", *Phys. Rev.* **D18** (1978) 2574.

[15] **GAMBIT** Collaboration, P. Athron *et al.*, "Status of the scalar singlet dark matter model", *Eur. Phys. J.* **C77** (2017), no. 8, 568, arXiv:1705.07931.

[16] E. Ma, "Verifiable radiative seesaw mechanism of neutrino mass and dark matter", *Phys. Rev.* **D73** (2006) 077301, arXiv:hep-ph/0601225.

[17] L. Lopez Honorez, E. Nezri, J. F. Oliver, and M. H. G. Tytgat, "The Inert Doublet Model: An Archetype for Dark Matter", *JCAP* **0702** (2007) 028, arXiv:hep-ph/0612275.

[18] A. Belyaev, G. Cacciapaglia, I. P. Ivanov, F. Rojas-Abatte, and M. Thomas, "Anatomy of the Inert Two Higgs Doublet Model in the light of the LHC and non-LHC Dark Matter Searches", *Phys. Rev.* **D97** (2018), no. 3, 035011, arXiv:1612.00511.

[19] A. Ilnicka, M. Krawczyk, and T. Robens, "Inert Doublet Model in light of LHC Run I and astrophysical data", *Phys. Rev.* **D93** (2016), no. 5, 055026, arXiv:1508.01671.

[20] J. Kalinowski, W. Kotlarski, T. Robens, D. Sokolowska, and A. F. Zarnecki, "The Inert Doublet Model at current and future colliders", in "6th Symposium on Prospects in the Physics of Discrete Symmetries (DISCRETE 2018) Vienna, Austria, November 26-30, 2018". 2019. arXiv:1903.04456.

[21] I. Engeln, "Phenomenological Comparison of the Dark Phases of the Next-to-Two-Higgs-Doublet Model", Master's thesis, KIT, Karlsruhe, 2018-03-07.

[22] I. Engeln, M. Mühlleitner, and J. Wittbrodt, "N2HDECAY: Higgs Boson Decays in the Different Phases of the N2HDM", *Comput. Phys. Commun.* **234** (2019) 256–262, arXiv:1805.00966.

[23] T. Biekötter, M. Chakraborti, and S. Heinemeyer, "A 96 GeV Higgs Boson in the N2HDM", *submitted to Eur. Phys. J.* **C**, 2019 arXiv:1903.11661.

[24] M. Muhlleitner, M. O. P. Sampaio, R. Santos, and J. Wittbrodt, "The N2HDM under Theoretical and Experimental Scrutiny", *JHEP* **03** (2017) 094, arXiv:1612.01309.

[25] V. D. Barger, J. L. Hewett, and R. J. N. Phillips, "New Constraints on the Charged Higgs Sector in Two Higgs Doublet Models", *Phys. Rev.* **D41** (1990) 3421–3441.

[26] A. Arbey, F. Mahmoudi, O. Stål, and T. Stefaniak, "Status of the Charged Higgs Boson in Two Higgs Doublet Models", *Eur. Phys. J.* **C78** (2018), no. 3, 182, arXiv:1706.07414.

[27] **ATLAS** Collaboration, G. Aad *et al.*, "Search for charged Higgs bosons in the $H^{\pm} \to tb$ decay channel in pp collisions at $\sqrt{s} = 8$ TeV using the ATLAS detector", *JHEP* **03** (2016) 127, arXiv:1512.03704.

[28] **ATLAS** Collaboration, M. Aaboud *et al.*, "Search for charged Higgs bosons produced in association with a top quark and decaying via $H^{\pm} \to \tau\nu$ using pp collision data recorded at $\sqrt{s} = 13$ TeV by the ATLAS detector", *Phys. Lett.* **B759** (2016) 555–574, arXiv:1603.09203.

[29] **ATLAS** Collaboration, M. Aaboud *et al.*, "Search for charged Higgs bosons decaying into top and bottom quarks at $\sqrt{s} = 13$ TeV with the ATLAS detector", *JHEP* **11** (2018) 085, arXiv:1808.03599.

[30] **ATLAS** Collaboration, M. Aaboud *et al.*, "Search for charged Higgs bosons decaying via $H^{\pm} \to \tau^{\pm}\nu_{\tau}$ in the τ+jets and τ+lepton final states with 36 fb^{-1} of pp collision data recorded at $\sqrt{s} = 13$ TeV with the ATLAS experiment", *JHEP* **09** (2018) 139, arXiv:1807.07915.

[31] **CMS** Collaboration, "Search for a charged Higgs boson decaying into top and bottom quarks in proton-proton collisions at 13TeV in events with electrons or muons", CMS-PAS-HIG-18-004, 2019

[32] **CMS** Collaboration, A. M. Sirunyan *et al.*, "Search for charged Higgs bosons in the H$^{\pm} \to \tau^{\pm}\nu_{\tau}$ decay channel in proton-proton collisions at $\sqrt{s} = 13$ TeV", arXiv:1903.04560.

[33] **ATLAS** Collaboration, G. Aad *et al.*, "Search for a Charged Higgs Boson Produced in the Vector-Boson Fusion Mode with Decay $H^{\pm} \to W^{\pm}Z$ using pp Collisions at $\sqrt{s} = 8$ TeV with the ATLAS Experiment", *Phys. Rev. Lett.* **114** (2015), no. 23, 231801, arXiv:1503.04233.

[34] **CMS** Collaboration, A. M. Sirunyan *et al.*, "Search for Charged Higgs Bosons Produced via Vector Boson Fusion and Decaying into a Pair of W and Z Bosons Using pp Collisions at $\sqrt{s} = 13$ TeV", *Phys. Rev. Lett.* **119** (2017), no. 14, 141802, arXiv:1705.02942.

[35] **ALEPH, DELPHI, L3, OPAL, LEP** Collaboration, G. Abbiendi *et al.*, "Search for Charged Higgs bosons: Combined Results Using LEP Data", *Eur. Phys. J.* **C73** (2013) 2463, arXiv:1301.6065.

[36] **DELPHI** Collaboration, J. Abdallah *et al.*, "Search for charged Higgs bosons at LEP in general two Higgs doublet models", *Eur. Phys. J.* **C34** (2004) 399–418, arXiv:hep-ex/0404012.

[37] **DELPHI** Collaboration, P. Abreu *et al.*, "Search for charged Higgs bosons at LEP-2", *Phys. Lett.* **B460** (1999) 484–497.

[38] **L3** Collaboration, P. Achard *et al.*, "Search for charged Higgs bosons at LEP", *Phys. Lett.* **B575** (2003) 208–220, arXiv:hep-ex/0309056.

[39] **OPAL** Collaboration, G. Abbiendi *et al.*, "Search for Charged Higgs Bosons in e^+e^- Collisions at $\sqrt{s} = 189 - 209$ GeV", *Eur. Phys. J.* **C72** (2012) 2076, arXiv:0812.0267.

[40] **OPAL** Collaboration, G. Abbiendi *et al.*, "Search for Higgs bosons in e^+e^- collisions at 183-GeV", *Eur. Phys. J.* **C7** (1999) 407–435, arXiv:hep-ex/9811025.

[41] **OPAL** Collaboration, G. Alexander *et al.*, "Search for charged Higgs bosons using the OPAL detector at LEP", *Phys. Lett.* **B370** (1996) 174–184.

[42] M. E. Peskin and T. Takeuchi, "A New constraint on a strongly interacting Higgs sector", *Phys. Rev. Lett.* **65** (1990) 964–967.

[43] M. E. Peskin and T. Takeuchi, "Estimation of oblique electroweak corrections", *Phys. Rev.* **D46** (1992) 381–409.

[44] S. Bertolini, "Quantum Effects in a Two Higgs Doublet Model of the Electroweak Interactions", *Nucl. Phys.* **B272** (1986) 77–98.

[45] W. Hollik, "Nonstandard Higgs Bosons in SU(2) X U(1) Radiative Corrections", *Z. Phys.* **C32** (1986) 291.

[46] X.-Q. Li, J. Lu, and A. Pich, "$B^0_{s,d} \to \ell^+\ell^-$ Decays in the Aligned Two-Higgs-Doublet Model", *JHEP* **06** (2014) 022, arXiv:1404.5865.

[47] X.-D. Cheng, Y.-D. Yang, and X.-B. Yuan, "Revisiting $B_s \to \mu^+\mu^-$ in the two-Higgs doublet models with Z_2 symmetry", *Eur. Phys. J.* **C76** (2016), no. 3, 151, arXiv:1511.01829.

[48] **CMS** Collaboration, V. Khachatryan *et al.*, "Search for neutral MSSM Higgs bosons decaying into a pair of bottom quarks", *JHEP* **11** (2015) 071, arXiv:1506.08329.

[49] **CMS** Collaboration, "Search for a narrow heavy resonance decaying to bottom quark pairs in the 13 TeV data sample", CMS-PAS-HIG-16-025, 2016

[50] **ATLAS** Collaboration, M. Aaboud *et al.*, "Search for Heavy Higgs Bosons A/H Decaying to a Top Quark Pair in pp Collisions at $\sqrt{s} = 8$ TeV with the ATLAS Detector", *Phys. Rev. Lett.* **119** (2017), no. 19, 191803, arXiv:1707.06025.

[51] **CMS** Collaboration, A. M. Sirunyan *et al.*, "Search for a light pseudoscalar Higgs boson produced in association with bottom quarks in pp collisions at $\sqrt{s} = 8$ TeV", *JHEP* **11** (2017) 010, arXiv:1707.07283.

[52] **CMS** Collaboration, A. M. Sirunyan *et al.*, "Search for beyond the standard model Higgs bosons decaying into a $\mathrm{b\bar{b}}$ pair in pp collisions at $\sqrt{s} = 13$ TeV", *JHEP* **08** (2018) 113, arXiv:1805.12191.

[53] **CMS** Collaboration, A. M. Sirunyan *et al.*, "Search for additional neutral MSSM Higgs bosons in the $\tau\tau$ final state in proton-proton collisions at $\sqrt{s} = 13$ TeV", *JHEP* **09** (2018) 007, arXiv:1803.06553.

[54] **CMS** Collaboration, G. Masetti, "Searches for BSM Higgs bosons in fermion decay channels with CMS", in "5th Large Hadron Collider Physics Conference (LHCP 2017) Shanghai, China, May 15-20, 2017". 2017. arXiv:1708.09651.

[55] **ATLAS** Collaboration, "Search for Higgs bosons decaying into di-muon in pp collisions at $\sqrt{s} = 13$ TeV with the ATLAS detector", ATLAS-CONF-2016-041, 2016

[56] **ATLAS** Collaboration, M. Aaboud *et al.*, "Search for scalar resonances decaying into $\mu^+\mu^-$ in events with and without b-tagged jets produced in proton-proton collisions at $\sqrt{s} = 13$ TeV with the ATLAS detector", *Submitted to: JHEP*, 2019 arXiv:1901.08144.

[57] **ATLAS** Collaboration, M. Aaboud *et al.*, "Search for additional heavy neutral Higgs and gauge bosons in the ditau final state produced in 36 fb^{-1} of pp collisions at $\sqrt{s} = 13$ TeV with the ATLAS detector", *JHEP* **01** (2018) 055, arXiv:1709.07242.

[58] **ATLAS** Collaboration, M. Aaboud *et al.*, "Search for Minimal Supersymmetric Standard Model Higgs bosons H/A and for a Z' boson in the $\tau\tau$ final state produced in pp collisions at $\sqrt{s} = 13$ TeV with the ATLAS Detector", *Eur. Phys. J.* **C76** (2016), no. 11, 585, arXiv:1608.00890.

[59] **CMS** Collaboration, "Search for a low-mass $\tau^+\tau^-$ resonance in association with a bottom quark in proton-proton collisions at $\sqrt{s} = 13$ TeV", arXiv:1903.10228.

[60] **CMS** Collaboration, A. M. Sirunyan *et al.*, "A search for pair production of new light bosons decaying into muons in proton-proton collisions at 13 TeV", *Submitted to: Phys. Lett.*, 2018 arXiv:1812.00380.

[61] **CMS** Collaboration, A. M. Sirunyan *et al.*, "Search for resonances in the mass spectrum of muon pairs produced in association with b quark jets in proton-proton collisions at $\sqrt{s} = 8$ and 13 TeV", *JHEP* **11** (2018) 161, arXiv:1808.01890.

[62] **ATLAS** Collaboration, G. Aad *et al.*, "Observation of a new particle in the search for the Standard Model Higgs boson with the ATLAS detector at the LHC", *Phys. Lett.* **B716** (2012) 1–29, arXiv:1207.7214.

[63] **CMS** Collaboration, S. Chatrchyan *et al.*, "Observation of a new boson at a mass of 125 GeV with the CMS experiment at the LHC", *Phys. Lett.* **B716** (2012) 30–61, arXiv:1207.7235.

[64] **CMS** Collaboration, "Search for new resonances in the diphoton final state in the mass range between 80 and 115 GeV in pp collisions at $\sqrt{s} = 8$ TeV", CMS-PAS-HIG-14-037, 2015

[65] **ATLAS** Collaboration, M. Aaboud *et al.*, "Search for resonances in diphoton events at $\sqrt{s}$=13 TeV with the ATLAS detector", *JHEP* **09** (2016) 001, arXiv:1606.03833.

[66] **ATLAS** Collaboration, M. Aaboud *et al.*, "Search for new phenomena in high-mass diphoton final states using 37 fb^{-1} of proton–proton collisions collected at $\sqrt{s} = 13$ TeV with the ATLAS detector", *Phys. Lett.* **B775** (2017) 105–125, arXiv:1707.04147.

[67] **CMS** Collaboration, A. M. Sirunyan *et al.*, "Search for a standard model-like Higgs boson in the mass range between 70 and 110 GeV in the diphoton final state in proton-proton collisions at $\sqrt{s} = 8$ and 13 TeV", *Phys. Lett.* **B793** (2019) 320–347, arXiv:1811.08459.

[68] **ATLAS** Collaboration, "Search for resonances in the 65 to 110 GeV diphoton invariant mass range using 80 fb^{-1} of pp collisions collected at $\sqrt{s} = 13$ TeV with the ATLAS detector", ATLAS-CONF-2018-025, 2018

[69] **ATLAS** Collaboration, M. Aaboud *et al.*, "Searches for heavy diboson resonances in pp collisions at $\sqrt{s} = 13$ TeV with the ATLAS detector", *JHEP* **09** (2016) 173, arXiv:1606.04833.

[70] **ATLAS** Collaboration, M. Aaboud *et al.*, "Search for resonant WZ production in the fully leptonic final state in proton-proton collisions at $\sqrt{s} = 13$ TeV with the ATLAS detector", *Phys. Lett.* **B787** (2018) 68–88, arXiv:1806.01532.

[71] **ATLAS** Collaboration, M. Aaboud *et al.*, "Search for heavy ZZ resonances in the $\ell^+\ell^-\ell^+\ell^-$ and $\ell^+\ell^-\nu\bar{\nu}$ final states using proton–proton collisions at $\sqrt{s} = 13$ TeV with the ATLAS detector", *Eur. Phys. J.* **C78** (2018), no. 4, 293, arXiv:1712.06386.

[72] **ATLAS** Collaboration, M. Aaboud *et al.*, "Search for heavy resonances decaying into WW in the $e\nu\mu\nu$ final state in pp collisions at $\sqrt{s} = 13$ TeV with the ATLAS detector", *Eur. Phys. J.* **C78** (2018), no. 1, 24, arXiv:1710.01123.

[73] **ATLAS** Collaboration, M. Aaboud *et al.*, "Searches for heavy ZZ and ZW resonances in the $\ell\ell qq$ and $\nu\nu qq$ final states in pp collisions at $\sqrt{s} = 13$ TeV with the ATLAS detector", *JHEP* **03** (2018) 009, arXiv:1708.09638.

[74] **ATLAS** Collaboration, G. Aad *et al.*, "Search for a high-mass Higgs boson decaying to a W boson pair in pp collisions at $\sqrt{s} = 8$ TeV with the ATLAS detector", *JHEP* **01** (2016) 032, arXiv:1509.00389.

[75] **ATLAS** Collaboration, G. Aad *et al.*, "Search for an additional, heavy Higgs boson in the $H \to ZZ$ decay channel at $\sqrt{s} = 8$ TeV in pp collision data with the ATLAS detector", *Eur. Phys. J.* **C76** (2016), no. 1, 45, arXiv:1507.05930.

[76] **CMS** Collaboration, A. M. Sirunyan *et al.*, "Search for a new scalar resonance decaying to a pair of Z bosons in proton-proton collisions at $\sqrt{s} = 13$ TeV", *JHEP* **06** (2018) 127, arXiv:1804.01939, [Erratum: JHEP03,128(2019)].

[77] **CMS** Collaboration, A. M. Sirunyan *et al.*, "Search for a heavy resonance decaying into a Z boson and a Z or W boson in 2l2q final states at $\sqrt{s} = 13$ TeV", *JHEP* **09** (2018) 101, arXiv:1803.10093.

[78] **CMS** Collaboration, "Search for H/A decaying into Z+A/H, with Z to ll and A/H to fermion pair", CMS-PAS-HIG-15-001, 2015

[79] **ATLAS** Collaboration, M. Aaboud *et al.*, "Combination of searches for heavy resonances decaying into bosonic and leptonic final states using 36 fb^{-1} of proton-proton collision data at $\sqrt{s} = 13$ TeV with the ATLAS detector", *Phys. Rev.* **D98** (2018), no. 5, 052008, arXiv:1808.02380.

[80] **CMS** Collaboration, A. M. Sirunyan *et al.*, "Search for heavy resonances decaying into a vector boson and a Higgs boson in final states with charged leptons, neutrinos and b quarks at $\sqrt{s} = 13$ TeV", *JHEP* **11** (2018) 172, arXiv:1807.02826.

[81] **ATLAS** Collaboration, M. Aaboud *et al.*, "Search for Higgs boson pair production in the $b\bar{b}WW^*$ decay mode at $\sqrt{s} = 13$ TeV with the ATLAS detector", *JHEP* **04** (2019) 092, arXiv:1811.04671.

[82] **ATLAS** Collaboration, M. Aaboud *et al.*, "Search for resonant and non-resonant Higgs boson pair production in the $b\bar{b}\tau^+\tau^-$ decay channel in pp collisions at $\sqrt{s} = 13$ TeV with the ATLAS detector", *Phys. Rev. Lett.* **121** (2018), no. 19, 191801, arXiv:1808.00336, [Erratum: Phys. Rev. Lett.122,no.8,089901(2019)].

[83] **ATLAS** Collaboration, M. Aaboud *et al.*, "Search for Higgs boson pair production in the $\gamma\gamma b\bar{b}$ final state with 13 TeV pp collision data collected by the ATLAS experiment", *JHEP* **11** (2018) 040, arXiv:1807.04873.

[84] **ATLAS** Collaboration, M. Aaboud *et al.*, "Search for Higgs boson pair production in the $\gamma\gamma WW^*$ channel using pp collision data recorded at $\sqrt{s} = 13$ TeV with the ATLAS detector", *Eur. Phys. J.* **C78** (2018), no. 12, 1007, arXiv:1807.08567.

[85] **CMS** Collaboration, A. M. Sirunyan *et al.*, "Search for resonances decaying to a pair of Higgs bosons in the $b\bar{b}q\bar{q}'\ell\nu$ final state in proton-proton collisions at $\sqrt{s} =$ 13 TeV", *Submitted to: JHEP*, 2019 arXiv:1904.04193.

[86] **CMS** Collaboration, A. M. Sirunyan *et al.*, "Combination of searches for Higgs boson pair production in proton-proton collisions at $\sqrt{s} = 13$ TeV", *Phys. Rev. Lett.* **122** (2019), no. 12, 121803, arXiv:1811.09689.

[87] **CMS** Collaboration, A. M. Sirunyan *et al.*, "Search for resonant pair production of Higgs bosons decaying to bottom quark-antiquark pairs in proton-proton collisions at 13 TeV", *JHEP* **08** (2018) 152, arXiv:1806.03548.

[88] **ATLAS** Collaboration, M. Aaboud *et al.*, "Search for heavy resonances decaying into a W or Z boson and a Higgs boson in final states with leptons and b-jets in 36 fb^{-1} of $\sqrt{s} = 13$ TeV pp collisions with the ATLAS detector", *JHEP* **03** (2018) 174, arXiv:1712.06518, [Erratum: JHEP11,051(2018)].

[89] **ATLAS** Collaboration, G. Aad *et al.*, "Search for a CP-odd Higgs boson decaying to Zh in pp collisions at $\sqrt{s} = 8$ TeV with the ATLAS detector", *Phys. Lett.* **B744** (2015) 163–183, arXiv:1502.04478.

[90] **CMS** Collaboration, A. M. Sirunyan *et al.*, "Search for a heavy pseudoscalar boson decaying to a Z and a Higgs boson at $\sqrt{s} = 13$ TeV", arXiv:1903.00941.

[91] **ATLAS** Collaboration, M. Aaboud *et al.*, "Search for heavy resonances decaying to a photon and a hadronically decaying $Z/W/H$ boson in pp collisions at $\sqrt{s} = 13$ TeV with the ATLAS detector", *Phys. Rev.* **D98** (2018), no. 3, 032015, arXiv:1805.01908.

[92] **ATLAS** Collaboration, M. Aaboud *et al.*, "Search for the Higgs boson produced in association with a vector boson and decaying into two spin-zero particles in the $H \to aa \to 4b$ channel in pp collisions at $\sqrt{s} = 13$ TeV with the ATLAS detector", *JHEP* **10** (2018) 031, arXiv:1806.07355.

[93] **CMS** Collaboration, A. M. Sirunyan *et al.*, "Search for an exotic decay of the Higgs boson to a pair of light pseudoscalars in the final state with two muons and two b quarks in pp collisions at 13 TeV", *Submitted to: Phys. Lett.*, 2018 arXiv:1812.06359.

[94] **CMS** Collaboration, A. M. Sirunyan *et al.*, "Search for an exotic decay of the Higgs boson to a pair of light pseudoscalars in the final state with two b quarks and two τ leptons in proton-proton collisions at $\sqrt{s} = 13$ TeV", *Phys. Lett.* **B785** (2018) 462, arXiv:1805.10191.

[95] **CMS** Collaboration, A. M. Sirunyan *et al.*, "Search for an exotic decay of the Higgs boson to a pair of light pseudoscalars in the final state of two muons and two τ leptons in proton-proton collisions at $\sqrt{s} = 13$ TeV", *JHEP* **11** (2018) 018, arXiv:1805.04865.

Chapter 8

Explanation for the LEP and CMS excesses at ~ 96 GeV

The discovery of the Higgs boson at ~ 125 GeV is in agreement with the SM prediction in which only a single physical Higgs boson is present. As already explained, many well motivated BMS models, such as SUSY models (see Sect. 2.5) or 2HDMs (see the introduction of Ch. 7), predict the existence of additional Higgs bosons. These additional particles might have escaped detection so far by either being too heavy, or by having a reduced coupling to the SM particles compared to the SM-like Higgs boson. The experimental searches for BSM Higgs bosons give crucial information about the allowed parameter space of such BSM models.

Even though there is no conclusive experimental evidence for the presence of an additional Higgs boson, there are two experimental excesses hinting to the existence of a Higgs boson, owing to the fact that they both appear at a similar mass of about 95 to 98 GeV. We will briefly describe the origin of the excesses here, focusing on what they tell us about the properties a Higgs boson with this mass should have to accommodate them simultaneously. For a detailed review about possible interpretations of the excesses in various different BSM models we refer to Refs. [1, 2]. A few of the possibilities considered are type I 2HDMs [3, 4], a radion model [5], a minimal dilaton model [6], a pseudo-Nambu Goldstone boson dark matter model [7], as well as supersymmetric models [8–12]. In the following we present our solutions in the $\mu\nu$SSM in Sect. 8.1 [9, 13] and in the N2HDM in Sect. 8.2 [14, 15].

LEP excess

The Large Electron-Positron (LEP) Collider measured an excess over the background in searches for the SM Higgs boson in the channel

$$e^+e^- \to Z(H \to b\bar{b}) \,, \tag{8.1}$$

i.e., the Higgstrahlung production in association with a decay of the Higgs boson to a pair of bottom quarks [16, 17]. A SM Higgs boson could be excluded up to masses of about ~ 110 GeV by this search. Nevertheless, a 2.3σ local excess was observed at a mass of roughly 98 GeV, where the mass resolution is rather bad due to the mass reconstruction of the b-jets. This corresponds to a signal strength of

$$\mu_{\text{LEP}} = \frac{\sigma\left(e^+e^- \to Z\phi \to Zb\bar{b}\right)}{\sigma^{\text{SM}}\left(e^+e^- \to ZH \to Zb\bar{b}\right)} = 0.117 \pm 0.057 \,, \tag{8.2}$$

where the excess is assumed to be caused by a new scalar particle ϕ, and μ_{LEP} measures the cross section normalized to the SM cross section for a hypothetical Higgs boson H with the same mass as ϕ. The value for μ_{LEP} was extracted in Ref. [8] using methods described in Ref. [18].

Since $\mu_{\text{LEP}} \sim 1/10$, and since no excess showed up at this mass scale in other searches at LEP, a possible candidate ϕ producing the signal necessarily has to have a reduced coupling to vector bosons compared to a SM Higgs boson of the order of

$$c^2_{\phi VV} = \frac{|g^{\text{BSM}}_{\phi VV}|^2}{|g^{\text{SM}}_{HVV}|^2} \sim 10\% - 20\% \,. \tag{8.3}$$

Thus, extensions of the SM incorporating gauge-singlet scalars who are able to acquire such an amount of coupling to the vector bosons via a substantial mixing with the SM-like Higgs boson at ∼ 125 GeV are ideal BSM models to accommodate the LEP excess.

CMS excess

The Compact Muon Solenoid (CMS) experiment at the LHC saw local excess over the SM background in Higgs-boson searches in the diphoton-decay channel in the Run I data with $\sim 2\sigma$ local significance [19] and in the Run II data with $\sim 3\sigma$ local significance [20]. Remarkably, the mass scale of the CMS excesses being at about ∼ 96 GeV are comparable to the mass scale of the LEP excess, taking into account the coarse mass resolution at LEP. Assuming a dominant production of the possibly new particle state via gluon-fusion (ggH), the excess corresponds to a signal strength of

$$\mu_{\text{CMS}} = \frac{\sigma\,(gg \to \phi \to \gamma\gamma)}{\sigma^{\text{SM}}\,(gg \to H \to \gamma\gamma)} = 0.6 \pm 0.2 \,. \tag{8.4}$$

First Atlas results in the Higgs-boson searches below 125 GeV in the diphoton channel were published in Ref. [21]. No excess in the mass range of the LEP and CMS excesses was observed. However, the upper limits on the cross section measured by Atlas is above the upper limits from the CMS measurement, even where CMS sees the excesses. Hence, the Atlas results neither confirm nor exclude the CMS excesses [1].

The CMS analyses was done assuming different production mechanism. The excess clearly appears in the analysis assuming ggH production and production in association with a pair of top quarks (ttH), whereas assuming vector-boson-fusion (VBF) production or the production in association with a vector boson (VH) yields a significantly reduced signal. Therefore, we demand that the new particle state ϕ is produced via ggH. This is contrary to the approach discussed in Refs. [3, 4] in which the second $\mathcal{CP}$-even Higgs boson of the type I 2HDM is used to accommodate the excesses. However, it is unclear if these solutions properly reproduce the peak in the ggF production channel, since they rely either on VBF+VH production [3], or on exotic production mechanisms via the decay of heavier BSM particles [4]. Then it is not obvious to what extend the signal will appear in the CMS analysis assuming ggF+ttH production, and not (as much) in the CMS analysis assuming VBF+VH production. Therefore, the explanation of the CMS excess in the ggH channel while simultaneously accommodating the LEP excess in the N2HDM, by using the additional gauge-singlet Higgs boson, is well motivated.

In contrast to μ_{LEP}, the signal strength corresponding to the CMS excess μ_{CMS} is relatively close to the prediction for a SM Higgs boson at the same mass. If one thinks of the new Higgs boson ϕ as gauge-singlet scalar that mixes with the SM-like Higgs boson,

$v_{iL}/\sqrt{2}$	Y_i^ν	A_i^ν	$\tan\beta$	μ	λ	A^λ	κ	A^κ	M_1
10^{-5}	10^{-7}	-1000	2	$[413; 418]$	0.6	956	0.035	$[-300; -318]$	100

M_2	M_3	$m^2_{\widetilde{Q}_{iL}}$	$m^2_{\widetilde{u}_{iR}}$	$m^2_{\widetilde{d}_{iR}}$	A_i^u	A_i^d	$(m^2_{\widetilde{e}})_{ii}$	A^e_{33}	$A^e_{11,22}$
200	1500	800^2	800^2	800^2	0	0	800^2	0	0

Table 8.1: Low-energy parameters for the scenario accommodating the LEP and CMS excesses in the $\mu\nu$SSM with one right-handed neutrino. Dimensionful parameters are given in GeV.

providing (as we argued before) a good interpretation of the LEP excess, then one faces the quest of reproducing the value $\mu_{\text{CMS}} \sim 0.6$ without finding too large values for μ_{LEP}. The only possibility to do so is to enhance the branching fraction of the decay of ϕ into a pair of photons, because the ggH production is suppressed by a similar amount as the VH production at LEP. In Sect. 8.1 we will see that in the $\mu\nu$SSM this issue cannot be resolved, such that the explication of both excesses can be accurate only up to the 1σ level.[1] In the N2HDM, on the other hand, no SUSY relations have to be obeyed, and a parameter space was found providing perfect agreement with μ_{LEP} and μ_{CMS}, while obeying all relevant theoretical and experimental constraints. The results are portrayed in Sect. 8.2.

8.1 Right-handed sneutrino in the $\mu\nu$SSM

In this section we will investigate if the gauge-singlet scalar fields in the $\mu\nu$SSM, i.e., the $\mathcal{CP}$-even right-handed sneutrinos, can reproduce both excesses simultaneously [9]. We first describe a benchmark point (BP) in the $\mu\nu$SSM with one right-handed neutrino in Sect. 8.1.1. Afterwards, we show a solution in the $\mu\nu$SSM with three right-handed neutrinos in Sect. 8.1.2. In the latter case, we are able to accurately accommodate the neutrino masses and mixings in agreement with experiment (see Sect. 6.3) on top of explaining the LEP and CMS excesses.

8.1.1 One family of right-handed neutrinos

In Tab. 8.1 we list the values of the parameters we used to account for a $\mathcal{CP}$-even right-handed sneutrino $h_1(\widetilde{\nu}_R^{\mathcal{R}})$ at $\sim$ 95–98 GeV and the SM-like Higgs boson h_2 at $\sim$ 125 GeV. The value for λ is large to account for a sizable Higgs-doublet component of h_1. Due to the contributions proportional to λ^2 to the tree-level mass of the SM-like Higgs boson (see Eq. (3.54)) no large quantum corrections are required to achieve a value of $\sim$ 125 GeV at loop level. Hence, $\tan\beta$ can be low and the soft trilinears $A^{u,d,e}$ are set to zero. The values of A^λ and $|A^\nu|$ are chosen to be around 1 TeV to get masses for the heavy MSSM-like Higgs and the left-handed sneutrinos of this order, so they do not play an important role in the following discussion. On the other hand, the value for κ is small to obtain a mass for the right-handed sneutrino below the SM-like Higgs-boson mass. The two parameters varied in this BP are μ and A^κ. By increasing μ the mixing of the right-handed sneutrino $h_1(\widetilde{\nu}_R^{\mathcal{R}})$ and the SM-like Higgs boson h_2 is increased. However, different

[1] The same conclusion were drawn for NMSSM solutions of both excesses, in which the extra singlet scalar takes on the role of ϕ [8, 10].

values of μ also modify the masses of h_1 and h_2. Therefore, different values of A^κ are used to keep the mass of the right-handed sneutrino in the correct range. Consequently, the results in this section will be displayed in the A^κ-μ plane.

Predictions for $\mu_{\rm LEP}$ and $\mu_{\rm CMS}$ were calculated using the narrow-width approximation. The ratios of cross sections and branching ratios between $\mu\nu$SSM prediction and SM prediction were approximated by effective coupling coefficients $c_{h_1\ldots}$ defined as the coupling of h_1 normalized to the coupling of a SM Higgs boson H at the same mass. Neglecting the vevs v_{iL}, the coupling coefficients to the SM fermions and the massive vector bosons are given at leading order by the admixture of the mass eigenstate h_i with the doublet-like Higgs fields H_d and H_u and β via

$$c_{h_i d\bar{d}} = \frac{U_{i1}^{H(2)}}{\cos\beta}\ , \quad c_{h_i u\bar{u}} = \frac{U_{i2}^{H(2)}}{\sin\beta}\ , \quad c_{h_i VV} = U_{i1}^{H(2)}\cos\beta + U_{i2}^{H(2)}\sin\beta\ , \tag{8.5}$$

where the partial two-loop plus resummation (called "two-loop" in the following, see Sect. 5.2) corrected mixing matrix elements $U_{ij}^{H,(2)}$ were calculated in the approximation of vanishing momentum.

We show in Fig. 8.1 the masses of h_1 and h_2 at the two-loop level $m_{h_1}^{(2)}$ and $m_{h_2}^{(2)}$ (top row), and the normalized couplings $|c_{h_i d\bar{d}}|$ (second row), $|c_{h_i u\bar{b}}|$ (third row) and $|c_{h_i VV}|$ (bottom row) of h_1 and h_2. The lower right corner (marked in gray) results in the right-handed sneutrino becoming tachyonic (at tree level). The largest mixing of the right-handed sneutrino and the SM-like Higgs boson is achieved where μ is largest and $|A^\kappa|$ is smallest. The mass of h_2 is in the allowed region for a SM-like Higgs boson at ~ 125 GeV assuming a theory uncertainty of 3 GeV. The coupling coefficients of the SM-like Higgs boson h_2 deviate from the SM prediction by approximately 10%. The LHC measurements of the SM-like Higgs boson couplings to fermions and massive gauge bosons are still not very precise [22], with uncertainties between 10 and 20% at the 1σ confidence level (obtained with the assumption that no BSM decays modify the total width of the SM-like Higgs boson). Therefore, considering current experimental uncertainties the BPs shown here cannot be excluded by the LHC measurements. However, possible future lepton colliders like the ILC could measure these couplings to a %-level [23, 24], which could probe most of the parameter space presented here. Seen from a more optimistic perspective, the precise measurement of the SM-like Higgs-boson couplings at future colliders could be used to make predictions for the properties of the lighter right-handed sneutrino in this scenario, whose coupling coefficients are directly related to the ones of the SM-like Higgs boson.

With the coupling coefficients for h_1 at hand, the singal strength for the LEP excess can be obtained by

$$\begin{aligned}
\mu_{\rm LEP}^{\mu\nu} &= \frac{\sigma^{\mu\nu}\left(Z^* \to Z h_1\right)}{\sigma^{\rm SM}\left(Z^* \to Z H\right)} \times \frac{{\rm BR}^{\mu\nu}\left(h_1 \to b\bar{b}\right)}{{\rm BR}^{\rm SM}\left(H \to b\bar{b}\right)} \\
&\approx \left|c_{h_1 VV}\right|^2 \times \frac{\Gamma_{b\bar{b}}^{\mu\nu}}{\Gamma_{b\bar{b}}^{\rm SM}} \times \frac{\Gamma_{\rm tot}^{\rm SM}}{\Gamma_{\rm tot}^{\mu\nu}} \\
&\approx \frac{\left|c_{h_1 VV}\right|^2 \times \left|c_{h_1 d\bar{d}}\right|^2}{\left|c_{h_1 d\bar{d}}\right|^2 \left({\rm BR}_{b\bar{b}}^{\rm SM} + {\rm BR}_{\tau\bar{\tau}}^{\rm SM}\right) + \left|c_{h_1 u\bar{u}}\right|^2 \left({\rm BR}_{gg}^{\rm SM} + {\rm BR}_{c\bar{c}}^{\rm SM}\right)}\ .
\end{aligned} \tag{8.6}$$

Here ${\rm BR}_{\ldots}^{\mu\nu}$ and ${\rm BR}_{\ldots}^{SM}$ denote branching ratios of h_1 and H in the $\mu\nu$SSM and the SM, respectively. Accordingly, $\Gamma_{\ldots}^{\mu\nu,{\rm SM}}$ are the decay widths, and $\Gamma_{\rm tot}^{\mu\nu,{\rm SM}}$ are the total width

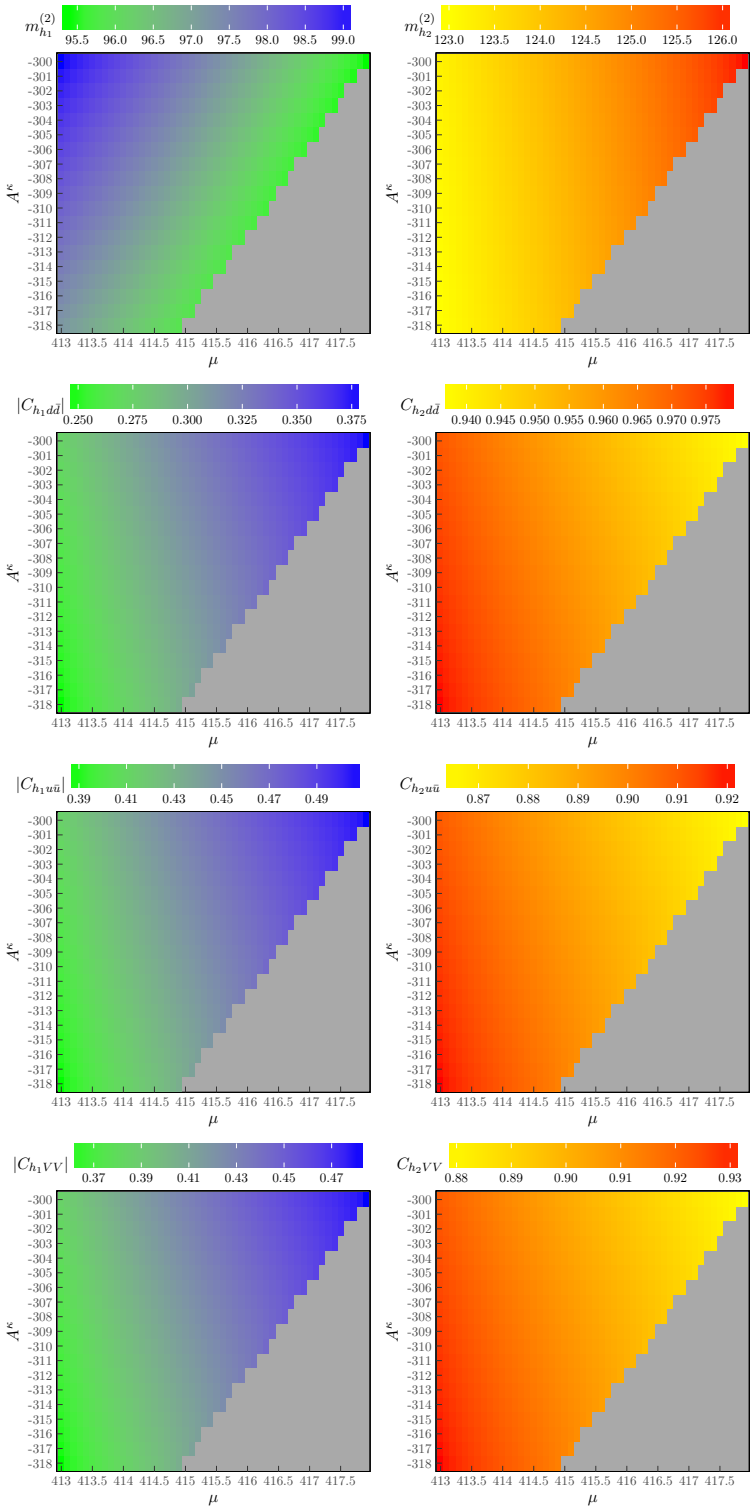

Figure 8.1: Properties of the lightest (*left*) and next-to-lightest (*right*) $\mathcal{CP}$-even scalar in the μ–A^κ plane. The couplings are normalized to the SM-prediction of a Higgs particle of the same mass. The gray area is excluded because the right-handed sneutrino becomes tachyonic at tree level. *First row:* two-loop masses, *second row:* coupling to down-type quarks, *third row:* coupling to up-type quarks, *fourth row:* coupling to massive gauge bosons.

of h_1 and H. In the second line the cross-section ratio was approximated by the square of the coupling coefficient $c_{h_1 VV}$. Similarly, in the third line we used the approximation

$$\frac{\Gamma^{\mu\nu}_{b\bar{b}}}{\Gamma^{\mathrm{SM}}_{b\bar{b}}} = |c_{h_1 d\bar{d}}|^2 \,, \tag{8.7}$$

where $c_{h_1 dd}$ determines the coupling of h_1 to down-type fermions. The expression in the denominator in Eq. (8.6) arises from the ratio of the total decay widths, by making use of the approximation

$$\frac{\Gamma^{\mu\nu}_{\mathrm{tot}}}{\Gamma^{\mathrm{SM}}_{\mathrm{tot}}} = \left|c_{h_1 d\bar{d}}\right|^2 (\mathrm{BR}^{\mathrm{SM}}_{b\bar{b}} + \mathrm{BR}^{\mathrm{SM}}_{\tau\bar{\tau}}) + |c_{h_1 u\bar{u}}|^2 (\mathrm{BR}^{\mathrm{SM}}_{gg} + \mathrm{BR}^{\mathrm{SM}}_{c\bar{c}}) \,. \tag{8.8}$$

Here, it was used that the loop-induced decay of h_1 into gluons is dominated by the diagrams with top quarks in the loop, such that

$$\Gamma^{\mu\nu}_{gg} = |c_{h_1 u\bar{u}}|^2 \, \Gamma^{\mathrm{SM}}_{gg} \,. \tag{8.9}$$

Apart from that, the two-body decays into off-shell vector bosons were neglected, because the branching ratios are very small ($\mathrm{BR}^{\mathrm{SM}}_{WW} \sim 0.5\%$ and $\mathrm{BR}^{\mathrm{SM}}_{ZZ} \sim 0.06\%$ for a SM Higgs boson at 95 GeV) [25, 26]). To finally calculate μ_{LEP} the SM branching ratios were taken from Ref. [26].

For the CMS excess we find

$$\begin{aligned}
\mu^{\mu\nu}_{\mathrm{CMS}} &= \frac{\sigma^{\mu\nu}(gg \to h_1)}{\sigma^{\mathrm{SM}}(gg \to H)} \times \frac{\mathrm{BR}^{\mu\nu}_{\gamma\gamma}}{\mathrm{BR}^{\mathrm{SM}}_{\gamma\gamma}} \\
&\approx |c_{h_1 u\bar{u}}|^2 \times \frac{\Gamma^{\mu\nu}_{\gamma\gamma}}{\Gamma^{\mathrm{SM}}_{\gamma\gamma}} \times \frac{\Gamma^{\mathrm{SM}}_{\mathrm{tot}}}{\Gamma^{\mu\nu}_{\mathrm{tot}}} \\
&\approx \frac{|c_{h_1 u\bar{u}}|^2 \times \left|c^{\mathrm{eff}}_{h_1\gamma\gamma}\right|^2}{\left|c_{h_1 d\bar{d}}\right|^2 (\mathrm{BR}^{\mathrm{SM}}_{b\bar{b}} + \mathrm{BR}^{\mathrm{SM}}_{\tau\bar{\tau}}) + |c_{h_1 u\bar{u}}|^2 (\mathrm{BR}^{\mathrm{SM}}_{gg} + \mathrm{BR}^{\mathrm{SM}}_{c\bar{c}})} \,.
\end{aligned} \tag{8.10}$$

The expression in the denominator again comes from the ratio of the total decay widths. In the second line the ggH production cross section ratio was approximated by

$$\frac{\sigma^{\mu\nu}(gg \to h_1)}{\sigma^{\mathrm{SM}}(gg \to h)} = |c_{h_1 u\bar{u}}|^2 \,, \tag{8.11}$$

exploiting the fact that the dominant diagram is the one with top quarks in the loop. The effective coupling coefficient of the h_i to photons $c^{\mathrm{eff}}_{h_i\gamma\gamma}$ has to be calculated in terms of the couplings to the W bosons and the up-type quarks, because both the diagram with W bosons and with top quarks in the loop contribute to the diphoton decay width. In the SM the decay of H to photons can be written as [27]

$$\Gamma^{\mathrm{SM}}_{\gamma\gamma} = \frac{G_\mu \, \alpha^2 \, m_h^3}{128\sqrt{2}\,\pi^3} \left|\frac{4}{3} A_{1/2}(\tau_t) + A_1(\tau_W)\right|^2 \,, \tag{8.12}$$

where G_μ is the Fermi-constant and the form factors $A_{1/2}$ and A_1 are given by

$$A_{1/2}(\tau) = 2\left(\tau + (\tau - 1)\arcsin^2\sqrt{\tau}\right)\tau^{-2} \,, \tag{8.13}$$

$$A_1(\tau) = -\left(2\tau^2 + 3\tau + 3(2\tau - 1)\arcsin^2\sqrt{\tau}\right)\tau^{-2} \,, \tag{8.14}$$

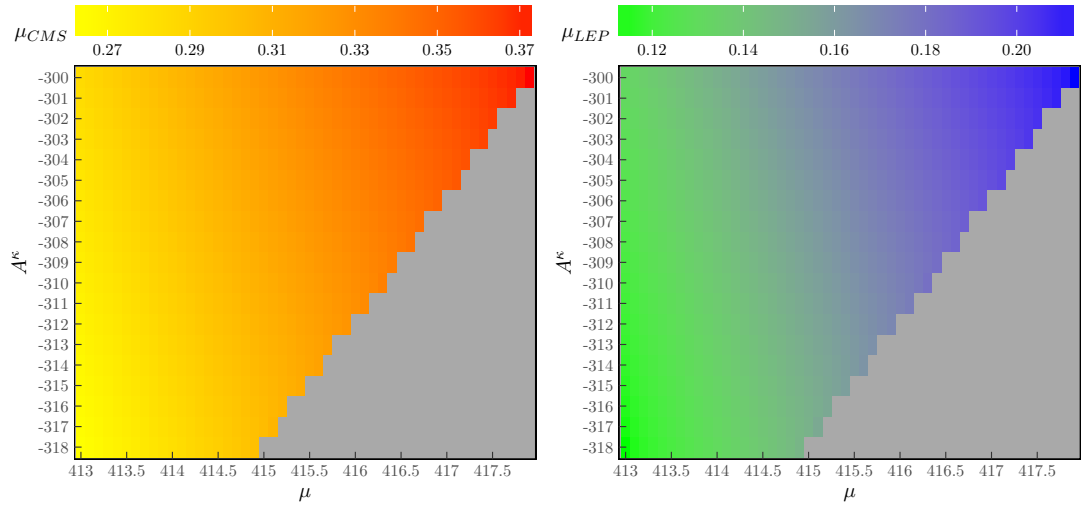

Figure 8.2: Signal strengths for the lightest $\widetilde{\nu}_R$-like neutral scalar at CMS ($pp \to h_1 \to \gamma\gamma$) (*left*) and LEP ($e^+e^- \to h_1 Z \to b\bar{b}Z$) (*right*) in the μ-A^κ plane. The gray area is excluded because the right-handed sneutrino becomes tachyonic at tree-level.

for $\tau \leq 1$, with $\tau_t = m_H^2/(4m_t^2)$ and $\tau_W = m_H^2/(4M_W^2)$. In our approximation the only difference between the $\mu\nu$SSM and the SM is that the couplings of h_i to the top quark and the W boson is modified by the coefficients $c_{h_i t\bar{t}}$ and $c_{h_i VV}$, so the effective coupling of the Higgses to photons in the $\mu\nu$SSM normalized to the SM predictions can be written as

$$\left|c^{\text{eff}}_{h_i\gamma\gamma}\right|^2 = \frac{\left|\frac{4}{3}c_{h_i t\bar{t}}A_{1/2}(\tau_t) + c_{h_i VV}A_1(\tau_W)\right|^2}{\left|\frac{4}{3}A_{1/2}(\tau_t) + A_1(\tau_W)\right|^2}\,. \tag{8.15}$$

Now, given the mass and the coupling coefficients of h_1, the signal strength for the CMS excess can be predicted by making use of Eq. (8.15) and Eq. (8.10).

We show the results for μ_{LEP} and μ_{CMS} in Fig. 8.2. While the LEP excess is easily reproduced in the observed parameter space, we cannot achieve the central value for μ_{CMS}, but only slightly smaller values. This is the result we expected from the reasoning at the beginning of this chapter. As already observed in Ref. [8], to explain the LEP excess a sizable coupling to bottom quarks is required. On the contrary, the only possibility to enhance the diphoton branching ratio, as required to accommodate the CMS excess, demands a small value for $c_{h_1 d\bar{d}}$ so that the denominator in Eq. (8.10) becomes small. Nevertheless, considering the large experimental uncertainties in μ_{CMS} and μ_{LEP}, the scenario presented in this section accommodates both excesses at approximately 1σ level, and motivates to keep on searching for light Higgs bosons in the still allowed mass window below ~ 125 GeV.

8.1.2 Three families of right-handed neutrinos

In the previous section we showed that both excesses can be accommodated simultaneously at the 1σ level in the $\mu\nu$SSM with just one right-handed neutrino, by means of a right-handed sneutrino at ~ 96 GeV that acquires substantial couplings to SM particles via its mixing with the SM-like Higgs boson. However, we did not include an accurate prediction of the properties of the neutrinos, because in the one-generation case at least one neutrino mass has to be generated via quantum corrections. On the contrary, in the $\mu\nu$SSM with three right-handed neutrinos, one can describe the mass differences and

$\tan\beta$	$\lambda_{1,2}$	λ_3	$\kappa_{111,222}$	κ_{333}	$v_{1,2R}$	v_{3R}	$A^\lambda_{1,2}$	A^λ_3	
1.945	0.01	$[0.538, 0.542]$	0.3	0.05	1200	$[884, 888]$	1000	$[806, 814]$	
A^ν_{ii}	$A^\kappa_{111,222}$	A^κ_{333}	A^u_3	$A^u_{1,2}$	$A^{d,e}$	$m_{\widetilde{Q},\widetilde{u},\widetilde{d},\widetilde{e}}$	M_1	M_2	M_3
-1000	-300	$[-124, -100]$	-650	0	0	1000	400	800	2700

Table 8.2: Same as in Tab. 8.1 for the $\mu\nu$SSM with three right-handed neutrinos

mixings of the neutrinos at tree level. As this is much more feasible, we present here BPs in the three-generation case in which on top of an explanation for the LEP and CMS excesses the neutrino sector is described in agreement with experimental data [13].

The values of the free parameters to fit the excesses are shown in Tab. 8.2. The $\mathcal{CP}$-even scalar $h_1(\widetilde{\nu}^{\mathcal{R}}_{\tau R})$ utilized to fit the excesses has dominant right-handed τ-sneutrino component. This is assured by setting $\kappa_{333} \ll \kappa_{111,222}$, so that $h_1(\widetilde{\nu}^{\mathcal{R}}_{\tau R})$ has a smaller mass than the other two right-handed sneutrinos. v_{3R} and A^κ_{333} are varied in a range in which the mass of $h_1(\widetilde{\nu}^{\mathcal{R}}_{\tau R})$ is roughly $\sim$ 95–98 GeV. A sufficiently large mixing of $h_1(\widetilde{\nu}^{\mathcal{R}}_{\tau R})$ with the SM-like Higgs boson $h_2(H^{\mathcal{R}}_u)$ at $\sim$ 125 GeV is achieved with a large value of $\lambda_3 \sim 0.54$, while $\lambda_{1,2} = 0.01$ are very small to avoid a very large effective μ-term. Alternatively, one could have used smaller values for $v_{1,2R}$, but then the other two $\mathcal{CP}$-even right-handed sneutrinos $\widetilde{\nu}^{\mathcal{R}}_{e,\mu\,R}$ would have been very light as well, potentially carrying away some doublet component via mixing with the SM-like Higgs boson which we here want to attribute to $h_1(\widetilde{\nu}^{\mathcal{R}}_{\tau R})$ at $\sim$ 96 GeV.[2] Since λ_3 is large, $h_2(H^{\mathcal{R}}_u)$ receives additional contribution to the tree-level mass. This is why $\tan\beta$ can be set to a small value, and, besides $A^u_3 = -650$ GeV, the soft trilinear parameters $A^{u,d,e}$ are set to zero. The signal strength μ_{CMS} effectively scales with $c_{h_1 t\bar{t}}$ to the power of four (see Eqs. (8.10) and (8.15)). Hence, a small value for $\tan\beta$ is eligible, because otherwise one suppresses the coupling of $h_1(\widetilde{\nu}^{\mathcal{R}}_{\tau R})$ to top quarks which scales with the inverse of $\sin\beta$ (see Eq. (8.5)). The parameters A^λ_i enter in the $\mathcal{CP}$-even scalar mass matrix elements $m^2_{\widetilde{\nu}^{\mathcal{R}}_{iR} H^{\mathcal{R}}_{d,u}}$ (see Eqs. (3.39) and (3.40)), so that they contribute to the mixing of the right-handed sneutrinos and the SM-like Higgs boson. We varied A^λ_3 in a range in which the mixing between $h_1(\widetilde{\nu}^{\mathcal{R}}_{\tau R})$ and $h_2(H^{\mathcal{R}}_u)$ is of the size to appropriately reproduce μ_{LEP}. Certainly, this is not an exhaustive parameter scan covering the complete parameter space, but the scan gives an idea of how the excesses can be accommodated in the three-generation case, and it resembles the solution we found in the $\mu\nu$SSM with one right-handed neutrino.

In Fig. 8.3 we show the results for the signal strength of the LEP excess μ_{LEP} (top) and of the CMS excess μ_{CMS} (bottom). In both plots the colors of the points encode the SM-like Higgs-boson mass $m_{h_2(H^{\mathcal{R}}_u)}$, while the mass of $h_1(\widetilde{\nu}^{\mathcal{R}}_{\tau R})$ is shown on the horizontal axis. The signal strengths were calculated using the same approach as explained in Sect. 8.1. One can immediately see that it is rather easy to achieve a value of $\mu_{\text{LEP}} \sim 0.117$, whereas the largest values for μ_{CMS} are roughly 1σ below the central value. Thus, we find the same result as in the one-generation case. The signal strengths μ_{LEP} and μ_{CMS} are fitted at the 1σ level. We verified that the BPs are in agreement with the experimental constraints on the SM-like Higgs boson with `HiggsSignals`, assuming a theoretical uncertainty of the SM-like Higgs-boson mass of 3 GeV.

In Fig. 8.4 we show the correlation of both signal strengths, with the colors indicating

[2] A scenario in which several right-handed sneutrinos give rise to the observed excesses is beyond the scope of this discussion and left for future work.

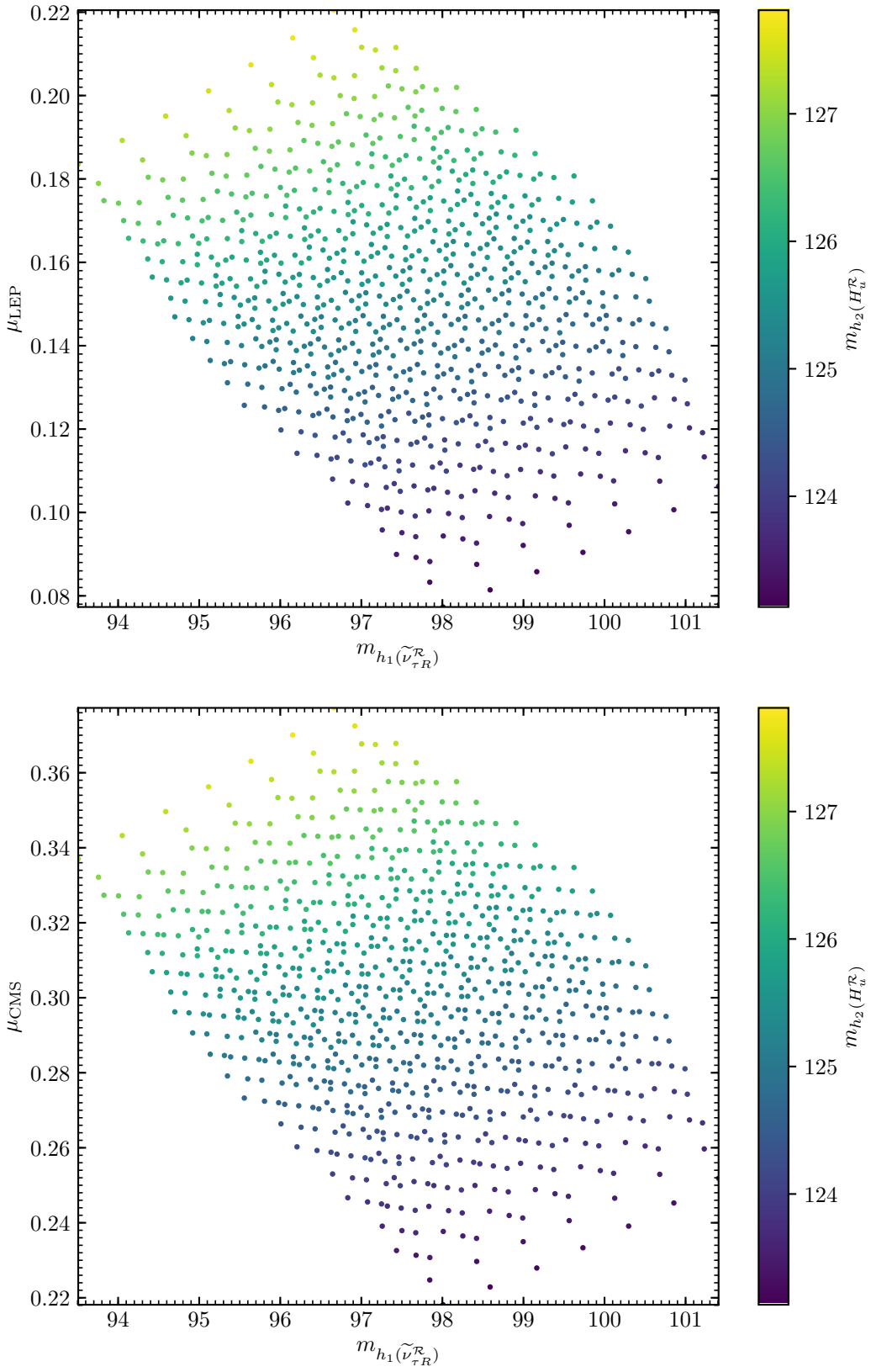

Figure 8.3: $\mu_{\rm LEP}$ *(top)* and for $\mu_{\rm CMS}$ *(bottom)* for each BP versus the mass of $h_1(\widetilde{\nu}^{\mathcal{R}}_{\tau R})$. The colors indicate the mass of the SM-like Higgs boson $h_2(H^{\mathcal{R}}_u)$.

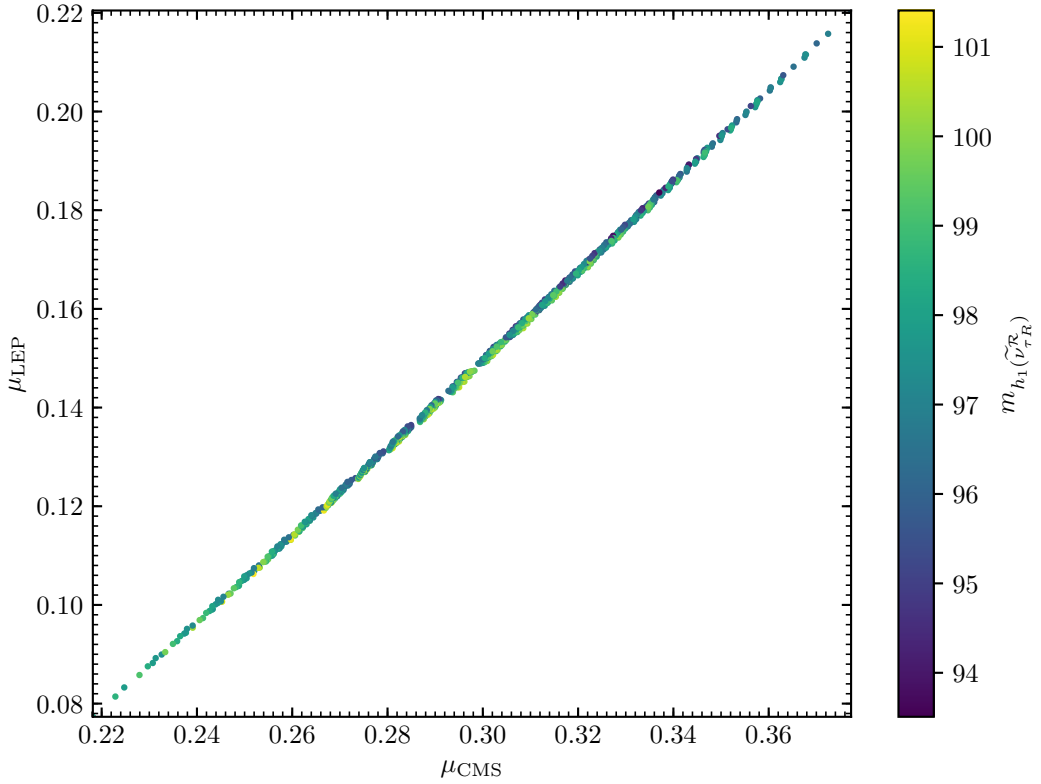

Figure 8.4: Correlation of $\mu_{\rm LEP}$ and $\mu_{\rm CMS}$, with the colors indicating the mass of $h_1(\widetilde{\nu}^{\mathcal{R}}_{\tau R})$.

the mass of $h_1(\widetilde{\nu}^{\mathcal{R}}_{\tau R})$. The strong correlation one can see has its origin in the fact that both signal strengths increase with the amount of doublet-component of $h_1(\widetilde{\nu}^{\mathcal{R}}_{\tau R})$. Due to the SUSY relations in the scalar potential, the coupling coefficient $c_{h_1 d\bar{d}}$ cannot be suppressed without suppressing $c_{h_1 u\bar{u}}$. Consequently, no large enhancement to the branching ratio of $h_1(\widetilde{\nu}^{\mathcal{R}}_{\tau R})$ into a diphoton pair can be achieved. The dominant terms mixing the right-handed sneutrinos $\widetilde{\nu}^{\mathcal{R}}_{iR}$ with the doublet fields $H^{\mathcal{R}}_d$ and $H^{\mathcal{R}}_u$ scale equally with λ_i, A^{λ}_i, κ_{ijk} and v_{iR} at tree level, as can be seen in Eqs. (3.39) and (3.40). The only difference are the factors v_d and v_u in each equation. This difference cannot be exploited too much, because, as mentioned before, $\tan\beta$ should not be too far from one. This is why an extensive scan of the vast parameter space of the $\mu\nu$SSM would be necessary to find parameter points in which $\mu_{\rm CMS}$ is further enhanced without increasing $\mu_{\rm LEP}$ too much. However, this lies beyond the scope of this thesis.

Instead, we will focus on the rest of the spectrum which heavily depends on the values of the neutrino Yukawa couplings Y^{ν}_{ij} and the vevs of the left-handed sneutrinos v_{iL}, once the remaining parameters are fixed to the values listed in Tab. 8.2. We show in Tab. 8.3 two possible sets of parameters that accommodate accurate neutrino masses and mixings in the BPs of this section. The phenomenology related to $h_1(\widetilde{\nu}^{\mathcal{R}}_{\tau R})$ and $h_2(H^{\mathcal{R}}_u)$ does not depend on the values of Y^{ν}_{ij} and v_{iL}. Its branching ratios are dominantly given by the mixing-effects with the SM-like Higgs boson which is not suppressed by the small neutrino Yukawa couplings Y^{ν}_{ij}.

In contrast to the scenarios we presented in Ch. 6, we make use of non-zero values of the off-diagonal elements of Y^{ν}_{ij} in BP2. This simplifies the accommodation of neutrino properties in agreement with experimental data, because there are six more free parameters that can be adjusted. The price to pay is that there is usually more than one

	$Y^\nu_{11}/10^{-8}$	$Y^\nu_{12}/10^{-8}$	$Y^\nu_{13}/10^{-8}$	$Y^\nu_{21}/10^{-8}$	$Y^\nu_{22}/10^{-8}$	$Y^\nu_{23}/10^{-8}$
BP1	8.109	0	0	0	11.54	0
BP2	7.088	1.181	−0.3404	1.902	12.38	1.783
	$Y^\nu_{31}/10^{-8}$	$Y^\nu_{32}/10^{-8}$	$Y^\nu_{33}/10^{-8}$	$v_{1L}/10^{-4}$	$v_{2L}/10^{-4}$	$v_{3L}/10^{-4}$
BP1	0	0	88.55	0.1890	2.601	1.871
BP2	−0.2103	0.6923	1.383	0.0179	2.072	3.673
BP1	$m_{\lambda_4}(\nu_{\tau R})$	$m_{A_1}(\widetilde{\nu}^{\mathcal{I}}_{\tau R})$	$m_{H_1^+}(\widetilde{\mu}_L)$	$m_{A_2}(\widetilde{\nu}^{\mathcal{I}}_{\mu L})$	$m_{h_3}(\widetilde{\nu}^{\mathcal{R}}_{\mu L})$	$m_{\lambda_5}(\widetilde{H}_{d,u})$
	78	97-109	283	285	285	$323-326$
BP2	$m_{\lambda_4}(\nu_{\tau R})$	$m_{h_1}(\widetilde{\nu}_{\tau L})$	$m_{A_1}(\widetilde{\nu}_{\tau L})$	$m_{H_1^+}(\widetilde{\tau}_L)$	$m_{A_2}(\widetilde{\nu}_{\tau R})$	$m_{\lambda_5}(\widetilde{H}_{d,u})$
	78	79	79	98	97-109	$323-326$

Table 8.3: Parameter sets BP1 and BP2 used to fit the neutrino oscillation data accurately. In the last four rows we list the masses of the six lightest non-SM particles (in addition to $\widetilde{\nu}^{\mathcal{R}}_{\tau R}$ at ~ 96 GeV) for each BP. Dimensionful parameters are given in GeV.

set of parameters of Y^ν_{ij} and v_{iL} that give accurate predictions for the neutrino sector. We show two distinct BPs, because in the $\mu\nu$SSM the scalar sector is deeply related to the neutrino sector. Different sets of parameters predict fundamentally different scalar spectra. Since there is no theoretical argument that the neutrino Yukawa couplings have to be diagonal, we used the additional freedom to present a BP in which, on top of the explanation of the LEP and the CMS excesses with $h_1(\widetilde{\nu}^{\mathcal{R}}_{\tau R})$ at ~ 96 GeV, there are a bunch of other light scalars possibly in reach of future colliders.

In both BP1 and BP2 the lightest BSM particle is the right-handed τ-neutrino $\nu_{\tau R}$. This is because a small value for κ_{333} is used decrease the mass of $h_1(\widetilde{\nu}^{\mathcal{R}}_{\tau R})$. Consequently, also the mass of the corresponding neutrino $m_{\nu_{\tau R}}$ is small (see Eq. (3.88)). However, $m_{\nu_{\tau R}}$ is above half the SM-like Higgs-boson mass, so the decay of $h_2(H^{\mathcal{R}}_u)$ into a pair of $\nu_{\tau R}$ is kinematically impossible. The striking difference between BP1 and BP2 is the mass scale of the left-handed $\mathcal{CP}$-even and $\mathcal{CP}$-odd τ-sneutrinos $\widetilde{\nu}^{\mathcal{R},\mathcal{I}}_{\tau L}$ and the slepton $\widetilde{\tau}_L$. In BP2 the Yukawa coupling Y^ν_{33} is the smallest diagonal element of Y^ν_{ij}, and the vev corresponding to the third family of left-handed sneutrinos v_{3L} is the largest of the three. This reduces the masses of $\widetilde{\nu}^{\mathcal{R},\mathcal{I}}_{\tau L}$ (see Eq. (3.48)) and $\widetilde{\tau}_L$ (see Eq. (3.86)) to values below the SM-like Higgs-boson mass. In BP1, on the other hand, v_{2L} is the largest of the three left-handed vevs, and therefore the left-handed μ-sneutrinos and μ-slepton are the lightest left-handed sfermions, although still more than twice as heavy as the SM-like Higgs boson. This illustrates that the parameters relating the neutrino sector and the scalar sector of the $\mu\nu$SSM have a profound impact on the phenomenology of a certain BP.

BP2 can give rise to additional interesting signal at colliders. A dedicated analysis of the collider phenomenology of light left-handed τ-sneutrinos/sleptons at the LHC can be found in Refs. [28, 29]. In Ref. [29] it was also shown that there are no lower limits on the sneutrino masses and slepton masses from LEP applicable to the $\mu\nu$SSM. An important feature is that the decay of $\widetilde{\nu}_{\tau L}$ can be displaced, because its decays to SM particles are suppressed by the small values for Y^ν_{ij}. In Refs. [28, 29] it is assumed that the left-handed sneutrino is the LSP. This is not the case here, since the right-handed τ-neutrino is even lighter. Signals at colliders from $\nu_{\tau R}$ are not expected, because it is a gauge singlet, thus

cannot be produced directly. In principle, it can be produced indirectly via the decay of the sfermions. However, the spectrum is very compressed, such that a pair production of $\nu_{\tau R}$ from the decays of $\widetilde{\nu}_{\tau R}$ at $\sim$ 96 GeV or the SM-like Higgs boson at $\sim$ 125 GeV is kinematically forbidden, and the production of a pair of a right- and a left-handed τ-neutrino is suppressed by the size of Y^{ν}_{33}.

8.2 Singlet-like scalar in the N2HDM

Our investigations in the framework of the $\mu\nu$SSM show that it is possible to explain the LEP and the CMS excesses at the 1σ level, where the limitations arise from the precise form of the scalar potential that has to obey SUSY relations. The same conclusions were drawn in the NMSSM [8, 10]. This fact motivated to examine if an even better fit can be achieved in a non-SUSY model containing a gauge-singlet scalar field. Thus, we analyzed in Refs. [14, 15] a possible explanation of the excesses in the N2HDM, by considering a Higgs boson with a dominant singlet-component and a mass of $\sim$ 96 GeV. We briefly explain in the following why only the type II and the type IV N2HDM (see Sect. 7.2) can potentially accommodate both excesses simultaneously. Afterwards, we state the relevant theoretical and experimental constraints that have to be taken into account. From there we derive appropriate values for the input parameters (see Eq. (7.26)). In Sect. 8.2.2 and Sect. 8.2.2 we show our results of the parameter scans in the type II and the type IV N2HDM, respectively. Finally, we discuss the prospects for current and future experiments to be able to test our scenario in Sect. 8.2.4.

Which type?

As already discussed in the introduction of this chapter, the LEP excess demands that the Higgs boson at $\sim$ 96 GeV should have a squared coupling to massive vector bosons of $\sim$ 0.1 times that of the SM Higgs boson of the same mass. For the CMS excess, on the other hand, it appears to be difficult at first sight to accommodate the large signal strength, because one expects a suppression of the loop-induced coupling to gluons and photons. However, it turns out that it is possible to overcompensate this suppression by decreasing the total width of the singlet-like scalar, leading to an enhancement of the branching ratio of the new scalar to the $\gamma\gamma$ final state. The different types of the N2HDM behave differently in this regard, based on how the doublet fields are coupled to the quarks and leptons. We summarize the general idea of our solution in Tab. 8.4, and argue that only the type II and type IV (flipped) N2HDM can accommodate both excesses simultaneously with a dominantly singlet-like scalar h_1 at $\sim$ 96 GeV.

The first condition is that the coupling of h_1 to b-quarks has to be suppressed to enhance the decay rate of the decay into $\gamma\gamma$, as the total decay width at this mass is still dominated by the decay to $b\bar{b}$. The second condition is that one must not decrease the coupling to t-quarks too much, because the decay width to photons strongly depends on the t-quark loop contribution. Moreover, the ggH production cross section is dominated at leading order by the diagram with t-quarks in the loop. Thus, a decreased coupling of h_1 to t-quarks implies a lower production cross section at the LHC. As one can deduce from Tab. 8.4, in type I and the lepton-specific type III N2HDM the coupling coefficients (see Sect. 7.2) are the same for up- and down-type quarks, because only one Higgs doublet field is coupled to the quarks (see Tab. 7.1). Thus, it is impossible to satisfy both of the above criteria simultaneously in these models, and they fail to accommodate both the CMS and the LEP excesses.

	Decrease $c_{h_1 b\bar{b}}$	No decrease $c_{h_1 t\bar{t}}$	No enhancement $c_{h_1 \tau\bar{\tau}}$
type I	✓ (R_{12}/s_β)	✗ (R_{12}/s_β)	✓ (R_{12}/s_β)
type II	✓ (R_{11}/c_β)	✓ (R_{12}/s_β)	✓ (R_{11}/c_β)
lepton-specific	✓ (R_{12}/s_β)	✗ (R_{12}/s_β)	✗ (R_{11}/c_β)
flipped	✓ (R_{11}/c_β)	✓ (R_{12}/s_β)	✗ (R_{12}/s_β)

Table 8.4: Conditions that have to be satisfied to accommodate the LEP and CMS excesses simultaneously with a light $\mathcal{CP}$-even scalar h_1 with dominant singlet component. In brackets we state the relevant coupling coefficients $c_{h_1 f\bar{f}}$ for the conditions for each type.

One could of course go to the 2HDM-limit of the N2HDM by taking the singlet scalar to be decoupled, and reproduce the results observed previously in Refs. [3, 4]. Therein both excesses are accommodated placing the second $\mathcal{CP}$-even Higgs boson in the corresponding mass range. These solutions imply that the ggH production mode no longer dominates the total production cross section and the CMS excess can only be explained by considering the contributions from other modes of production like VBF and associated production with vector bosons (VH) etc. As was explained in the introduction of this chapter, we discard these solutions, as the excess clearly appears in the ggH production mode.

Having discarded the type I and type III scenario, we now concentrate on the remaining two possibilities. In type II and the flipped type IV scenario, each of the doublet fields Φ_1 and Φ_2 couple to either up- or down-type quarks, and it is possible to control the size of the coupling coefficients $c_{h_i t\bar{t}}$ and $c_{h_i b\bar{b}}$ independently. The singlet-like scalar h_1 acquires its couplings to fermions through the mixing with the doublet fields. This effectively yields one more degree of freedom to adjust its couplings independently for up- and down-type quarks. From the dependence of the mixing matrix elements R_{11} and R_{12} on the mixings angles α_i, as stated in Eq. (7.9), one can deduce that the relevant parameter in this case is α_1. For

$$|\alpha_1| \to \pi/2 \,, \tag{8.16}$$

the up-type doublet component of h_1 is large and the down-type doublet component goes to zero. Thus, large values of α_1 will correspond to a suppression of the decay width to $b\bar{b}$, while simultaneously not suppressing the decay width to $\gamma\gamma$. Consequently, considering that the total decay width of h_1 is dominated by the decay width to $b\bar{b}$, the limit shown in Eq. (8.16) corresponds to en enhancement of the branching ration of the diphoton decay of h_1.

A third condition is related to the coupling of h_1 to leptons. If it is increased, the decay to a pair of τ-leptons is enhanced. Similar to the decay to b-quarks, it would compete with the diphoton decay and suppress the signal strength required for the CMS excess. However, this condition is not as significant as the former two, owing to the smaller τ-Yukawa coupling and the missing color factor, so that $(Y_3^e)^2 \ll 9(Y_3^d)^2$. Still, as we will see in our numerical evaluation, it is the reason why it is easier to fit the CMS excess in the type II model than in the flipped type IV scenario. In the latter the coupling coefficient to leptons $c_{h_1 l\bar{l}}$ is equal to the one to up-type quarks $c_{h_1 u\bar{u}}$. Thus, in the region where the diphoton branching ratio is enhanced, also decay width of the decay into $\tau\bar{\tau}$ is large, and both channels will compete. In the type II scenario, on the other hand, $c_{h_1 l\bar{l}}$ is equal to the coupling to down-type quarks $c_{h_1 d\bar{d}}$, meaning that in

the relevant parameter region both the decay to b-quarks and the decay to τ-leptons are suppressed.

8.2.1 Theoretical constraints

The N2HDM faces important constraints coming from tree-level perturbartive unitarity, stability of the vacuum and the condition that the vacuum should be a global minimum of the potential. We briefly describe these constraints below and how they were accounted for in our scans.

- Tree-level perturbative unitarity conditions ensure that the potential remains perturbative up to very high energy scales. These conditions were calculated in Ref. [30] by demanding that the amplitudes of the scalar quartic interactions leading to $2 \to 2$ scattering processes remain below the value of 8π at tree level.
- The values for the input parameters have to correspond to a true vacuum. In particular, that means that the scalar potential (see Eq. (7.2)) must be bounded from below, i.e., that it remains positive when the field values approach infinity. The necessary and sufficient conditions for boundedness from below are given in Ref. [31]. The same conditions can be found in Ref. [30] in the notation adopted in this thesis.
- We impose the condition that the vacuum is a global minimum of the potential. Although this condition can be avoided in the case of a metastable vacuum with the tunneling time to the real minimum being larger than the age of the universe, we do not explore this possibility in this analysis.[3]

All the theoretical constraints mentioned above were taken into account in our analysis by scanning the scalar potential with the help of the public code `ScannerS` [33] in which the conditions are implemented by default for the N2HDM [30].

Experimental constraints

In Sect. 7.3 we described already the phenomenological consequences related to the presence of the additional Higgs bosons in the broken phase of the N2HDM. Several experimental constraints are implemented into `ScannerS`. Unfortunately, some of these were outdated and did not include the most recent experimental data. Therefore, we supplemented the most recent ones by linking the parameter points from `ScannerS` to the more recent versions of other public codes. Here, we list the relevant experimental constraints, and give the tools other than `ScannerS` used to take them into account, if this was necessary. The necessary input for these codes, such as branching ratios and effective coupling coefficients (see Eqs. (7.29) and (7.30)), were obtained by using the `Scanners` interface with the spectrum generator `N2HDECAY` [30, 34, 35].

- Direct searches at colliders: We used the public code `HiggsBounds v.5.3.2` [36–40] to check each BP against exclusion limits at the 95% confidence level from Higgs-boson searches at LEP, Tevatron and LHC.
- Flavor physics: We took over the 2HDM exclusion regions in the $\tan\beta$-$M_{H^\pm}$ from Ref. [41]. The dominant constraints from $\mathrm{BR}(B \to X_s\gamma)$ and ΔM_{B_s} depend in very good approximation only on the charged Higgs boson sector which is unchanged

[3] Shortly after we published our results, an analysis of metastable parameter configurations of the N2HDM potential was published [32]. However, the conditions for valid metastable points are not yet available in a public computer code. Considering the possibility of metastability is left for future work.

in the N2HDM, so that the same bounds can be applied (see Sect. 7.3 for more details).

- SM-like Higgs boson: Constraints from SM-like Higgs-boson observables were taken into account in a twofold way. Firstly, `ScannerS` checks the signal strengths

$$\frac{\mu_F}{\mu_V} \,, \quad \mu_F^{\gamma\gamma} \,, \quad \mu_F^{ZZ} \,, \quad \mu_F^{WW} \,, \quad \mu_F^{\tau\tau} \,, \quad \mu_F^{bb} \,, \tag{8.17}$$

as they are quoted in Ref. [22], where an agreement within $\pm 2\sigma$ is required. The signal strengths are defined as

$$\mu_F^{xx} = \mu_F \frac{\mathrm{BR}_{\mathrm{N2HDM}}(h_i \to xx)}{\mathrm{BR}_{\mathrm{SM}}(H \to xx)} \,. \tag{8.18}$$

Here, the production cross sections associated with couplings to fermions normalized to the SM prediction are defined as

$$\mu_F = \frac{\sigma_{\mathrm{N2HDM}}(\mathrm{ggH}) + \sigma_{\mathrm{N2HDM}}(\mathrm{bbH})}{\sigma_{\mathrm{SM}}(\mathrm{ggH})} \,. \tag{8.19}$$

The production in association with a pair of b-quarks (bbH) is neglected in the SM. In N2HDM it can be enhanced by $\tan\beta$, so that it has to be taken into account. The VBF production cross section and the VH production cross section are given by the coupling coefficient c_{h_2VV},

$$\mu_V = \frac{\sigma_{\mathrm{N2HDM}}(\mathrm{VBF})}{\sigma_{\mathrm{SM}}(\mathrm{VBF})} = \frac{\sigma_{\mathrm{N2HDM}}(VH)}{\sigma_{\mathrm{SM}}(VH)} = c^2_{h_2VV} \,, \tag{8.20}$$

using the fact that QCD corrections cancel in the ratio of the vector boson fusion cross sections in the N2HDM and the SM [30]. The ggH and bbH cross sections are provided by `ScannerS` with the help of data tables obtained using the public code `SusHi` [42, 43]. Since this approach does not capture the most recent measurements related to the SM-like Higgs boson, we verified in a second step the agreement of the BPs with all currently available measurements using the public code `HiggsSignals v.2.2.3` [44–46]. The complete list of implemented experimental data can be found on the `HiggsSignals` web page [47]. In our scans, we will show the reduced χ^2,

$$\chi^2_{\mathrm{red}} = \frac{\chi^2}{n_{\mathrm{obs}}} \,, \tag{8.21}$$

where χ^2 is provided by `HiggsSignals` and $n_{\mathrm{obs}} = 101$ is the number of experimental observations considered.

- EWPO: `ScannerS` calculates the one-loop corrections to the oblique parameters for models with an arbitrary number of Higgs doublets and singlets from Ref. [48]. This calculation is valid under the criteria that the gauge group is the SM $SU(2) \times U(1)$, and that particles beyond the SM have suppressed couplings to light SM fermions. Both conditions are fulfilled in the N2HDM. Under these assumptions, the corrections are independent of the Yukawa sector of the N2HDM, and therefore the same for all types. In 2HDMs there is a strong correlation between T and U, and T is the most sensitive of the three oblique parameters. Thus, U is much smaller in points not excluded by an extremely large value of T [49], and the contributions to U can safely be dropped. Therefore, we require that the prediction for S and T are within the 2σ ellipse, corresponding to $\chi^2 = 5.99$ for two degrees of freedom. By default `ScannerS` verifies that the S, T and U parameters are within the 2σ ellipsoid with three degrees of freedom, corresponding to $\chi^2 = 7.81$. Due to the correlation of T and U our approach yields even stronger constraints.

Details of the scans

In the following sections we present our analyses in the type II and type IV scenario in which the excesses can be accounted for.[4] We performed a scan over the relevant parameters using the public code `ScannerS`. Following the discussion about the various experimental and theoretical constrains, we chose to scan the following range of input parameters:

$$\begin{aligned} 95\text{ GeV} \leq & m_{h_1} \leq 98\text{ GeV}\,, \quad m_{h_2} = 125.09\text{ GeV}\,, \quad 400\text{ GeV} \leq m_{h_3} \leq 1000\text{ GeV}\,, \\ & 400\text{ GeV} \leq m_A \leq 1000\text{ GeV}\,, \quad 650\text{ GeV} \leq M_{H^\pm} \leq 1000\text{ GeV}\,, \\ & 0.5 \leq \tan\beta \leq 4\,, \quad 0 \leq m_{12}^2 \leq 10^6\text{ GeV}^2\,, \quad 100\text{ GeV} \leq v_S \leq 1500\text{ GeV}\,. \end{aligned} \tag{8.22}$$

The parameter ranges were scanned uniformly, i.e., a flat prior distribution is applied. The lower limit of $M_{H^\pm} \geq 650$ GeV arises from the flavor constraints (see Eq. (7.37)). The lower limits on m_{h_3} and m_A avoid very strong bounds from collider searches [41], while the upper bound of 1 TeV assures that the additional Higgs bosons will not have masses far beyond the reach of the LHC.

We will make use of the possibility to set additional constraints on the singlet admixture of each $\mathcal{CP}$-even scalar particle which is provided by `ScannerS`. To enforce that the lightest scalar has the dominant singlet admixture, we impose

$$65\% \leq \Sigma_{h_1} \leq 90\%\,, \tag{8.23}$$

while for the SM-like Higgs boson we impose a lower limit on the singlet admixture of

$$\Sigma_{h_2} \geq 10\%\,. \tag{8.24}$$

This assures that there is at least some doublet component in h_1 in each BP which is necessary to fit the excesses. We checked explicitly that BPs with $\Sigma_{h_2} < 10\%$ cannot explain the excesses with an accuracy better than 1σ, because the doublet component of h_1 is too small.

Our aim is to increase the up-type component of h_1 compared to its down-type component, thus obtaining BPs with enhanced branching ratio of h_1 into the $\gamma\gamma$ final state, for which the limit shown in Eq. (8.16) is a necessary condition. In this limit the coupling coefficients of the SM-like Higgs boson h_2 to quarks can be approximated by

$$c_{h_2 t\bar{t}} \sim \mp\frac{s_{\alpha_2} s_{\alpha_3}}{s_\beta} \quad \text{and} \quad c_{h_2 b\bar{b}} \sim \mp\frac{c_{\alpha_3}}{c_\beta}\,. \tag{8.25}$$

Consequently, if α_2 and α_3 would have opposite signs, one would enter the wrong-sign Yukawa coupling regime, in which it is harder to accommodate the SM-like Higgs-boson properties, especially for low values of $\tan\beta$. Also the possible singlet-component of h_2 is more limited [30]. To avoid entering the wrong-sign Yukawa coupling regime, we therefore impose an additional constraint on the mixing angles α_i, i.e.,

$$\alpha_2 \cdot \alpha_3 > 0\,. \tag{8.26}$$

This condition also removes uninteresting parameter regions with small values of $|\alpha_1|$. Because of the global minimum conditions, $|\alpha_1|$ can only be small when the condition in

[4] Similar scans have been performed also for the N2HDM type I and III (lepton specific). We confirmed the negative result expected from the arguments given in Sect. 8.2. Consequently, we do not show any of these results here.

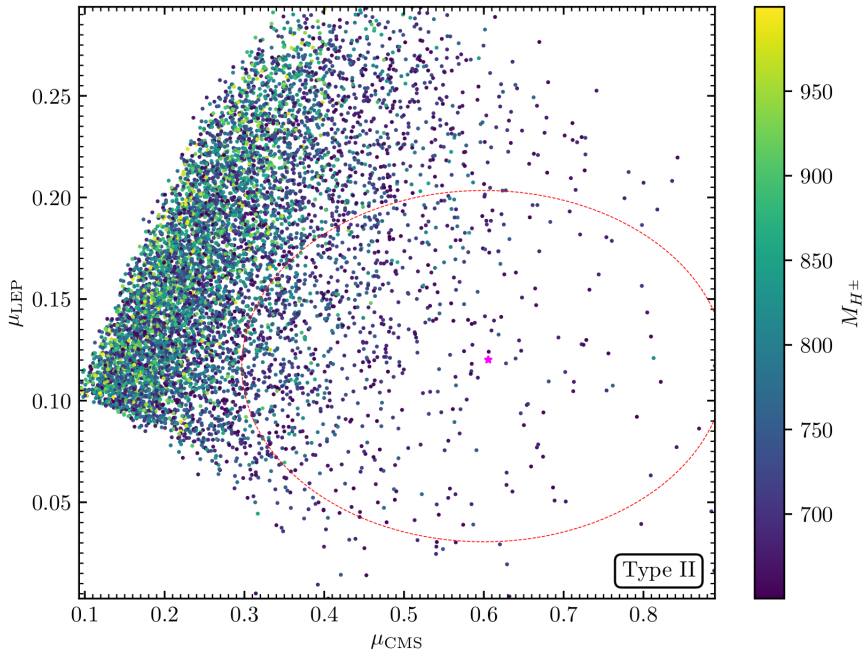

Figure 8.5: Type II: the signal strengths $\mu_{\rm CMS}$ and $\mu_{\rm LEP}$ are shown for each scan point respecting the experimental and theoretical constrains. The 1σ region of both excesses is shown by the red ellipse. The colors show the mass of the charged Higgs. The magenta star is the best-fit point. The lowest (highest) value of $M_{H^\pm}$ inside the 1σ ellipse is 650.03 (964.71) GeV.

Eq. (8.26) is not fulfilled. The quality of the fit to the excesses for each BP will be given in terms of the χ^2 defined by

$$\chi^2_{\rm CMS-LEP} = \frac{(\mu_{\rm LEP} - 0.117)^2}{0.057^2} + \frac{(\mu_{\rm CMS} - 0.6)^2}{0.2^2} \,, \tag{8.27}$$

quantifying the quadratic deviation w.r.t. the measured values for the signal strengths, assuming that there is no correlation between both signals. We refer to the BP with smallest $\chi^2_{\rm CMS-LEP}$ in each scan as the "best-fit point". In principle, we could have combined the χ^2 obtained from `HiggsSignals` regarding the SM-like Higgs-boson observables with the χ^2 defined above regarding the LEP and the CMS excesses. In that case, however, the total χ^2 would be strongly dominated by the SM-like Higgs-boson contribution from `HiggsSignals` due to the sheer amount of signal strength observables implemented. Consequently, we refrain from performing such a combined χ^2 analysis.

8.2.2 Type II

We show the result of our scan in the type II scenario in Figs. 8.5-8.7 in the plane of the signal strengths $\mu_{\rm LEP}$ and $\mu_{\rm CMS}$ for each BP. The best-fit point w.r.t. the two excesses is marked by a magenta star. The density of points has no physical meaning and is a pure artifact of the "flat prior" in our parameter scan. The red dashed line corresponds to the 1σ ellipse, i.e., to $\chi^2_{\rm CMS-LEP} = 2.30$ for two degrees of freedom. The left boundary of the points arises from the condition written in Eq. (8.26). The lower bounds on $\mu_{\rm LEP}$ and $\mu_{\rm CMS}$ follow from the upper limit on the singlet component of h_2 shown in Eq. (8.23).

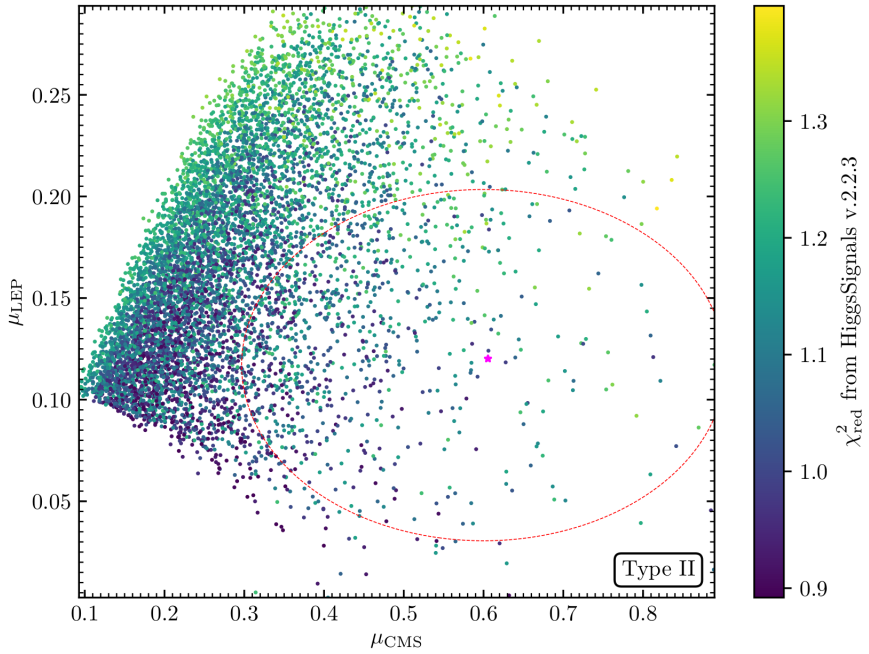

Figure 8.6: Type II: as in Fig. 8.5, but here the colors indicate the $\chi^2_{\rm red}$ from HiggsSignals. The best-fit point (magenta) has $\chi^2_{\rm red} = 1.237$ with 101 observations considered. The lowest (highest) value of $\chi^2_{\rm red}$ inside the 1σ ellipse is 0.9052 (1.3304).

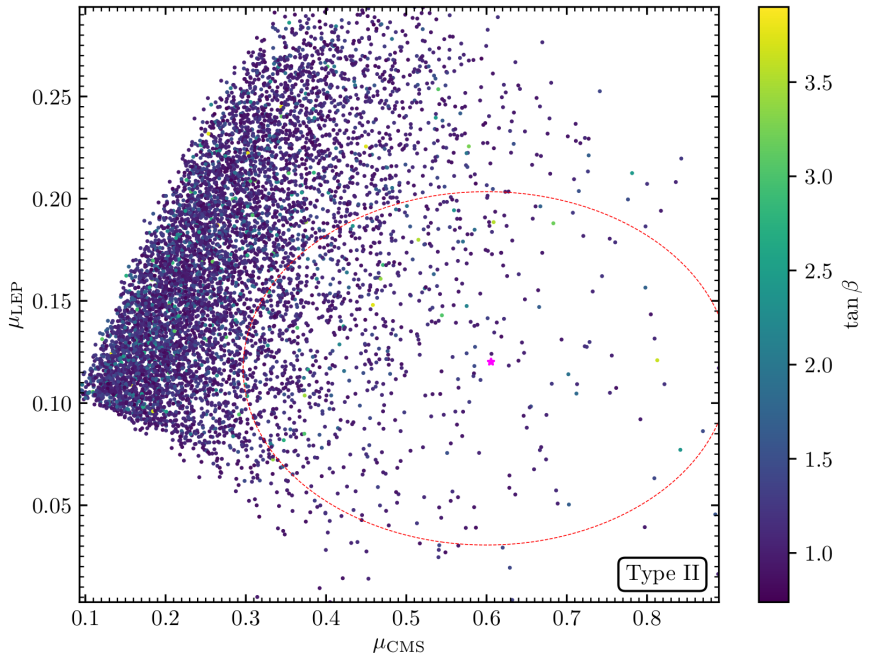

Figure 8.7: Type II: as in Fig. 8.5, but here the colors indicate the value of $\tan\beta$. The lowest (highest) value of $\tan\beta$ inside the 1σ ellipse is 0.7970 (3.748).

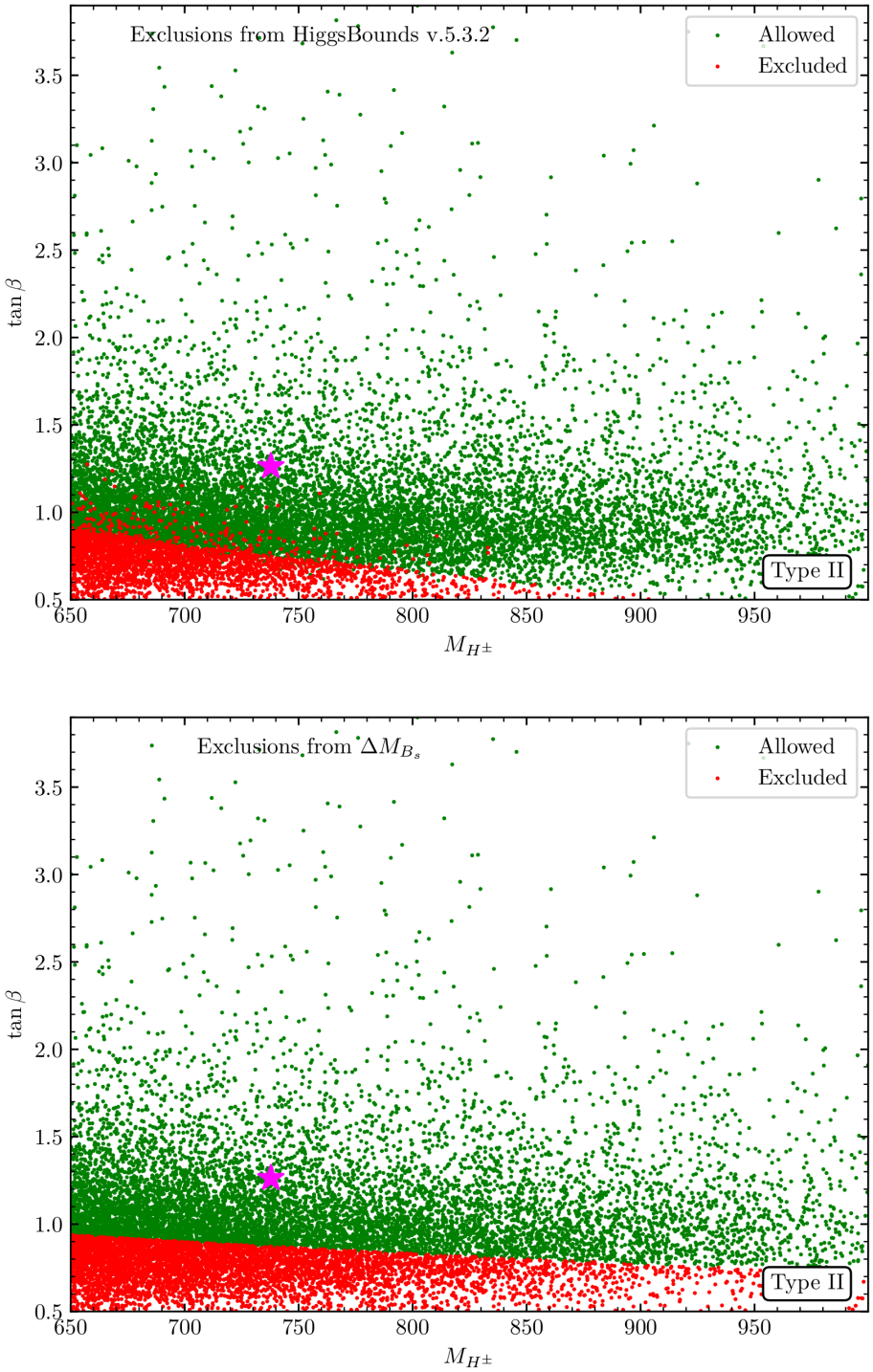

Figure 8.8: Type II: Allowed (*green*) and excluded (*red*) points considering direct searches (*top*) and flavor physics (*bottom*) in the $M_{H^\pm}$-$\tan\beta$ plane. The magenta star is the best-fit point.

m_{h_1}	m_{h_2}	m_{h_3}	m_A	$M_{H^\pm}$		
96.5263	125.09	535.86	712.578	737.829		
$\tan\beta$	α_1	α_2	α_3	m_{12}^2	v_S	
1.26287	1.26878	−1.08484	−1.24108	80644.3	272.72	
$\mathrm{BR}_{h_1}^{bb}$	$\mathrm{BR}_{h_1}^{gg}$	$\mathrm{BR}_{h_1}^{cc}$	$\mathrm{BR}_{h_1}^{\tau\tau}$	$\mathrm{BR}_{h_1}^{\gamma\gamma}$	$\mathrm{BR}_{h_1}^{WW}$	$\mathrm{BR}_{h_1}^{ZZ}$
0.5048	0.2682	0.1577	0.0509	$2.582 \cdot 10^{-3}$	0.0137	$1.753 \cdot 10^{-3}$
$\mathrm{BR}_{h_2}^{bb}$	$\mathrm{BR}_{h_2}^{gg}$	$\mathrm{BR}_{h_2}^{cc}$	$\mathrm{BR}_{h_2}^{\tau\tau}$	$\mathrm{BR}_{h_2}^{\gamma\gamma}$	$\mathrm{BR}_{h_2}^{WW}$	$\mathrm{BR}_{h_2}^{ZZ}$
0.5916	0.0771	0.0288	0.0636	$2.153 \cdot 10^{-3}$	0.2087	0.0261
$\mathrm{BR}_{h_3}^{tt}$	$\mathrm{BR}_{h_3}^{gg}$	$\mathrm{BR}_{h_3}^{h_1h_1}$	$\mathrm{BR}_{h_3}^{h_1h_2}$	$\mathrm{BR}_{h_3}^{h_2h_2}$	$\mathrm{BR}_{h_3}^{WW}$	$\mathrm{BR}_{h_3}^{ZZ}$
0.8788	$2.537 \cdot 10^{-3}$	0.0241	0.0510	$3.181 \cdot 10^{-3}$	0.0261	0.0125
BR_{A}^{tt}	BR_{A}^{gg}	$\mathrm{BR}_{A}^{Zh_1}$	$\mathrm{BR}_{A}^{Zh_3}$	BR_{A}^{bb}		
0.6987	$1.771 \cdot 10^{-3}$	0.1008	0.1981	$5.36 \cdot 10^{-4}$		
$\mathrm{BR}_{H^\pm}^{tb}$	$\mathrm{BR}_{H^\pm}^{Wh_3}$	$\mathrm{BR}_{H^\pm}^{Wh_1}$				
0.6000	0.3004	0.0984				

Table 8.5: Parameters of the best-fit point and branching ratios of the Higgs bosons in the type II scenario. Dimensionful parameters are given in GeV and the angles are given in radian.

In Fig. 8.5 the colors of the points indicate the value of $M_{H^\pm}$. Lower values for $M_{H^\pm}$ are preferred to fit the diphoton signal μ_{CMS}. We emphasize that the dependence of the branching ratio of h_1 into diphotons, and therefore of μ_{CMS}, on $M_{H^\pm}$ is due to the positive correlation between $M_{H^\pm}$ and the total decay width of h_1. When $M_{H^\pm}$ becomes larger the constraints from the oblique parameters induce also larger masses of the heavy Higgs boson m_{h_3} and the $\mathcal{CP}$-odd Higgs boson m_A. These masses are related to the mixing angles in the scalar sector via the tree-level perturbative unitarity and global minimum conditions. A large suppression of the total decay width of h_1, and thus an enhancement of $\mathrm{BR}_{h_1}^{\gamma\gamma}$, turns out to be more difficult to achieve for larger m_{h_3}, $M_{H^\pm}$ and M_A. The additional contributions to the diphoton decay width of diagrams with the charged Higgs boson in the loop has a minor dependence on $M_{H^\pm}$ for $M_{H^\pm} > 650$ GeV $\gg m_{h_1}$.

In Fig. 8.6 the colors indicate the reduced χ^2 (see Eq. (8.21)) from the test of the SM-like Higgs-boson properties with `HiggsSignals`. Various points fit both excesses simultaneously while also accommodating the properties of the SM-like Higgs boson h_2 at 125 GeV. This is quite remarkable, considering the fact that h_2 is contaminated substantially with a singlet component (see Eq. (8.24)).

We show in Fig. 8.7 a plot with the colors indicating the value of $\tan\beta$. An overall tendency can be observed that values of about $\tan\beta \sim 1$ are preferred in our scan. However, we find points covering the whole $\tan\beta$-range used in our scan within the 1σ ellipse of the excesses. In combination, the preference for low values of $M_{H^\pm}$ and $\tan\beta$ give rise to the fact that the scenario presented here will be in reach of direct searches for charged Higgs bosons at the LHC. In addition, flavor physics observables provide strict exclusion limits in this region of the parameter space (see the discussion in Sect. 7.3) [50].

This is illustrated in Fig. 8.8. In the previous plots we only showed BPs that passed

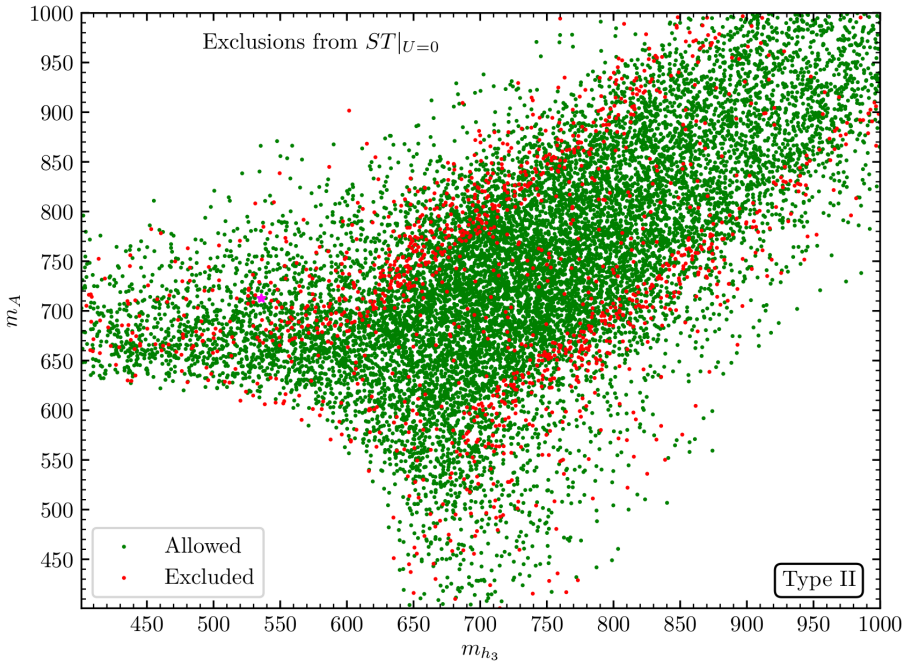

Figure 8.9: Type II: Points generated by `ScannerS` that fulfill the constraints on the STU parameters (*green*) in the $m_{h_3} - m_A$ plane. The points in *red* do not fulfill the constraints on ST with U assumed to be vanishing, which we imposed additionally in our scans (see Sect. 8.2.1).

all experimental constraints. In Fig. 8.8 we show also the rejected BPs in the $\tan\beta - M_{H^\pm}$ plane. In the left plot the red points were discarded because of constraints from direct searches using `HiggsBounds`, and in green the BPs that passed these constraints. In the right plot the same is shown regarding flavor physics observables. For values of $\tan\beta < 1$ direct searches are very constraining. The experimental analysis responsible for this excluded region is the search for charged Higgs bosons produced in association with a t- and a b-quark, and the subsequent decay of the charged Higgs boson to a tb-pair, performed by ATLAS [50]. Comparing to the right plot, we see that in the region of lower values of $M_{H^\pm}$, where the excesses are reproduced most "easily", bounds from flavor physics cover a similar parameter space than the direct searches for additional Higgs bosons. Values of $\tan\beta < 0.7$ are ruled out for the whole range of $M_{H^\pm}$, because of constraints from ΔM_{B_s}. For values of $M_{H^\pm}$ larger than ~ 750 GeV this constraint is far more restrictive than the constraints from collider searches.

In Tab. 8.5 we show the values of the free parameters and the relevant branching ratios of the singlet-like scaler h_1, the SM-like Higgs boson h_2 as well as all other (heavier) Higgs bosons of the model for the best-fit point of our scan which is highlighted with a magenta star in the plots. Remarkably, the branching ratio for the singlet-like scalar to photons is larger than the one of the SM-like Higgs boson. As explained in Sect. 8.2, this is achieved by a value of $\alpha_1 = 1.268 \sim \pi/2$. The most important BRs for the heavy Higgs bosons are those to the heaviest quarks, $h_3 \to t\bar{t}$, $A \to t\bar{t}$ and $H^\pm \to tb$, offering interesting prospects for future searches.

The presence of the extra singlet-like scalar h_1 leads to one more decay channel of $H^\pm$ into a $W^\pm$ boson and a $\mathcal{CP}$-even Higgs boson h_i compared to the 2HDM. Thus, these decays might provide crucial information regarding the possibility of distinguishing the

N2HDM from the 2HDM (see Sect. 8.2.4 for details). In almost the same manner, the decay of the $\mathcal{CP}$-odd Higgs boson A into the $Zh_{1,3}$ final state, with branching ratios of $\mathrm{BR}_A^{Zh_1} \sim 10\%$ and $\mathrm{BR}_A^{Zh_3} \sim 20\%$, respectively, might be detectable at the LHC or future colliders.

In the best-fit point, constraints from the oblique parameters lead to a $\mathcal{CP}$-odd Higgs boson mass m_A close to the mass of the charged Higgs boson $M_{H^\pm}$. As was explained in Sect. 7.3, the alternative criterion to be in agreement with EWPOs is that m_{h_3} is close to $M_{H^\pm}$, in which case m_A is not constrained regarding the STU parameters. In our scans, both possibilities occur, as can be seen in Fig. 8.9 in which we plot the BPs that fulfill the condition on STU implemented in `ScannerS`, and in red the points that, on top of that, fulfill the condition on ST, assuming U is vanishing (see Sect. 8.2.1). Note that there are no BPs with both m_A and m_{h_3} below ~ 650 GeV, because of the lower limit of $M_{H^\pm} \geq 650$ GeV.

The value of $\tan\beta$ in Tab. 8.5 is close to one, meaning that the best-fit point might be in range of future improved constraints both from direct searches at colliders as well as from flavor physics (see Fig. 8.8). More optimistically speaking, deviations from the SM predictions are expected in those observables if our explanation of the LEP and CMS excesses are implemented by nature. From the values for the mixing angles α_i we derive a singlet component of h_2 of $\Sigma_{h_2} \sim 19.5\%$. Therefore, deviations from the SM predictions are present in observables related to the SM-like Higgs boson which might be detectable at future collider experiments. We will discuss experimental prospects in detail in Sect. 8.2.4.

8.2.3 Type IV - flipped

The second type of the N2HDM where we expect to be able to fit both excesses simultaneously is the type IV or flipped scenario. We performed a scan over the same parameter ranges as stated in Eqs. (8.22), (8.23) and (8.24), and again imposing the condition shown in Eq. (8.26). We show the results of this scan in Figs. 8.10-8.12. As before, the colors indicate the charged Higgs-boson mass in Fig. 8.10, the reduced χ^2 from `HiggsSignals` in Fig. 8.11, and the value of $\tan\beta$ in Fig. 8.12, and only BPs fulfilling all theoretical and experimental constraints are depicted.

As in the type II scenario, a large number of BPs fit both the LEP and the CMS excesses simultaneously, while being in agreement with the measurements of the SM-like Higgs-boson properties (see Fig. 8.11). Various points inside the 1σ ellipse have a χ^2_{red} from `HiggsSignals` below one, indicating that the signal-strength predictions for the SM-like Higgs boson are on average within the 1σ uncertainties of each measurement. Similar to the type II analysis a clear preference of small values for $M_{H^\pm}$ and $\tan\beta$ is visible, also for the points outside the 1σ ellipse.

The exclusion boundaries from direct searches and from flavor physics are practically unchanged to the ones we found in the type II scenario. We show in Fig. 8.13 the allowed and excluded points of our scan considering only the collider searches (top) and flavor-physics observables (bottom) in the $\tan\beta$-$M_{H^\pm}$ plane. The most sensitive direct search is, as in type II, the production of $H^\pm$ in association with a tb-pair, and subsequent decay of $H^\pm$ to a tb-pair. For values of $\tan\beta < 1$, points with a charged Higgs mass up to 900 GeV can be excluded. The excluded region from flavor physics observable in the bottom plot of Fig. 8.13 is derived from predictions to the meson mass difference ΔM_{B_s}, which is unchanged w.r.t. the one from the type II scenario. The ΔM_{B_s} constraint is the dominant one regarding flavor observables for the range of $M_{H^\pm}$ and $\tan\beta$ scanned

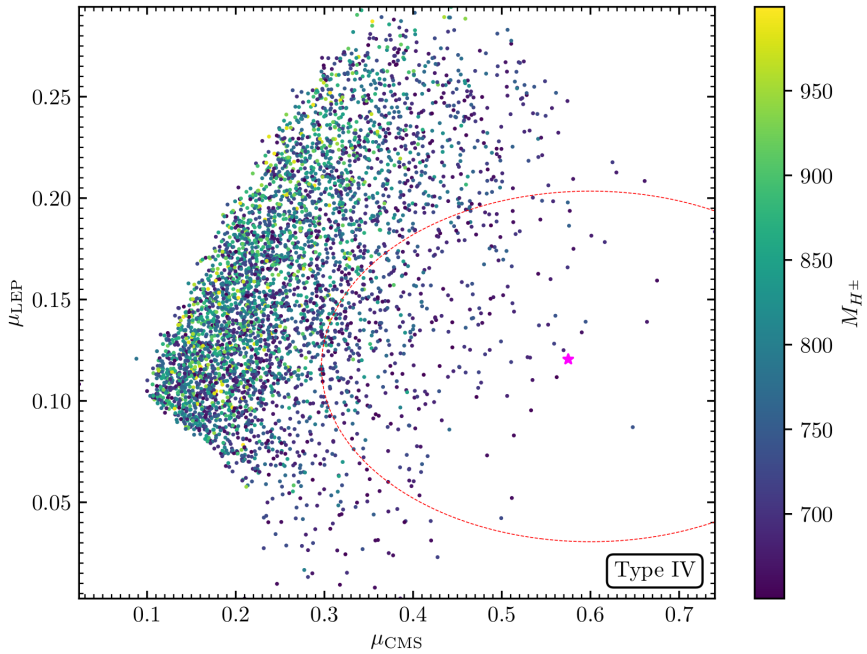

Figure 8.10: Type IV: the signal strengths $\mu_{\rm CMS}$ and $\mu_{\rm LEP}$ for each scan point respecting the experimental and theoretical constrains. The 1σ region of both excesses is shown by the red ellipse. The colors show the mass of the charged Higgs. The magenta star indicates the best-fit point. The lowest (highest) value of $M_{H^\pm}$ inside the 1σ ellipse is 650.01 (931.85) GeV.

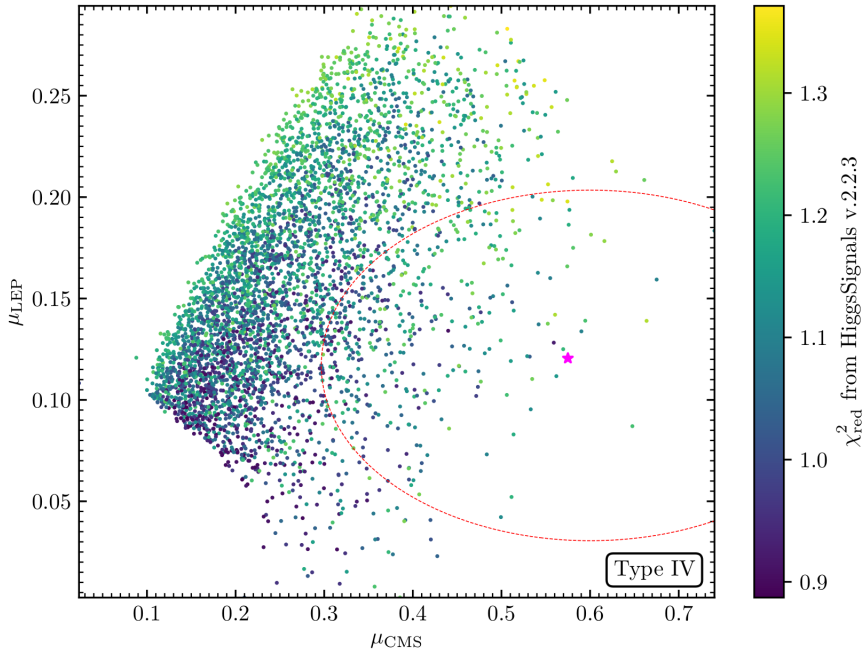

Figure 8.11: Type IV: as in Fig. 8.10, but here the colors indicate the $\chi^2_{\rm red}$ from HiggsSignals. The best-fit point (magenta) has $\chi^2_{\rm red} = 1.11286$ with 101 observations considered. The lowest (highest) value of $\chi^2_{\rm red}$ within the 1σ ellipse is 0.9073 (1.3435).

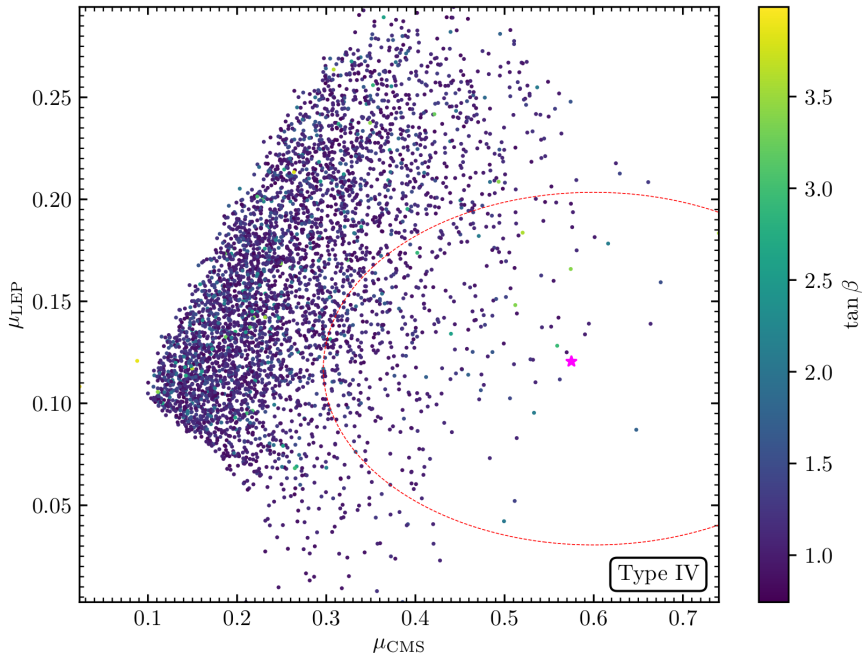

Figure 8.12: Type IV: as in Fig. 8.5, but here the colors indicate the value of $\tan\beta$. The lowest (highest) value of $\tan\beta$ within the 1σ ellipse is 0.7935 (3.592).

m_{h_1}	m_{h_2}	m_{h_3}	m_A	$M_{H^\pm}$		
97.8128	125.09	485.998	651.502	651.26		
$\tan\beta$	α_1	α_2	α_3	m_{12}^2	v_S	
1.3147	1.27039	−1.02829	−1.32496	41034.1	647.886	
$\text{BR}_{h_1}^{bb}$	$\text{BR}_{h_1}^{gg}$	$\text{BR}_{h_1}^{cc}$	$\text{BR}_{h_1}^{\tau\tau}$	$\text{BR}_{h_1}^{\gamma\gamma}$	$\text{BR}_{h_1}^{WW}$	$\text{BR}_{h_1}^{ZZ}$
0.4074	0.2071	0.1189	0.2483	$2.139 \cdot 10^{-3}$	0.0135	$1.579 \cdot 10^{-3}$
$\text{BR}_{h_2}^{bb}$	$\text{BR}_{h_2}^{gg}$	$\text{BR}_{h_2}^{cc}$	$\text{BR}_{h_2}^{\tau\tau}$	$\text{BR}_{h_2}^{\gamma\gamma}$	$\text{BR}_{h_2}^{WW}$	$\text{BR}_{h_2}^{ZZ}$
0.5363	0.0939	0.0345	0.0758	$2.247 \cdot 10^{-3}$	0.2267	0.0284
$\text{BR}_{h_3}^{tt}$	$\text{BR}_{h_3}^{gg}$	$\text{BR}_{h_3}^{h_1h_1}$	$\text{BR}_{h_3}^{h_1h_2}$	$\text{BR}_{h_3}^{h_2h_2}$	$\text{BR}_{h_3}^{WW}$	$\text{BR}_{h_3}^{ZZ}$
0.8078	$2.707 \cdot 10^{-3}$	0.0124	$2.111 \cdot 10^{-3}$	0.0119	0.1085	0.0517
BR_{A}^{tt}	BR_{A}^{gg}	$\text{BR}_{A}^{Zh_1}$	$\text{BR}_{A}^{Zh_2}$	$\text{BR}_{A}^{Zh_3}$	BR_{A}^{bb}	
0.7090	$1.940 \cdot 10^{-3}$	0.1007	$9.652 \cdot 10^{-3}$	0.1780	$6.49 \cdot 10^{-4}$	
$\text{BR}_{H^\pm}^{tb}$	$\text{BR}_{H^\pm}^{Wh_3}$	$\text{BR}_{H^\pm}^{Wh_1}$				
0.6820	0.2046	0.1024				

Table 8.6: Parameters of the best-fit point and branching ratios of the Higgs bosons in the type IV scenario. Dimensionful parameters are given in GeV and the angles are given in radian.

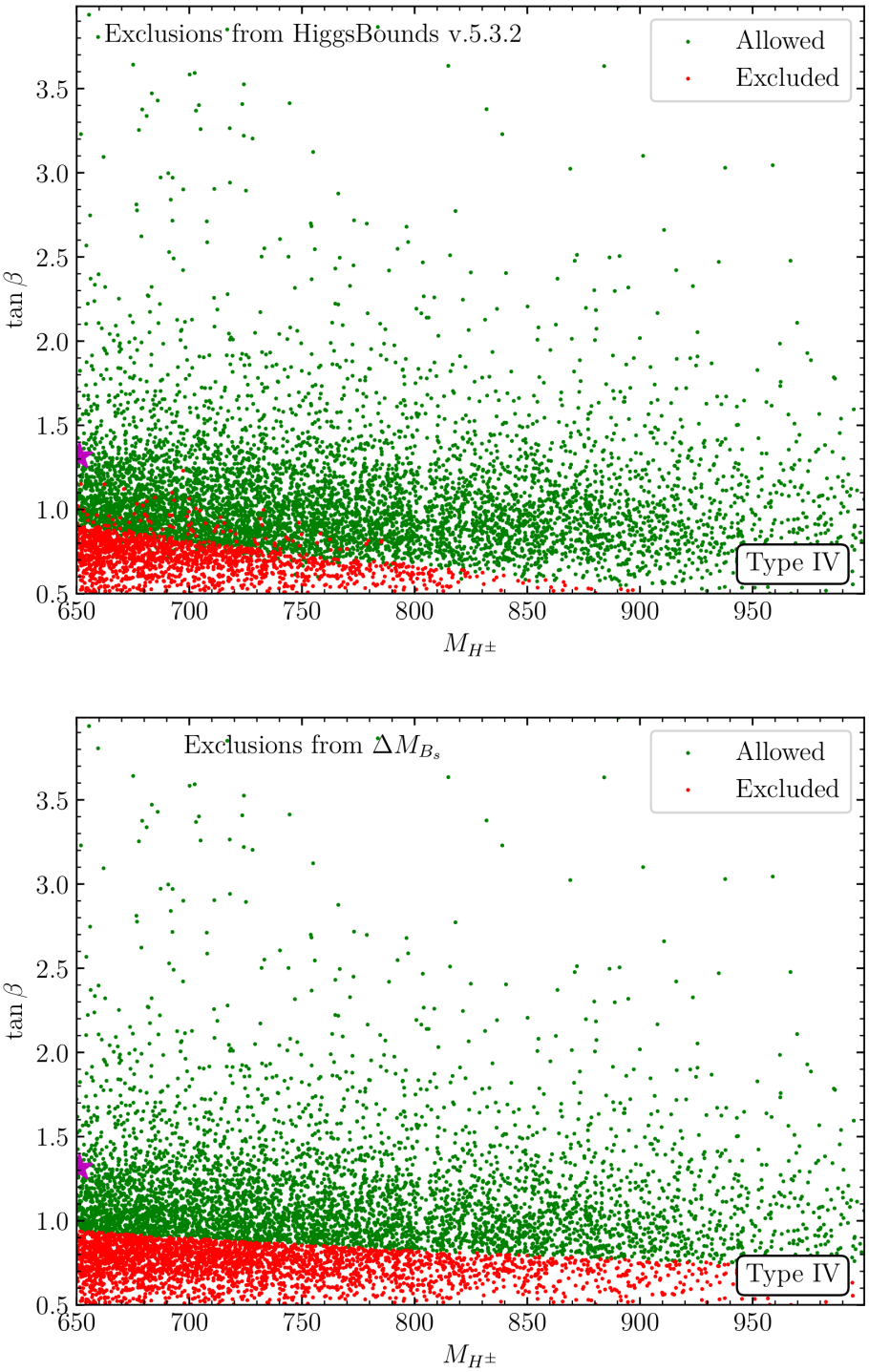

Figure 8.13: Allowed (*green*) and excluded (*red*) points considering direct searches (*left*) and flavor physics (*right*) in the $M_{H^\pm}$-tan β plane. The magenta star is the best-fit point.

here, assuming that the exclusions from BR($B_s \to \mu^+\mu^-$) constraints in the 2HDM do not change by more than 20% due to the presence of the additional real singlet in the N2HDM [41].

The details of our best-fit point of the scan in the N2HDM type IV, indicated with the magenta star in Figs. 8.10-8.13, are listed in Tab. 8.6. The value of the charged Higgs-boson mass is just on the lower end of the scanned range. Comparing to the best-fit point of our scan in the N2HDM type II, shown in Tab. 8.5, we observe that the values for $\tan\beta$ and the mixing angles in the $\mathcal{CP}$-even scalar sector α_i are very similar. This is due to the fact that the effective coefficients of the couplings of the Higgs bosons to quarks and gauge bosons are the same. The decays of the heavier Higgs bosons are similar to the type II best-fit point. In particular, the decays of the heavy $\mathcal{CP}$-even Higgs boson h_3 into a pair of lighter $\mathcal{CP}$-even states $h_{1,2}$ is not prominent in both the best-fit points in type II and type IV. The range scanned for m_{h_3} is well above the threshold where the decay into a pair of top quarks becomes possible which is always dominant in this regime. As in the best-fit point of the scan in the type II scenario, the decays of the charged Higgs boson $H^\pm$ or the $\mathcal{CP}$-odd Higgs boson A into a gauge boson plus a $\mathcal{CP}$-even Higgs boson h_1 or h_3 are more promising signals. For BPs, in which $m_{h_3} \sim M_{H^\pm}$ and m_A smaller, the decay of h_3 to the ZA final state is present instead. This decay can also lead to interesting collider signatures.

The striking difference between the best-fit points in both types is that, even though the suppression of the branching ratio of h_1 to b-quarks is larger in type IV, the branching ratio of the decay of h_1 into photons remains smaller. As already discussed in Sect. 8.2, in the parameter region in which the excesses can be accommodated, there is an enhancement of the decay width into τ-leptons in type IV, whereas in type II the decay is suppressed in this regime. Hence, the value of $\mathrm{BR}_{h_1}^{\tau\tau}$ in Tab. 8.6 is roughly five times larger than the one in Tab. 8.5.

This circumstance is not a particular feature of the best-fit point, but a general difference between type II and type IV. To illustrate this, we show in Fig. 8.14 the branching ratio for the decay of h_1 into a diphoton pair for type II (top) and type IV (bottom) as a function of the absolute value of the ratio of the effective coupling coefficients $c_{h_1 b\bar{b}}$ and $c_{h_1 t\bar{t}}$. The blue and red points are the ones lying inside and outside the 1σ ellipse regarding $\chi^2_{\mathrm{CMS-LEP}}$, respectively. When $|c_{h_1 b\bar{b}}/c_{h_1 t\bar{t}}|$ is small, $\mathrm{BR}_{h_1}^{\gamma\gamma}$ receives an enhancement and it is possible to fit the CMS excess. This is why the blue points in Fig. 8.14 are located below a certain value of the ratio of the couplings on the horizontal axis. On average, the type II scenario features larger values of $\mathrm{BR}_{h_1}^{\gamma\gamma}$. We can understand this by comparing the branching ratios for the decay of h_1 into a pair of τ-leptons which is shown in Fig. 8.15. Here, the conceptual difference between the type II model and the flipped scenario becomes visible. In the region, in which the excesses can be fitted, $\mathrm{BR}_{h_1}^{\tau\tau}$ is suppressed in type II, but enhanced in type IV, owing to the fact that the coupling to leptons scales with the same factor as $c_{h_1 b\bar{b}}$ in type II, but proportional to $c_{h_1 t\bar{t}}$ in type IV.

In Fig. 8.16 we show the predicted signal strengths for both excesses, with colors indicating the singlet component of h_1. Comparing both plots, it becomes apparent that the circumstance described above yields a substantial suppression of μ_{CMS} in the type IV scenario compared to the type II scenario. For similar values of the singlet component Σ_{h_1}, the type II scenario can reach larger μ_{CMS}, whereas the size of μ_{LEP} is very similar in both scenarios. Remarkably, the type II scenario can reach values of $\mu_{\mathrm{CMS}} \sim 1$, meaning that the signal strength prediction for μ_{CMS} is as big as the one of a hypothetical SM-like

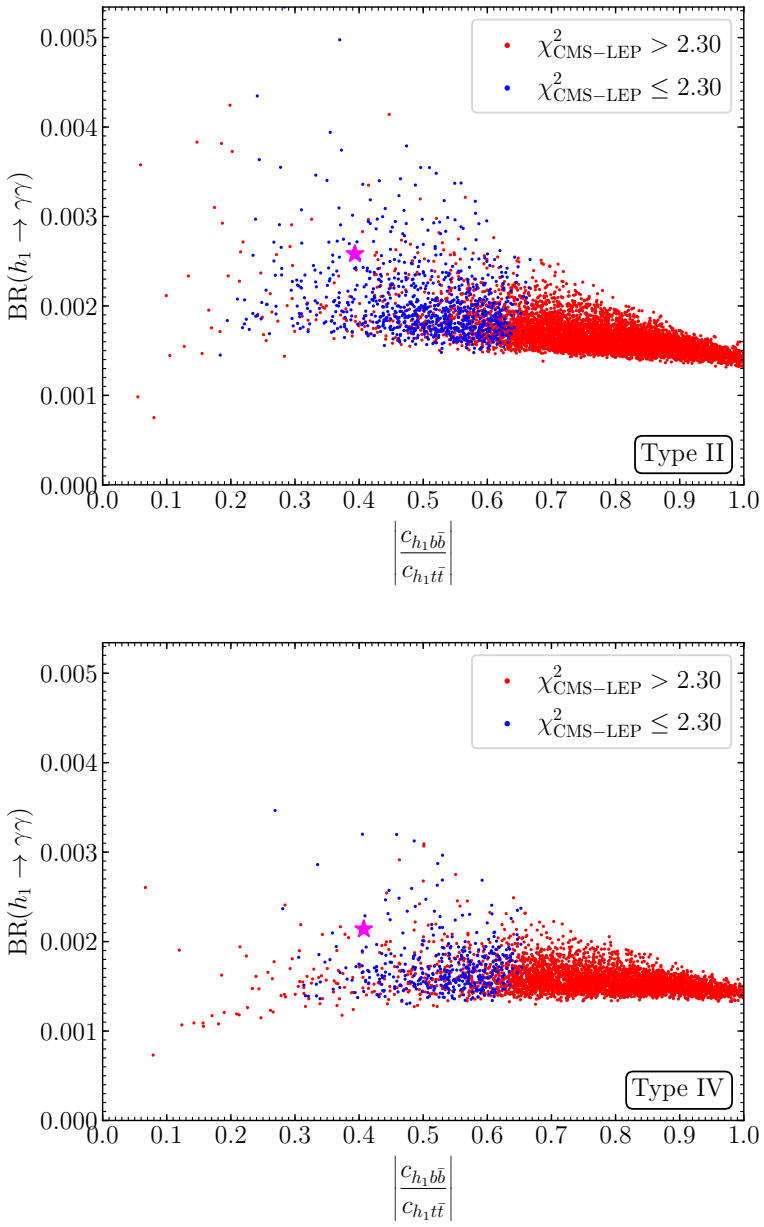

Figure 8.14: Branching fraction of the decay of h_1 into two photons for each BP respecting the experimental and theoretical constrains in the type II (*top*) and the type IV scenario (*bottom*), as a function of the ratio of the coupling of h_1 to bottom and top quarks normalized to the SM prediction. The blue points have $\chi^2_{\text{CMS-LEP}} \leq 2.30$, while the red points have $\chi^2_{\text{CMS-LEP}} > 2.30$.

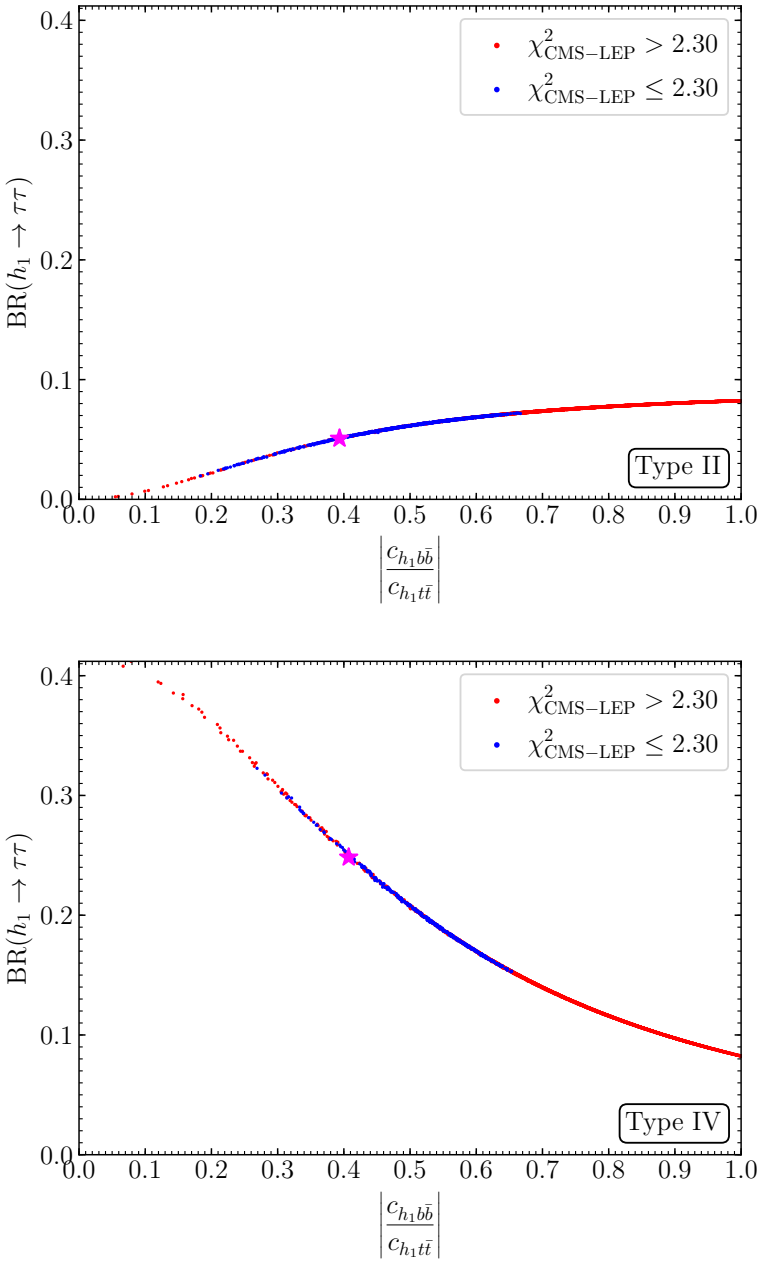

Figure 8.15: As in Fig. 8.14 for the branching fraction of the decay of h_1 into two τ-leptons.

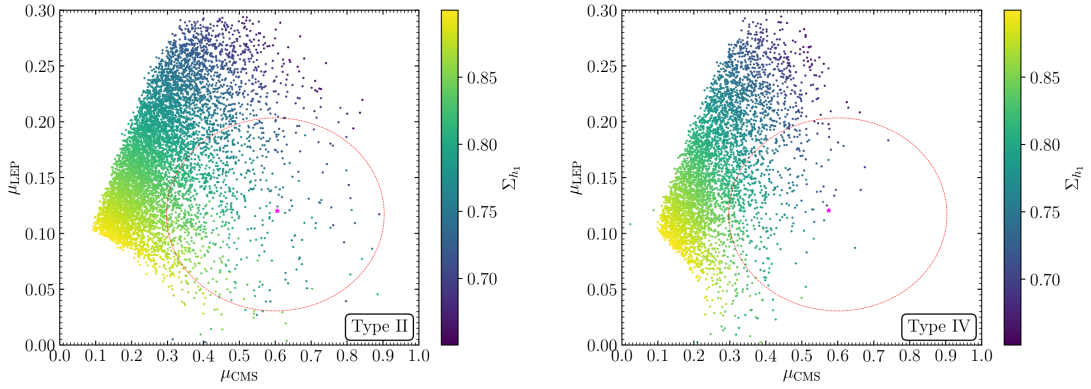

Figure 8.16: Signal strengths μ_{CMS} and μ_{LEP} for each parameter point respecting the experimental and theoretical constrains in the type II (*left*) and the type IV scenario (*right*). The 1σ region of both excesses is shown by the red ellipse. The colors show the singlet component of h_1. The magenta star is the best-fit point.

Higgs boson at the same mass, even though it is dominantly singlet-like. In the type IV scenario, on the other hand, there is no point above the upper 1σ limit of $\mu_{\text{CMS}} = 0.8$.

8.2.4 Prospects

Our explanation of the LEP and CMS excesses, making use of a singlet-like Higgs boson that acquires substantial couplings to the SM particle sector via its mixing with the SM-like Higgs boson leads to two distinct ways of testing the scenario at current and future collider experiments. Firstly, the couplings of the SM-like Higgs boson are modified w.r.t. SM prediction. Precise measurements of these couplings at the LHC, and perhaps a future lepton collider like the ILC, will constrain these deviations to high precision. Secondly, the additional Higgs bosons, such as the singlet-like scalar with a mass of ~ 96 GeV, can be produced directly at particle colliders. Being close to the Z-boson peak, a discovery of h_1 at 5σ confidence level at the LHC is particularly challenging, since a hadron collider generally suffers a huge amount of hadronic background activity. Thus, at the LHC searches for the other Higgs bosons might be more promising. However, a future lepton collider like the ILC could improve the prospects on the direct detection of light Higgs boson significantly. We briefly discuss both possibilities of testing our scenario experimentally, i.e., indirectly via the SM-like Higgs-boson couplings or directly via searches for additional Higgs bosons, in the following.

Indirect searches

Currently, uncertainties on the measurement of the coupling strengths of the SM-like Higgs boson at the LHC are still large. At the 1σ level, they are of the same order or larger than the modifications of the couplings present in our analysis in the N2HDM [22, 51, 52]. Once the complete $300\,\text{fb}^{-1}$ collected at the LHC are analyzed, the statistical uncertainties will be drastically reduced, yielding tighter constraints on the coupling coefficients. Even more improved constraints are expected from the LHC after the high-luminosity upgrade (HL-LHC), when the planned amount of $3000\,\text{fb}^{-1}$ integrated luminosity will have been collected [23]. Furthermore, a future linear e^+e^- collider like the ILC could improve the precision measurements of the Higgs-boson couplings, far beyond the preci-

sion of the LHC [23, 53].[5] A lepton collider not only has drastically reduced background compared to a hadron collider, but is also capable of measuring the total width of the SM-like Higgs boson (and thus also the coupling modifiers) without model assumptions, by measuring the recoil energy in the Higgstrahlung production channel.

Starting from the assumptions that no deviations from the SM predictions will be found, several studies have been performed to estimate the future constraints on the coupling modifiers of the SM-like Higgs boson at the LHC [23, 54–57] and the ILC [23, 58–63]. We compare here our BPs to the expected precisions of the LHC and the ILC as they are reported in Refs. [62, 63], however neglecting possible correlations of the coupling modifiers.

In Fig. 8.17 we show the effective coupling coefficient of the SM-like Higgs boson h_2 to τ-leptons on the horizontal axis against the coupling coefficient to b-quarks (top) and to t-quarks (bottom) for type II (blue) and type IV (red), for the points that passed all the experimental and theoretical constraints. In particular, we verified that the points are in agreement with the LHC measurements of the SM-like Higgs-boson properties using `HiggsSignals`. In the top plot the blue points lie on a diagonal line, because in type II the couplings to leptons and to down-type quarks scale identically. Similarly, in the bottom plot the red points lie on the diagonal, because in type IV the coupling to leptons scales in the same way as the coupling to up-type quarks. The current measurements on the coupling modifiers by ATLAS [51] and CMS [52] are shown as black ellipses, although their uncertainties are still very large.

The magenta ellipses in each plot show the expected precision of the HL-LHC measurements taken from from Ref. [63]. The current uncertainties and the HL-LHC analysis are based on the coupling modifier, or κ-framework, in which the tree-level couplings of the SM-like Higgs boson to vector bosons, the top quark, the bottom quark, the τ- and the μ-lepton, and the three loop-induced couplings to $\gamma\gamma$, gg and $Z\gamma$ receive a factor κ_i quantifying potential modifications from the SM predictions. These modifiers are then constrained using a global fit to projected HL-LHC data assuming no deviation from the SM prediction will be found. The uncertainties found for the κ_i can directly be applied to the future precision of the coupling modifiers $c_{h_i\ldots}$ we use here. We stress that the κ-framework is not model-independent, and can potentially underestimate uncertainties compared to an effective field theory approach. In Fig. 8.17 we depict the uncertainties obtained under the assumptions that no decay of the SM-like Higgs boson to BSM particles is present ($\Gamma_{h_2}^{\mathrm{BSM}} = 0$), and that current systematic uncertainties will be reduced in addition to the reduction of statistical uncertainties due to the increased statistics.

The green and the orange ellipses show the expected uncertainties when the HL-LHC results are combined with projected data from the ILC after the 250 GeV phase and the 500 GeV phase, respectively, taken from Ref. [62]. This analysis is based on a pure effective field theory calculation. Thus, it can in principle capture modifications of the SM-like Higgs-boson couplings that go beyond a simple rescaling, as is assumed in the κ-framework. Therefore, to be able to combine both approaches, the effective field theory calculation was done supplementing further assumptions. This concerns, in particular, the couplings to vector bosons. Modifications that are impossible in the κ-framework were excluded artificially in the effective field theory approach, by recasting the fit setting two parameters related to the couplings to the Z boson and the W boson to zero (for details we refer to Ref. [62]). This theory input required for the combined

[5] Similar results can be obtained for CLIC, FCC-ee and CEPC. We will focus on the ILC prospects here using the results of Ref. [53].

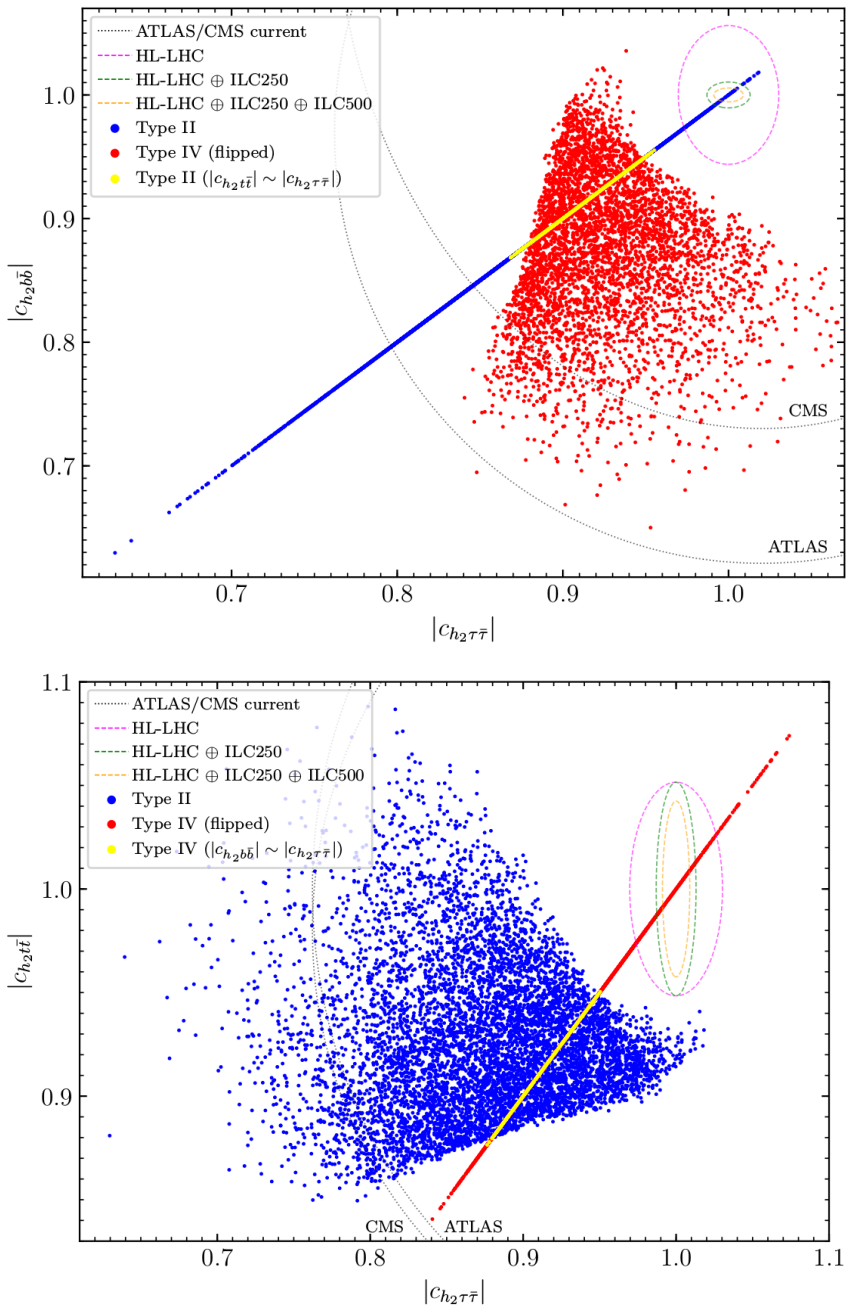

Figure 8.17: BPs of our analysis in the type II (*blue*) and type IV (*red*) scenario in the $|c_{h_2\tau\bar{\tau}}|$-$|c_{h_2b\bar{b}}|$ plane (*top*) and the $|c_{h_2\tau\bar{\tau}}|$-$|c_{h_2t\bar{t}}|$ plane (*bottom*). In the upper plot we highlight in yellow the points of the type II scenario that overlap with points from the type IV scenario in the lower plot, i.e., points with $|c_{h_2t\bar{t}}| \sim |c_{h_2b\bar{b}}| \sim |c_{h_2\tau\bar{\tau}}|$. In the lower plot we highlight in yellow the points of the type IV scenario that overlap with points from the type II scenario in the upper plot. The dashed ellipses are the projected uncertainties at the HL-LHC [63] (*magenta*) and the ILC [62] (*green* and *orange*) of the measurements of the coupling modifiers at the 68% confidence level, assuming that no deviation from the SM prediction will be found (more details in the text). We also indicate with the dotted black lines the 1σ ellipses of the current measurements from CMS [52] and ATLAS [51].

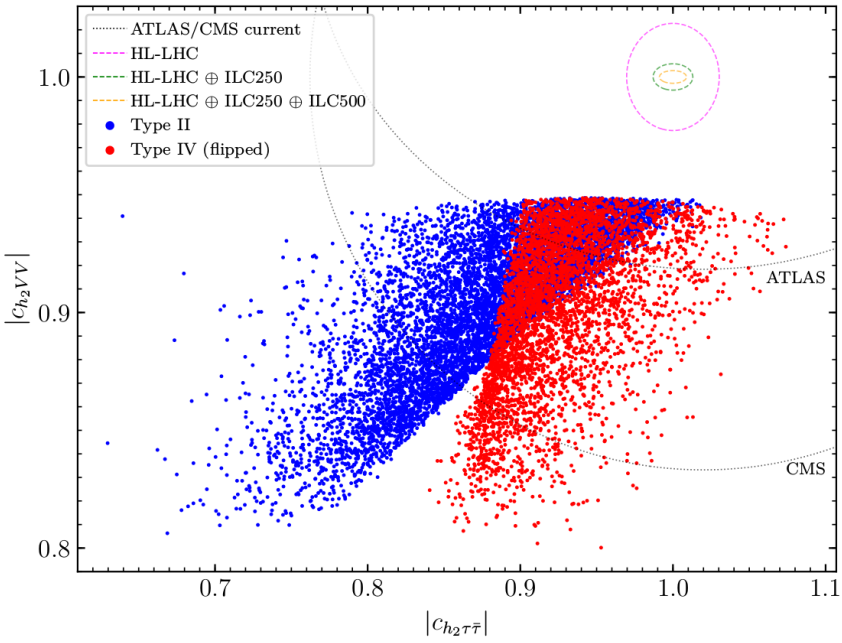

Figure 8.18: As in Fig. 8.17, but with $|c_{h_2VV}|$ on the vertical axis.

LHC+ILC analysis has to be kept in mind in the following, when we quote specific future uncertainties.

While current constraints on the SM-like Higgs-boson properties allow for large deviations of the couplings of up to 40%, the allowed parameter space will be significantly reduced by the expected constraints from the HL-LHC and the ILC. For instance, the uncertainty of the coupling to b-quarks will shrink below 4% at the HL-LHC, and of the coupling to τ-leptons it is expected to be at 2% at the HL-LHC. The ILC could reduce these uncertainties further to the per-mille level. For the coupling to t-quarks, on the other hand, the ILC cannot improve substantially the expected uncertainty of the HL-LHC (but permit a model-independent analysis). Still, a reduction of the uncertainty by roughly a factor of three is expected. The modifications of the SM-like Higgs-boson couplings in our BPs are many times larger than the anticipated experimental uncertainties. Thus, our explanation of the LEP and the CMS excesses within the N2HDM is testable indirectly using future precision measurements of the SM-like Higgs-boson couplings. This is especially important, since these measurement (at least at the HL-LHC) will be carried out in the near future, so that our solution will be experimentally inspected without demanding any experimental analysis specifically dedicated to our scenario.

Comparing both plots in Fig. 8.17, we see that there are no BPs coinciding with the SM prediction regarding the three coupling coefficients shown. This implies that, once these couplings are measured precisely by the HL-LHC and the ILC, a deviation of the SM prediction has to arise in at least one of the couplings, if our explanation of the excesses is correct. Accordingly, if no deviation from the SM prediction regarding these couplings will be measured, our explanation would be ruled out entirely. Of course, as we explicitly demanded a lower limit on the singlet component of the SM-like Higgs boson of $\Sigma_{h_2} \geq 10\%$ in our scans, the second lightest Higgs boson unavoidably exhibits deviations from the SM regarding the coupling coefficients. However, BPs with $\Sigma_{h_2} < 10\%$ cannot accommodate both excesses, as we checked with dedicated scans, because in that case the doublet component of h_1 is too small. Hence, the conclusions drawn here are not

affected by demanding $\Sigma_{h_2} \geq 0.1$.

In case a deviation from the SM prediction will be found, the predicted scaling behavior of the coupling coefficients in the type II scenario (upper plot) and the type IV scenario (lower plot), might lead to distinct possibilities for the two models to accommodate these possible deviations. Precision measurements of the SM-like Higgs-boson couplings could then be used to exclude either the type II or the type IV scenario. This holds for all points except the ones highlighted in yellow in Fig. 8.17. The yellow points are a subset of points of our scans that, if such deviations of the SM-like Higgs-boson couplings will be measured, could correspond to a BP of both the scan in the type II and the type IV scenario. However, this subset of points is confined to the diagonal lines of both plots which constitutes a very specific region of the overall allowed parameter space. For the type II scenario, in the upper plot, the yellow points are determined by the additional constraint that $|c_{h_2 t\bar{t}}| \sim |c_{h_2 \tau\bar{\tau}}|$ which is exactly true in the type IV scenario. For the type IV scenario, in the lower plot, the yellow points are determined by the additional constraint that $|c_{h_2 b\bar{b}}| \sim |c_{h_2 \tau\bar{\tau}}|$ which is exactly true in the type II scenario.

For completeness we show in Fig. 8.18 the absolute value of the coupling modifier of the SM-like Higgs boson w.r.t. the vector boson couplings $|c_{h_2 VV}|$ on the vertical axis. Again, the parameter points of both types show deviations larger than the projected experimental uncertainty at HL-LHC and ILC. The BPs closest to the SM prediction correspond to the ones with lowest singlet component Σ_{h_2}. One can show that

$$|c_{h_2 VV}|^2 \sim 1 - \Sigma_{h_2} \ , \tag{8.28}$$

so that there are no BPs above $|c_{h_2 VV}| \sim 0.95$ due to the uppwe limit of $\Sigma_{h_2} \geq 0.1$ in our scans. However, as already emphasized, BPs with lower Σ_{h_2}, potentially lying within the colored ellipse in Fig. 8.18, cannot accommodate the LEP and CMS excesses, so that they are of no relevance here.

Direct searches

Direct searches for additional Higgs bosons are promising ways of testing our scenarios. As already mentioned, despite the fact that the diphoton bump has persisted through LHC Run I and II, a definite discovery of the possible 96 GeV Higgs boson is particularly challenging at the LHC. However, it is worth exploring the possibility of discovering the remaining Higgs boson of the N2HDM in future runs of the LHC. The search for the charged Higgs bosons appears to be promising in the region of low $\tan\beta$, where we already encountered strong bounds from current searches (see Figs. 8.8 and 8.13). Stronger constraints or discovery signs of a charged Higgs boson in the region between 600 GeV and 950 GeV are expected once more data is collected. Prospects for a 5σ discovery in the charged Higgs-boson searches can be found in Ref. [64].

For larger values of $\tan\beta$ the production of the charged Higgs boson in association with a decay into a W boson and a lighter $\mathcal{CP}$-even Higgs boson is a very promising signal. As already emphasized in Sect. 8.2.2, these signatures are particularly interesting, because they can be used to distinguish between the N2HDM and the 2HDM. We show in Figs. 8.19-8.21 the branching ratios of the charged Higgs boson decaying into $W^\pm h_i$ final states as a function of $M_{H^\pm}$ for the BPs that fulfill all theoretical and experimental constraints in the type II scenario (the situation is analogues in type IV). The colors indicate if the value of $\chi^2_{\text{CMS}-\text{LEP}}$ is below or above 2.30 for each BP. The decay into the SM-like Higgs boson h_2 shown in Fig. 8.20 is the smallest of the three. This is because the

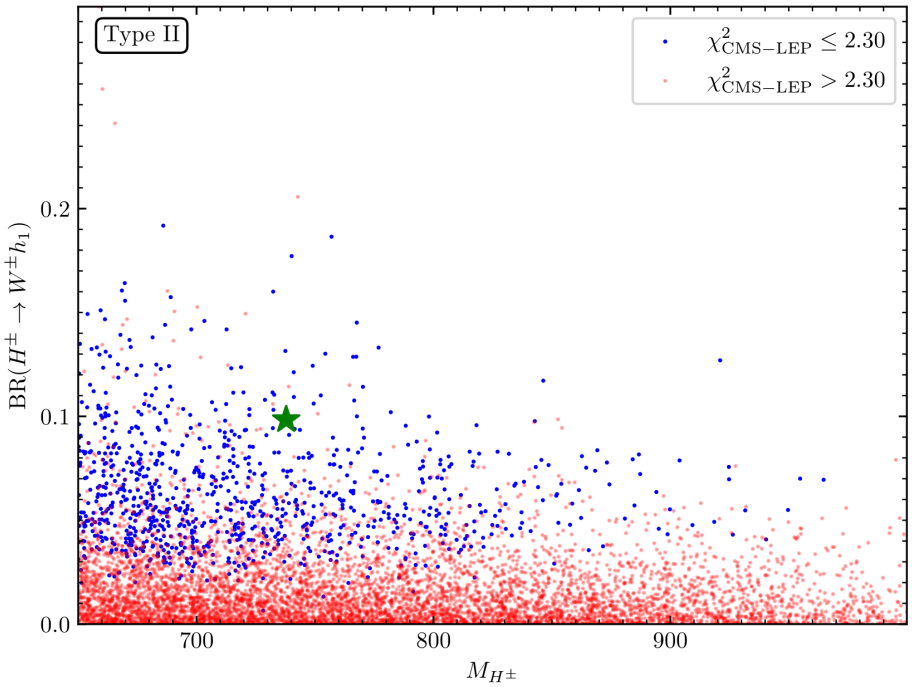

Figure 8.19: Type II: $\text{BR}(H^\pm \to W^\pm h_1)$ versus $M_{H^\pm}$ for the points fulfilling all theoretical and experimental constraints, with the colors indicating if the point fits both excesses within 1 σ accuracy (*blue*) or not (*red*).

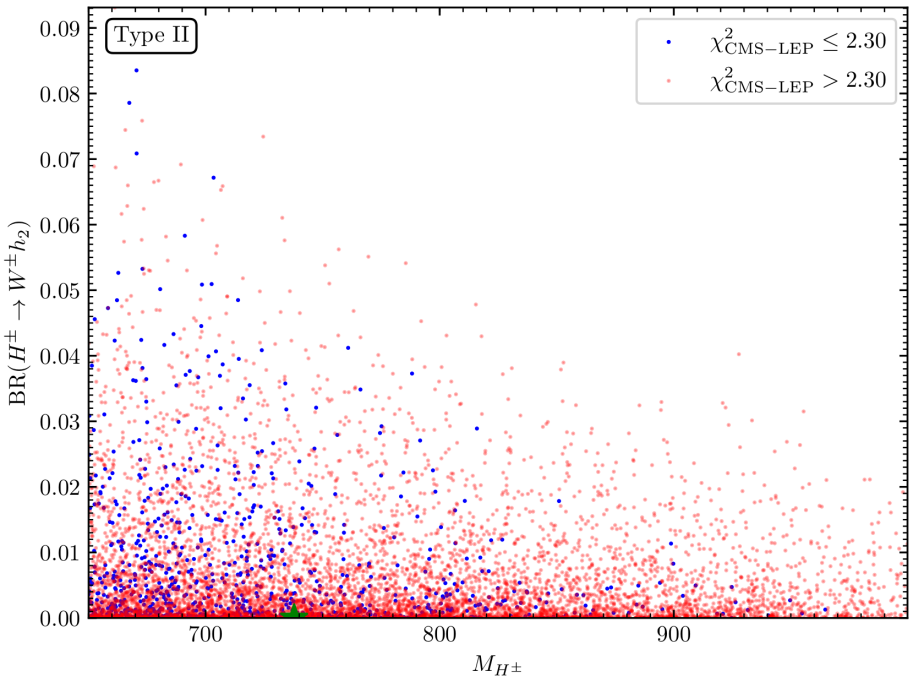

Figure 8.20: Type II: As in Fig. 8.19 for $\text{BR}(H^\pm \to W^\pm h_2)$.

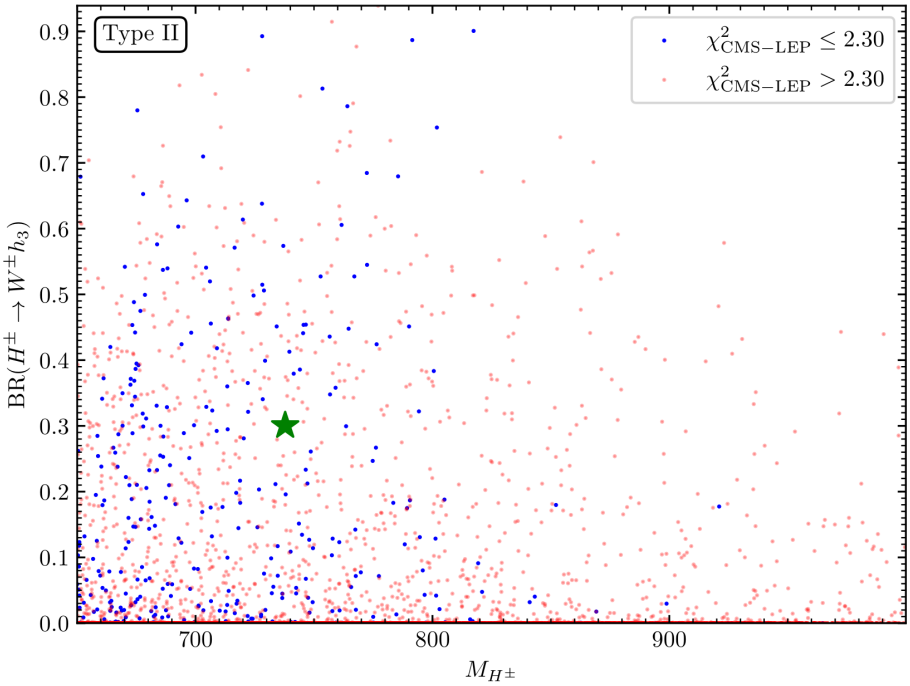

Figure 8.21: Type II: As in Fig. 8.19 for $\text{BR}(H^\pm \to W^\pm h_3)$.

tree-level couplings $c_{H^\pm W^\pm h_i}$ vanish in the limit in which the corresponding h_i becomes SM-like (see Tab. 6 in Ref. [30]). The decay into the heavy Higgs boson h_3 (see Fig. 8.21) is the largest of the three if kinematically possible. This is in complete analogy to the 2HDM. However, in the N2HDM the decay with the light singlet-like scalar h_1 in the final state provides a third option with fairly large branching ratios. For our solution to the LEP and CMS excesses this is of particular importance, because, as can bee seen in Fig. 8.21, the BPs that fit the excesses at the 1σ level (blue) tend to have larger branching ratios. The reason for this is that both the signal strengths μ_{LEP} and μ_{CMS}, as well as the couplings of h_1 to gauge bosons, demand a sizable doublet component. Thus, the decay $H^\pm \to W^\pm h_1$ could constitute a promising signal related to $H^\pm$ beyond the decays to third family lepton, and precise information about the branching ratios could help to distinguish the N2HDM from the 2HDM. The prospects for the searches for the heavy neutral Higgs bosons or the $\mathcal{CP}$-odd Higgs boson A, decaying dominantly to $t\bar{t}$, may also be promising. However, we are not aware of corresponding HL-LHC projections. The decays of h_3 or A into a Z boson and a lighter Higgs boson can be relevant for future searches looking for Higgs cascades.

In contrast to the LHC, e^+e^- colliders show good prospects for the search of light scalars [53, 65], such that the singlet-like Higgs boson at ~ 96 GeV can be looked for directly. The main production channel in this mass range is the Higgsstrahlung process $e^+e^- \to h_1 Z$. The LEP collaboration has previously performed such searches [16], which resulted in the 2σ excess given by μ_{LEP}. The ILC, with its much higher luminosity and the possibility of using polarized beams, has a substantially higher potential to discover such particles.

In Fig. 8.22 and Fig. 8.23 we show the bounds from LEP and the projected bounds from the ILC on the cross section for the Higgsstrahlung production of h_1 normalized to the SM prediction which is given here by the coupling coefficient $c_{h_1 VV}$ squared, in association with a subsequent decay of h_1 to a pair of b-quarks. The expected bounds for

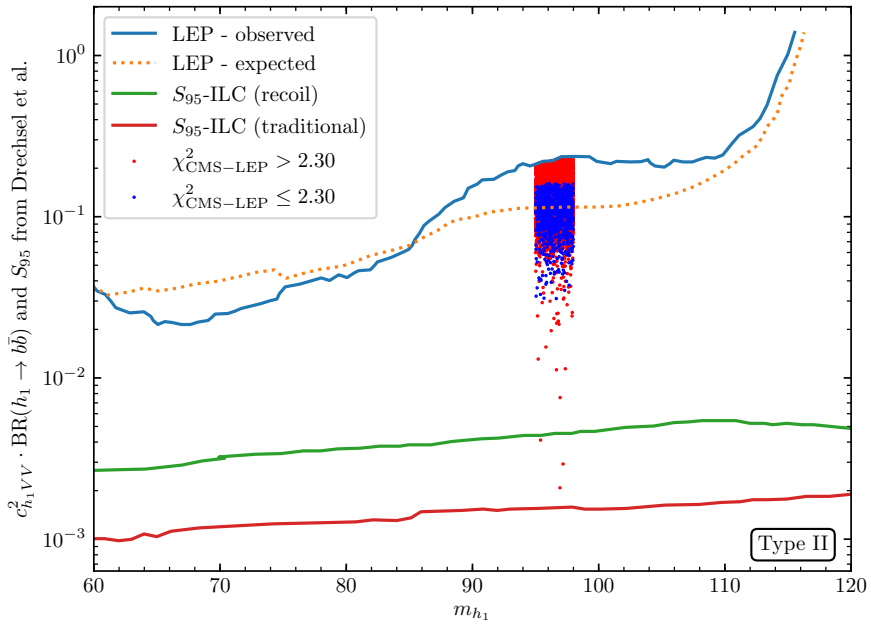

Figure 8.22: The 95% CL expected (*orange dashed*) and observed (*blue*) upper bounds on the Higgsstrahlung production process with associated decay of the scalar to a pair of bottom quarks at LEP [16]. Expected 95% CL upper limits on the Higgsstrahlung production process normalized to the SM prediction S_{95} at the ILC using the traditional (*red*) and the recoil technique (*green*) as described in the text [53]. Also shown are the points of our scan in the type II scenario which lie within (*blue*) and outside (*red*) the 1σ ellipse regarding the CMS and the LEP excesses.

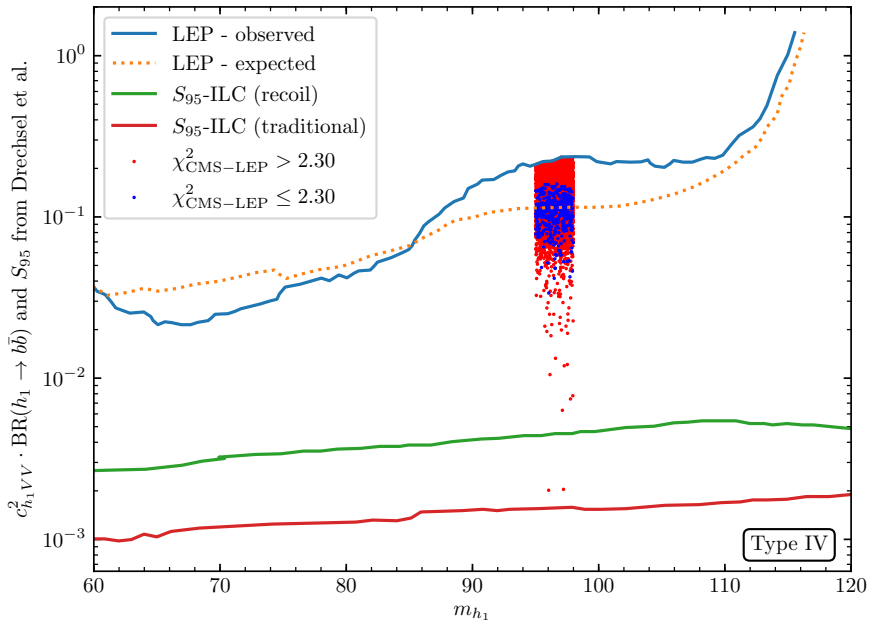

Figure 8.23: As in Fig. 8.22, but with the BPs of the scan in the type IV scenario.

the ILC correspond to a center-of-mass energy of $\sqrt{s} = 250$ GeV with beam polarizations (P_{e^-}, P_{e^+}) of $(-80\%, +30\%)$, and an integrated luminosity of $2000\,\text{fb}^{-1}$ [53]. The quantity S_{95} used in Ref. [53] corresponds to an upper limit at the 95% confidence level on the cross section times branching ratio generated within the 'background only' hypothesis, where the cross section has been normalized to the reference SM-Higgs cross section and the BRs have been assumed to coincide with the SM values. Hence, we take the obtained limits to be valid for the total cross section times branching ratio. The green bound is obtained using the more conservative recoil technique, where only the recoil mass distribution of the di-muon system produced in Z decay is analyzed [66]. The red bound, on the other hand, is obtained in the context of the traditional method which is based on the particular decay mode $h_1 \to b\bar{b}$, along with Z decays to $\mu^+\mu^-$ final states (see Ref. [53] for details). The traditional method achieves stronger constraints, but introduces more model dependence into the analysis, since a particular decay mode of h_1 is exploited. The colored points shown in Fig. 8.22 and Fig. 8.23 are the points of our scans in the type II and type IV scenario satisfying all the theoretical and experimental constraints.

One immediately sees that the BPs of our scans can in both the type II and the type IV scenario be covered completely by searches at the ILC for additional Higgs bosons below ~ 125 GeV. Depending on c_{h_1VV}, i.e., the light Higgs-boson production cross section, h_1 can be produced and analyzed in detail at the ILC. An analysis of the corresponding experimental precision of the light Higgs-boson couplings is beyond the scope of this thesis.

Bibliography

[1] S. Heinemeyer and T. Stefaniak, "A Higgs Boson at 96 GeV?!", in "7th International Workshop on Prospects for Charged Higgs Discovery at Colliders (CHARGED 2018) Uppsala, Sweden, September 25-28, 2018". 2018. arXiv:1812.05864.

[2] S. Heinemeyer, "A Higgs boson below 125 GeV?!", *Int. J. Mod. Phys.* **A33** (2018), no. 31, 1844006.

[3] P. J. Fox and N. Weiner, "Light Signals from a Lighter Higgs", *JHEP* **08** (2018) 025, arXiv:1710.07649.

[4] U. Haisch and A. Malinauskas, "Let there be light from a second light Higgs doublet", *JHEP* **03** (2018) 135, arXiv:1712.06599.

[5] F. Richard, "Search for a light radion at HL-LHC and ILC250", arXiv:1712.06410.

[6] L. Liu, H. Qiao, K. Wang, and J. Zhu, "A light scalar in the Minimal Dilaton Model in light of the LHC constraints", *Chin. Phys.* **C43** (2019), no. 2, 023104.

[7] J. M. Cline and T. Toma, "Pseudo-Goldstone dark matter confronts cosmic ray and collider anomalies", arXiv:1906.02175.

[8] J. Cao, X. Guo, Y. He, P. Wu, and Y. Zhang, "Diphoton signal of the light Higgs boson in natural NMSSM", *Phys. Rev.* **D95** (2017), no. 11, 116001, arXiv:1612.08522.

[9] T. Biekötter, S. Heinemeyer, and C. Muñoz, "Precise prediction for the Higgs-boson masses in the $\mu\nu$SSM", *Eur. Phys. J.* **C78** (2018), no. 6, 504, arXiv:1712.07475.

[10] F. Domingo, S. Heinemeyer, S. Paßehr, and G. Weiglein, "Decays of the neutral Higgs bosons into SM fermions and gauge bosons in the $\mathcal{CP}$-violating NMSSM", *Eur. Phys. J.* **C78** (2018), no. 11, 942, arXiv:1807.06322.

[11] W. G. Hollik, S. Liebler, G. Moortgat-Pick, S. Paßehr, and G. Weiglein, "Phenomenology of the inflation-inspired NMSSM at the electroweak scale", arXiv:1809.07371.

[12] K. Choi, S. H. Im, K. S. Jeong, and C. B. Park, "A 96 GeV Higgs boson in the general NMSSM", arXiv:1906.03389.

[13] T. Biekötter, S. Heinemeyer, and C. Muñoz, "Precise prediction for the Higgs-Boson Masses in the $\mu\nu$SSM with three right-handed neutrino superfields", arXiv:1906.06173.

[14] T. Biekötter, M. Chakraborti, and S. Heinemeyer, "A 96 GeV Higgs Boson in the N2HDM", *submitted to Eur. Phys. J.* **C**, 2019 arXiv:1903.11661.

[15] T. Biekötter, M. Chakraborti, and S. Heinemeyer, "An N2HDM Solution for the possible 96 GeV Excess", *18th Hellenic School and Workshops on Elementary Particle Physics and Gravity (CORFU2018) Corfu, Greece, August 31-September 28, 2018*, 2019 arXiv:1905.03280.

[16] **OPAL, DELPHI, LEP Working Group for Higgs boson searches, ALEPH, L3** Collaboration, R. Barate *et al.*, "Search for the standard model Higgs boson at LEP", *Phys. Lett.* **B565** (2003) 61–75, arXiv:hep-ex/0306033.

[17] **ALEPH, DELPHI, L3, OPAL, LEP Working Group for Higgs Boson Searches** Collaboration, S. Schael *et al.*, "Search for neutral MSSM Higgs bosons at LEP", *Eur. Phys. J.* **C47** (2006) 547–587, arXiv:hep-ex/0602042.

[18] A. Azatov, R. Contino, and J. Galloway, "Model-Independent Bounds on a Light Higgs", *JHEP* **04** (2012) 127, arXiv:1202.3415, [Erratum: JHEP04,140(2013)].

[19] **CMS** Collaboration, "Search for new resonances in the diphoton final state in the mass range between 80 and 115 GeV in pp collisions at $\sqrt{s} = 8$ TeV", CMS-PAS-HIG-14-037, 2015

[20] **CMS** Collaboration, A. M. Sirunyan *et al.*, "Search for a standard model-like Higgs boson in the mass range between 70 and 110 GeV in the diphoton final state in proton-proton collisions at $\sqrt{s} = 8$ and 13 TeV", *Phys. Lett.* **B793** (2019) 320–347, arXiv:1811.08459.

[21] **ATLAS** Collaboration, "Search for resonances in the 65 to 110 GeV diphoton invariant mass range using 80 fb^{-1} of pp collisions collected at $\sqrt{s} = 13$ TeV with the ATLAS detector", ATLAS-CONF-2018-025, 2018

[22] **ATLAS, CMS** Collaboration, G. Aad *et al.*, "Measurements of the Higgs boson production and decay rates and constraints on its couplings from a combined

ATLAS and CMS analysis of the LHC pp collision data at $\sqrt{s} = 7$ and 8 TeV", *JHEP* **08** (2016) 045, arXiv:1606.02266.

[23] S. Dawson *et al.*, "Working Group Report: Higgs Boson", in "Proceedings, 2013 Community Summer Study on the Future of U.S. Particle Physics: Snowmass on the Mississippi (CSS2013): Minneapolis, MN, USA, July 29-August 6, 2013". 2013. arXiv:1310.8361.

[24] A. Arbey *et al.*, "Physics at the e+ e- Linear Collider", *Eur. Phys. J.* **C75** (2015), no. 8, 371, arXiv:1504.01726.

[25] A. Denner, S. Heinemeyer, I. Puljak, D. Rebuzzi, and M. Spira, "Standard Model Higgs-Boson Branching Ratios with Uncertainties", *Eur. Phys. J.* **C71** (2011) 1753, arXiv:1107.5909.

[26] **LHC Higgs Cross Section Working Group** Collaboration, S. Heinemeyer *et al.*, "Handbook of LHC Higgs Cross Sections: 3. Higgs Properties", arXiv:1307.1347.

[27] A. Djouadi, "The Anatomy of electro-weak symmetry breaking. I: The Higgs boson in the standard model", *Phys. Rept.* **457** (2008) 1–216, arXiv:hep-ph/0503172.

[28] P. Ghosh, I. Lara, D. E. Lopez-Fogliani, C. Munoz, and R. Ruiz de Austri, "Searching for left sneutrino LSP at the LHC", *Int. J. Mod. Phys.* **A33** (2018), no. 18n19, 1850110, arXiv:1707.02471.

[29] I. Lara, D. E. López-Fogliani, C. Muñoz, N. Nagata, H. Otono, and R. Ruiz De Austri, "Looking for the left sneutrino LSP with displaced-vertex searches", *Phys. Rev.* **D98** (2018), no. 7, 075004, arXiv:1804.00067.

[30] M. Muhlleitner, M. O. P. Sampaio, R. Santos, and J. Wittbrodt, "The N2HDM under Theoretical and Experimental Scrutiny", *JHEP* **03** (2017) 094, arXiv:1612.01309.

[31] K. G. Klimenko, "On Necessary and Sufficient Conditions for Some Higgs Potentials to Be Bounded From Below", *Theor. Math. Phys.* **62** (1985) 58–65, [Teor. Mat. Fiz.62,87(1985)].

[32] P. M. Ferreira, M. Mühlleitner, R. Santos, G. Weiglein, and J. Wittbrodt, "Vacuum Instabilities in the N2HDM", arXiv:1905.10234.

[33] R. Coimbra, M. O. P. Sampaio, and R. Santos, "ScannerS: Constraining the phase diagram of a complex scalar singlet at the LHC", *Eur. Phys. J.* **C73** (2013) 2428, arXiv:1301.2599.

[34] A. Djouadi, J. Kalinowski, and M. Spira, "HDECAY: A Program for Higgs boson decays in the standard model and its supersymmetric extension", *Comput. Phys. Commun.* **108** (1998) 56–74, arXiv:hep-ph/9704448.

[35] J. M. Butterworth *et al.*, "THE TOOLS AND MONTE CARLO WORKING GROUP Summary Report from the Les Houches 2009 Workshop on TeV Colliders", in "Physics at TeV colliders. Proceedings, 6th Workshop, dedicated to Thomas Binoth, Les Houches, France, June 8-26, 2009". 2010. arXiv:1003.1643.

[36] P. Bechtle, O. Brein, S. Heinemeyer, G. Weiglein, and K. E. Williams, "HiggsBounds: Confronting Arbitrary Higgs Sectors with Exclusion Bounds from LEP and the Tevatron", *Comput. Phys. Commun.* **181** (2010) 138–167, arXiv:0811.4169.

[37] P. Bechtle, O. Brein, S. Heinemeyer, G. Weiglein, and K. E. Williams, "HiggsBounds 2.0.0: Confronting Neutral and Charged Higgs Sector Predictions with Exclusion Bounds from LEP and the Tevatron", *Comput. Phys. Commun.* **182** (2011) 2605–2631, arXiv:1102.1898.

[38] P. Bechtle, O. Brein, S. Heinemeyer, O. Stal, T. Stefaniak, G. Weiglein, and K. Williams, "Recent Developments in HiggsBounds and a Preview of HiggsSignals", *PoS* **CHARGED2012** (2012) 024, arXiv:1301.2345.

[39] P. Bechtle, O. Brein, S. Heinemeyer, O. Stål, T. Stefaniak, G. Weiglein, and K. E. Williams, "HiggsBounds – 4: Improved Tests of Extended Higgs Sectors against Exclusion Bounds from LEP, the Tevatron and the LHC", *Eur. Phys. J.* **C74** (2014), no. 3, 2693, arXiv:1311.0055.

[40] P. Bechtle, S. Heinemeyer, O. Stal, T. Stefaniak, and G. Weiglein, "Applying Exclusion Likelihoods from LHC Searches to Extended Higgs Sectors", *Eur. Phys. J.* **C75** (2015), no. 9, 421, arXiv:1507.06706.

[41] A. Arbey, F. Mahmoudi, O. Stål, and T. Stefaniak, "Status of the Charged Higgs Boson in Two Higgs Doublet Models", *Eur. Phys. J.* **C78** (2018), no. 3, 182, arXiv:1706.07414.

[42] R. V. Harlander, S. Liebler, and H. Mantler, "SusHi: A program for the calculation of Higgs production in gluon fusion and bottom-quark annihilation in the Standard Model and the MSSM", *Comput. Phys. Commun.* **184** (2013) 1605–1617, arXiv:1212.3249.

[43] R. V. Harlander, S. Liebler, and H. Mantler, "SusHi Bento: Beyond NNLO and the heavy-top limit", *Comput. Phys. Commun.* **212** (2017) 239–257, arXiv:1605.03190.

[44] P. Bechtle, S. Heinemeyer, O. Stål, T. Stefaniak, and G. Weiglein, "*HiggsSignals*: Confronting arbitrary Higgs sectors with measurements at the Tevatron and the LHC", *Eur. Phys. J.* **C74** (2014), no. 2, 2711, arXiv:1305.1933.

[45] O. Stål and T. Stefaniak, "Constraining extended Higgs sectors with HiggsSignals", *PoS* **EPS-HEP2013** (2013) 314, arXiv:1310.4039.

[46] P. Bechtle, S. Heinemeyer, O. Stål, T. Stefaniak, and G. Weiglein, "Probing the Standard Model with Higgs signal rates from the Tevatron, the LHC and a future ILC", *JHEP* **11** (2014) 039, arXiv:1403.1582.

[47] See: https://higgsbounds.hepforge.org/downloads.html.

[48] W. Grimus, L. Lavoura, O. M. Ogreid, and P. Osland, "The Oblique parameters in multi-Higgs-doublet models", *Nucl. Phys.* **B801** (2008) 81–96, arXiv:0802.4353.

[49] G. Funk, D. O'Neil, and R. M. Winters, "What the Oblique Parameters S, T, and U and Their Extensions Reveal About the 2HDM: A Numerical Analysis", *Int. J. Mod. Phys.* **A27** (2012) 1250021, arXiv:1110.3812.

[50] **ATLAS** Collaboration, M. Aaboud *et al.*, "Search for charged Higgs bosons decaying into top and bottom quarks at $\sqrt{s} = 13$ TeV with the ATLAS detector", *JHEP* **11** (2018) 085, arXiv:1808.03599.

[51] **ATLAS Collaboration** Collaboration, "Combined measurements of Higgs boson production and decay using up to 80 fb^{-1} of proton–proton collision data at $\sqrt{s} =$ 13 TeV collected with the ATLAS experiment", ATLAS-CONF-2018-031, CERN, Geneva, Jul 2018

[52] **CMS** Collaboration, A. M. Sirunyan *et al.*, "Combined measurements of Higgs boson couplings in proton-proton collisions at $\sqrt{s} = 13$ TeV", *Submitted to: Eur. Phys. J.*, 2018 arXiv:1809.10733.

[53] P. Drechsel, G. Moortgat-Pick, and G. Weiglein, "Sensitivity of the ILC to light Higgs masses", in "International Workshop on Future Linear Collider (LCWS2017) Strasbourg, France, October 23-27, 2017". 2018. arXiv:1801.09662.

[54] **CMS** Collaboration, "Projected Performance of an Upgraded CMS Detector at the LHC and HL-LHC: Contribution to the Snowmass Process", in "Proceedings, 2013 Community Summer Study on the Future of U.S. Particle Physics: Snowmass on the Mississippi (CSS2013): Minneapolis, MN, USA, July 29-August 6, 2013". 2013. arXiv:1307.7135.

[55] **CMS, ATLAS** Collaboration, A. Tricomi, "Prospects of the high luminosity LHC from ATLAS and CMS", *PoS* **EPS-HEP2015** (2015) 121.

[56] **ATLAS** Collaboration, "Projections for measurements of Higgs boson signal strengths and coupling parameters with the ATLAS detector at a HL-LHC", ATL-PHYS-PUB-2014-016, Oct 2014

[57] M. Slawinska, "High-luminosity LHC prospects with the upgraded ATLAS detector", *PoS* **DIS2016** (2016) 266, arXiv:1609.08434.

[58] D. M. Asner *et al.*, "ILC Higgs White Paper", in "Proceedings, 2013 Community Summer Study on the Future of U.S. Particle Physics: Snowmass on the Mississippi (CSS2013): Minneapolis, MN, USA, July 29-August 6, 2013". 2013. arXiv:1310.0763.

[59] H. Ono and A. Miyamoto, "A study of measurement precision of the Higgs boson branching ratios at the International Linear Collider", *Eur. Phys. J.* **C73** (2013), no. 3, 2343, arXiv:1207.0300.

[60] C. Dürig, K. Fujii, J. List, and J. Tian, "Model Independent Determination of HWW coupling and Higgs total width at ILC", in "International Workshop on Future Linear Colliders (LCWS13) Tokyo, Japan, November 11-15, 2013". 2014. arXiv:1403.7734.

[61] K. Fujii *et al.*, "Physics Case for the 250 GeV Stage of the International Linear Collider", DESY-17-155, KEK-PREPRINT-2017-31, LAL-17-059, SLAC-PUB-17161, 2017 arXiv:1710.07621.

[62] P. Bambade *et al.*, "The International Linear Collider: A Global Project", DESY 19-037, FERMILAB-FN-1067-PPD, IFIC/19-10, JLAB-PHY-19-2854, KEK Preprint 2018-92, LAL/RT 19-001, SLAC-PUB-17412, 2019 arXiv:1903.01629.

[63] **Physics of the HL-LHC Working Group** Collaboration, M. Cepeda *et al.*, "Higgs Physics at the HL-LHC and HE-LHC", arXiv:1902.00134.

[64] M. Guchait and A. H. Vijay, "Probing Heavy Charged Higgs Boson at the LHC", *Phys. Rev.* **D98** (2018), no. 11, 115028, arXiv:1806.01317.

[65] Y. Wang, J. List, and M. Berggren, "Search for Light Scalars Produced in Association with Muon Pairs for $\sqrt{s} = 250$ GeV at the ILC", in "International Workshop on Future Linear Collider (LCWS2017) Strasbourg, France, October 23-27, 2017". 2018. arXiv:1801.08164.

[66] **OPAL** Collaboration, G. Abbiendi *et al.*, "Decay mode independent searches for new scalar bosons with the OPAL detector at LEP", *Eur. Phys. J.* **C27** (2003) 311–329, arXiv:hep-ex/0206022.

Chapter 9

Conclusions

The discovery of the Higgs boson with a mass of ~ 125 GeV is a ground-breaking moment in the history of particle physics. So far it is the only fundamental scalar particle observed in nature. Considering the current experimental uncertainties, the new particle behaves as the Higgs boson predicted by the SM. Each model proposed to incorporate new physics has to accommodate the new particle state. However, in contrast to the SM, many BSM models predict extended Higgs sectors with more than a single Higgs boson. There is still no experimental evidence for additional Higgs bosons, yielding bounds on the parameter space of these models. Complementary, precise measurements of known observables provide constraints, as the presence of additional particles can alter the theory predictions indirectly. In particular, the properties of the SM-like Higgs boson can show deviations in models with extended Higgs sectors due to mixing effects. Thus, the Higgs boson acts as a sensor for BSM phenomena.

In the scope of this thesis the extended Higgs sectors of two different BSM models were investigated. The first model was the $\mu\nu$SSM that, in addition to the general attractive features related to the presence of Susy, can accommodate neutrino masses and mixings in agreement with experimental data via a seesaw mechanism at the electroweak scale. The $\mu\nu$SSM requires the existence of right-handed neutrinos. The scalar Susy partners of the neutrinos contribute to the EWSB, yielding a complicated but phenomenologically rich Higgs sector. The second model that was investigated was the N2HDM. This model results from enhancing the SM particle content by a second Higgs doublet field and a real scalar gauge-singlet field. The N2HDM comprises the phenomenology of various BSM models, for instance certain Susy models in which the presence of the aforementioned particles results from theoretical considerations, so that the N2HDM is a well motivated extension of the SM.

The work in the $\mu\nu$SSM was aimed to perform the complete one-loop renormalization of the neutral scalar sector at the one-loop level. At first, a renormalization prescription for the one-generation case, i.e., the $\mu\nu$SSM with on right-handed neutrino superfield, was established. Subsequently, the approach was extended to the more realistic three-generation case, i.e., the $\mu\nu$SSM with three right-handed neutrino superfields. So far, higher-order corrections in the $\mu\nu$SSM had been restricted to $\overline{\text{DR}}$ calculations in which the relations between model parameters and physical observables, e.g., particle masses, are rather obscure. In our renormalization prescription, OS renormalization conditions were deployed whenever this was eligible, thus taking advantage of direct relations between model parameters and observables. As soon as OS conditions are implemented, the renormalization cannot be automated anymore (in contrast to pure $\overline{\text{DR}}$ calculations), but

has to be reconsidered for each model studied. Therefore, we gave a detailed description of the renormalization conditions applied both in the one- and in the three-generation case of the $\mu\nu$SSM. The renormalization of the neutral scalar sector was used to attain the higher-order corrections to the masses of the neutral scalars.

Our analysis in the one-generation case was aimed to identify the conceptual differences to the MSSM and the NMSSM. The appearance of kinetic mixing and non-diagonal soft mass parameters which have their origin in the breaking of lepton-number conservation and R-parity led to a larger number of counterterms and more complicated expressions for the renormalization conditions. The numerical impact of genuine $\mu\nu$SSM-like corrections, i.e., corrections beyond the NMSSM, to the SM-like Higgs-boson mass were shown to be negligible compared to the parametric theory uncertainty, and also exceeded by the (anticipated) experimental uncertainty. This indicates that via the incorporation of state-of-the-art MSSM-like higher-order corrections the theoretical uncertainty of our Higgs-boson mass prediction is of the same level of accuracy as in the NMSSM. However, one-loop corrections to the masses of relatively light left-handed sneutrinos were shown to be potentially even larger than the tree-level masses, owing to the large hierarchy between the vevs of left-handed sneutrinos and the remaining neutral scalar fields. We illustrated the phenomenology of the scalar sector of the $\mu\nu$SSM in representative scenarios, in which we obtained numerical results for a SM-like Higgs-boson mass consistent with the experimental bounds. In addition, the scenarios presented feature additional light scalars. One of them, namely the $\mathcal{CP}$-even right-handed sneutrino, was demonstrated to be able to reproduce at the 1σ level two experimental excesses measured at LEP and CMS at ~ 96 GeV.

As already mentioned, the subsequent analysis in the $\mu\nu$SSM extended the renormalization procedure to the three-generation case. Here both the $\mathcal{CP}$-even and $\mathcal{CP}$-odd scalar sectors are further enhanced by a second and a third right-handed sneutrino. This yields a drastic increase in the total number of parameters. Apart from that, a second source of kinetic mixing of the scalar fields arises, since the three right-handed sneutrinos share the same quantum numbers. The resulting renormalization procedure, again exploiting OS conditions where that was adequate, was described in detail. The numerical analysis in the three-generation case exhibits two main differences compared to the one-generation case. Firstly, there are three instead of one gauge-singlet scalar fields present. Their mixing with the SM-like Higgs boson can, without taking into account experimental constraints, be arbitrarily large. Secondly, the presence of three instead of one right-handed neutrino yields also three light neutrino masses at tree level instead of just one. Because of this, we were able for the first time to evaluate the masses and mixings in the neutral scalar sector with high precision, while simultaneously reproducing the experimental neutrino data, i.e., mass differences and mixing angles. We illustrated the unique relations between scalar and fermionic sectors of the $\mu\nu$SSM in scenarios in which the SM-like Higgs boson is accompanied by one or more light right-handed sneutrinos. One of these was substantially mixed with the SM-like Higgs boson. We explicitly showed that in these kind of scenarios the non-universality of genuine $\mu\nu$SSM parameters w.r.t. their generation indices results in contributions to the SM-like Higgs-boson mass of ~ 1 GeV in experimentally allowed parameter regions.

The investigations in the N2HDM were focused particularly on a more accurate fit to the two experimental excesses at ~ 96 GeV measured at LEP and CMS. Since we saw that in the $\mu\nu$SSM, where Susy relations constrain the form of the scalar potential, the accommodation of the excesses is limited, we aimed for a better fit in a model without

Susy. The N2HDM was a natural candidate, as the particle content of the Higgs sector resembles the one of the $\mu\nu$SSM, where also a gauge-singlet scalar field is present in addition to two Higgs doublet fields. Taking into account all relevant constraints, we specified the relevant parameter space of the N2HDM in which a Higgs boson with a mass of ~ 96 GeV, having a dominant singlet component, can reproduce both excesses simultaneously in perfect agreement with the experimental signal-strenghts measurements. Furthermore, we demonstrated that only the type II and type IV N2HDM can provide a Higgs boson reproducing both signals accurately. In these types the couplings of the Higgs bosons to down-type and up-type fermions can be adjusted independently. This is crucial to attribute the desired properties to the ~ 96 GeV Higgs boson. Finally, we investigated how our proposed scenario can (and will) be tested at future colliders. We found that the scenario can be ruled out entirely if the future SM-like Higgs-boson coupling measurements at the HL-LHC will not find deviations from the SM predictions. A future e^+e^- collider like the ILC could produce the ~ 96 GeV Higgs boson from our analysis in large numbers, and would be able to precisely measure its branching ratios.

Conclusiones

El descubrimiento del bosón de Higgs con una masa de $\sim$ 125 GeV es un hito en la historia de la física de partículas. Hasta ahora, es la única partícula escalar observada en la naturaleza. Teniendo en cuenta las incertidumbres de los experimentos actuales, la nueva partícula se comporta tal y como se había previsto según el modelo estandar (SM). Cada modelo propuesto para incorporar nueva física también ha de acomodar esta partícula. Sin embargo, al contrario que el SM, muchas teorías más allá del SM (BMS) predicen un sector de Higgs extendido, que tiene más que un bosón de Higgs. Todavía no hay pruebas experimentales de que bosones de Higgs adicionales existan. Como consecuencia, hay que tener en cuenta restricciones sobre el espacio de parámetros de modelos BSM. Además, las medidas precisas de los observables conocidos producen restricciones de forma indirecta. En concreto, las propiedades del bosón de Higgs podrían verse afectadas por la presencia de otros escalares. En este sentido, el bosón de Higgs puede actuar como un sensor de fenómenos BSM.

Durante el desarollo de la tesis, investigamos los sectores de Higgs de dos modelos distintos. El primer modelo fue el $\mu\nu$SSM. El $\mu\nu$SSM es un modelo supersimétrico, que es capaz de acomodar las masas y mezclas de los neutrinos en concordancia con los valores medidos experimentalmente, mediante un mecanismo de seesaw a la escala electrodébil. El $\mu\nu$SSM require la existencia de neutrinos right-handed. Las parejas supersimétricas de los neutrinos contribuyen a la ruptura de la simetría electrodébil. Esto da lugar a un sector de Higgs complejo, pero con una fenomenología muy rica. El segundo modelo que investigamos fue el N2HDM. En el N2HDM se añaden otro campo de Higgs doblete y un campo escalar real al contenido del sector de Higgs del SM. El N2HDM comprende la fenomenología de varios modelos BSM en los que están presentes bosones de Higgs adicionales de este tipo. Por ello, el N2HDM es un modelo bien motivado.

Nuestro trabajo en el $\mu\nu$SSM se centró en llevar a cabo la renormalización completa a nivel de un loop del potencial de los escalar neutrales. En primer lugar, desarrollamos una prescripción de renormalización para el caso de una generación, es decir, para el $\mu\nu$SSM con un neutrino right-handed. Después extendimos el método para el caso más realista de tres generaciones, es decir, el $\mu\nu$SSM con tres neutrinos right-handed. Hasta ahora, los cálculos de las correcciones de órdenes superiores estaban limitados únicamente a esquemas de renormalización $\overline{\text{DR}}$ en los cuales las relaciones entre los parámetros del modelo y los observables, por ejemplo la masa de una partícula, no quedan de todo claras. En nuestra prescripción de renormalización en la que usamos condiciones on-shell (OS) nos aprovechamos de las relaciones directas entre parámetros y observables. Una vez implementadas las condiciones OS, ya no se puede automatizar la renormalización (a diferencia de los esquemas $\overline{\text{DR}}$). En cada modelo investigado hay que reconsiderar la renormalización. Por ello, catalogamos en detalle las condiciones de renormalización aplicadas en el caso de una y tres generaciones del $\mu\nu$SSM. Utilizamos la renormalización del potencial de los escalares neutrales para obtener las correcciones de órdenes superiores

para las masas de los escalares.

El análisis del caso de una generación se centró en identificar las diferencias conceptuales respecto al MSSM y NMSSM. Debido a la ruptura de la conservación del número leptónico y de R-paridad aparecen términos cinéticos mezclados y términos no diagonales de masas soft. Esto da lugar a un número total de contratérminos más grande y, a la vez, a expresiones más complicadas para las condiciones de renormalización. Mostramos que el impacto numérico de las contribuciones específicas del $\mu\nu$SSM que contribuyen a la masa del bosón de Higgs del SM es desdeñable comparado con las incertidumbres teóricas y experimentales. Esto indica que, una vez incorporadas las correcciones de órdenes superiores del MSSM, nuestra predicción de la masa del bosón de Higgs del SM tiene la misma exactitud que los cálculos correspondientes en el NMSSM. Sin embargo, demostramos también que las correcciones a nivel de un loop para las masas de sneutrinos left-handed pueden ser de la misma magnitud que las masas de las mismas a nivel clásico, debido a la jerarquía entre vevs de los sneutrinos left-handed y el resto de escalares. Illustramos la fenomenología del sector escalar del $\mu\nu$SSM en escenarios representativos en los que obtuvimos resultados numéricos para la masa del bosón de Higgs del SM consistente con el valor experimental. Además, los escenarios contienen escalares adicionales con masas bajas. Uno de estos, en concreto el sneutrino right-handed par bajo $\mathcal{CP}$, es capaz de reproducir a nivel de 1σ dos excesos experimentales medidos con los colisionadores LEP y LHC alrededor de ~ 96 GeV.

Como ya hemos mencionado, el análisis siguiente en el $\mu\nu$SSM extendió la prescripción de renormalización al caso de tres generaciones. En este caso, los sectores escalares pares e impares bajo $\mathcal{CP}$ tienen un segundo y tercer sneutrino right-handed. Describimos en detalle la renormalización del potencial de Higgs, incorporando de nuevo condiciones OS. El análisis numérico en el caso de tres generaciones muestra dos diferencias importantes con respeto al caso de una generación. En primer lugar, hay tres singletes en vez de uno en el sector de Higgs, y todos se pueden mezclar con el bosón de Higgs del SM. En segundo lugar, la presencia de tres neutrinos right-handed da lugar a tres masas en vez de una a tree level para los neutrinos left-handed. Por ello, fuimos capaz de calcular con precisión las masas y las mezclas de los escalares neutrales y simultáneamente reproducir los datos experimentales relacionados con los neutrinos: sus diferencias de masas y sus ángulos de mezcla. Ilustramos las relaciones especiales que existen entre el sector escalar y el sector fermiónico del $\mu\nu$SSM en escenarios en los que por lo menos uno de los sneutrinos right-handed tiene una masa parecida a la del bosón de Higgs del SM. Debido a ello puede haber una mezcla considerable entre los dos. Demostramos que la predicción de la masa del bosón de Higgs del SM se ve afectada por efectos no universales de los parámetros específicos del $\mu\nu$SSM. Por ejemplo, valores no universales para los parámetros λ_i dieron lugar a variaciones de ~ 1 GeV en escenarios que cumplían las restricciones experimentales.

Nuestra investigación en el N2HDM se centró en lograr un ajuste aún mejor de los dos excesos medidos alrededor de ~ 96 GeV. Dado que vimos que en el $\mu\nu$SSM, en el cual las relaciones supersimétrias restringen la forma del potencial escalar, la incorporación de los excesos está limitada, pretendimos mejorar el ajuste en un modelo no supersimétrico. El N2HDM es un candidato natural, porque el contenido de partículas se parece al del $\mu\nu$SSM en el cual también están presentes un campo escalar real yu un segundo campo de Higgs doblete. Teniendo en cuenta todas las restricciones experimentales, especificamos el espacio de parámetros en el que un bosón de Higgs con una masa de ~ 96 GeV, que tiene una componente dominante del campo singlete, es capaz de reproducir las

señales en concordancia perfecta con las medidas. Además, demostramos que solo el tipo II y el tipo IV del N2HDM poseen un bosón de Higgs que reproduzca las dos señales a la vez. En estos tipos de construcciones se pueden ajustar independientemente los acoplamientos de los bosones de Higgs con los fermiones tipo up y tipo down. Esto es fundamental para atribuir las propiedades deseadas al bosón de Higgs a ~ 96 GeV. Por último, investigamos cómo colisionadores futuros podrán comprobar el escenario prupuesto. Descubrimos que el HL-LHC puede descartar el escenario, si no se miden desviaciones con respecto a las predicciones en las medidas de los acoplamientos del bosón de Higgs del SM. Un posible colisionador e^+e^- como el ILC sería capaz de producir el bosón de Higgs a ~ 96 GeV de nuestro analisis en cantidades muy grandes y podría medir los branching ratios con una precisión muy elevada.